Pretargeted radioimmunodetection and -therapy in colorectal cancer

Rafke Schoffelen

Pretargeted radioimmunodetection and -therapy in colorectal cancer; PhD thesis, Radboud University Nijmegen, The Netherlands

Cover designed by: Joost van Moll and Rafke Schoffelen, technical assistance: Jonathan A. Disselhorst en Morten B. Hansen

Layout by: Jonathan A. Disselhorst and Rafke Schoffelen

Printed by: Ipskamp Drukkers B.V., Enschede

Financially supported by: the Dutch Cancer Society (KWF Kankerbestrijding), grant no. KUN 2008-4038

Pretargeted radioimmunodetection and -therapy in colorectal cancer

Proefschrift

ter verkrijging van de graad van doctor
aan de Radboud Universiteit Nijmegen,
op gezag van de rector magnificus prof. mr. S.C.J.J. Kortmann,
volgens besluit van het college van decanen
in het openbaar te verdedigen op
maandag 26 november 2012 om 10.30 uur precies

door
Rafke Schoffelen
geboren op 30 mei 1983
te Tilburg

Promotoren:

Prof. dr. O.C. Boerman
Prof. dr. W.J.G. Oyen
Prof. dr. W.T.A. van der Graaf

Manuscriptcommissie:

Prof. dr. L.F.A.G. Massuger
Prof. dr. J.H.A.M. Kaanders
Prof. dr. G.A.M.S. van Dongen

Paranimfen:

Gerben M. Franssen
Sanne Schoffelen

Table of contents

1

Outline

Metastatic colorectal cancer

Metastatic colorectal cancer (CRC) is diagnosed in more than 1.2 million patients annually and is responsible for more than 600,000 deaths per year worldwide (*1*). Patient survival mainly depends on the development of distant metastases (mCRC), which occurs in half of the patients. During the last decade, the therapeutic options for mCRC patients have increased, where after the addition of two new chemotherapeutic agents, oxaliplatin and irinotecan, two classes of monoclonal antibodies (MAb), against the vascular endothelial growth factor (bevacizumab), and against the epidermal growth factor receptor (cetuximab and panitumumab) were introduced in the clinical practice. Currently, the combination or successive regimens with these agents resulted in study populations in a median overall survival of 20 months (*2, 3*). However, these therapies cause in a subset of patients significant toxicity, such as diarrhoea, hand-foot skin reaction, fatigue, or sensory neuropathy (*4-6*). In addition, despite this improvement in survival, eventually most patients have disease progression, as they become refractory to these treatments. Only patients with a limited number of metastases have a chance for cure by radical surgery, in general combined with chemotherapy, which results in a increased 5-year survival up to almost 50% (*7, 8*). However, initial curative resection of metastases often fails, due to inoperable disease discovered at laparotomy (*9*), or recurrent disease during follow-up, which occurs in >50% of the cases (*10, 11*). Moreover, only a minority of patients is eligible for this surgical resection of metastases and the chance of complete tumour resection depends on the number, localization and size of metastatic tumour lesions (*12*). Therefore, there is need for improved and early detection of small metastases to avoid futile major surgery (*13*), and prevent delay in the start of palliative chemotherapy.

Currently, conventional imaging is performed with anatomical techniques, such as computed tomography (CT) and ultrasonography. However, these modalities require anatomic alterations to detect tumours, while their low contrast resolution limits the discrimination from soft tissues. Therefore, small tumours are missed, resulting in futile laparotomies and progression into overt-recurrences. Positron emission tomography (PET) with ^{18}F-fluorodeoxyglucose (FDG) is a more recent molecular imaging technique. FDG accumulates in cells with increased glucose metabolism, such as cancer cells, granulocytes and macrophages. The increased uptake in tumours generally leads to high contrast images. Multimodality imaging with hybrid PET/CT combining anatomy depicted by CT with molecular information from PET, is now widely available, and results in adequate diagnostic work-up of patients with CRC. FDG-PET/CT has high sensitivity and high negative predictive value for staging patients with CRC (*14, 15*), and therefore has an established role in the diagnostic process of patients with mCRC. In the pre-operative phase it changes patient management in >25% of patients, mainly by detecting extrahepatic disease (*9, 16, 17*). However, since FDG is a nonspecific tracer, it also has uptake in other tissues with increased metabolism (e.g., physiological uptake in the bowel, uptake in (post-surgical) inflammatory or infec-

tious lesions). This may cause diagnostic dilemmas as malignant disease may then not be excluded with sufficient confidence (*18-20*).

Radiolabeled monoclonal antibodies

As indicated above, both diagnostic and therapeutic challenges remain in patients with mCRC, i.e. [1] the need for a sensitive, but also specific imaging modality to detect small CRC tumours at an early stage, and [2] the need for an effective and less toxic systemic therapy for mCRC or for adjuvant treatment after surgery. These needs could potentially be met by antibody-guided radionuclide targeting. MAb directed against tumour-associated antigens can be used to selectively target radioactivity to tumour cells, while sparing normal tissues. These antibodies, or antibody-derived molecules, can be labelled with a wide variety of radionuclides, either for imaging or therapy. Moreover, imaging and therapy can be elegantly combined, a strategy designated as theranostics. Pre- and post-therapy imaging can be used to predict or measure the deposition of therapeutic agents.

Radioimmunotherapy (RIT) aims to selectively deliver radionuclides to the tumour lesions, and has some advantages over other therapeutic approaches for treatement of mCRC. For example, tumour cells that do not express the target antigen can still be killed due to crossfire effect, i.e. radiation emitted by radionuclides bound to neighbouring tumour cells. Furthermore, in contrast to chemotherapeutics and unconjugated MAb for treatemt of mCRC, radiolabelled MAb do not induce drug resistance, alternation of downstream signalling pathways, nor increased growth factor receptor.

Radioimmunotherapy in mCRC

For CRC, the mostly targeted tumour-associated antigen is carcinoembryonic antigen (CEA), which is overexpressed in 95% of CRC and is almost absent in normal tissues. CEA concentrations in tumours are on average 60-fold higher than in nonmalignant tissues (*21*). CEA is a glycoprotein consisting of 60% carbohydrate and a molecular mass of 180–200 kDa. CEA is attached to the cell membrane by a glycosyl phosphatidylinositol anchor and is released as a soluble form into the circulation probably by a phospholipase C or phospholipase D (*22, 23*). CEA is readily available on the outside of the membrane. Anti-CEA monoclonal antibodies bound to CEA-isotopes on the tumour cell surface are internalized, but this takes place only slowly and to a limited extent (*24, 25*).

The efficacy of RIT using radiolabelled anti-CEA MAb in mCRC has been investigated in various preclinical studies. Behr *et al.* demonstrated that in a nude mouse model for lung metastases of CRC, RIT with an ^{131}I-anti-CEA antibody cured half of the animals whereas equitoxic chemotherapy only prolonged life for a few weeks (*26*). Koppe *et al.* compared the effect of different radionuclides used in RIT with a radiolabelled anti-CEA-IgG in a mouse model with small peritoneal xenografts, and

showed that ^{177}Lu and ^{131}I were suitable radionuclides to be used in RIT (*27*).
In a phase I/II clinical trial, Behr *et al.* investigated the pharmacokinetics, dosimetry, toxicity and antitumor activity of ^{131}I-anti-CEA antibody in patients with CEA-expressing tumors, mainly of colorectal origin. Tumour absorbed doses inversely correlated with the tumour size. Only modest antitumor effects were observed (*28*). The pivotal clinical study of RIT that demonstrated its therapeutic potential in mCRC patients, was a phase II trial performed by Liersch *et al.* in patients with small volume disease. An ^{131}I-labelled anti-CEA IgG was given in an adjuvant setting to patients after liver metastasectomy. RIT resulted in an improved overall survival (OS) as compared to a comparable group of patients who did not receive adjuvant therapy (5 years OS 42.1% and 15.8% for RIT and controls, respectively) (*29, 30*).
Although RIT is effective in non-Hodgkin's lymphoma, which has led to the registration of two radiolabelled anti-CD20 MAb preparations (*31-34*), the efficacy of RIT in solid tumours is modest, mainly because these tumour lesions are less radiosensitive. To improve therapeutic efficacy of RIT in solid tumours, further escalation of radioactivity doses is required to guide higher absorbed doses to these tumours. However, radiolabelled MAb are not the solution as these have a slow blood clearance, causing continuous radiation exposure of the bone marrow due to long-circulating radioactivity. This results in dose-limiting bone marrow suppression without sufficient radiation doses being delivered to solid tumours. Therefore, to guarantee acceptable absorbed doses to normal tissue, the tumour-to-normal tissue ratios should be improved.
Different approaches of engineering or modification of antibodies have been developed to accelerate blood clearance of the radioactive agent and to improve targeting of tumours: MAb fragments such as Fab, $F(ab')_2$ fragments have been produced, as well as other MAb-derived constructs such a single-chain antibodies (scFv), minibodies and diabodies (*35-38*). Using these MAb fragments red marrow doses are indeed reduced, at the expense, however, ofincreased radiation doses to the kidneys, due to renal excretion and tubular retention of the radionuclides. Several methods to lower the kidney radiation doses have been developed (*39, 40*), but these may be insufficiently efficient to prevent renal failure.

Pretargeting

A very promising technique to improve tumour-to-normal tissue ratios is pretargeting. In pretargeting, the targeting of the tumour and the delivery of the radionuclide to the tumor are separated in two steps. For this purpose, MAb have been developed, which have affinity for a tumour-associated antigen as well as for a smaller radiolabelled molecule. First, the unlabelled MAb construct is infused, and when the MAb has cleared from the blood and has accumulated in the tumour, the radiolabelled small molecule is administered which is subsequently trapped in the tumour by the other binding site of the MAb (*Figure 1*). These smaller radiolabelled molecules used in pretargeting

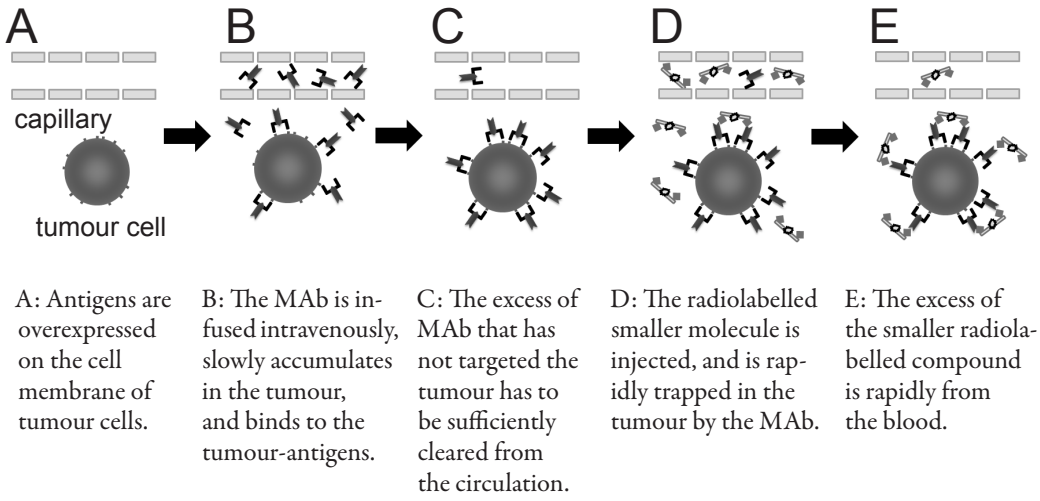

Figure 1: Schematic representation of pretargeting strategy. The tumour is pretargeted with a bispecific MAb, and in the second step a smaller radiolabelled molecule is administered (*41*).

extravasate more rapidly, thus targeting the tumours faster while also clearing more rapidly from the circulation than the full-sized radiolabelled MAb in conventional radioimmunodetection or RIT (*41*).

Two main MAb-based pretargeting approaches can be distinguished: strategies that use (strept)avidin and biotin, and those that use bispecific monoclonal antibodies (bsMAb) *(41).* The first approach is based on the extremely high affinity of the non-mammalian avidin or bacterial analog streptavidin to biotin ($K_a=10^{15}$ M^{-1}) (*42, 43*). Various strategies were developed, mainly using biotin as the radionuclide carrier. A streptavidin-conjugated IgG was used to pretarget the tumour and to capture the radiolabeled biotin. In another method a MAb-biotin conjugate is administered first, followed by a (strept)avidin injection followed by injection of the radiolabelled biotin. The biotin-avidin-based strategies has several disadvantages compared to the strategy with bsMAb. Firstly, (strept)avidin is immunogenic and cannot be humanized (*44*). Furthermore, due to the extremely high affinity of avidin for biotin, these two agents also strongly bind in the circulation, leading to enhanced circulatory half-life of the labelled compound and reduction of tumour uptake. Therefore, a clearing agent is needed to remove the excess antibody conjugate from the blood prior to administration of the radiolabelled compound (*41*).
BsMAb contain both a Fab-fragment that binds the tumour-associated antigen as well as a Fab-fragment that binds to a hapten. A hapten is a chemical structure that can induce an antibody response when it is coupled to a carrier molecule, but not by itself. The anti-hapten antibodies can be induced in mice. Both parts of the bsMAb

can be humanized with standard techniques. Due to the lower affinity of the bsMAb-hapten binding (Kd = 10^{-9} M) as compared to avidin-biotion binding (Kd = 10^{-15} M), bsMAb-hapten complexes that are formed in the circulation again dissociate. So, for pretargeting with bsMAb no clearing agent is required, which makes its clinical implementation less complicated than pretargeting with avidin-biotin *(41)*.

Initially, bsMAb were developed that bind chetal-metal complexes, such as DTPA-^{111}In as haptens. These chetal-metal haptens could either be used as separate agents, or they could be conjugated to a peptide. To improve the tumour binding properties of the radiolabelled peptide, two haptens can be conjugated, resulting in a divalent peptide (*45*). Le Doussal *et al.* demonstrated that divalent peptides had higher tumour uptake and stability, a phenomenom known as affinity enhancement (*46*). A pretargeting system based on an anti-CEA × anti-DTPA-indium bsmAb and a ^{131}I-labelled di-DTPA-tyrosyl-lysine peptide was studied in patients with CEA-expressing tumours. In patients (n=29) with recurrent medullary thyroid carcinoma, a statistically significant increase in the survival was observed compared to historical controls (*47*).

The binding affinity of an anti-chelate MAb may be affected by the chelated metal. Therefore, a more flexible system was developed with an antibody that has affinity for another part of a hapten-peptide complex than the chelating moiety. Recently, peptides substituted with two haptens, histamine-succinyl-glycine (HSG), in combination with anti-tumor x anti-HSG bsMAb were designed (*48*). The di-HSG-peptides can be conjugated with various chelating moieties (DTPA, DOTA, N_3S-chelates, etc.), and consequently with a wide variety of radionuclides, like ^{111}In and ^{99m}Tc for SPECT imaging (*49*), with ^{124}I, ^{68}Ga or ^{18}F for PET imaging (*50, 51*), or with ^{131}I, ^{90}Y and ^{177}Lu for pretargeted RIT (*48*).

Until recently, the bsMAbs used in pretargeting were either produced by fusing two hybridoma Ab-producing cells using the quadroma technology or by chemical conjugation of Fab-fragments. Karacay et al. demonstrated that a bsMAb with divalent reactivity for the tumour antigen leads to higher tumour uptake of a divalent hapten (*52*). Therefore, a new method, called the Dock-and-Lock (DNL) technology, has been developed to produce humanized trivalent Fab bsMAb constructs (molecular size: 157 kDa) with two binding sites for the tumour-associated antigen and one anti-HSG-Fab fragment to bind the HSG-groups on the radiolabeled peptide (*53, 54*). The DNL technology is based on the dimerization and docking sequences of cAMP-dependent protein A-kinase. Two anti-tumour Fab fragments are fused with the dimerization sequence. The dimeric sequence of the anti-tumour $F(ab)_2$ has high affinity for a sequence that is fused to the anti-hapten Fab (=docking). Furthermore, cysteine residues are placed on four location to form disulfide bridges to stabilize the trivalent bispecific antibody construct (=locking) (*54, 55*). DNL constructs have been developed for different tumour types and their specific antigens, such as B-cell lymphoma, pancreatic cancer, prostate cancer and significant responses have been reported in animals with subcutaneous xenografts (*45, 56*).

Pretargeting agents for CRC

For CRC the trivalent anti-CEACAM5 x anti-HSG bsMAb construct, TF2 (molecular weight 157 kDa), and IMP288 peptide (1456 Da) have been produced by IBC Pharmaceuticals, Inc., and Immunomedics, Inc. (Morris Plains, NJ, USA). TF2 is engineered from the 679 anti-HSG monoclonal antibody, and two humanized anti-CEACAM5 Fab-fragments derived from the humanized anti-CEACAM5 MAb, hMN-14 antibody, or labetuzumab *(21)*. MAb 679 binds to HSG with a high affinity (Ka ~ 10^{10} M^{-1}), while it does not react with histamine (Ka < 10^{4} M^{-1}) (*57*), and hMN-14 has a high affinity for CEACAM5 (Ka ~ 10^{9} M^{-1}) (*58*).
IMP288 is a DOTA-conjugated D-Tyr-D-Lys-D-Glu-D-Lys tetrapeptide in which both ε-NH_2 groups of the lysine residues are substituted with a HSG-moiety: 7,10-tetra-azacyclododecane-N,N',N'',N'''-tetraacetic acid (DOTA)-D-Tyr-D-Lys(HSG)-D-Glu-D-Lys(HSG)-NH_2 (*Figure 2*) (*51*). A particular favourable characteristic of this peptide is the lack of reabsorption in the kidneys.

Radionuclides

For immuno-PET ^{124}I has been used with directly radiolabeled antibody constructs for a large part because radioiodine will not be retained in normal tissues, and thus more reasonable tumour/tissue ratios can be achieved (*58*). However, the costs and relatively poor imaging properties of ^{124}I are considerable barriers to the development of

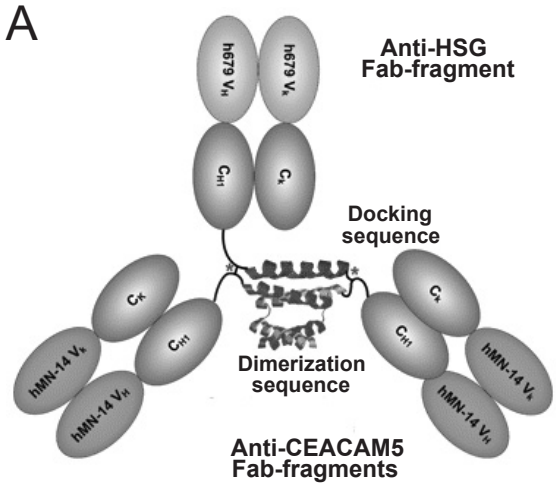

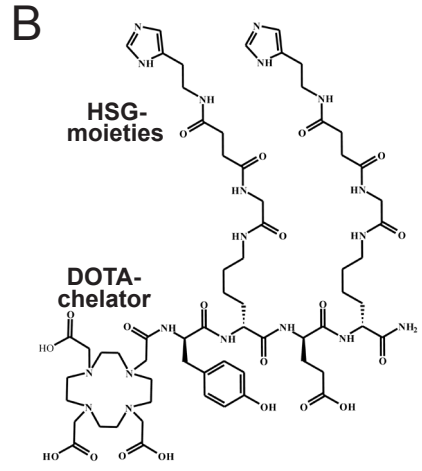

Figure 2: Pretargeting agents for CRC.
A: Schematic representation of the components of TF2, formed by the DNL method. The Fab of an anti-CEA antibody, hMN14, is dimerized. The dimerized construct is linked to the anti-HSG Fab, resulting in a tri-Fab bsMAb construct *(53)* (Reprinted by permission of the Society of Nuclear Medicine)

B: Chemical structure of IMP288, a DOTA-conjugated D-Tyr-D-Lys-D-Glu-D-Lys tetrapeptide in which the lysine residues are substituted with a HSG-moiety (*59*) (Reprinted by permission of the American Association of Cancer Research).

products based on this radionuclide. The short physical half-life of ^{18}F (110 min.) and ^{68}Ga (68 min.) can be used effectively in pretargeting to enhance detection sensitivity. The half-life of ^{68}Ga very well matches the fast kinetics of the peptide in the pretargeting system. A further advantage of ^{68}Ga is the availibility of a $^{68}Ge/^{68}Ga$ generator that can be eluted twice daily, avoiding the need for an on-site cyclotron.
For RIT the selection of the radionuclide is crucial to obtain an optimal balance between the therapeutic effect and the side effects. The β-emitting radionuclides that are most often used in RIT are ^{131}I, ^{90}Y and ^{177}Lu. There are several factors that must be taken into account when determining which of these is most suitable for a particular application. The physical properties, like half-life and energy of the beta particles, as well as differences in biological processes influence their impact. The physical half-life should match the blood clearance rate and the tumour residence time of the radiolabelled agent. ^{177}Lu has a relatively long half-life (6.7 days) compared to ^{90}Y (2.7 days). Furthermore, ^{177}Lu has low-energy beta particles (E_{max}= 498 keV), with a maximum penetration range in tissue of 2.5 mm, while ^{90}Y has a high energy (E_{max}= 2.28 MeV), resulting in a longer penetration range in tissue (maximum 12.0 mm). Therefore, ^{177}Lu may be useful in the treatment of small volume or micro metastatic cancer, and ^{90}Y would be more appropriate for larger tumours, especially when the intratumoural distribution is heterogeneous.
The *in vivo* processing after tumour-binding is different for radioiodine (^{131}I) than for radiometals (^{177}Lu, ^{90}Y). A radiolabelled peptide can be internalized by the target cell. Subsequently, it is enzymatically degraded in the lysosomes. In that case, radioiodine is again excreted from the cells, while radiometals will be trapped in the lysosomes. Therefore, the use of radiometals may result in longer tumour retention of the beta-emitter, causing higher absorbed doses (*27*).

Dosimetry

Ionizing radiation due to energy emitted by radiopharmaceuticals and deposited in tissues, may cause changes in atoms or molecules and thus damage cells. This might result in biologic effects: either therapeutic effects or toxicity, depending on the amount of radiation and the organ. The energy absorbed per unit mass (absorbed dose) is expressed in joules per kilogram, or grays (Gy).
The measurement and calculation of the absorbed dose is called radiation dosimetry. The absorbed dose can be calculated for the total body or for specific organs of interest (target organs). Some organs might contain significant concentrations of the radionuclide (source organs).
The absorbed dose can predict the therapeutic potential of new radiopharmaceuticals. Knowledge of the absorbed dose in healthy organs after administration of that radiopharmaceutical is mandatory to estimate the risk for radiation-related side-effects of healthy tissues. In RIT, red bone marrow and nephrotoxicity could be dose-limiting,

and therefore estimation of the radiation doses to the bone marrow and kidneys are crucial to determine the maximum dose that can be administered safely. A maximum absorbed dose of 2 Gy to the bone marrow is generally accepted to be safe (*59, 60*). Based on data from external beam radiotherapy a kidney dose of 23 Gy results in a 5% probability of developing radiation nephropathy within five years (*61*). In clinical trials with radiolabeled peptides, radiation doses that did not exceed 27 Gy to the kidneys, rarely caused long term renal failure (*62, 63*).

For accurate estimation of the absorbed dose in organs of interest, quantification of the time dependent activity distribution in the total body and the tissues is necessary. The most frequently used techniques to determine the residence times of the activity in the tissues are: [1] whole body gamma camera imaging at various time points and [2] serial measurements of radioactivity concentration in blood, urine and feces. These data can be used to calculate the cumulated activity, i.e. the sum of all nuclear transitions in the region. The cumulated activity divided by the administered activity is called the residence time. To convert residence times of the source organs into absorbed dose for target doses, not only the uptake and retention of activity in the source organs are important, but also other factors should be taken into account. Factors such as the physical half-life of the radionuclide, the types and energies of the emitted radiations, the sizes, shapes and distances of the source and target organs and the tissue between those organs determine the absorbed dose. To incorporate these factors in the calculations, the Medical Internal Radiation Dose (MIRD) scheme has been developed. It beholds conversion factors calculated for different phantoms (adult male/female, newborn, children etc.), hundreds of different radionuclides and all source and target organs (*64*). A FDA-approved software package that calculates the absorbed dose values using the MIRD scheme is the OLINDA/EXM program (Vanderbilt University, 2003).

Image vs blood-based methods to estimate the radiation dose to the red marrow

The red bone marrow dose can be calculated using two different methods: image-based or blood-based. In the image-based method, scintigraphic images are used to draw a region of interest (ROI) over a part of the body with high bone marrow contents, e.g. lumbar vertebrae, or skull. When planar images are used, the lumbar vertebrae will suffer from overlap of abdominal organs. Therefore, a part of the skull, i.e. the cranium, can be used as ROI for the red marrow, avoiding overlapping organs. The ROI of the cranium should be drawn as two separate left and right parts, to exclude the central, blood-rich part of the skull (*65*). The red bone marrow mass in the cranium is defined as the 0.119 fraction of the total red bone marrow mass in the body, as described in the ICRP23's Reference Man (*66*).

A second method for red marrow dose estimates is the blood-derived method as described by Shen *et al.* (*67, 68*). The blood-based method can only be applied if [1] no bone marrow or bone metastases are present, [2] the radiolabeled agents administered

do not bind to any blood, bone marrow, or bone components, and [3] the radiolabeled agents administered do not show aspecific retention in bone marrow. Weight and height of the individual patient are used to calculate the total blood mass (*69, 70*). This methods calculates the red marrow dose as a sum of the marrow self-dose (source organ = target organ) and the absorbed dose of the other organs. For the self-dose, the blood activity concentration is used as a surrogate for the bone marrow concentration, as the activity in the circulating blood is distributed within the extracellular fluid space of the red marrow. To convert the blood concentration into a bone marrow concentration, the patient's haematocrit and the extracellular fluid fraction are used. For the other organs that could be a source to the red marrow, the mean total body absorbed dose has been found to approximate the contributions of all separate organs, when corrected for the patient-specific body weight (*71*).
The most widely used method for dosimetry is planar whole body gamma camera imaging. Because overlapping organs and inhomogeneous background distribution might cause measurement errors, SPECT imaging could improve the accuracy of dosimetry, also for tumours. However, quantitative SPECT imaging is much more time-consuming and complex than calculation based on planar imaging.

Scope of the studies described in this thesis

The goal of this thesis was to examine the feasibility, specificity and sensitivity of pretargeted immuno-PET with anti-CEACAM5 x anti-HSG bsMAb (TF2) and ^{68}Ga- or ^{18}F-labelled di-HSG-peptide (IMP288) as imaging modality for CEA-positive colorectal xenografts in mice, both in subcutaneous as well in orthotopic tumours.
Moreover, the feasibility of image-guided therapy using pretargeted immunoSPECT with TF2 and ^{111}In-IMP288 for monitoring tumor targeting and –growth in mice, and for individual activity dosing in patients was investigated.
Furthermore, the therapeutic efficacy and toxicity of pretargeted RIT with TF2 and ^{177}Lu-IMP288 was studied in the same animal models, as well in a first clinical dose-finding study in patients with advanced colorectal cancer.
Finally, the added value of 3D voxel based dosimetry to estimate tumour and red marrow absorbed doses was determined.

References

1. Global Cancer Facts & Figures 2nd Edition, Atlanta: *American Cancer Society*; 2011.
2. Tol J, Koopman M, Cats A, et al. Chemotherapy, bevacizumab, and cetuximab in metastatic colorectal cancer. *N Engl J Med.* 2009;360:563-72.
3. Van Cutsem E, Köhne CH, Láng I, et al. Cetuximab plus irinotecan, fluorouracil, and leucovorin as first-line treatment for metastatic colorectal cancer: updated analysis of overall survival according to tumor KRAS and BRAF mutation status. *J Clin Oncol.* 2011;29:2011-9.
4. Koopman M, Antonini NF, Douma J, et al. Randomised study of sequential versus combination chemotherapy with capecitabine, irinotecan and oxaliplatin in advanced colorectal cancer, an interim safety analysis. A Dutch Colorectal Cancer Group (DCCG) phase III study. *Ann Oncol.* 2006;17:1523-8.

5. Heras P, Kritikos K, Hatzopoulos A, et al. Efficacy and safety of capecitabine and oxaliplatin combination as second-line treatment in advanced colorectal cancer. *Am J Ther.* 2009;16:319-22.
6. Eng C. Toxic effects and their management: daily clinical challenges in the treatment of colorectal cancer. *Nat Rev Clin Oncol.* 2009;6:207-18.
7. Jones RP, Jackson R, Dunne DF, et al. Systematic review and meta-analysis of follow-up after hepatectomy for colorectal liver metastases. *Br J Surg.* 2012;99:477-86.
8. Neeff H, Hörth W, Makowiec F, et al. Outcome after resection of hepatic and pulmonary metastases of colorectal cancer. *J Gastrointest Surg.* 2009;13:1813-20.
9. Wiering B, Krabbe PF, Jager GJ, Oyen WJ, Ruers TJ. The impact of fluor-18-deoxyglucose-positron emission tomography in the management of colorectal liver metastases. *Cancer.* 2005;104:2658-2670.
10. Adam R, Delvart V, Pascal G, et al. Rescue surgery for unresectable colorectal liver metastases downstaged by chemotherapy: a model to predict long-term survival. *Ann Surg.* 2004;240:644-657; discussion 657-648.
11. Alberts SR, Horvath WL, Sternfeld WC, et al. Oxaliplatin, fluorouracil, and leucovorin for patients with unresectable liver-only metastases from colorectal cancer: a North Central Cancer Treatment Group phase II study. *J Clin Oncol.* 2005;23:9243-9249.
12. Fong Y, Fortner J, Sun RL, Brennan MF, Blumgart LH. Clinical score for predicting recurrence after hepatic resection for metastatic colorectal cancer: analysis of 1001 consecutive cases. *Ann Surg.* 1999;230:309-318; discussion 318-321.
13. Park IJ, Kim HC, Yu CS, et al. Efficacy of PET/CT in the accurate evaluation of primary colorectal carcinoma. *Eur J Surg Oncol.* 2006;32:941-947.
14. Chowdhury FU, Shah N, Scarsbrook AF, Bradley KM. [18F]FDG PET/CT imaging of colorectal cancer: a pictorial review. *Postgrad Med J.* 2010;86:174-182.
15. Esteves FP, Schuster DM, Halkar RK. Gastrointestinal tract malignancies and positron emission tomography: an overview. *Semin Nucl Med.* 2006;36:169-181.
16. Llamas-Elvira JM, Rodriguez-Fernandez A, Gutierrez-Sainz J, et al. Fluorine-18 fluorodeoxyglucose PET in the preoperative staging of colorectal cancer. *Eur J Nucl Med Mol Imaging.* Jun 2007;34(6):859-867.
17. Tzimas GN, Koumanis DJ, Meterissian S. Positron emission tomography and colorectal carcinoma: an update. *J Am Coll Surg.* 2004;198:645-652.
18. Dirisamer A, Schima W, Heinisch M, et al. Detection of histologically proven peritoneal carcinomatosis with fused 18F-FDG-PET/MDCT. *Eur J Radiol.* 2009;69:536-541.
19. Even-Sapir E, Parag Y, Lerman H, et al. Detection of recurrence in patients with rectal cancer: PET/CT after abdominoperineal or anterior resection. *Radiology.* 2004;232:815-822.
20. Metser U, Miller E, Lerman H, Even-Sapir E. Benign nonphysiologic lesions with increased 18F-FDG uptake on PET/CT: characterization and incidence. *AJR Am J Roentgenol.* 2007;189:1203-1210.
21. Boucher D, Cournoyer D, Stanners CP, Fuks A. Studies on the control of gene expression of the carcinoembryonic antigen family in human tissue. *Cancer Res.* 1989;49:847-852.
22. Thomas P, Toth CA, Saini KS, Jessup JM, Steele G, Jr. The structure, metabolism and function of the carcinoembryonic antigen gene family. *Biochim Biophys Acta.* 1990;1032:177-189.
23. Thompson JA, Grunert F, Zimmermann W. Carcinoembryonic antigen gene family: molecular biology and clinical perspectives. *J Clin Lab Anal.* 1991;5:344-366.
24. Ford CH, Tsaltas GC, Osborne PA, Addetia K. Novel flow cytometric analysis of the progress and route of internalization of a monoclonal anti-carcinoembryonic antigen antibody. *Cytometry.* 1996;23:228-240.
25. Stein R, Juweid M, Mattes MJ, Goldenberg DM. Carcinoembryonic antigen as a target for radioimmunotherapy of human medullary thyroid carcinoma: antibody processing, targeting, and experimental therapy with 131I and 90Y labeled MAbs. *Cancer Biother Radiopharm.* 1999;14:37-47.
26. Behr TM, Memtsoudis S, Vougioukas V, et al. Radioimmunotherapy of colorectal cancer in small volume disease and in an adjuvant setting: preclinical evaluation in comparison to equitoxic chemotherapy and initial results of an ongoing phase-I/II clinical trial. *Anticancer Res.* 1999;19:2427-2432.
27. Koppe MJ, Bleichrodt RP, Soede AC, et al. Biodistribution and therapeutic efficacy of (125/131)I-, (186)Re-, (88/90)Y-, or (177)Lu-labeled monoclonal antibody MN-14 to carcinoembryonic antigen in mice with small peritoneal metastases of colorectal origin. *J Nucl Med.* 2004;45:1224-1232.
28. Behr TM, Sharkey RM, Juweid ME, et al. Phase I/II clinical radioimmunotherapy with an iodine-131-labeled anti-carcinoembryonic antigen murine monoclonal antibody IgG. *J Nucl Med.* 1997;38:858-870.
29. Liersch T, Meller J, Bittrich M, Kulle B, Becker H, Goldenberg DM. Update of carcinoembryonic antigen

radioimmunotherapy with (131)I-labetuzumab after salvage resection of colorectal liver metastases: comparison of outcome to a contemporaneous control group. *Ann Surg Oncol.* 2007;14:2577-2590.
30. Liersch T, Meller J, Kulle B, et al. Phase II trial of carcinoembryonic antigen radioimmunotherapy with 131I-labetuzumab after salvage resection of colorectal metastases in the liver: five-year safety and efficacy results. *J Clin Oncol.* 2005;23:6763-6770.
31. Gordon LI, Witzig T, Molina A, et al. Yttrium 90-labeled ibritumomab tiuxetan radioimmunotherapy produces high response rates and durable remissions in patients with previously treated B-cell lymphoma. *Clin Lymphoma.* 2004;5:98-101.
32. Wiseman GA, Gordon LI, Multani PS, et al. Ibritumomab tiuxetan radioimmunotherapy for patients with relapsed or refractory non-Hodgkin lymphoma and mild thrombocytopenia: a phase II multicenter trial. *Blood.* 2002;99:4336-4342.
33. Witzig TE, Flinn IW, Gordon LI, et al. Treatment with ibritumomab tiuxetan radioimmunotherapy in patients with rituximab-refractory follicular non-Hodgkin's lymphoma. *J Clin Oncol.* 2002;20:3262-3269.
34. Witzig TE, Gordon LI, Cabanillas F, et al. Randomized controlled trial of yttrium-90-labeled ibritumomab tiuxetan radioimmunotherapy versus rituximab immunotherapy for patients with relapsed or refractory low-grade, follicular, or transformed B-cell non-Hodgkin's lymphoma. *J Clin Oncol.* 2002;20:2453-2463.
35. Behr T, Becker W, Hannappel E, Goldenberg DM, Wolf F. Targeting of liver metastases of colorectal cancer with IgG, F(ab')2, and Fab' anti-carcinoembryonic antigen antibodies labeled with 99mTc: the role of metabolism and kinetics. *Cancer Res.* 1995;55:5777s-5785s.
36. Colcher D, Goel A, Pavlinkova G, Beresford G, Booth B, Batra SK. Effects of genetic engineering on the pharmacokinetics of antibodies. *Q J Nucl Med.* 1999;43:132-139.
37. Olafsen T, Wu AM. Antibody vectors for imaging. *Semin Nucl Med.* May 2010;40(3):167-181.
38. Rudnick SI, Adams GP. Affinity and avidity in antibody-based tumor targeting. *Cancer Biother Radiopharm.* 2009;24:155-161.
39. Behr TM, Sharkey RM, Sgouros G, et al. Overcoming the nephrotoxicity of radiometal-labeled immunoconjugates: improved cancer therapy administered to a nude mouse model in relation to the internal radiation dosimetry. *Cancer.* 1997;80:2591-2610.
40. Vegt E, de Jong M, Wetzels JF, et al. Renal toxicity of radiolabeled peptides and antibody fragments: mechanisms, impact on radionuclide therapy, and strategies for prevention. *J Nucl Med.* Jul 2010;51(7):1049-1058.
41. Boerman OC, van Schaijk FG, Oyen WJ, Corstens FH. Pretargeted radioimmunotherapy of cancer: progress step by step. *J Nucl Med.* 2003;44:400-411.
42. Paganelli G, Magnani P, Fazio F. Pretargeting of carcinomas with the avidin-biotin system. *Int J Biol Markers.* 1993;8:155-159.
43. Hnatowich DJ, Virzi F, Rusckowski M. Investigations of avidin and biotin for imaging applications. *J Nucl Med.* 1987;28:1294-1302.
44. Chinol M, Casalini P, Maggiolo M, et al. Biochemical modifications of avidin improve pharmacokinetics and biodistribution, and reduce immunogenicity. *Br J Cancer.* 1998;78:189-197.
45. Karacay H, McBride WJ, Griffiths GL, et al. Experimental pretargeting studies of cancer with a humanized anti-CEA x murine anti-[In-DTPA] bispecific antibody construct and a (99m)Tc-/(188)Re-labeled peptide. *Bioconjug Chem.* 2000;11:842-854.
46. Le Doussal JM, Martin M, Gautherot E, Delaage M, Barbet J. In vitro and in vivo targeting of radiolabeled monovalent and divalent haptens with dual specificity monoclonal antibody conjugates: enhanced divalent hapten affinity for cell-bound antibody conjugate. *J Nucl Med.* 1989;30:1358-1366.
47. Chatal JF, Campion L, Kraeber-Bodere F, et al. Survival improvement in patients with medullary thyroid carcinoma who undergo pretargeted anti-carcinoembryonic-antigen radioimmunotherapy: a collaborative study with the French Endocrine Tumor Group. *J Clin Oncol.* 2006;24:1705-1711.
48. Sharkey RM, McBride WJ, Karacay H, et al. A universal pretargeting system for cancer detection and therapy using bispecific antibody. *Cancer Res.* 2003;63:354-363.
49. Sharkey RM, Cardillo TM, Rossi EA, et al. Signal amplification in molecular imaging by pretargeting a multivalent, bispecific antibody. *Nat Med.* Nov 2005;11(11):1250-1255.
50. Griffiths GL, Chang CH, McBride WJ, et al. Reagents and methods for PET using bispecific antibody pretargeting and 68Ga-radiolabeled bivalent hapten-peptide-chelate conjugates. *J Nucl Med.* 2004;45(1):30-39.
51. McBride WJ, Zanzonico P, Sharkey RM, et al. Bispecific antibody pretargeting PET (immunoPET) with an 124I-labeled hapten-peptide. *J Nucl Med.* 2006;47:1678-1688.

52. Karacay H, Sharkey RM, McBride WJ, et al. Pretargeting for cancer radioimmunotherapy with bispecific antibodies: role of the bispecific antibody's valency for the tumor target antigen. *Bioconjug Chem.* 2002;13:1054-1070.
53. Goldenberg DM, Rossi EA, Sharkey RM, McBride WJ, Chang CH. Multifunctional antibodies by the Dock-and-Lock method for improved cancer imaging and therapy by pretargeting. *J Nucl Med.* 2008;49:158-163.
54. Rossi EA, Goldenberg DM, Cardillo TM, McBride WJ, Sharkey RM, Chang CH. Stably tethered multifunctional structures of defined composition made by the dock and lock method for use in cancer targeting. *Proc Natl Acad Sci U S A.* 2006;103:6841-6846.
55. Sharkey RM, Chang CH, Rossi EA, McBride WJ, Goldenberg DM. Pretargeting: taking an alternate route for localizing radionuclides. *Tumour Biol.* 2012.
56. Sharkey RM, Karacay H, Litwin S, et al. Improved therapeutic results by pretargeted radioimmunotherapy of non-Hodgkin's lymphoma with a new recombinant, trivalent, anti-CD20, bispecific antibody. *Cancer Res.* 2008;68(13):5282-90.
57. Morel A, Darmon M, Delaage M. Recognition of imidazole and histamine derivatives by monoclonal antibodies. *Mol Immunol.* 1990;27(10):995-1000.
58. Sharkey RM, Goldenberg DM, Goldenberg H, et al. Murine monoclonal antibodies against carcinoembryonic antigen: immunological, pharmacokinetic, and targeting properties in humans. *Cancer Res.* 1990;50:2823-2831.
59. Schoffelen R, Sharkey RM, Goldenberg DM, et al. Pretargeted immuno-positron emission tomography imaging of carcinoembryonic antigen-expressing tumors with a bispecific antibody and a 68Ga- and 18F-labeled hapten peptide in mice with human tumor xenografts. *Mol Cancer Ther.* 2010;9:1019-1027.
60. Scala RJ. Biologic effects of ionizing radiation. In: P.J. Early BDS, ed. Principles and Practice of Nuclear Medicine. St Louis: Mosby; 1995:123-127.
61. Siegel JA, Pawlyk DA, Lee RE, et al. Tumor, red marrow, and organ dosimetry for 131I-labeled anti-carcinoembryonic antigen monoclonal antibody. *Cancer Res.* 1990;50:1039s-1042s.
62. Barone R, Borson-Chazot F, Valkema R, et al. Patient-specific dosimetry in predicting renal toxicity with (90)Y-DOTATOC: relevance of kidney volume and dose rate in finding a dose-effect relationship. *J Nucl Med.* 2005;46 Suppl 1:99S-106S.
63. Valkema R, Pauwels SA, Kvols LK, et al. Long-term follow-up of renal function after peptide receptor radiation therapy with (90)Y-DOTA(0),Tyr(3)-octreotide and (177)Lu-DOTA(0), Tyr(3)-octreotate. *J Nucl Med.* 2005;46 :83S-91S.
64. Kraeber-Bodere F, Faivre-Chauvet A, Ferrer L, et al. Pharmacokinetics and dosimetry studies for optimization of anti-carcinoembryonic antigen x anti-hapten bispecific antibody-mediated pretargeting of Iodine-131-labeled hapten in a phase I radioimmunotherapy trial. *Clin Cancer Res.* 2003;9:3973S-3981S.
65. Stabin MG, Sparks RB, Crowe E. OLINDA/EXM: the second-generation personal computer software for internal dose assessment in nuclear medicine. *J Nucl Med.* 2005;46(6):1023-1027.
66. Visser E, Postema E, Boerman O, Visschers J, Oyen W, Corstens F. Software package for integrated data processing for internal dose assessment in nuclear medicine (SPRIND). *EJNMMI* 2007;34:413-421.
67. Report of the task group on reference man. *Ann ICRP.* 1979;3:iii.
68. Shen S, DeNardo GL, Sgouros G, O'Donnell RT, DeNardo SJ. Practical determination of patient-specific marrow dose using radioactivity concentration in blood and body. *J Nucl Med.* Dec 1999;40(12):2102-2106.
69. Shen S, Meredith RF, Duan J, et al. Improved prediction of myelotoxicity using a patient-specific imaging dose estimate for non-marrow-targeting (90)Y-antibody therapy. *J Nucl Med.* 2002;43(9):1245-1253.
70. Wennesland R, Brown E, Hopper J, Jr., et al. Red cell, plasma and blood volume in healthy men measured by radiochromium (Cr51) cell tagging and hematocrit: influence of age, somatotype and habits of physical activity on variance after regression of volumes to height and weight combined. *J Clin Invest*. 1959;38:1065-1077.
71. Brown E, Hopper J, Jr., Hodges JL, Jr., Bradley B, Wennesland R, Yamauchi H. Red cell, plasma, and blood volume in the healthy women measured by radiochromium cell-labeling and hematocrit. *J Clin Invest.* 1962;41:2182-2190.
72. Shen S, DeNardo GL, Macey DJ, et al. Practical determination of organ S values for individual patients for therapy. *Nucl Med Biol.* 1997;24:447-449.

2

Pretargeted immuno-PET imaging of CEA-expressing tumours with a bispecific antibody and a ^{68}Ga- and ^{18}F-labelled hapten-peptide in mice with human tumour xenografts

Rafke Schoffelen[1], Robert M. Sharkey[2], David M. Goldenberg[2], Gerben M. Franssen[1], William J. McBride[3], Edmund A. Rossi[4], Chien-Hsing Chang[3], Peter Laverman[1], Jonathan A. Disselhorst[1], Annemarie Eek[1], Winette T.A. van der Graaf[5], Wim J.G. Oyen[1], and Otto C. Boerman[1]

Molecular cancer therapeutics 2010;9:1019-1027

[1] Radboud University Nijmegen Medical Centre, dept. of Nuclear Medicine, Nijmegen, Netherlands
[2] Garden State Cancer Center, Morris Plains, New Jersey, USA
[3] IBC Pharmaceuticals, Morris Plains, New Jersey, USA
[4] Immunomedics, Inc., Morris Plains, New Jersey, USA
[5] Radboud University Nijmegen Medical Centre, dept. of Medical Oncology, Nijmegen, Netherlands

Abstract

Background

^{18}F-Fluorodeoxyglucose (^{18}F-FDG) is the most common molecular imaging agent in oncology, with a high sensitivity and specificity for detecting a number of cancers. Antibodies could enhance specificity; therefore, procedures were developed for radiolabelling a small (1.5 kD) hapten-peptide with ^{68}Ga or ^{18}F to compare their specificity to ^{18}F-FDG for detecting tumours using a pretargeting procedure.

Methods

Mice were implanted with carcinoembryonic (CEA; CEACAM5)-expressing LS174T human colonic tumours, a CEA-negative tumour, or an inflammation was induced in thigh muscle. A bispecific monoclonal (bsMAb) anti-CEA x anti-hapten antibody was given to mice, and 16 h later, 5 MBq of ^{68}Ga- or ^{18}F-labelled hapten-peptides were administered intravenously.

Results

Within 1 h, tissues showed high and specific targeting of the ^{68}Ga-IMP288, with 10.7 ± 3.6 %ID/g uptake in the tumour and very low uptake in normal tissues (e.g., tumour/blood 69.9 ± 32.3), in a CEA-negative tumour (0.35 ± 0.35 %ID/g), and inflamed muscle (0.72 ± 0.20 %ID/g). ^{18}F-FDG localized efficiently in the tumour (7.42 ± 0.20 %ID/g), but also in the inflamed muscle (4.07 ± 1.13 %ID/g) and in a number of normal tissues; thus, pretargeted ^{68}Ga-IMP288 provided better specificity and sensitivity. PET/CT images reinforced the improved specificity of the pretargeting method. ^{18}F-labelled IMP499 distributed similarly in the tumour and normal tissues as the ^{68}Ga-labelled IMP288, indicating that either radiolabelled hapten-peptide could be used.

Conclusions

Thus, pretargeted immuno-PET performs exceptionally well with short-lived radionuclides, and is a highly sensitive procedure that is more specific than ^{18}F-FDG-PET.

Introduction

Radiolabelled antibody targeting of tumour-associated antigens often requires several days for adequate visualization of tumours due to the slow pharmacokinetics and accretion of intact antibodies in tumours (*1*). The use of antibody fragments and engineered antibody formats (such as $F(ab')_2$, Fab', diabodies, minibodies or scFv) has improved radioimmunodetection only to a limited extent. Tumour uptake of most antibody fragments is much lower than that of an IgG, resulting in reduced signal strength in the tumours, which can contribute to uncertainties in interpretation (*2*). Pretargeting techniques were developed to improve radioimmunotargeting of tumours (*3-5*). In pretargeting, an unlabelled bifunctional reagent with affinity for the tumour and a small radiolabelled molecule is given in advance of the radiolabelled compound (*3, 4, 6*). Two main antibody-based pretargeting approaches can be distinguished: strategies that use (strept)avidin and biotin, and those that use bispecific monoclonal antibodies (bsMAb). The disadvantages of the biotin-avidin-based approaches are the immunogenicity of (strept)avidin and the need for a clearing agent to remove the antibody conjugate from the blood (*3*). A bsMAb, which can be humanized to reduce immunogenicity, will bind a tumour-associated antigen and a hapten. Coupling 2 haptens together improves peptide uptake and stability by a process known as affinity enhancement (*7*). Chelate-metal complexes, such as DTPA-In, have been used as haptens (*8*). More recently, peptides substituted with the hapten, histamine-succinylglycine (HSG), in combination with anti-HSG bsMAbs have provided a more flexible system, because these HSG-substituted peptides can be conjugated with various chelating moieties (DTPA, DOTA, N_3S-chelates, etc.). As a result they can be labelled with a wide variety of radionuclides, like ^{111}In and ^{99m}Tc for SPECT imaging (*6*), with ^{124}I for PET imaging (*9, 10*), or with ^{131}I, ^{90}Y and ^{177}Lu for pretargeted radioimmunotherapy (*11*).

Previous studies illustrated the enhanced sensitivity of pretargeted imaging for detecting cancer (6,10,12), with superior results of pretargeting compared to the directly radiolabelled antibody fragment. In a micrometastatic human colon cancer model, tumour nodules no larger than 0.3 mm in diameter were detected in the lungs of athymic mice with the ^{124}I-labelled di-HSG-peptide (*12*). This study highlighted the exceptional sensitivity of the pretargeting procedure, but herein we also wanted to examine the specificity of pretargeting, and therefore included a model of sterile inflammation. Earlier studies were performed with ^{124}I because it was commercially available and the chemistry for iodination was well known. However, ^{124}I is not an ideal radionuclide for PET imaging due to its high-energy positrons and considerable expense. Its long half-life ($t_{½}$ = 4.2 days) has been an advantage for directly radiolabelled antibodies that require extended periods for adequate contrast to develop, which only takes 1 h with pretargeting, making this method more amenable to short-lived positron emitting radionuclides. There are currently two radionuclides with exceptional imaging

properties for PET, namely ^{68}Ga and ^{18}F, and their half-lives are well matched with the pharmacokinetics of the radiolabelled peptide (^{68}Ga t½ = 68 min; and ^{18}F, t½ = 110 min). ^{68}Ga is a relative newcomer to nuclear medicine, and in addition to its physical properties, it is readily available in a nearly carrier-free state from an in-house ^{68}Ge/^{68}Ga generator.

Herein we report the first pretargeting studies with this ^{68}Ga-labelled peptide. ^{18}F has been the gold standard for PET studies. It is abundantly available and inexpensive, but the chemistry involved in preparing labelled products can be challenging. We recently reported a simplified approach for preparing ^{18}F-labelled peptides that involves the formation of ^{18}F-aluminum complexes that can then be simply bound to a chelate on a peptide (*13*). Thus, another objective of this study was to compare a ^{68}Ga- and an ^{18}F-labelled peptide with pretargeting.

In summary, we show the feasibility of using ^{68}Ga- or ^{18}F-labelled di-HSG-peptides in pretargeting, and further demonstrate the improved specificity afforded by pretargeting by including a comparison of ^{18}F-FDG and an inflammation model.

Methods

Pretargeting reagents TF2, IMP288 and IMP499

The bsMAb, TF2, and the peptides IMP288 and IMP499, were provided by Immunomedics (Morris Plains, NJ, USA). TF2 is an engineered trivalent bispecific antibody composed of a humanized anti-histamine-succinyl-glycine (HSG) Fab-fragment derived from the 679 anti-HSG monoclonal antibody (*14*), and two humanized anti-CEA Fab-fragments derived from the hMN-14 antibody or labetuzumab (*14, 15*), formed into a 157 kD protein by the Dock-and-Lock procedure (*16, 17*). The immunoreactive fraction of TF2 for binding to CEA, determined in a Lindmo assay (*18*) on fixed LS174T cells, exceeded 85%. Gel fitration chromatography showed that TF2 could bind >90% of ^{68}Ga-IMP288 peptide. TF2 was labelled with ^{125}I (Perkin Elmer, Waltham, MA) by the iodogen method (*19*), to a specific activity of 58 MBq/nmol. ^{125}I-labelled TF2 was purified by eluting the reaction mixture with PBS, 0.5 % *w/v* bovine serum albumin (BSA) (Sigma Chemicals, St. Louis, MO, USA) on a PD-10 column (GE Healthcare Bio-Sciences AB, Uppsala, Sweden).

IMP288 was synthesized and purified as described by McBride et al. (10). It is a DOTA-conjugated D-Tyr-D-Lys-D-Glu-D-Lys tetrapeptide in which both lysine residues are substituted with a HSG-moiety via their ε-aminogroup: 7,10-tetra-azacyclododecane-N,N',N'',N'''-tetraacetic acid (DOTA)-D-Tyr-D-Lys(HSG)-D-Glu-D-Lys(HSG)-NH_2 (*Figure 1A*). A similar peptide, IMP499, was conjugated with 1,4,7-tri-azacyclononane-N,N',N''-triacetic acid (NOTA) instead of DOTA, to facilitate labelling with ^{18}F (*Figure 1B*). To improve the conjugation of the NOTA chelator an alanine residue was used as a spacer (*13*).

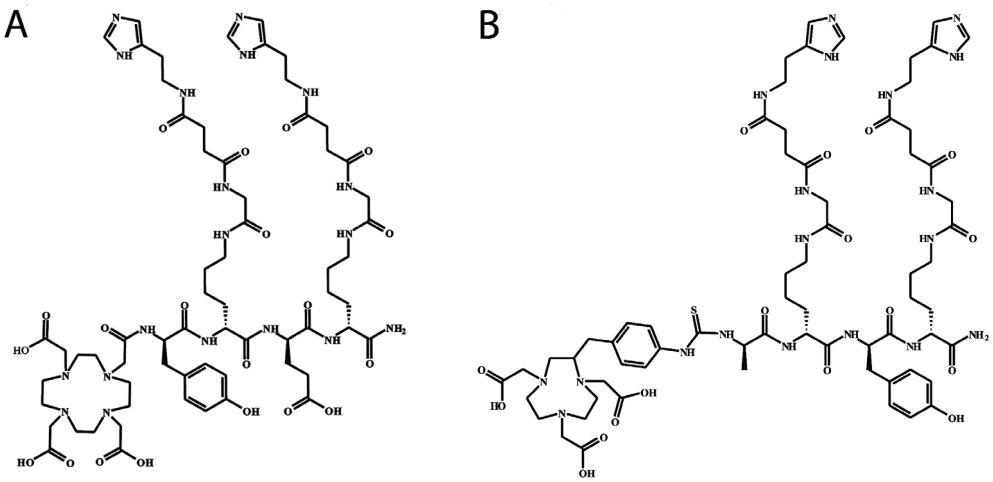

Figure 1. Chemical structures of IMP288 (A) and IMP449 (B). Both are Tyr-D-Lys-D-Glu-D-Lys tetrapeptides in which both lysine residues are substituted with a HSG-moiety via their ε-aminogroup. IMP288 is conjugated with DOTA: 7,10-tetra-azacyclododecane-N,N',N'',N'''-tetraacetic acid and IMP449 is conjugated with NOTA: 1,4,7-tri-azacyclononane-N,N',N''-triacetic acid.

Labelling of IMP288 or IMP499

IMP288 was labelled with ^{111}In (Covidien, Petten, The Netherlands) at 32 MBq/nmol under strict metal-free conditions. Briefly, 11 MBq ^{111}In was added to 12 μg IMP288 in 0.25 M ammonium acetate (NH_4Ac) buffer, pH 5.6, and after 20 min at 95 °C , 10 μL 50 mM ethylenediaminetetraacetic acid (EDTA) was added to complex any unbound ^{111}In.

IMP288 was labelled with ^{68}Ga eluted from a TiO-based 1,110 MBq ^{68}Ge/^{68}Ga generator (Cyclotron Co. Ltd., Obninsk, Russia) using 0.1 M ultrapure HCl (J.T. Baker, Deventer, The Netherlands). Five, 1-ml fractions were collected and the second fraction was used for labelling the peptide. One volume of 1.0 M HEPES buffer, pH 7.0, was added to 3.4 nmole IMP288. Four volumes of ^{68}Ga eluate (380 MBq) were added and the mixture was heated at 95 °C for 20 min. EDTA (50 mM) was added to a final concentration of 5 mM to complex the non-chelated $^{68}Ga^{3+}$, followed by purification on a 1-mL Oasis HLB-cartridge (Waters, Milford, MA). After washing the cartridge with water, the peptide was eluted with 25% ethanol.

IMP499 was labelled with ^{18}F as described by McBride et al. (*13*). [^{18}F]Fluoride (555-740 MBq; B.V. Cyclotron VU, Amsterdam, The Netherlands) was eluted from a QMA cartridge with 0.4 M $KHCO_3$. Four 200-μL fractions were collected in vials containing 3 μL 2 mM $AlCl_3$ in 0.1 M sodium acetate buffer, pH 4. The fraction with highest activity was used. The $Al[^{18}F]^{2+}$ activity was added to a vial containing IMP499 (230 μg) and ascorbic acid (10 mg). The mixture was incubated at 100 °C for 15 min, then

purified by reversed phase-high performance liquid chromatography (RP-HPLC; Phenomenex Onyx monolithic C18 column, Torrance, CA), using a linear gradient of 97% A to 100% B in 30 min (Buffer A: 0.1% TFA in water; Buffer B: 0.1% TFA in acetonitrile, flow rate: 3 mL/min). After adding one volume of water, the peptide was purified on a 1-mL Oasis HLB cartridge. After washing with water, the radiolabelled peptide was eluted with 50% ethanol.

Quality control of the radiolabelled preparations

Radiochemical purity was determined using instant thin-layer chromatography (ITLC) on silica-gel strips (Pall Life Sciences, Ann Arbor, MI) using 0.1 M citrate buffer, pH 6.0 as the mobile phase. The colloid content of the radiolabelled peptide was determined by ITLC-SG using a 1:1 v/v solution of 0.15 M NH_4Ac, pH 5.5, MeOH as the mobile phase.
^{111}In-IMP288, ^{68}Ga-IMP288 and ^{18}F-IMP499 were analyzed by RP-HPLC (Agilent 1100 series, Agilent Technologies, Palo Alto, CA) on a RP C_{18} column (Alltima, 5 μm, 4.6 x 250 mm, Alltech, Deerfield, IL), using a flow rate of 1.0 ml/min with a linear gradient of 97% A and 3% to 100% B, over 15 min buffer A: 0.1 % TFA in water and buffer B: 0.1 % TFA in acetonitrile. Radiochemical purity of ^{125}I-TF2, ^{111} In- and ^{68}Ga- IMP288 and ^{18}F-IMP499 preparations always exceeded 95%.

Animal experiments

All studies were approved by the institutional Animal Welfare Committee of the Radboud University Medical Centre Nijmegen, and conducted in accordance with their guidelines (revised Dutch Act on Animal Experimentation, 1997). Male nude BALB/c mice (6-8 weeks old), weighing 20-25 grams, received a subcutaneous injection with 0.2 mL of a suspension of 1 x 10^6 LS174T, a CEA-expressing human colon carcinoma cell line (CCL-188, American Type Culture Collection, Rockville, MD, passage 7). In some studies, animals were co-implanted with SK-RC52 cells, a human renal cancer cell line that is negative for CEA (*20*). The CEA production of LS174T in the ATCC seed stock was 1944 ng per milion cells in 10 days. Homogenized tissue of subcutaneous LS174T and SK-RC52 tumours during 10 days, grown in nude BALB/c mice, showed that the LS174T tumour had a CEA content of 17745 ng per million cells, whereas the SK-RC52 tumour had no detectable CEA content. Studies were initiated when the tumours reached a size of about 0.1-0.3 g.
In separate studies, animals bearing an LS174T xenograft in one hind leg were injected in the other hind limb muscle with 50 μl of turpentine to induce an inflammatory reaction (*21*).
TF2 was given intravenously and 16 hours later, radiolabelled IMP288 was given in 0.2 mL. This interval was shown previously to be sufficient to clear TF2 from the circulation (*15*). In some studies, ^{125}I-TF2, (0.4 MBq) was co-injected with unlabelled

TF2. One hour after the injection of ^{68}Ga-labelled peptide, and two hours after injection of ^{18}F-IMP499, mice were euthanized by CO_2 /O_2, and blood was obtained by cardiac puncture.
PET images were acquired with an Inveon animal PET/CT scanner (Siemens Preclinical Solutions, Knoxville, TN) with an intrinsic spatial resolution of 1.5 mm (*22*). The animals were placed in a supine position. PET emission scans were acquired for 15 min, preceded by CT scans for anatomical reference (spatial resolution 113 μm, 80 kV, 500 μA, exposure time 300 msec). Scans were reconstructed using Inveon Acquisition Workplace software (version 1.2, Siemens Preclinical Solutions, Knoxville, TN, USA) using a 3D ordered subset expectation maximization/maximum a posteriori (OSEM3D/MAP) algorithm with the following parameters: matrix 256 x 256 x 159, pixel size 0.43 x 0.43 x 0.8 mm^3 and MAP prior β of 0.5.
After imaging, tumour and organs of interest were dissected, weighed and counted in a gamma counter with appropriate energy windows for ^{125}I, ^{111}In, ^{68}Ga or ^{18}F. The percentage-injected dose per gram tissue (%ID/g) was calculated.

Statistic analysis

All mean values are given ± standard deviation. Statistical analysis was performed using a non-parametric, two-tailed Mann Whitney test using GraphPad InStat software (version 4.00, GraphPad Software). The level of significance was set at $p<0.05$.

Results

Dose optimization

The effect of the TF2 dose on tumour targeting with a fixed amount of IMP288 (0.01 or 0.1 nmole; 15 or 150 ng, respectively) was determined. Groups of five mice were injected intravenously with 0.10, 0.25, 0.50 or 1.0 nmol TF2, labelled with a trace amount of ^{125}I (0.4 MBq). Two hours after injection of ^{111}In-IMP288 (0.01 nmol, 0.4 MBq), the biodistribution of the radiolabels was determined.
TF2 cleared rapidly from blood and normal tissues. Eighteen hours after injection, the blood concentration was less than 0.45 %ID/g at all TF2 doses tested. TF2 tumour uptake was 3.5 %ID/g, independent of TF2 dose up to 1.0 nmol (data not shown). At all TF2 doses, ^{111}In-IMP288 accumulated effectively in the tumour, with increasing uptake associated with higher TF2 doses (*Figure 2A*). At the 0.01 nmole ^{111}In-IMP288 dose, tumour uptake peaked at 26.2 ± 3.8 %ID/g. With 0.01 nmol of IMP288, the highest tumour targeting and tumour-to-blood ratios were achieved with 1.0 nmol TF2 (TF2:IMP288 molar ratio = 100:1). The kidneys had the highest normal organ accretion of ^{111}In-IMP288 (1.75 ± 0.27 %ID/g); all other normal tissues had very low uptake.

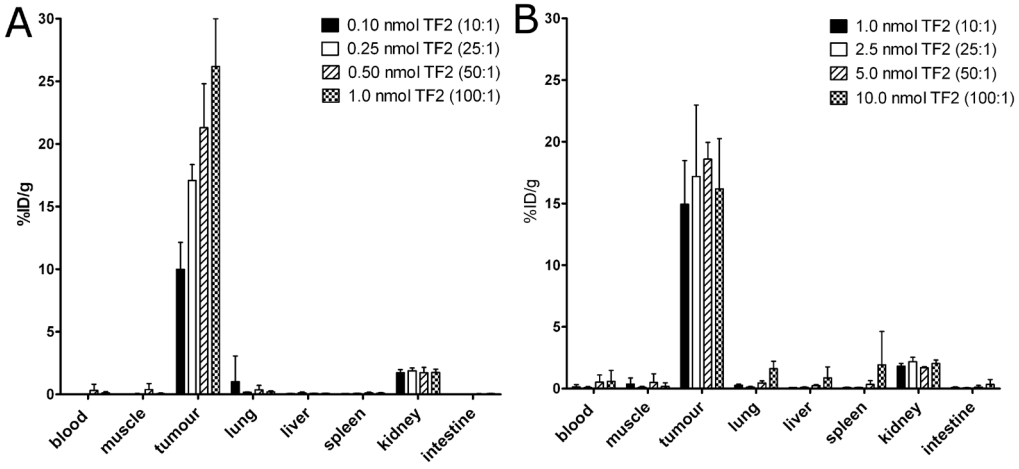

Figure 2. Biodistribution of ^{111}In-IMP288 1 h after i.v. injection, following pretargeting with escalating doses TF2 in BALB/c nude mice with a s.c. CEA-expressing LS174T tumour. Two peptide doses were tested (A: 0.01 nmol ^{111}In-IMP288; B: 0.10 nmol ^{111}In-IMP288). Values are given as means ± standard deviation (n=5).

With ^{68}Ga-labelled IMP288, a minimum of 5-10 MBq ^{68}Ga was required for PET imaging performed 1 h after injection. At a maximum specific activity of 50-125 MBq/nmol at the time of injection, at least 0.1-0.25 nmol of ^{68}Ga-IMP288 had to be administered. A separate group of LS174T-bearing mice received the same TF2:IMP288 molar ratios as were tested above, but with 0.1 nmol IMP288, 1.0, 2.5, 5.0 or 10.0 nmol of TF2 was administered. The percent uptake of TF2 in the tumour decreased from 3.21 ± 0.61 %ID/g at the 1.0 nmole dose to 1.16 ± 0.27 %ID/g with 10.0 nmol, suggesting the antigen in the tumour was saturated. In contrast to the results at the 0.01 nmole dose, tumour uptake with 0.1 nmole of ^{111}In-IMP288 was not affected by the TF2 dose, but it did not exceed about 15 %ID/g at all doses tested (*Figure 2B*). Based on these data, a bsMAb dose of 6.0 nmol was selected for targeting 0.1-0.25 nmol of ^{68}Ga-IMP288 to the tumour.

PET imaging

Five mice bearing an LS174T CEA-expressing tumor in the right flank and SK-RC52, a CEA-negative tumour in the left flank were administered 6.0 nmol ^{125}I-TF2 intravenously. After 16 h, the mice received 5 MBq ^{68}Ga-IMP288 (0.25 nmol, specific activity of 20 MBq/nmol). A separate group of three mice received the same amount of ^{68}Ga-IMP288 alone, without pretargeting with TF2. PET/CT scans of the mice were acquired 1 h after injection of the ^{68}Ga-IMP288.

The biodistribution of ^{125}I-TF2 and ^{68}Ga-IMP288 in mice are shown in *Figure 3A*. High uptake of the bsMAb (2.17 ± 0.50 %ID/g) and peptide (10.7 ± 3.6 %ID/g) in the tumour was observed, with very low accretion in the normal tissues (tumour-to-blood ratio for ^{68}Ga-IMP288: 64 ± 22). Most importantly, targeting of ^{68}Ga-IMP288 in the CEA-negative tumour SK-RC52 was very low (0.35 ± 0.35 %ID/g). Likewise, tumours that were not pretargeted with TF2 had a low uptake of ^{68}Ga-IMP288 (0.20 ± 0.03 %ID/g), indicating that the specific accumulation of IMP288 in the CEA-expressing LS174T tumour was derived from the pre-localization of the bsMAb.

The specific uptake of ^{68}Ga-IMP288 in the CEA-expressing tumour pretargeted with TF2 was clearly visualized in the PET image acquired 1 h after injection, without any localization in the negative tumour (*Figure 3B*). Uptake in the tumour was evaluated quantitatively by drawing regions of interest (ROI), using a 50% threshold of maximum intensity. A region in the abdomen was used as background region. The tumour-to-background ratio in the image of the mouse that received TF2 and ^{68}Ga-IMP288 was 38.2 at 1 h.

In the next studies, two groups of five mice bearing a s.c. LS174T tumour in the right hind leg and an turpentine-induced inflammatory focus in the left thigh muscle were examined to assess the specificity of the pretargeting procedure compared to ^{18}F-FDG. Three days after the induction of the inflammatory lesion, one group of mice received 6.0 nmol TF2, followed 16 h later by 5 MBq ^{68}Ga-IMP288 (0.25 nmol). The other group received ^{18}F-FDG (5 MBq). Mice were fasted for 10 hours prior to the injection and anesthetized and kept warm at 37 °C until euthanasia, 1 h post-injection.
Figure 4A shows an example of a mouse that received the TF2-pretargeted ^{68}Ga-IMP288, showing efficient accretion of the radiolabelled peptide in the tumour, while the inflamed muscle was not visualized. In contrast, both tumour and inflammation were visible in the mice that received ^{18}F-FDG (*Figure 4B*). In mice given ^{68}Ga-IMP288, the tumour-to-inflamed tissue ratio by SUV analysis was 5.4 and the tumour-to-background ratio was 48. ^{18}F-FDG uptake had a tumour-to-inflamed muscle ratio of 0.83, and the tumour-to-background ratio was 2.4.

At necropsy, uptake of ^{68}Ga-IMP288 measured in the inflamed muscle was only 0.72 ± 0.20 %ID/g, but tumour uptake was 8.73 ± 1.60 %ID/g ($p<0.05$, *Figure 5*). The tumour-to-blood ratio of ^{68}Ga-IMP288 in these mice was 69.9 ± 32.3; the inflamed muscle-to-blood ratio was 5.9 ± 2.9; and the tumour-to-inflamed muscle ratio was 12.5 ± 2.1. ^{18}F-FDG accreted efficiently in the tumour (7.42 ± 0.20 %ID/g, tumour-to-blood ratio 6.24 ± 1.5, *Figure 5*), but also accumulated substantially in the inflamed muscle (4.07 ± 1.13 %ID/g), with an inflamed muscle-to-blood ratio of 3.4 ± 0.5, and a tumour-to-inflamed muscle ratio of 1.97 ± 0.71.

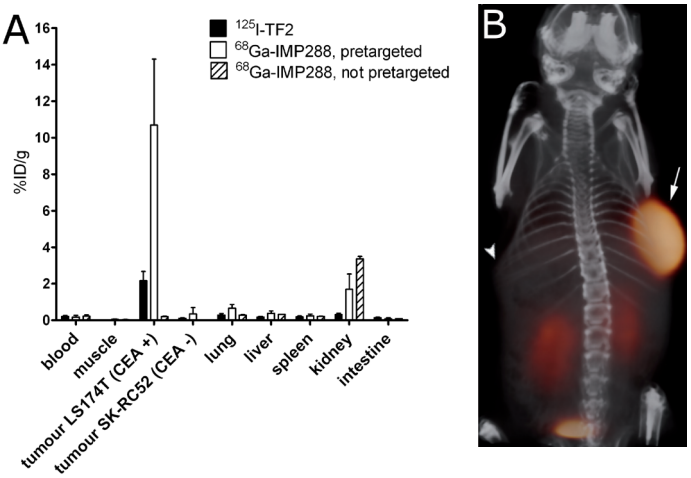

Figure 3A: Biodistribution of 6.0 nmol ^{125}I-TF2 (0.37 MBq) and 0.25 nmol ^{68}Ga-IMP288 (5 MBq), 1 h after i.v. injection of ^{68}Ga-IMP288 in BALB/c nude mice with a s.c. LS174T and SK-RC52 tumour. Values are given as means ± SD (n=5) (A).

Figure 3B: PET/CT image (3D volume rendered) of a BALB/c nude mouse with a s.c. LS174T CEA-expressing tumour in the right flank (arrow) and a s.c. SK-RC52 tumour, a non-CEA-producing, tumour in the left flank (arrowhead), that received 6.0 nmol TF2 and 5 MBq ^{68}Ga-IMP288 (0.25 nmol) intravenously with a 16-hour interval, imaged one hour after ^{68}Ga-IMP288 injection (B).

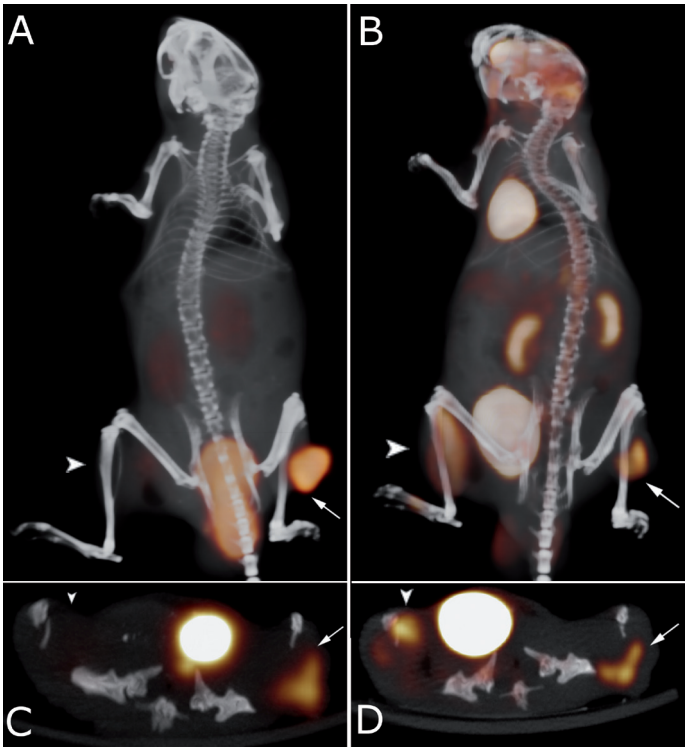

Figure 4. PET/CT images of a BALB/c nude mouse with a s.c. LS174T tumour (0.1 g) on the right hind leg (arrow) and a inflammation in the left thigh muscle (arrowhead), that received 5 MBq ^{18}F-FDG, and one day later 6.0 nmol TF2 and 5 MBq ^{68}Ga-IMP288 (0.25 nmol) with a 16-hour interval. The animal was imaged one hour after ^{18}F-FDG and ^{68}Ga-IMP288 injections. The panel shows the 3D volume rendering of the pretargeted immuno-PET scan (A) and of the FDG-PET scan (B), and the transverse sections of the tumour region of the pretargeted immuno-PET scan (C), and of the FDG-PET scan (D).

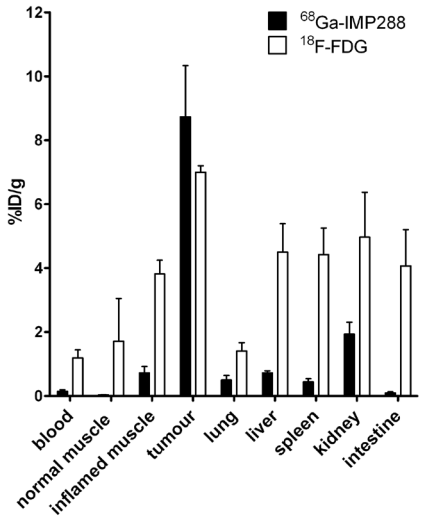

Figure 5. Biodistribution of 5 MBq FDG and 5 MBq ^{68}Ga-IMP288 (0.25 nmol) 1 h after injection, following pretargeting with 6.0 nmol TF2 in BALB/c nude mice with a s.c. CEA-expressing LS174T tumour. Values are given as means ± standard deviation (n=5).

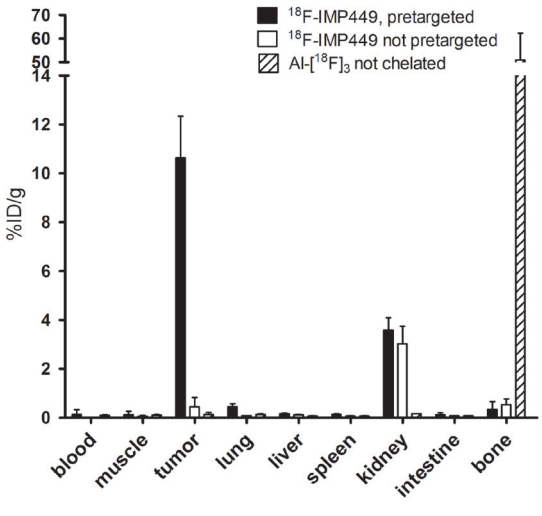

Figure 6. Biodistribution of 0.25 nmol ^{18}F-IMP449 (5 MBq) 1 hour after injection, following pretargeting with 6.0 nmol TF2 16 hours earlier, biodistribution of ^{18}F-IMP449 without pretargeting, or biodistribution of Al[^{18}F]$^{2+}$ in BALB/c nude mice with a s.c. CEA-expressing LS174T tumour. Values are given as means ± standard deviation.

Finally, the pretargeted immuno-PET imaging method was tested using the ^{18}F-labelled peptide, IMP499. Five mice received 6.0 nmol TF2, followed 16 h later by 5 MBq ^{18}F-IMP499 (0.25 nmol). Three additional mice received 5 MBq ^{18}F-IMP499 without prior administration of TF2, while two mice were injected with Al[^{18}F]$^{2+}$ (3 MBq). Uptake of ^{18}F-IMP499 at 1 h in tumours pretargeted with TF2 was high (10.6 ± 1.7 %ID/g) (*Figure 6*), whereas it was very low in the non-pretargeted mice (0.45 ± 0.38 %ID/g). Al[^{18}F]$^{2+}$ accumulated in the bone (50.9 ± 11.4 %ID/g), while uptake of IMP499 peptide in the bone was very low (0.54 ± 0.2 %ID/g), indicating that the ^{18}F-IMP499 was stable *in vivo*. Importantly, the biodistribution of ^{18}F-IMP499 in the TF2 pretargeted mice was very similar to that of ^{68}Ga-IMP288, indicating the suitability for either of these radiolabelled agents for use in pretargeted PET imaging. Pretargeted immuno-PET images with ^{18}F-IMP499 showed the same intensity in the tumour as those with ^{68}Ga-IMP288, but the resolution of the ^{18}F-images was better than the ^{68}Ga-images (*Figure 7*). The tumour-to-background ratio of the ^{18}F-IMP499 signal was 66.

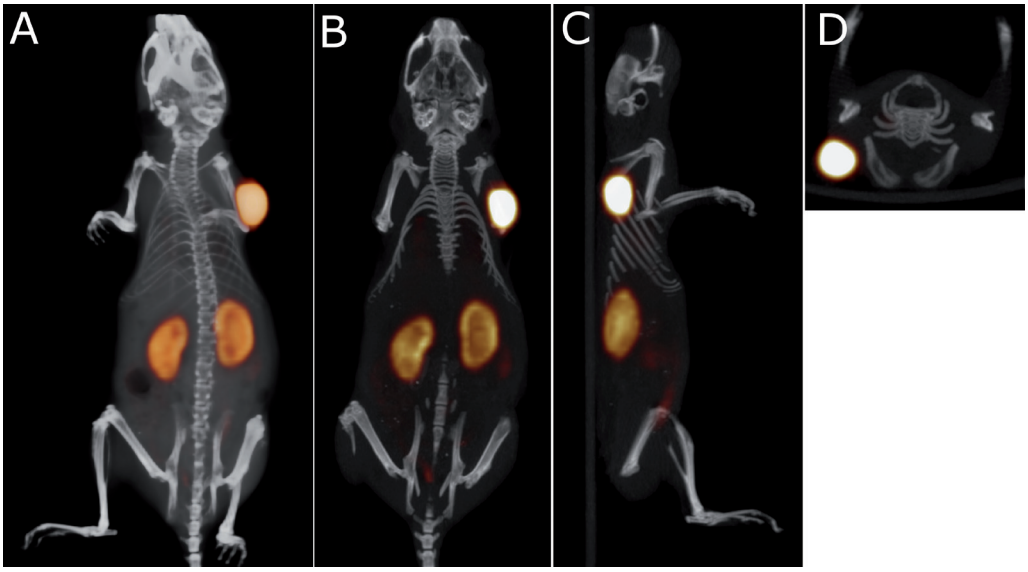

Figure 7. Static PET/CT imaging study of a BALB/c nude mouse with a subcutaneous LS174T tumour (0.1 g) on the right side, that received 6.0 nmol TF2 and 0.25 nmol ^{18}F-IMP449 (5 MBq) intravenously with a 16-hour interval. The animal was imaged one hour after injection of ^{18}F- IMP449. The panel shows the 3D volume rendering (A: posterior view), and cross-sections at the tumour region (B: coronal, C: sagittal, D: transversal).

Discussion

Several important conclusions can be made from the present study. Pretargeting affords the possibilities of utilizing antibody-based imaging techniques with short-lived radionuclides, such as ^{68}Ga and ^{18}F, that are ideally suited for PET imaging. Before the use of ^{18}F-FDG and PET imaging, radiolabelled antibodies were being developed commercially for the detection of colorectal, ovarian, lung, and prostate cancers using single-photo computed emission tomography imaging systems (*23*). However, all of these imaging methods suffered from relatively poor contrast, even when radiolabelled antibody fragments were used (*24*). Unquestionably, the advent of ^{18}F-FDG provided the necessary platform for the development of molecular imaging based on the newly developed PET imaging systems, and as a result, most of these antibody-imaging agents have been withdrawn from the market. Since then, molecular engineering has fostered a new era for antibodies, making it possible to craft many different forms with more favorable blood clearance and targeting potential (*25*). Still, many of these new constructs require considerable time for good tumour uptake and contrast to develop, and therefore radionuclides with longer half-lives, such as ^{64}Cu and ^{124}I, are often used.

For example, Cai et al. reported an attempt to use a directly radiolabelled ^{18}F-anti-CEA diabody for imaging (*26*). While this type of construct has very favorable pharmacokinetic properties, maximum tumour uptake in LS174T xenografts obtained at 1 h post- injection was only 2.7 %ID/g, along with 2.0 %ID/g in the blood and higher uptake in the other major organs. Low, but favorable tumour/tissue ratios required 4-6 h to develop. ^{124}I has been used with directly radiolabelled antibody constructs for a large part because radioiodine will not be retained in normal tissues, and thus more reasonable tumour/tissue ratios can be achieved than with a radiometal (*27*). However, the added expense and relatively poor imaging properties of this radionuclide are considerable barriers to the development of products based on ^{124}I. As our studies show, the short physical half-life of ^{18}F and ^{68}Ga can be used effectively in pretargeting to enhance detection sensitivity.

The half-life of ^{68}Ga is well matched to the kinetics of the IMP288 peptide in the pretargeting system. ^{68}Ga can be eluted twice daily from a ^{68}Ge/^{68}Ga generator, avoiding the need for an on-site cyclotron. However, the high energy of the positrons emitted by ^{68}Ga (1.9 MeV) limits the spatial resolution of the acquired images to 3 mm, while the intrinsic resolution of the microPET system is as low as 1.5 mm (*22*). In the clinical setting, the penetration range of ^{68}Ga positrons does not reduce the resolution of the images. For these studies, the procedure to label IMP288 with ^{68}Ga was optimized, resulting in a one-step labelling technique. We found that purification on a C18/HLB cartridge was required to remove the ^{68}Ga colloid that is inevitably formed when the peptide was labelled at specific activities exceeding 150 GBq/nmol at 95 °C. ^{68}Ga colloid accumulates in tissues of the reticuloendothelial system (liver, spleen, and bone marrow), deteriorating image quality, but it could be effectively reduced by rapid purification on a C18-cartridge. Radiolabelling and purification for administration could be accomplished within 45 minutes.

^{18}F, the most widely used radionuclide in PET, has an even more favorable half-life for pretargeted PET imaging (t½ = 110 min). Therefore, in this study, the NOTA-conjugated peptide, IMP499, was labelled with ^{18}F, as recently described by McBride et al. (*13*). We showed that this method produces a preparation that is stable *in vivo*. Similar to labelling with ^{68}Ga, it is a one-step procedure, which currently requires HPLC purification to remove the unlabelled peptide to enhance specific activity. Labelling yield was as high as 50%. Interestingly, the biodistribution of ^{18}F-IMP499 was similar to that of ^{68}Ga-labelled IMP288, suggesting that the new labelling method using NOTA to chelate Al[^{18}F]$^{2+}$ turns the ^{18}F-label into a residualizing radionuclide. Presumably, the peptide undergoes proteolytic degradation in the lysosomes and its radiolabelled catabolite, containing Al[^{18}F]$^{2+}$-NOTA, is trapped in the lysosomes, as has been described for radiometals.

In contrast to FDG-PET, pretargeted radioimmunodetection is a tumour-specific imaging modality. Although a high sensitivity and specificity for FDG-PET in detecting recurrent colorectal cancer lesions has been reported in patients (*28*), FDG-PET

images could lead to diagnostic dilemmas in discriminating malignant from benign, highly metabolic lesions, such as inflammation. Earlier studies in animal models have highlighted the improvements that an antibody-based pretargeting procedure can provide in comparison to ^{18}F-FDG, focusing primarily on its enhanced sensitivity (*12*) . In this study, we addressed the specificity of pretargeting in relation to its ability to discriminate inflammatory lesions from cancer. As expected, ^{18}F-FDG had high uptake in the tumour, but this was only 2-fold higher than the uptake in the inflammatory lesion. In contrast, tumour uptake was at least 10-fold higher in the tumour as compared to the inflammatory lesion with the antibody-based pretargeting method. Additionally, we showed that pretargeting specifically localizes in the intended target, with a 30-times higher concentration in the antigen-positive tumour than in a negative tumour. Thus, with evidence for appreciable improvements in both sensitivity and specificity, bsMAb-based pretargeting procedures could provide important new tools for detecting cancer.

This pretargeting method is a 2-step process that first requires the administration of the unlabelled bsMAb. Rather than using a clearing agent, the bsMAb are designed in a manner to minimize their residence time in the blood. Despite its size equaling that of an IgG (i.e., 157 kD), TF2 is cleared very quickly. The long circulatory half-life of IgG is only partly determined by its large size, and is mainly due to the presence of the C_H2 domain, which enables recycling via FcRn-receptors (*29*). It has been shown that C_H2 domain-deleted variants of IgG (121 kDa) clear much faster from the blood than intact IgG (*30, 31*). TF2 is an engineered trivalent antibody derived from three Fab-fragments and lacks any C_H2 domain.

These studies also provide new insights into this pretargeting method. Earlier studies examined the effects of increasing the bsMAb with a fixed amount of the peptide in mice with GW-39 human colonic tumours. It was reported that beyond a 10:1 molar ratio of bsMAb:peptide, the amount of peptide that could be delivered to the tumour did not increase (*32*). Using a low peptide dose level (0.01 nmol), we found tumour uptake in the LS174T model increased as the moles of bsMAb were increased from 0.1 to 1 nmole, reaching a maximum uptake of ~25 %ID/g with 1 nmole of TF2 (i.e., a 100:1 mole ratio) with minimal changes in blood and normal tissue uptake.

Compared to earlier studies, a number of factors contributed to the need for injecting considerably more hapten-peptide in these studies, including the size and age of the ^{68}Ga-generator, yields after purification, and the natural decay of the product that required a minimum of 5 MBq to be administered for imaging. Thus, a separate biodistribution study was performed to examine a similar dose-response with 10-fold more IMP288 (0.1 nmole). Despite administering increasing amounts of TF2 at the same mole ratios used with 0.01 nmole of IMP288, tumour uptake remained highly favorable, but remained at a constant level of ~15 %ID/g over a TF2 dose range of 1 to 10 nmoles. TF2 tumour uptake showed a constant level of ~3 %ID/g over a dose range from 0.1 to 1.0 nmol, but at the 2.5 nmol dose the percent uptake began to

decline, reducing to ~1 %ID/g at 10 nmole. As a result, at the high IMP288 dose (0.1 nmol), increasing the TF2 dose did not result in higher tumour uptake of radiolabelled IMP288. These data suggest that at TF2 doses exceeding 2.5 nmol, saturation of CEA in the tumour (with TF2) occurs. Thus, in pretargeting, exceptionally favorable targeting at lower specific activities can be achieved, but a higher fractional uptake results at its highest specific activity.

Conclusions

Pretargeted immuno-PET with an anti-CEA bsMAb and a ^{68}Ga- or ^{18}F-hapten-peptide is a rapid, highly specific and sensitive imaging modality for the detection CEA-positive tumours.

References

1. Jain RK. Physiological barriers to delivery of monoclonal antibodies and other macromolecules in tumors. *Cancer Res.* Feb 1 1990;50(3 Suppl):814s-819s.
2. Sharkey RM, Karacay H, Cardillo TM, et al. Improving the delivery of radionuclides for imaging and therapy of cancer using pretargeting methods. *Clin Cancer Res.* Oct 1 2005;11(19 Pt 2):7109s-7121s.
3. Boerman OC, van Schaijk FG, Oyen WJ, Corstens FH. Pretargeted radioimmunotherapy of cancer: progress step by step. *J Nucl Med.* Mar 2003;44(3):400-411.
4. Chang CH, Sharkey RM, Rossi EA, et al. Molecular advances in pretargeting radioimunotherapy with bispecific antibodies. *Mol Cancer Ther.* May 2002;1(7):553-563.
5. Reardan DT, Meares CF, Goodwin DA, et al. Antibodies against metal chelates. *Nature.* Jul 18-24 1985;316(6025):265-268.
6. Sharkey RM, Cardillo TM, Rossi EA, et al. Signal amplification in molecular imaging by pretargeting a multivalent, bispecific antibody. *Nat Med.* Nov 2005;11(11):1250-1255.
7. Le Doussal JM, Martin M, Gautherot E, Delaage M, Barbet J. In vitro and in vivo targeting of radiolabeled monovalent and divalent haptens with dual specificity monoclonal antibody conjugates: enhanced divalent hapten affinity for cell-bound antibody conjugate. *J Nucl Med.* Aug 1989;30(8):1358-1366.
8. Karacay H, McBride WJ, Griffiths GL, et al. Experimental pretargeting studies of cancer with a humanized anti-CEA x murine anti-[In-DTPA] bispecific antibody construct and a (99m)Tc-/(188)Re-labeled peptide. *Bioconjug Chem.* Nov-Dec 2000;11(6):842-854.
9. Griffiths GL, Chang CH, McBride WJ, et al. Reagents and methods for PET using bispecific antibody pretargeting and 68Ga-radiolabeled bivalent hapten-peptide-chelate conjugates. *J Nucl Med.* Jan 2004;45(1):30-39.
10. McBride WJ, Zanzonico P, Sharkey RM, et al. Bispecific antibody pretargeting PET (immunoPET) with an 124I-labeled hapten-peptide. *J Nucl Med.* Oct 2006;47(10):1678-1688.
11. Sharkey RM, McBride WJ, Karacay H, et al. A universal pretargeting system for cancer detection and therapy using bispecific antibody. *Cancer Res.* Jan 15 2003;63(2):354-363.
12. Sharkey RM, Karacay H, Vallabhajosula S, et al. Metastatic human colonic carcinoma: molecular imaging with pretargeted SPECT and PET in a mouse model. *Radiology.* Feb 2008;246(2):497-507.
13. McBride WJ, Sharkey RM, Karacay H, et al. A novel method of 18F radiolabeling for PET. *J Nucl Med.* Jun 2009;50(6):991-998.
14. Morel A, Darmon M, Delaage M. Recognition of imidazole and histamine derivatives by monoclonal antibodies. *Mol Immunol.* Oct 1990;27(10):995-1000.

15. Sharkey RM, Goldenberg DM, Goldenberg H, et al. Murine monoclonal antibodies against carcinoembryonic antigen: immunological, pharmacokinetic, and targeting properties in humans. *Cancer Res.* May 1 1990;50(9):2823-2831.
16. Goldenberg DM, Rossi EA, Sharkey RM, McBride WJ, Chang CH. Multifunctional antibodies by the Dock-and-Lock method for improved cancer imaging and therapy by pretargeting. *J Nucl Med.* Jan 2008;49(1):158-163.
17. Rossi EA, Goldenberg DM, Cardillo TM, McBride WJ, Sharkey RM, Chang CH. Stably tethered multifunctional structures of defined composition made by the dock and lock method for use in cancer targeting. *Proc Natl Acad Sci U S A.* May 2 2006;103(18):6841-6846.
18. Lindmo T, Boven E, Cuttitta F, Fedorko J, Bunn PA, Jr. Determination of the immunoreactive fraction of radiolabeled monoclonal antibodies by linear extrapolation to binding at infinite antigen excess. *J Immunol Methods.* Aug 3 1984;72(1):77-89.
19. Fraker PJ, Speck JC, Jr. Protein and cell membrane iodinations with a sparingly soluble chloroamide, 1,3,4,6-tetrachloro-3a,6a-diphrenylglycoluril. *Biochem Biophys Res Commun.* Feb 28 1978;80(4):849-857.
20. Ebert T, Bander NH, Finstad CL, Ramsawak RD, Old LJ. Establishment and characterization of human renal cancer and normal kidney cell lines. *Cancer Res.* Sep 1 1990;50(17):5531-5536.
21. van der Laken CJ, Boerman OC, Oyen WJ, et al. In vivo expression of interleukin-1 receptors during various experimentally induced inflammatory conditions. *J Infect Dis.* May 1998;177(5):1398-1401.
22. Visser EP, Disselhorst JA, Brom M, et al. Spatial resolution and sensitivity of the Inveon small-animal PET scanner. *J Nucl Med.* Jan 2009;50(1):139-147.
23. Van de Wiele C, Revets H, Mertens N. Radioimmunoimaging. Advances and prospects. *Q J Nucl Med Mol Imaging.* Dec 2004;48(4):317-325.
24. Goldenberg DM. Perspectives on oncologic imaging with radiolabeled antibodies. *Cancer.* Dec 15 1997;80(12 Suppl):2431-2435.
25. Wu AM, Olafsen T. Antibodies for molecular imaging of cancer. *Cancer J.* May-Jun 2008;14(3):191-197.
26. Cai W, Olafsen T, Zhang X, et al. PET imaging of colorectal cancer in xenograft-bearing mice by use of an 18F-labeled T84.66 anti-carcinoembryonic antigen diabody. *J Nucl Med.* Feb 2007;48(2):304-310.
27. Sharkey RM, Motta-Hennessy C, Pawlyk D, Siegel JA, Goldenberg DM. Biodistribution and radiation dose estimates for yttrium- and iodine-labeled monoclonal antibody IgG and fragments in nude mice bearing human colonic tumor xenografts. *Cancer Res.* Apr 15 1990;50(8):2330-2336.
28. Huebner RH, Park KC, Shepherd JE, et al. A meta-analysis of the literature for whole-body FDG PET detection of recurrent colorectal cancer. *J Nucl Med.* Jul 2000;41(7):1177-1189.
29. Ghetie V, Ward ES. FcRn: the MHC class I-related receptor that is more than an IgG transporter. *Immunol Today.* Dec 1997;18(12):592-598.
30. Chinn PC, Morena RA, Santoro DA, et al. Pharmacokinetics and tumor localization of (111)in-labeled HuCC49DeltaC(H)2 in BALB/c mice and athymic murine colon carcinoma xenograft. *Cancer Biother Radiopharm.* Apr 2006;21(2):106-116.
31. Slavin-Chiorini DC, Kashmiri SV, Lee HS, et al. A CDR-grafted (humanized) domain-deleted antitumor antibody. *Cancer Biother Radiopharm.* Oct 1997;12(5):305-316.
32. Sharkey RM, Karacay H, Richel H, et al. Optimizing bispecific antibody pretargeting for use in radioimmunotherapy. *Clin Cancer Res.* Sep 1 2003;9(10 Pt 2):3897S-3913S.

3

Pretargeted immuno-PET imaging of CEA-expressing intraperitoneal human colonic tumour xenografts: a new sensitive detection method

Rafke Schoffelen[1], Winette T.A. van der Graaf[2], Robert M. Sharkey[3], Gerben M. Franssen[1], William J. McBride[4], Chien-Hsing Chang[5], Peter Laverman[1], David M. Goldenberg[3], Wim J.G. Oyen[1] and Otto C. Boerman[1]

EJNMMI research. 2012;2:5

[1] Radboud University Nijmegen Medical Centre, dept. of Nuclear Medicine, Nijmegen, Netherlands
[2] Radboud University Nijmegen Medical Centre, dept. of Medical Oncology, Nijmegen, Netherlands
[3] Garden State Cancer Center, Morris Plains, New Jersey, USA
[4] Immunomedics, Inc., Morris Plains, New Jersey, USA
[5] IBC Pharmaceuticals, Morris Plains, New Jersey, USA

Abstract

Background

In this study, pretargeted immuno-PET with a bispecific monoclonal anti-carcinoembryonic antigen (CEA; CEACAM5) x anti-hapten antibody (bsMAb) and a small (1.5 kD) peptide labelled with ^{68}Ga was compared to ^{18}F-FDG-PET for detecting intraperitoneal (i.p.) CEA-expressing human colonic tumour xenografts in nude mice.

Methods

Two groups of female BALB/c nude mice were inoculated with LS174T human colonic tumour cells i.p. One group received 5 MBq ^{18}F-FDG, and the other received i.v. injections of the bsMAb, followed 16 h later with 5 MBq of ^{68}Ga-labelled peptide. One hour after the radiolabelled peptide or FDG was given, micro-PET/CT images were acquired. Thereafter, the uptake of the ^{68}Ga or ^{18}F in dissected tissue was determined.

Results

Within one hour, high uptake of ^{68}Ga-labelled peptide in the tumour lesions (23.4 ± 7.2% ID/g) and low background activity levels were observed (e.g., tumour-to-intestines ratio 58 ± 22). This resulted in clear visualization of all intra-abdominal tumour lesions ≥ 10 μL, and even some tumours as small as 5 μL (2mm diameter). ^{18}F-FDG efficiently localized in the tumours (8.7 ± 3.1 % ID/g), but also showed physiological uptake in various normal tissues (e.g., tumour-to-intestines ratio, 3.9 ± 1.1).

Conclusions

Pretargeted immuno-PET with bsMAb and a ^{68}Ga-labelled peptide could be a very sensitive imaging method for imaging colonic cancer, disclosing occult lesions.

Introduction

Colorectal cancer is a frequently diagnosed cancer type. It is the third most common cancer in both men and women in the Western world (*1, 2*). The overall five-year survival is 40–60% (*3, 4*). The prognosis is mainly determined by the presence of local or distant metastases, especially in the liver and peritoneum, which occur in half the patients. Only patients with a limited number of liver or lung metastases have a chance for cure by extensive surgery, in general combined with chemotherapy. However, up to half of the patients selected for metastasectomy have inoperable disease at laparotomy (*5*). Therefore, preoperative staging for detecting extrahepatic disease is crucial to avoid futile major surgery (*6*). Specific detection of malignant colorectal tumour lesions could be achieved by (pretargeted) antibody-guided radionuclide imaging. The combination of the specificity of antibody targeting and the sensitivity of PET is very promising. Radiolabelled antibodies have been tested for the detection of several cancer types. However, imaging with radiolabelled whole antibodies requires a relatively long interval between injection and imaging acquisition for adequate contrast to develop, due to the slow accretion of intact antibodies in tumours and their slow clearance (*7*). Pretargeting techniques were developed to improve radioimmunotargeting of tumours (*8*). A two-step pretargeting method using bispecific monoclonal antibodies (bsMAb) has been developed. First an unlabelled bsMAb with affinity for both the tumour and a small radiolabelled molecule is injected. When the bsMAb has cleared from the blood and has accumulated in the tumour, a radiolabelled, hapten-conjugated peptide is administered that clears rapidly from the blood and the body, but is trapped in the tumour by the anti-hapten binding arm of the bsMAb (*9-11*). Such a pretargeting method allows imaging within one hour after injection of the radiolabelled peptide, with high contrast, in animal models. Coupling two haptens together improves peptide uptake and stability by a process known as affinity enhancement (*12*). Chelate-metal complexes, such as DTPA-In, have been used as haptens (*13*).
FDG-PET/CT has an established role in the work-up of patients with metastasized colorectal cancer, and could change patient management in >25% of patients (*14-16*). Other clinical indications for PET-scanning in patients with colorectal cancer are the detection of disease recurrence and characterization of undefined lesions on conventional imaging (*17-20*). However, since FDG is a nonspecific tracer, it also has uptake in other tissues (e.g., physiological uptake in the bowel, uptake in (post-surgical) inflammatory or infectious lesions). FDG-PET frequently causes diagnostic dilemmas in assessing peritoneal disease (*21-24*).
In the present study, we examined the sensitivity of pretargeting with a bispecific monoclonal anti-carcinoembryonic antigen (CEA) x anti-histamine-succinyl-glycine (HSG) antibody, TF2, and a ^{68}Ga-labelled peptide, IMP288. Pretargeted immuno-PET was compared to ^{18}F-FDG-PET in a preclinical orthotopic model in mice with small, intraperitoneally growing, CEA-expressing colonic tumour lesions.

Methods

Pretargeting reagents TF2 and IMP288

The bsMAb, TF2, and the peptide IMP288, were provided by Immunomedics (Morris Plains, NJ, USA). The preparation of TF2 and binding properties have previously been described (*25-29*). Gel fitration chromatography showed that TF2 bound >90% of ^{68}Ga-IMP288 peptide. IMP288 was synthesized and purified as described by McBride et al. (*30*). IMP288 is a DOTA-conjugated D-Tyr-D-Lys-D-Glu-D-Lys tetrapeptide in which both lysine residues are substituted with a HSG-moiety via their ε-aminogroup: 7,10-tetra-azacyclododecane-N,N',N'',N'''-tetraacetic acid (DOTA)-D-Tyr-D-Lys(HSG)-D-Glu-D-Lys(HSG)-NH_2.
TF2 was labelled with ^{125}I (Perkin Elmer, Waltham, MA) by the iodogen method as described previously (*31*), to a specific activity of 58 MBq/nmol. ^{125}I-labelled TF2 was purified by eluting the reaction mixture with PBS, 0.5 % w/v bovine serum albumin (BSA) (Sigma Chemicals, St. Louis, MO, USA) on a PD-10 column (GE Healthcare Bio-Sciences AB, Uppsala, Sweden). IMP288 was labelled with ^{68}Ga as described previously (*32*). Radiolabelling and purification for administration could be accomplished within 45 minutes. The final product was adjusted to have a specific activity of 20 MBq/nmol at the moment of injection.
^{18}F-FDG was obtained from B.V. Cyclotron VU, Amsterdam, The Netherlands.

Quality control of the radiolabelled preparations

Radiochemical purity of the radiolabelled TF2 and IMP288 preparations was determined as described previously (*32*). In all experiments, the radiochemical purity of ^{125}I-TF2, and ^{68}Ga-IMP288 preparations exceeded 95%.

Animal experiments

All studies were approved by the Institutional Animal Welfare Committee of the Radboud University Nijmegen Medical Centre, and conducted in accordance with their guidelines (revised Dutch Act on Animal Experimentation, 1997). Animals were accustomed to laboratory conditions for one week before use and housed in individually ventilated cages isolators under standard laboratory conditions (temperature 20-24 °C, relative humidity 50-60 %, 12-h light-dark cycle), with free access to animal chow and water.
Female nude BALB/c mice (6-8 weeks old), weighing 20 to 25 g, received an intraperitoneal injection of 0.5 mL of a suspension of 1 x 10^6 LS174T cells, a CEA-expressing human colon carcinoma cell line (CCL-188; passage 7; American Type Culture Collection).

PET imaging

Three weeks after tumour cell inoculation, one group of five mice was injected intravenously with 5.0 nmol TF2 (0.2 mL), labelled with a trace amount of ^{125}I (0.4 MBq). Sixteen hours later, ^{68}Ga-IMP288 (5 MBq/025 nmol) was administered intravenously in 0.2 mL as described previously (*32*). The other group of five mice received 5 MBq ^{18}F-FDG intravenously (i.v.). Mice were fasted for 10 hours before the ^{18}F-FDG-injection and anesthetized and kept warm at 37°C. Mice were euthanized one hour after the injection of ^{68}Ga-IMP288 or ^{18}F-FDG by CO_2/O_2 asphyxiation, followed by cardiac puncture to obtain blood.

PET/CT scans of the mice were acquired one hour after the injection of ^{68}Ga-IMP288 or ^{18}F-FDG with an Inveon animal PET/CT scanner (Siemens Preclinical Solutions) having an intrinsic spatial resolution of 1.5 mm (*33*). The animals were placed in a supine position. PET emission scans were acquired for 15 minutes, preceded by CT scans for anatomical reference (spatial resolution 113 μm; 80 kV; 500 μA; exposure time 300 ms). Scans were reconstructed using Inveon Acquisition Workplace software (version 1.5; Siemens Preclinical Solutions) using a three-dimensional ordered subset expectation maximization/maximum a posterior algorithm with the following parameters: matrix 256 x 256 x 159; pixel size 0.43 x 0.43 x 0.8 mm^3; and maximum a posteriori prior β 0.5.

After the scans, mice were dissected and the abdomen were systematically and meticulously examined for tumours. The location of each lesion was documented, weighed, measured, and then the activity in each lesion was determined in a gamma counter. The other organs of interest were weighed and counted in a gamma counter with standards prepared from the injected products, using appropriate energy windows for radionuclide of interest. The percentage of the injected dose per gram tissue (% ID/g) was calculated. The correlation between the weight and uptake of ^{125}I-TF2 as ^{68}Ga-IMP288 per lesion was calculated.

Immunohistochemistry

Immunohistochemical analysis of CEA was performed on 4 μM thick formalin-fixed, paraffin-embedded tissue sections. The sections were deparaffinized in xylol and rehydrated through a graded ethanol into water. Endogenous peroxidase, slides was blocked with 3% hydrogen peroxide in phosphate buffered saline (10 min at room temperature). Then sections were blocked with 20% normal goat serum (Vector Laboratories Inc., Burlingame, USA) in 1% bovine serum albumin (BSA)-PBS (30 min at RT). Subsequently, tumour sections were incubated with a 1:12000 dilution of polyclonal rabbit anti-CEA antibody (A0115, Dako, Glostrup, Denmark) overnight at 4°C, followed by incubation with a goat-anti-rabbit biotinylated secondary antibody (1/200 in 1% BSA-PBS) (Vector Laboratories Inc., Burlingame, USA) for 30 min RT. Finally, avidin–biotin–enzyme complex (Vector Laboratories) was applied

for 30 min at 37°C and 3,39-diaminobenzidine was used to develop the tumour sections. Human coloncarcinoma was used as a positive control, and substitution of the primary antibody with 1% BSA-PBS was used as the negative control.

Analysis of the PET images

PET/CT images were scored by a blinded, independent, experienced nuclear physician (W.O.), being asked to record the presence of intra-abdominal tumour lesions. When lesions were present, he was asked to draw a region of interest (ROI) around the tumour. Each lesion was given a number on a 1-3 scale that defined the reader's confidence in that the uptake was related to a tumour (definitely, probably or possibly tumour). The imaging findings were then compared with the tumour lesions found at dissection. The detection rates for tumours <10 μL and ≥10 μL were calculated, corresponding with a sphere diameter of < 2.7 or ≥ 2.7 mm respectively.

Statistical analysis

Statistical analysis was performed using the SPSS software (Chicago, IL) and GraphPad Prism version 5.00 for Windows (GraphPad Software, San Diego USA). Means and standard deviations were used to describe continuous data, unless stated otherwise. Correlations were determined using a Spearman's correlation test. The level of significance was set at $p<0.05$.

Results

Tumour growth

Three weeks after the intraperitoneal injection of the LS174T cells, mice did not show clinical signs of discomfort or change in body weight. At dissection, the abdomen contained multiple solid tumour lesions (median n=10 per mouse; range 4-17). Most frequent localizations were at the rectovesical pouch, mesentery, subhepatic, -splenic and -phrenic space. Some tumour nodules were adjoining in groups of two or three lesions. Three-dimensional caliper measurements indicated that the maximum diameter of the tumour lesions varied between 1 and 15 millimetres (median 5), and weights varied between 0.3 and 650 mg (median 16 mg).

Biodistribution

The biodistribution of ^{125}I-TF2 and ^{68}Ga-IMP288 in the mice is shown in *Figure 1A*. High uptake of the bsMAb (3.73 ± 1.2% ID/g) and peptide (23.4 ± 7.2% ID/g) in the tumour lesions was observed, with very low accretion in the normal organs. This

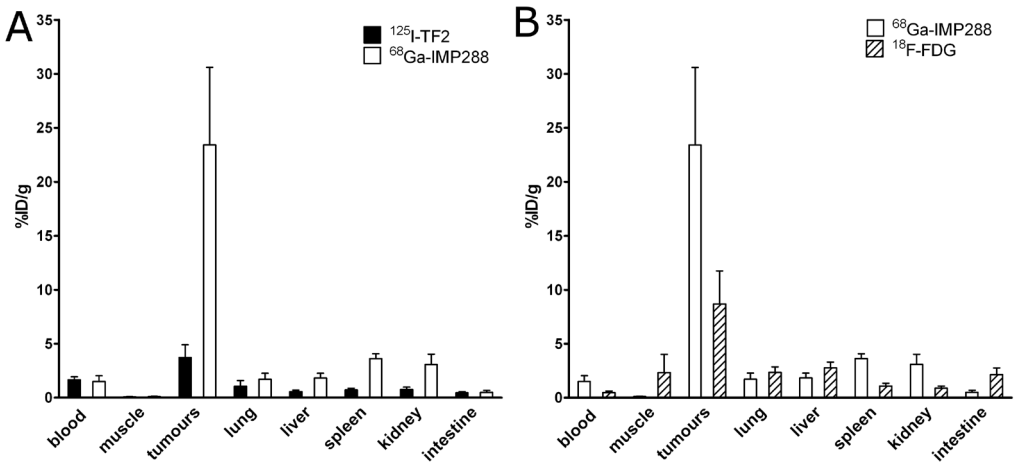

Figure 1A: Biodistribution of 6.0 nmol ^{125}I-TF2 (0.37 MBq) and 0.25 nmol ^{68}Ga-IMP288 (5 MBq), 1 h after i.v. injection of ^{68}Ga-IMP288 in BALB/c nude mice with intraperitoneal.CEA-expressing LS174T tumours. Values are given as means ± standard deviation (n=5).
Figure 1B: Biodistribution of 0.25 nmol ^{68}Ga-IMP288 (5 MBq), ^{18}F-FDG (5 MBq), 1 h after i.v. injection in BALB/c nude mice with intraperitoneal CEA-expressing LS174T tumours. Values are given as means ± standard deviation (n=5).

resulted in high tumour-to-normal-tissue ratios of ^{68}Ga-IMP288 (e.g., tumour-to-intestine ratio: 58 ± 22, tumour-to-liver ratio: 15 ±3). ^{18}F-FDG localized efficiently in the tumours (8.7 ± 3.1 % ID/g) (*Figure 1B*), but with physiological uptake in various normal tissues, with lower tumour-to-normal tissue ratios (e.g., tumour-to-intestines 3.9 ± 1.1, tumour-to-liver: 2.9 ± 0.5).
Tumour uptake both of ^{125}I-TF2 and ^{68}Ga-IMP288 correlated inversely with tumour size, as shown in *Figure 2A* and *2B* (Spearman's ρ=-0.66, $p<0.05$, and Spearman's ρ=-0.63, $p<0.05$, respectively).

PET/CT images

Immuno-PET with TF2 and ^{68}Ga-IMP288 resulted in clear delineation of the tumours. An example of a PET/CT image is shown in *Figure 3A*. It shows the cross sections through several tumours lesions. The photographs show their localization in the abdomen as well as their size. Apart from the activity in the bladder, very low uptake in normal tissues was seen. Due to the highly specific uptake in the tumour lesions and low background concentration, the immuno-PET/CT images could even be used to guide the localization of tumour lesions during dissection. Tumours that were more difficult to find macroscopically, because they were localized in the retroperitoneal cavities or posterior to the liver, were easily seen and localized on the images.
Interestingly, one lesion that was macroscopically doubtful to be a tumour, and show-

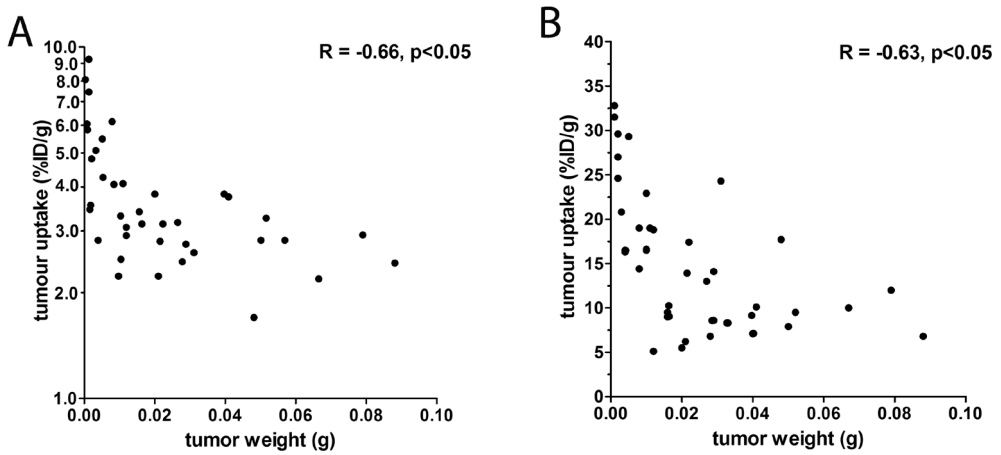

Figure 2: Correlation between tumour uptake of ^{125}I-TF2 (A) and ^{68}Ga-IMP288 (B) and tumour size (Spearman's rho = -0.66, p<0.05, and Spearman's rho = -0.63, p<0.05, respectively).

ing minimal uptake on immuno-PET, had an activity concentration as low as 0.49% ID/g. This uptake level was much lower than that of the other lesions in the same animal (range 16.3-29.6 % ID/g). This lesion with the low uptake was shown by immunohistochemistry to consist >90% of necrotic tissue and infiltrated leukocytes, lacking CEA-expression, and had only a small rim of vital tumour cells (*Figure 4*), which explains its low signal on immuno-PET.

In contrast, it was more difficult to discriminate the tumour lesions from other intra-abdominal structures on the FDG-PET images, because the uptake in the tumours was only slightly higher than in the intestines, as is shown in *Figure 3B*. FDG-PET images showed physiological uptake in the brain and the myocardium. To illustrate the low uptake of the pretargeting peptide in the background, the immuno-PET/CT and FDG-PET/CT images of mice without intraperitoneal tumours, which were imaged according the same scanning protocol, are shown in *Figure 3C* and *3D*. In pretargeted immuno-PET/CT images, only a low signal in the kidneys was observed, whereas no uptake was observed in the other normal organs. The FDG-PET/CT image of the animal without abdominal tumours clearly showed uptake in the bowel.

Sensitivity

There was a major difference in the number of detected lesions with immuno-PET/CT compared with FDG-PET/CT. Table 1 shows the number of tumours that were correctly aligned by the independent nuclear physician for each imaging method. For pretargeted immuno-PET all tumour lesions ≥10 μL were detected (100%, 23/23). Separate analysis for the smaller lesions, <10 μL, showed a detection rate of 20% (3/15). The score on the probability scale was 'definitely positive' for 88% of the delin-

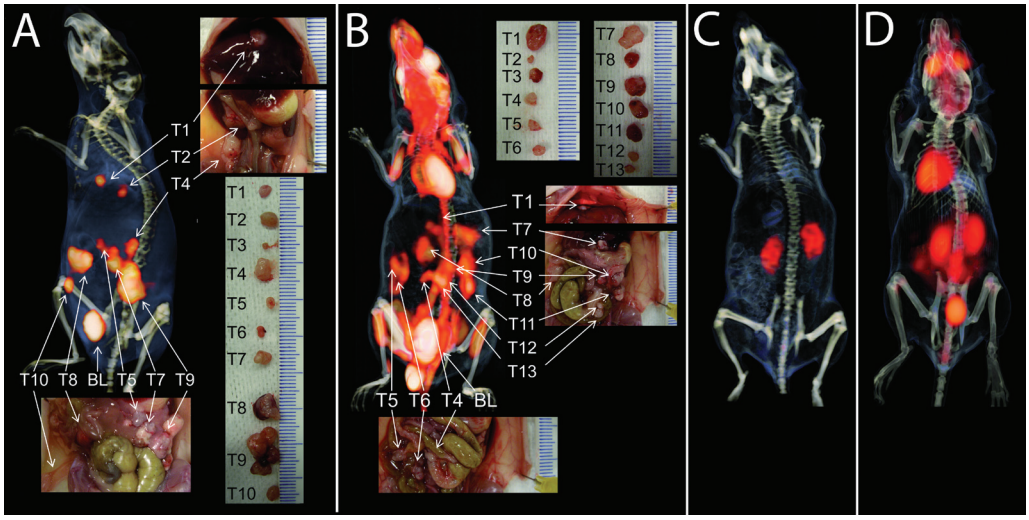

Figure 3: 3D-volume rendering of the pretargeted immuno-PET scan (A) and of the FDG-PET/CT scan (B) of BALB/c nude mice with intraperitoneal LS174T tumours, that received 6.0 nmol TF2 and 5 MBq ^{68}Ga-IMP288 (0.25 nmol) with a 16-hour interval (A) or ^{18}F-FDG (B). The animals were imaged one hour after ^{68}Ga-IMP288 or ^{18}F-FDG injection. Digital pictures were made during dissection to localize and measure individual tumours. On the pretargeted immuno-PET/CT images (A), all dissected tumours were very clearly distinguishable, except for the two very small tumours (1.2 and 4.7 µL respectively). In the FDG-PET/CT images (B) arrows are pointed at the localizations where tumours were found at dissection, but the signal was difficult to be discriminated from intestines. *Figure 3c* and 3d show the PET/CT images of mice without intraperioneal images after TF2 and ^{68}Ga-IMP288 injection (C) or ^{18}F-FDG injection (D).

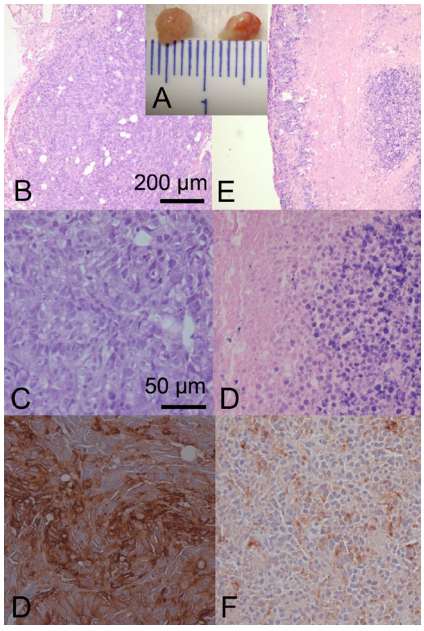

Figure 4: Two tumour lesions dissected from the abdomen of a BALB/c nude mouse that received ^{68}Ga-IMP288 after pretargeting with TF2. One lesion (A: left lesion) showed normal vital tumour cells on microscopic HE- and CEA-stained images (B: HE, 5x zoom; C: HE, 20x zoom, D: CEA, 20x zoom), and high specific tumour uptake of ^{68}Ga-IMP288 (17.7 % ID/g). On the contrary, another lesion in the same animal (A: right lesion) showed much lower tumour activity concentration (0.49% ID/g) in biodistribution and a much lower signal on the PET/CT images. This result was explained by the HE-sections and CEA-stained images showing >90% of non-vital tumour tissue (necrosis and infiltrated lymphocytes), lacking CEA-expression (E: HE, 5x zoom; F: HE, 20x zoom, G: CEA, 20x zoom).

eated lesions. In contrast, in the FDG-PET images, the detection rate of the tumours ≥10 μL was only 48% (13/27). A similar small proportion of the smaller lesions were found by FDG-PET/CT compared to immuno-PET/CT (25%, 3/12). Interestingly, the nuclear medicine physician was much less confident about aligning the ROIs in the FDG-PET/CT images. For none of the lesions he scored 'definitely positive', and only 'possibly positive' for 69% (11/16).

Table 1: Number of tumours that were correctly aligned by the independent nuclear physician for pretargeted immuno-PET/CT and FDG-PET/CT, and confidence rate defined by the reader.

		Pretargeted immuno-PET/CT	FDG-PET/CT
Tumours > 10 μL	Disssected	23	27
	Detected in images	23 (100%)	13 (48%)
Tumours < 10 μL	Disssected	15	12
	Detected in images	3 (20%)	3 (25%)
Probability assigned by nuclear physician	Definitely positive	23 (88%)	0
	Possibly positive	3 (12%)	11 (69%)
	Probably positive	0	5 (31%)

Discussion

This study showed that pretargeted immuno-PET is a very sensitive imaging modality to detect CEA-expressing tumour lesions in an orthotopic mouse model. The intraperitoneal tumours were clearly delineated with a high tumour-to-background contrast, providing high sensitivity: all tumour lesions ≥10 μL were detected with this method, at a very good confidence rate. The smallest lesions that were detected had a volume as low as 5-8 μL, which is in the same range of the spatial resolution of the dedicated animal PET scanner.

The animal model used in this study was well characterized by Koppe et al (*34*). The human colon carcinoma cell line LS174T has a reproducible growth pattern in BALB/c nude mice after intraperitoneal injection. Three weeks after tumour cell inoculation small tumour nodules were observed in the rectovesical pouch, mesentery, subhepatic, -splenic and -phrenic space. The preclinical model mimics peritoneal disease of patients with metastasized colorectal cancer (*35*).

In a previous imaging study, we demonstrated the feasibility of pretargeted immuno-PET using ^{68}Ga- or ^{18}F-labelled di-HSG-peptides in mice with subcutaneous tumours (*32*). In the current study, the activity concentration of the ^{68}Ga-labelled IMP288 in

the intraperitoneal tumours was similar to that in the subcutaneous tumours (*32, 36*). In our intraperitoneal tumour model the variation in tumour size was much wider than in the subcutaneous model. Our biodistribution results showed an inverse relationship between tumour weight and activity concentration. This correlation corresponds with the findings of other investigators (*37-40*). Sharkey et al. showed specific uptake of ^{124}I-labelled peptide after pretargeting with TF2 in microdisseminated human colon cancer colonies in the lungs of nude mice. In that model, high tumour-to-non-tumour ratios were obtained, illustrating the excellent tumour targeting potential of the pretargeting strategy (*41*).

FDG-PET/CT has shown high sensitivity and negative predictive value in diagnosing CRC (*42, 43*). Therefore, it was used in the present study as a reference method. The imaging quality of FDG-PET in this preclinical study was optimized by minimizing uptake of FDG in other organs by anaesthesia, fasting and warming of the animals (*44*). Its uptake in the myocardium, brain, intestines and liver is comparable to the clinical situation. The ratios between normal and tumour tissue might have been appeared to be less favourable than in patients, which might have compromised the detection of the tumours.

Based on our preclinical results we feel that pretargeted immuno-PET can be of additive value in the clinical setting. When staging patients with primary tumours in detection of eventual metastases, a highly sensitive and specific imaging method is required. Furthermore, in patients to be screened prior to curative liver metastatectomy, the disclosure of occult extrahepatic lesions will prevent useless operations. Moreso, immuno-PET can help to select patients who could undergo radioimmunotherapy. As the pretargeting system with the DOTA-conjugated peptides is very flexible, it can be labelled with a broad variety of radionuclides, like ^{90}Y and ^{177}Lu for pretargeted radioimmunotherapy, or with ^{111}In and ^{99m}Tc for SPECT imaging. Our preclinical results show similar biodistribution of the ^{111}In/^{177}Lu- or ^{68}Ga-peptide labelled (*36*). Images about targeting of known, non-biopsied lesions, can confirm antigen expression and accessibility of the therapeutic dose. Information on the biodistribution and pharmacokinetics can help to adjust treatment regimes by providing dosimetry data. This could be used to optimize dosing and to avoid toxicities.

For clinical application, ^{68}Ga has some major advantages. It is readily available in a nearly carrier-free state from an in-house ^{68}Ge/^{68}Ga generator. IMP288-DOTA can be stably and rapidly labelled with ^{68}Ga. Its half-life matches the pharmacokinetics of the peptide. In the present study, the positron range of ^{68}Ga (median range 3.5 mm) might have limited image resolution. Visser et al showed that with the intrinsic spatial resolution (approximately 1.5 mm) of our state of the art small-animal PET scanner, the finite positron range has become the limiting factor for the overall spatial resolution and activity recovery in small structures imaged with ^{68}Ga (*33*). Combined with the partial volume effect, this could explain the lower detection rate of the smallest tumour lesions with pretargeted immuno-PET, despite of the higher radioactivity

concentration of TF2 and ^{68}Ga-IMP288 in the smaller tumours.
Due the flexibility of the di-HSG-peptides, the use of other PET-radionuclides for this pretargeting system can be explored. ^{18}F, the most widely used positron emitting radioisotope, would be suitable due to its short positron range in tissue (0.62 mm), which might increase the image resolution. McBride and, subsequently, Laverman, McBride and colleagues developed an innovative and rapid method for labelling peptides with ^{18}F based on a metal chelator (*45, 46*). The biodistribution and PET-images in the subcutaneous LS174T tumours in nude mice showed the feasibility of this approach (*32*). Translation of this preclinical imaging method to the clinical situation will show the effect of the intrinsic resolution of the clinical PET-scanner in combination with the spatial resolution of the radionuclide.

Conclusions

In summary, this study indicates that pretargeted immuno-PET with TF2 and ^{68}Ga-IMP288 is a specific and sensitive method for detecting colon cancer in a preclinical model. Further clinical trials should focus on the diagnostic accuracy of pretargeted immuno-PET and determine its additional value in the clinical setting.

Acknowledgements

We thank Bianca Lemmers-van de Weem, Kitty Lemmens-Hermans, Jonathan Disselhorst, and Melissa Roeffen for technical assistance.
The work was supported by the Dutch Cancer Society (KWF Kankerbestrijding) grant no. KUN 2008-4038, and National Institutes of Health grant (National Institute of Biomedical Imaging and Bioengineering, R43 EB003751).

References

1. Jemal A, Siegel R, Ward E, Murray T, Xu J, Thun MJ. Cancer statistics, 2007. *CA Cancer J Clin.* Jan-Feb 2007;57(1):43-66.
2. National Cancer Institute: https//www.cancer.gov. Accessed July 4 2011.
3. Parkin DM. Global cancer statistics in the year 2000. *Lancet Oncol.* Sep 2001;2(9):533-543.
4. National Institute for Clinical Excellence: www.nice.org. Improving outcomes in colorectal cancers, manual update. Available at. Accessed July 4, 2011.
5. Hughes KS, Simon R, Songhorabodi S, et al. Resection of the liver for colorectal carcinoma metastases: a multi-institutional study of patterns of recurrence. *Surgery.* Aug 1986;100(2):278-284.
6. Ruers TJ, Wiering B, van der Sijp JR, et al. Improved selection of patients for hepatic surgery of colorectal liver metastases with (18)F-FDG PET: a randomized study. *J Nucl Med.* Jul 2009;50(7):1036-1041.
7. Jain RK. Physiological barriers to delivery of monoclonal antibodies and other macromolecules in tumors. *Cancer Res.* Feb 1 1990;50(3 Suppl):814s-819s.
8. Reardan DT, Meares CF, Goodwin DA, et al. Antibodies against metal chelates. *Nature.* Jul 18-24 1985;316(6025):265-268.

9. Boerman OC, van Schaijk FG, Oyen WJ, Corstens FH. Pretargeted radioimmunotherapy of cancer: progress step by step. *J Nucl Med.* Mar 2003;44(3):400-411.
10. Chang CH, Sharkey RM, Rossi EA, et al. Molecular advances in pretargeting radioimunotherapy with bispecific antibodies. *Mol Cancer Ther.* May 2002;1(7):553-563.
11. Sharkey RM, Cardillo TM, Rossi EA, et al. Signal amplification in molecular imaging by pretargeting a multivalent, bispecific antibody. *Nat Med.* Nov 2005;11(11):1250-1255.
12. Le Doussal JM, Martin M, Gautherot E, Delaage M, Barbet J. In vitro and in vivo targeting of radiolabeled monovalent and divalent haptens with dual specificity monoclonal antibody conjugates: enhanced divalent hapten affinity for cell-bound antibody conjugate. *J Nucl Med.* Aug 1989;30(8):1358-1366.
13. Karacay H, McBride WJ, Griffiths GL, et al. Experimental pretargeting studies of cancer with a humanized anti-CEA x murine anti-[In-DTPA] bispecific antibody construct and a (99m)Tc-/(188)Re-labeled peptide. *Bioconjug Chem.* Nov-Dec 2000;11(6):842-854.
14. Wiering B, Krabbe PF, Jager GJ, Oyen WJ, Ruers TJ. The impact of fluor-18-deoxyglucose-positron emission tomography in the management of colorectal liver metastases. *Cancer.* Dec 15 2005;104(12):2658-2670.
15. Park IJ, Kim HC, Yu CS, et al. Efficacy of PET/CT in the accurate evaluation of primary colorectal carcinoma. *Eur J Surg Oncol.* Nov 2006;32(9):941-947.
16. Llamas-Elvira JM, Rodriguez-Fernandez A, Gutierrez-Sainz J, et al. Fluorine-18 fluorodeoxyglucose PET in the preoperative staging of colorectal cancer. *Eur J Nucl Med Mol Imaging.* Jun 2007;34(6):859-867.
17. Tzimas GN, Koumanis DJ, Meterissian S. Positron emission tomography and colorectal carcinoma: an update. *J Am Coll Surg.* Apr 2004;198(4):645-652.
18. Topal B, Flamen P, Aerts R, et al. Clinical value of whole-body emission tomography in potentially curable colorectal liver metastases. *Eur J Surg Oncol.* Mar 2001;27(2):175-179.
19. Pelosi E, Deandreis D. The role of 18F-fluoro-deoxy-glucose positron emission tomography (FDG-PET) in the management of patients with colorectal cancer. *Eur J Surg Oncol.* Feb 2007;33(1):1-6.
20. Herbertson RA, Scarsbrook AF, Lee ST, Tebbutt N, Scott AM. Established, emerging and future roles of PET/CT in the management of colorectal cancer. *Clin Radiol.* Mar 2009;64(3):225-237.
21. Rosenbaum SJ, Lind T, Antoch G, Bockisch A. False-positive FDG PET uptake--the role of PET/CT. *Eur Radiol.* May 2006;16(5):1054-1065.
22. Metser U, Miller E, Lerman H, Even-Sapir E. Benign nonphysiologic lesions with increased 18F-FDG uptake on PET/CT: characterization and incidence. *AJR Am J Roentgenol.* Nov 2007;189(5):1203-1210.
23. Even-Sapir E, Parag Y, Lerman H, et al. Detection of recurrence in patients with rectal cancer: PET/CT after abdominoperineal or anterior resection. *Radiology.* Sep 2004;232(3):815-822.
24. Dirisamer A, Schima W, Heinisch M, et al. Detection of histologically proven peritoneal carcinomatosis with fused 18F-FDG-PET/MDCT. *Eur J Radiol.* Mar 2009;69(3):536-541.
25. Goldenberg DM, Rossi EA, Sharkey RM, McBride WJ, Chang CH. Multifunctional antibodies by the Dock-and-Lock method for improved cancer imaging and therapy by pretargeting. *J Nucl Med.* Jan 2008;49(1):158-163.
26. Lindmo T, Boven E, Cuttitta F, Fedorko J, Bunn PA, Jr. Determination of the immunoreactive fraction of radiolabeled monoclonal antibodies by linear extrapolation to binding at infinite antigen excess. *J Immunol Methods.* Aug 3 1984;72(1):77-89.
27. Morel A, Darmon M, Delaage M. Recognition of imidazole and histamine derivatives by monoclonal antibodies. *Mol Immunol.* Oct 1990;27(10):995-1000.
28. Rossi EA, Goldenberg DM, Cardillo TM, McBride WJ, Sharkey RM, Chang CH. Stably tethered multifunctional structures of defined composition made by the dock and lock method for use in cancer targeting. *Proc Natl Acad Sci U S A.* May 2 2006;103(18):6841-6846.
29. Sharkey RM, Goldenberg DM, Goldenberg H, et al. Murine monoclonal antibodies against carcinoembryonic antigen: immunological, pharmacokinetic, and targeting properties in humans. *Cancer Res.* May 1 1990;50(9):2823-2831.
30. McBride WJ, Zanzonico P, Sharkey RM, et al. Bispecific antibody pretargeting PET (immunoPET) with an 124I-labeled hapten-peptide. *J Nucl Med.* Oct 2006;47(10):1678-1688.
31. Fraker PJ, Speck JC, Jr. Protein and cell membrane iodinations with a sparingly soluble chloroamide, 1,3,4,6-tetrachloro-3a,6a-diphrenylglycoluril. *Biochem Biophys Res Commun.* Feb 28 1978;80(4):849-857.
32. Schoffelen R, Sharkey RM, Goldenberg DM, et al. Pretargeted immuno-positron emission tomography imaging of carcinoembryonic antigen-expressing tumors with a bispecific antibody and a 68Ga- and 18F-labeled

hapten peptide in mice with human tumor xenografts. *Mol Cancer Ther.* Apr 2010;9(4):1019-1027.
33. Visser EP, Disselhorst JA, Brom M, et al. Spatial resolution and sensitivity of the Inveon small-animal PET scanner. *J Nucl Med.* Jan 2009;50(1):139-147.
34. Koppe MJ, Hendriks T, Boerman OC, Oyen WJ, Bleichrodt RP. Radioimmunotherapy is an effective adjuvant treatment after cytoreductive surgery of experimental colonic peritoneal carcinomatosis. *J Nucl Med.* Nov 2006;47(11):1867-1874.
35. De Gaetano AM, Calcagni ML, Rufini V, Valenza V, Giordano A, Bonomo L. Imaging of peritoneal carcinomatosis with FDG PET-CT: diagnostic patterns, case examples and pitfalls. *Abdom Imaging.* May-Jun 2009;34(3):391-402.
36. Schoffelen R, van der Graaf WT, Franssen G, et al. Pretargeted 177Lu radioimmunotherapy of carcinoembryonic antigen-expressing human colonic tumors in mice. *J Nucl Med.* Nov 2010;51(11):1780-1787.
37. Sharkey RM, Primus FJ, Goldenberg DM. Antibody protein dose and radioimmunodetection of GW-39 human colon tumor xenografts. *Int J Cancer.* May 15 1987;39(5):611-617.
38. Moshakis V, McIlhinney RA, Raghavan D, Neville AM. Localization of human tumour xenografts after i.v. administration of radiolabeled monoclonal antibodies. *Br J Cancer.* Jul 1981;44(1):91-99.
39. Hagan PL, Halpern SE, Dillman RO, et al. Tumor size: effect on monoclonal antibody uptake in tumor models. *J Nucl Med.* Mar 1986;27(3):422-427.
40. Blumenthal RD, Sharkey RM, Kashi R, Natale AM, Goldenberg DM. Influence of animal host and tumor implantation site on radio-antibody uptake in the GW-39 human colonic cancer xenograft. *Int J Cancer.* Dec 15 1989;44(6):1041-1047.
41. Sharkey RM, Karacay H, Vallabhajosula S, et al. Metastatic human colonic carcinoma: molecular imaging with pretargeted SPECT and PET in a mouse model. *Radiology.* Feb 2008;246(2):497-507.
42. Chowdhury FU, Shah N, Scarsbrook AF, Bradley KM. [18F]FDG PET/CT imaging of colorectal cancer: a pictorial review. *Postgrad Med J.* Mar 2010;86(1013):174-182.
43. Esteves FP, Schuster DM, Halkar RK. Gastrointestinal tract malignancies and positron emission tomography: an overview. *Semin Nucl Med.* Apr 2006;36(2):169-181.
44. Fueger BJ, Czernin J, Hildebrandt I, et al. Impact of animal handling on the results of 18F-FDG PET studies in mice. *J Nucl Med.* Jun 2006;47(6):999-1006.
45. Laverman P, McBride WJ, Sharkey RM, et al. A novel facile method of labeling octreotide with (18) F-fluorine. *J Nucl Med.* Mar 2010;51(3):454-461.
46. McBride WJ, Sharkey RM, Karacay H, et al. A novel method of 18F radiolabeling for PET. *J Nucl Med.* Jun 2009;50(6):991-998.

4

Pretargeted ^{177}Lu radioimmunotherapy of CEA-expressing human colonic tumours in mice

Rafke Schoffelen[1], Winette T.A. van der Graaf[2], Gerben M. Franssen[1], Robert M. Sharkey[3], David M. Goldenberg[3], William J. McBride[4], Edmund A. Rossi[5], Annemarie Eek[1], Wim J.G. Oyen[1] and Otto C. Boerman[1]

Journal of nuclear medicine. 2010;51:1780-1787

[1] Radboud University Nijmegen Medical Centre, dept. of Nuclear Medicine, Nijmegen, Netherlands
[2] Radboud University Nijmegen Medical Centre, dept. of Medical Oncology, Nijmegen, Netherlands
[3] Garden State Cancer Center, Morris Plains, New Jersey, USA
[4] Immunomedics, Inc., Morris Plains, New Jersey, USA
[5] IBC Pharmaceuticals, Morris Plains, New Jersey, USA

Abstract

Background

Pretargeted radioimmunotherapy (PRIT) with bispecific antibodies in combination with a radiolabelled peptide reduces the radiation dose to normal tissues, especially the bone marrow. In this study, the optimization, therapeutic efficacy and toxicity of PRIT of colon cancer with a ^{177}Lu-labelled peptide was determined in mice with CEA-expressing human tumours.

Methods

To obtain the optimal therapeutic efficacy, several strategies were evaluated to increase the total amount of radioactivity targeted to subcutaneous (s.c.) LS174T colon cancer tumours in BALB/c nude mice. First, the maximum amount of bispecific anti-CEA x anti-hapten antibody, TF2, and the peptide, IMP288, that could be targeted was determined. Furthermore, the tumour targeting of repeated administrations of radiolabelled IMP288 was investigated. Mice received one TF2 injection followed by multiple IMP288 gifts (3 h interval), or multiple cycles with each IMP288 administration preceded by a new TF2 injection (72 h interval). PRIT was administered at maximum doses of TF2, and ^{177}Lu-labelled IMP288 in groups of nine mice with s.c. LS174T tumours. Mice received one, two or three successive cycles treatment (26 MBq/mouse/cycle) or carrier only. Primary endpoint was survival; secondary endpoints were tumour growth, body weight, bone marrow and renal toxicity.

Results

The highest amount of radioactivity delivered to a s.c. colon tumour was achieved by administering 5.0 nmol TF2 and 0.28 nmol IMP288 in three successive cycles with each IMP288 preceded with a new TF2 injection (72 h interval). PRIT effectively delayed tumour growth and prolonged survival significantly. Higher activity doses, administered in successive cycles, correlated with longer survival: the median survival of untreated mice was 13 days (range 6-20), whereas that of mice treated with one, two or three cycles of PRIT was 24 (range 24-31), 45 days (range 38->130), and 65 days (range 48->130), respectively. Toxicity was limited: no significant changes in mean body weight were measured. Minimal changes in leukocyte counts were measured two and three weeks p.i., with full recovery within seven weeks after treatment. Platelet counts were unaffected. Serum creatinine was not increased significantly, thus there was no indication of acute renal toxicity.

Conclusions

This study indicates that in mice PRIT is an effective treatment modality against colon cancer with limited toxicity.

Introduction

The survival of patients with colorectal cancer depends mainly on the development of distant metastases. In patients with metastasized disease, chemotherapy with capecitabine, oxaliplatin and irinotecan used in combination protocols prolongs median overall survival from 8.0 months to 11.7 months *(1)*. The addition of bevacizumab to those chemotherapy schedules increases median overall and progression free survival by 3.7-4.7 months *(2)*, resulting in an overall survival of more than 20 months in patients with metastatic disease *(3)*.

Novel systemic strategies are needed for patients who become refractory or intolerant to these treatments. Radioimmunotherapy (RIT), the selective targeting of tumour-associated antigens expressed on the tumour cells with radiolabelled antibodies, is an attractive candidate. This concept has been investigated extensively and has proven to be effective in patients with non-Hodgkin lymphoma *(4-7)*, leading to approval of two radiolabelled anti-CD20 monoclonal antibody preparations: ^{90}Y-ibritumomab tiuxetan (Zevalin®, Bayer Schering Pharma AG) and ^{131}I-tositumomab® (Bexxar, GlaxoSmithKline). While RIT has not been as successful in solid tumours, presumably because these tumours are less radiosensitive, an ^{131}I-labelled anti-CEACAM5 IgG given to colorectal cancer patients as an adjuvant therapy after resection of hepatic metastases improved survival compared to a contemporaneous group of patients *(8, 9)*. The activity dose in RIT is limited by myelotoxicity as a result of the continuous radiation exposure of the red marrow by the slow-clearing antibody. Pretargeting techniques were developed to circumvent this problem *(10)*. In pretargeting, an unlabelled bifunctional reagent, with affinity for the tumour and a small radiolabelled molecule, is administered to pre-localize in the tumour *(11-13)*. In this approach, a bispecific monoclonal antibody (bsMAb) is administered intravenously and given time to accumulate in the tumour and clear from the circulation. Then, a radiolabelled hapten-peptide is given that clears rapidly from the blood and body, but is trapped in the tumour by the anti-hapten binding arm of the bsMAb. This greatly reduces the radiation dose to normal tissues, especially the bone marrow. The retention of the radiolabelled hapten-peptide in the tumour is enhanced when two haptens are included in the hapten-peptide *(14)*.

In our pretargeting system, peptides are substituted with the hapten histamine-succinyl-glycine (HSG), creating a flexible pretargeting system, because these HSG-substituted peptides can be conjugated with various chelating moieties (DTPA, NOTA, DOTA, N_3S-chelates, etc.), so that the peptide can be radiolabelled stably with a variety of radionuclides, such as ^{111}In and ^{99m}Tc for SPECT imaging *(13)*, with ^{18}F and ^{68}Ga for PET imaging *(15-18)*, or with ^{131}I, ^{90}Y, and ^{177}Lu for pretargeted radioimmunotherapy (PRIT) *(19)*.

Until recently, the bsMAbs used in pretargeting were either produced by chemical conjugation of Fab-fragments or via the quadroma technology. A new method, the Dock-

and-Lock (DNL) technology as described previously *(20, 21)*. Using DNL constructs to target B-cell lymphoma and pancreatic cancer, significant therapeutic responses have been reported in animals with subcutaneous xenografts, using a ^{90}Y-labelled di-HSG-peptide *(22. 23)*. The DOTA-di-HSG-peptide can also be stably labelled with ^{177}Lu. Herein, we report the optimization, therapeutic efficacy and toxicity of an anti-CEA DNL bsMAb construct in combination with a ^{177}Lu-labelled di-HSG peptide in mice bearing carcinoembryonic antigen (CEA)-expressing tumours.

Methods

Pretargeting reagents TF2 and IMP288

The trivalent anti-CEACAM5 x anti-HSG bsMAb construct, TF2 (MW 157 kDa), and IMP288 peptide (molecular weight 1456 Da) were provided by IBC Pharmaceuticals, Inc., and Immunomedics, Inc. (Morris Plains, NJ, USA). The preparation and binding properties of TF2 have previously been described *(21, 24-26)*. Size-exclusion chromatography showed that TF2 could bind >90% of the added ^{111}In-IMP288 peptide. IMP288 was synthesized and purified as described by McBride et al. *(16)*.
In some studies ^{125}I-TF2 (0.4 MBq), was co-injected with unlabelled TF2 to confirm tumour accretion. IMP288 was labelled with either ^{111}In for biodistribution studies or with ^{177}Lu for radioimmunotherapy. Mice received TF2 and IMP288 intravenously in 0.2-0.3 mL phosphate-buffered saline (PBS), 0.5% bovine serum albumin (BSA).
TF2 was radioiodinated with a trace amount of ^{125}I (Perkin Elmer, Waltham, MA) by the iodogen method and ^{125}I-labelled TF2 was purified as described previously *(27)*.
IMP288 was labelled with ^{111}In (Covidien, Petten, The Netherlands) at a specific activity of 32 MBq/nmol and with ^{177}Lu (IDB Holland BV, Baarle Nassau, The Netherlands) at a specific activity of 86 MBq/nmol and radiolabelling was performed as described previously *(18)*.
Radiochemical purity of the radiolabelled TF2 and IMP288 preparations was determined using instant thin-layer chromatography (ITLC) on silica-gel strips (Pall Life Sciences, Ann Arbor, MI). The percentage of radiolabelled TF2 was determined using 0.1 M citrate buffer, pH 6.0, as the mobile phase. To determine the percentage of radiolabelled IMP288 0.1 M NH_4Ac : 0.1 M EDTA was used as the mobile phase. Furthermore, ^{111}In-IMP288 and ^{177}Lu-IMP288 were analyzed by RP-HPLC as described previously *(18)*. Radiochemical purity of ^{125}I-TF2, ^{111} In- and ^{177}Lu- IMP288 preparations always exceeded 95%.

Animal experiments

The experiments were performed in male nude BALB/c mice (6-8 weeks old), weighing 20-25 g. Mice were accustomed to laboratory conditions for at least one week before

experimental use and were housed under non-sterile standard conditions in filter-topped cages with free access to animal chow and water. All studies were approved by the institutional Animal Welfare Committee of the Radboud University Nijmegen Medical Center, and conducted in accordance with their guidelines (revised Dutch Act on Animal Experimentation, 1997).
Tumour xenografts were induced by subcutaneous inoculation of 0.2 mL of a suspension of 1 x 10^6 LS174T cells, a CEA-expressing human colon carcinoma cell line (American Type Culture Collection, Rockville, MD, USA). TF2 and IMP288 were injected intravenously in 0.2-0.3 mL, with an interval of 16 hours, as this period was shown to be sufficient to clear TF2 from the circulation, to allow for IMP288 tumour targeting without significant complexation in the circulation.

Biodistribution studies

In this study, the maximum amount of IMP288 that could be captured by LS174T tumours (0.02-0.2 g) was assessed. First, the optimal TF2 dose that could bind the maximal amount of IMP288 in the tumour was determined. Groups of 5 tumour-bearing nude mice were injected intravenously with 1.3, 2.5, 5.0 or 10.0 nmol TF2 (~0.2 to 1.57 mg), labelled with a trace amount of ^{125}I (0.4 MBq), and 16 hours later, 0.10 nmol IMP288 was given. One hour after injection of IMP288, all mice were euthanized by CO_2/O_2 asphyxiation. Blood was obtained by cardiac puncture, and tumour and organs of interest were dissected, weighed and counted in a gamma counter with standards prepared from the injected products, using appropriate energy windows for radionuclide used. The percentage-injected dose per gram tissue (% ID/g) was calculated.
Subsequently, the maximum amount of IMP288 that could be captured under these pretargeting conditions was assessed. Therefore, groups of five mice received 5.0 nmol of TF2 intravenously, and 16 hours later, 0.035, 0.070, 0.140, 0.280 or 0.410 nmol IMP288 (50, 100, 200, 400 or 600 ng, respectively) was given, labelled with a trace amount of ^{111}In (0.4 MBq). One hour later, all mice were euthanized for determination of tumour uptake and organ distribution.
In a third experiment, the accumulation and retention in the tumour of the maximum TF2 and IMP288 doses was investigated. Tumour-bearing nude mice received 5.0 nmol ^{125}I-TF2 (0.4 MBq) intravenously, and 16 h later, 0.28 nmol of ^{111}In-IMP288 (0.4 MBq). Groups of 5 mice were euthanized at 1, 6, 24 and 48 hours for determination of tumour uptake and organ distribution.
The radioactivity of ^{177}Lu that could be delivered was limited by the maximum peptide mass, as the maximum specific activity of ^{177}Lu-IMP288 was 90 MBq/nmol. A single dose of 25 MBq/0.28 nmol IMP288, which was the maximal IMP288 dose that was specifically targeted to the tumour, was well below the maximum tolerated radioactivity level. Therefore, our treatment strategy included the use of repeated treatment

cycles. Biodistribution studies were performed to assess two different approaches. The first strategy examined was to administer multiple injections of the radiolabelled peptide after a single injection of the bsMAb. The tumour uptake was measured in three groups of five mice that received one 5.0-nmol dose of TF2, and then 16 h later, one, two or three injections of 0.28 nmol IMP288 were given, with each IMP288 injection separated by 3 h. In the multiple-dosed groups, only the last dose of IMP288 was labelled with ^{111}In.
The second strategy investigated whether subsequent injections of IMP288 could be targeted more efficiently by preceding each IMP288 with a new TF2 injection. Three groups of five mice received one, two or three cycles of 5.0 nmol TF2 combined 16 h later with 0.28 nmol IMP288, with each cycle separated by 72 h. In the multiple-dosed groups, the last dose of TF2 was labelled with ^{125}I and the last dose of IMP288 was labelled with ^{111}In. One hour after the injection of ^{111}In-labelled peptide, mice were euthanized and dissection and analyses were performed as described above.

Pretargeted radioimmunotherapy studies

The therapeutic efficacy of PRIT with TF2 and ^{177}Lu-IMP288 was determined by random assignment of 9 mice with subcutaneous LS174T xenografts per group. Therapy studies were initiated 10 days after tumour inoculation, when the median tumour size was 40 mm^3 (range: 12-120 mm^3). They received one, two or three treatment cycles of TF2 (5.0 nmol) and ^{177}Lu-IMP288 (26 MBq/0.28 nmol per cycle), or PBS, 0.5% BSA, with each cycle separated by 3 days, because this regime resulted in the highest absolute amount of radiolabelled peptide in the tumours.
The primary endpoint was overall survival. The secondary endpoint was toxicity, with special attention to myelosuppression and acute renal toxicity. This was evaluated by monitoring general condition, body weight, blood cell counts and creatinine levels. Animals were observed daily by independent, experienced biotechnicians, measuring body weight and tumour size twice weekly. Standardized humane endpoints used to euthanize animals were: failure to eat/drink and losing ≥15% of body weight in 1 or 2 days, or losing ≥20% of their starting weight, or in the case of tumour progression, when tumour size exceeded 1.0 cm^3 or excessive ulceration. Tumour size was measured in three dimensions (length, width and height) with a caliper, and tumour volume was calculated, assuming tumours were ellipsoid shaped, using the formula: tumour volume (mm^3) = $4/3\pi$ x (length/2) x (width/2) x (height/2).

Blood samples of 0.1 mL were collected via submandibular bleeding, prior to therapy for baseline full blood counts and serum creatinine, and weekly starting two weeks after therapy. White blood cell counts and platelet counts were analyzed by the ADVIA 120 Hematology System (Siemens Medical Solutions Diagnostics, Deerfield, USA). Serum creatinine was analyzed by Aeroset (Abbott Diagnostics, USA). Timing

of the white blood cell and platelet count measurement were scheduled to determine the nadir, at two and three weeks after the first injection of ^{177}Lu-IMP288, and bone marrow recovery at seven weeks post-injection (p.i.).

Statistic analysis

All mean values are given ± standard deviations. Statistical analysis was performed using a non-parametric, two-tailed Mann Whitney test and Kruskal Wallis test using SPSS software (version 16.0). Survival curves were compared using the Log-rank test. The level of significance was set at $p<0.05$.

Results

Determination of the maximum peptide dose

The maximum amount of TF2 and IMP288 that could be targeted specifically to LS174T tumours was determined. As shown in *Figure 1A*, the percentage uptake of TF2 in the tumour decreased from 3.21 ± 0.61% ID/g at the 1.0 nmol dose to 1.16 ± 0.27% ID/g at 10.0 nmol. *Figure 1B* illustrates that the absolute amount of TF2 accreted specifically in the tumour (subtracting the blood concentration), illustrating that the total amount in the tumour did not increase at administered doses >5.0 nmol (i.e., antigen saturating dose). Therefore, the 5.0 nmol dose was selected for further PRIT experiments.

The maximum amount of IMP288 that could be captured in the tumour with this amount of TF2 was determined. At 1 h post-injection, ^{111}In-IMP288 accumulated effectively in the tumour at all peptide doses, with very low uptake in all normal tissues. The highest tumour uptake in terms of % ID/g was obtained at the 0.035 and 0.070 nmol IMP288 doses (18.8 ± 8.1 % ID/g and 23.3 ± 6.6% ID/g, respectively, P=0.33, Mann-Whitney exact test, two-tailed), with decreasing uptake at higher IMP288 doses (14.2 ± 6.6% ID/g, 9.6 ± 3.0% ID/g and 6.5± 2.2% ID/g at 0.140, 0.280 or 0.410 nmol, respectively) (*Figure 1C*). Most importantly, the absolute amount of peptide targeted to the tumours did not increase at injected peptide doses higher than 0.28 nmol IMP288 (*Figure 1D*). Therefore, this dose was selected for PRIT, as it would result in the highest amount of radioactivity in the tumour. For example, although 0.07 nmol of ^{177}Lu-IMP288 would allow 23% ID/g uptake, based on the specific activity of 90 MBq/nmol for ^{177}Lu-IMP288, only 6.3 MBq of ^{177}Lu-activity could be administered, delivering 1.45 MBq to the tumour, whereas with 0.28 nmol, even though the percent uptake is lower (~10% ID/g), 25.2 MBq could be administered, delivering 2.5 MBq to the tumour.

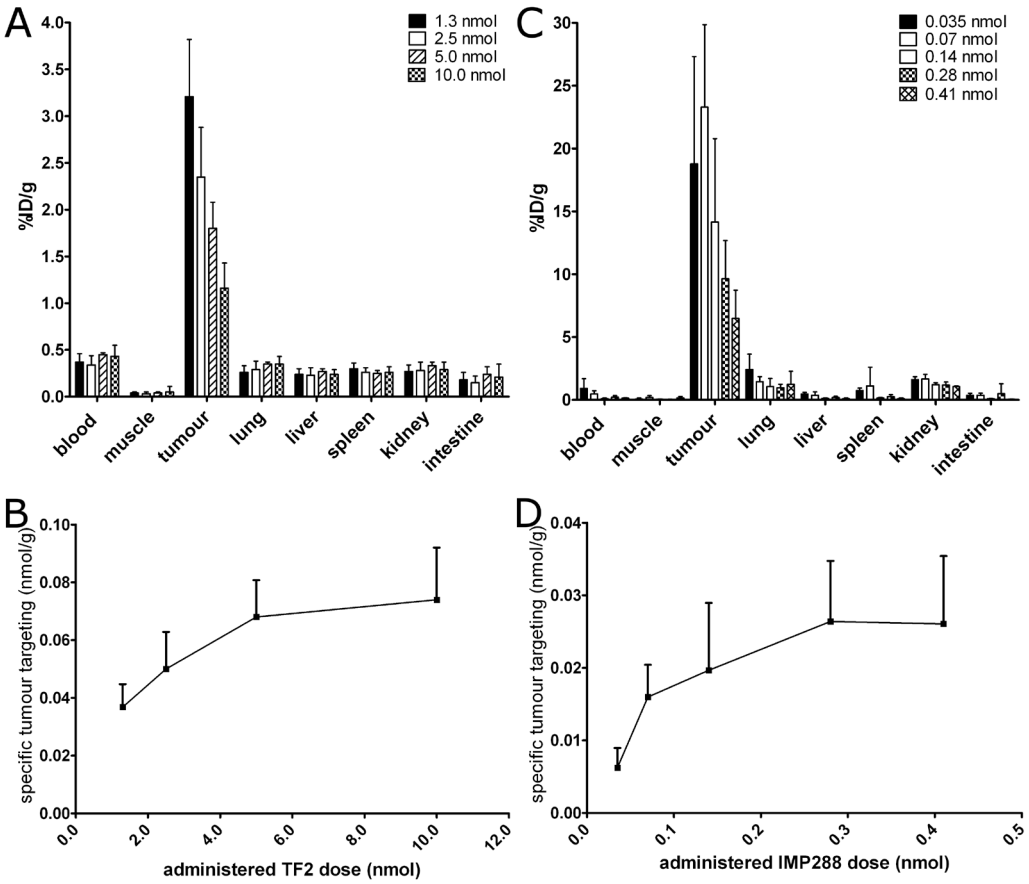

Figure 1: A and B show the biodistribution and specific tumor targeting of escalating bsMAb doses (1.0-10.0 nmol ^{125}I-TF2, 0.4MBq) in BALB/c nude mice with 0.02-0.2 g s.c. LS174T tumors. The bsMAb was followed by the injection of 0.10 nmol IMP288 16 h later, and one hour after that injection, the mice were euthanized. C and D show the biodistribution and specific tumor targeting of escalating peptide doses (0.035-0.41 nmol ^{111}In-IMP288, 0.4 MBq), injected 16 h after pretargeting with TF2 (5.0 nmol). Specific tumor targeting of ^{125}I-TF2 and ^{111}In-IMP288 was calculated as nmol per gram tumor, corrected for the blood concentration. Values represent means ± standard deviation (n=5).

Blood and tumour retention

Using 5.0 nmol TF2 and 0.28 nmol IMP288, tumour uptake and tissue distribution were examined over a 48-h period following an ^{111}In-IMP288 injection (*Figure 2*). TF2 cleared rapidly from blood and normal tissues, with <0.1% in the blood 17 hours after injection (1 h after ^{111}In-IMP288), but with tumour uptake averaging 1.3 ± 0.22% ID/g (*Figure 2A*). At this same time, ^{111}In-IMP288 tumour uptake was 11.3 ± 2.7% ID/g, with the kidneys having the highest uptake among normal tissues, aver-

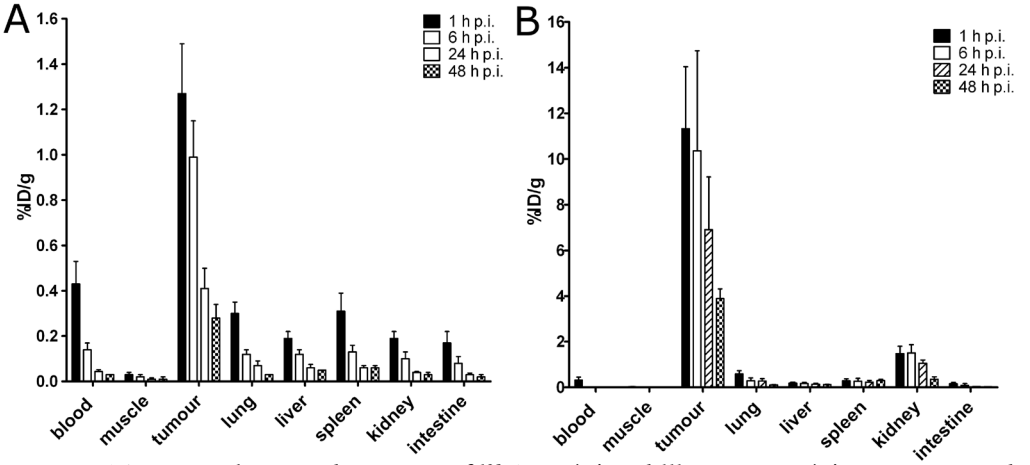

Figure 2. The accumulation and retention of ^{125}I-TF2 (A) and ^{111}In-IMP288 (B) in BALB/c nude mice with s.c. LS174T tumors. TF2 (5.0 nmol) and IMP288 (0.28 nmol) were injected, with animals necropsied at 1, 6, 24 and 48 hours post-^{111}In-IMP288 injection. Values represent means ± standard deviation (n=5).

aging 1.5 ± 0.3 % ID/g at this 1-h interval (*Figure 2B*). Tumour uptake of TF2 and IMP288 gradually decreased over time at a somewhat similar rate. Tumour-to-blood ratio exceeded 1,400:1 at all time points.

Successive cycles of therapy

The data from the previous study indicated that maximum radioactivity dose of ^{177}Lu-IMP288 that could be administered with 0.28 nmol of IMP288 was far below the expected MTD. Therefore, we evaluated the efficiency of successive doses of IMP288 (i.e., administering one dose of 5 nmol TF2, and 16 h later 3-hourly one, two or three 0.28 nmol ^{111}In-IMP288 injections, or one, two or three cycles of 5 nmol TF2, followed 16 h later by 0.28 nmol ^{111}In-IMP288 every 3 days).

The successive administrations of ^{111}In-IMP288 after one injection of TF2 resulted in significantly lower uptake of the second and third injection of peptide compared to the first injection (8.0 ± 1.1 % ID/g and 6.2 ± 1.0 % ID/g versus 14.3 ± 1.5 % ID/g, respectively; Mann-Whitney exact test, two-tailed: $p<0.05$) (*Figure 3A*). Administering an extra second and third dose of TF2 before each successive dose of IMP288, with a 3-day interval, resulted in similar tumour accretion of the second and third injections of bsMAb to that seen with the first injection (2.6 ± 0.4% ID/g, 2.0 ± 0.4% ID/g and 2.3 ± 0.1% ID/g at first, second and third dose respectively). Most importantly, in this regime the first and second doses of ^{111}In-IMP288 had similar uptake (14.7 ± 1.1 % ID/g and 14.3 ± 1.5 % ID/g, respectively, $p=0.91$, Mann-Whitney exact test, two-tailed), but by the third cycle, the ^{111}In-IMP288, uptake was slightly lower compared

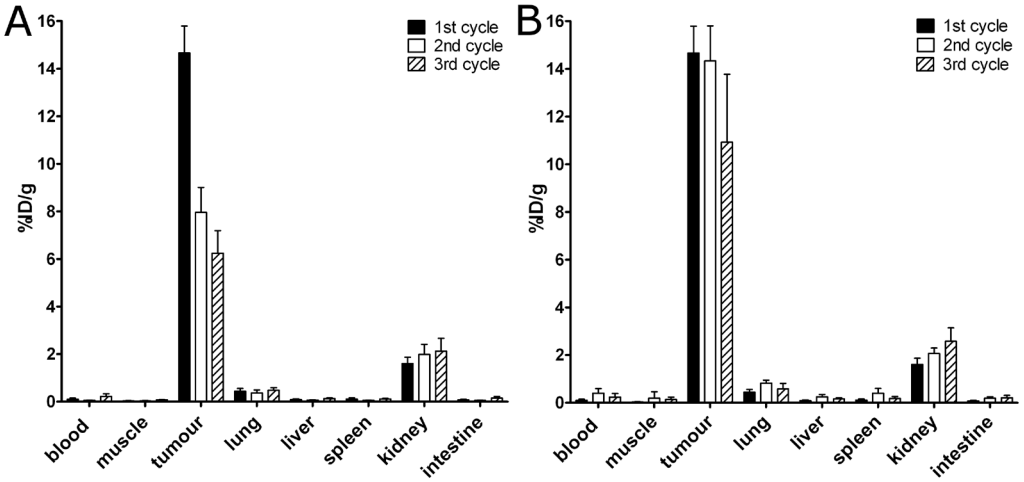

Figure 3. Biodistribution of successive administrations of ^{111}In-IMP288, 3-hourly (A) and of successive cycles of TF2 combined with ^{111}In-IMP288, 3-daily (B). A: Three groups of five mice received one injection of 5.0 nmol TF2 and 16 h later with one, two or three injections of 0.28 nmol IMP288, with each IMP288 injection separated by 3 h. B: Three groups of five mice received one, two or three cycles of 5.0 nmol TF2 and 0.28 nmol IMP288, with each cycle separated by 72 h. In each group, the last (or only) dose of IMP288 was labeled with ^{111}In. One hour after the IMP288-injection of labeled peptide, all mice were euthanized. Values represent means ± standard deviation (n=5).

to the first and the second injection (10.9 ± 2.8 % ID/g,, p= 0.018, Mann-Whitney exact test, two-tailed) (*Figure 3B*). Renal uptake also increased slightly with each progressive dose, but tumour/kidney ratios were always favorable (9.3 ± 1.3, 7.0 ± 1.0, and 4.3 ± 1.1 after the first, second and third cycle respectively). Thus, this latter approach was selected for therapeutic evaluation.

Pretargeted radioimmunotherapy

PRIT effectively delayed tumour growth compared to the control mice (*Figure 4*). Tumours in all untreated mice rapidly increased in size, while in the treated mice, the tumours did not start growing until day 14, 24 and 41 after one, two and three cycles of PRIT, respectively.

The survival of the animals in the four groups of mice is depicted in *Figure 5*. PRIT prolonged survival: the median survival of untreated mice was 13 days (range 6-20), whereas the median survival of mice treated with one, two, and three cycles PRIT was 24 (range 24-31), 45 (range 38->130), and 65 days (range 48->130) respectively, with significant differences between all pairs of survival curves ($p<0.001$, Log-Rank test), except for two cycles PRIT compared to three cycles ($p=0.22$, Log- Rank test).

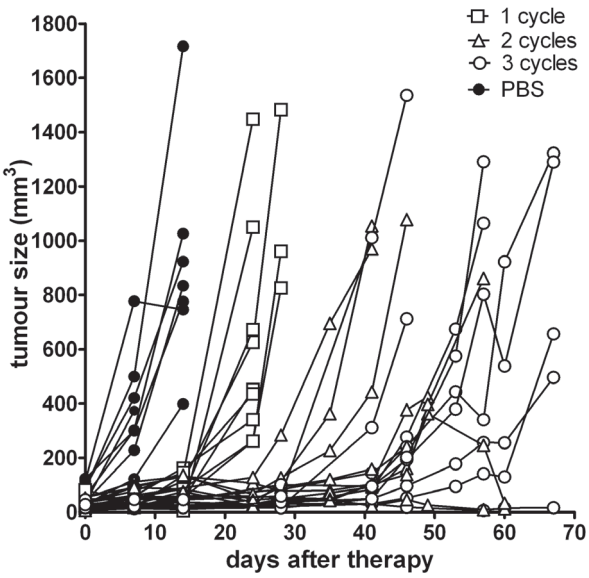

Figure 4. Tumor growth in mice that received one, two and three cycles of TF2 (5.0 nmol) and ^{177}Lu-IMP288 (26 MBq/0.28 nmol per cycle), or PBS. The size of the tumors of individual mice is depicted.

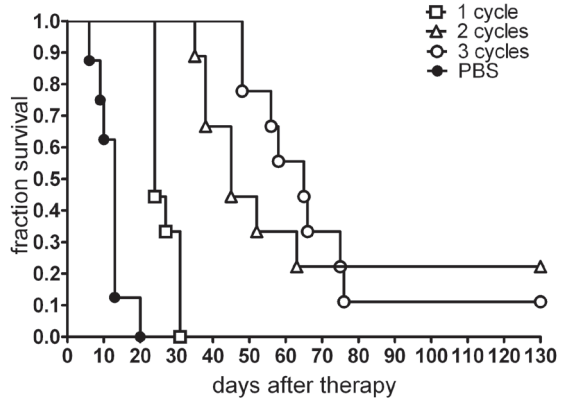

Figure 5. The survival of the animals in groups of 9 mice that were treated with one, two or three treatment cycles of TF2 (5.0 nmol) and ^{177}Lu-IMP288 (26 MBq/0.28 nmol per cycle), or PBS.

Toxicity due the PRIT was minimal. For all groups at all time points, body weight remained >93% of baseline, with no significant changes in mean body weight between the control and treated animals (P=0.85, Kruskal-Wallis test). Hematologic toxicity in the PRIT groups is illustrated by the leukocyte and platelet counts at two, three and seven weeks post-injection (p.i.) (*Figure 6A* and 6B). Seven weeks p.i., five animals of the group that received two cycles had already been euthanized due to excessive

tumour growth, while all mice that received three cycles of treatment were still alive. No differences in leukocyte and platelet counts were observed between the two- or three-cycle groups, so data of both groups were combined. A minimal, but statistically significant, decrease in leukocyte counts was measured two and three weeks after the start of treatment (median baseline counts, 6.9 x 10^9/L; two and three weeks p.i., 4.5 x 10^9/L and 4.6 x 10^9/L, respectively; p<0.001, Mann-Whitney exact test, two-tailed). Full recovery was observed at seven weeks after treatment (median counts seven weeks, 7.4 x 10^9/L; compared to baseline: P=0.95, Mann-Whitney exact test, two-tailed). No decrease in platelet counts was observed (median baseline counts, 972 x 10^9/L; two and three weeks, 964 and 991 x 10^9/L, respectively; compared to baseline: P=0.94, Mann-Whitney exact test, two-tailed). Serum creatinine at six and eight weeks after therapy was not increased significantly, as shown in *Figure 6C* (median = 14.0, 18.0 and 14.0 μmol/L at baseline, 6, and 8 weeks after therapy, respectively; Kruskal Wallis: P=0.94), indicating no evidence of acute nephrotoxicity in the treated mice.

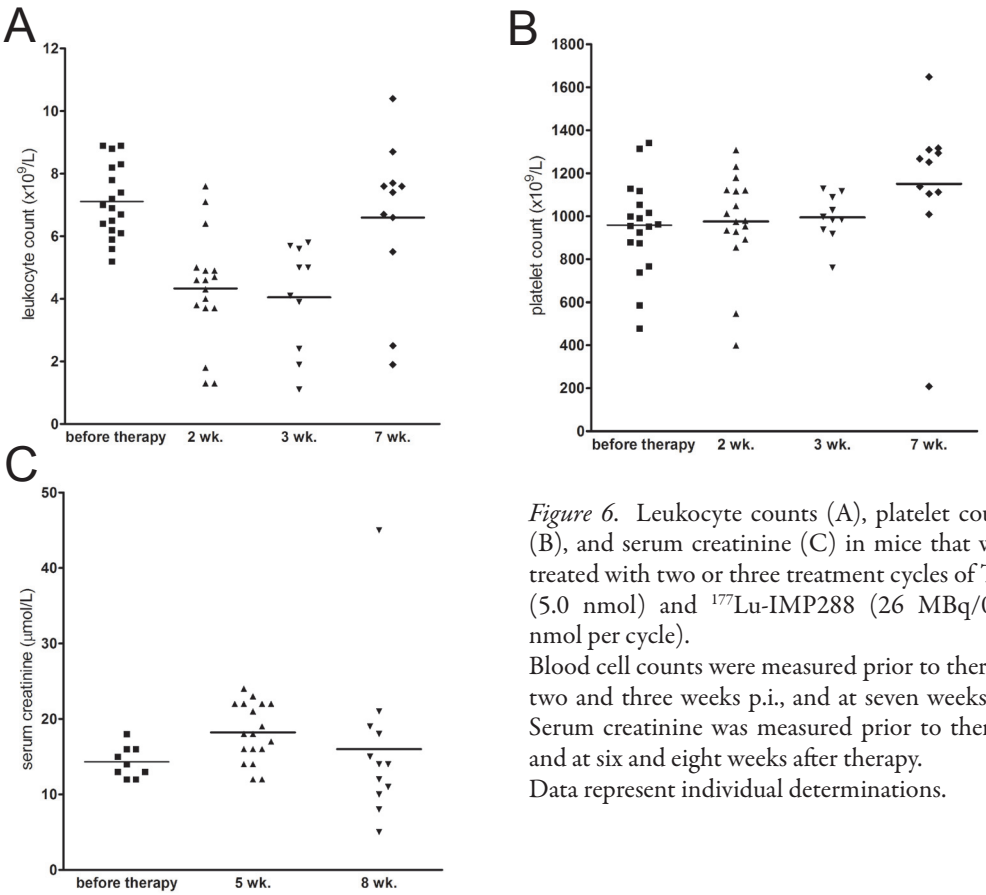

Figure 6. Leukocyte counts (A), platelet counts (B), and serum creatinine (C) in mice that were treated with two or three treatment cycles of TF2 (5.0 nmol) and ^{177}Lu-IMP288 (26 MBq/0.28 nmol per cycle).
Blood cell counts were measured prior to therapy, two and three weeks p.i., and at seven weeks p.i. Serum creatinine was measured prior to therapy and at six and eight weeks after therapy.
Data represent individual determinations.

Discussion

In this study we investigated the optimization of the pretargeting procedure for radioimmunotherapy using a new humanized recombinant DNL-bsMAb, TF2, with binding to CEACAM5, and the hapten, HSG, using a ^{177}Lu-labelled di-HSG-DOTA-peptide, IMP288. We demonstrate that using the optimal dose schedule, it can be an effective treatment modality for the treatment of CEA-positive human colonic tumours growing in mice.

All targeted therapies are limited by the amount and accessibility of the antigen. In this model system, where small tumour xenografts were used, the amount of radioactivity that could be delivered in a single treatment was limited by the amount and specific activity of IMP288 that could be given with antigen-saturating amounts of the bsMAb. We recently reported an evaluation of this same pretargeting system for PET imaging using ^{68}Ga- and ^{18}F-labelled peptides *(18)*, and found, like in this study, 5 nmol (800 μg) of TF2 saturated the amount of antigen in LS174T tumours. Thus, this amount of bsMAb was the upper limit that should be used in this pretargeting setting *(28)*. Using 5 nmol of TF2, the optimal IMP288 dose was next determined, finding that 0.28 nmol of IMP288 essentially saturated the amount of bsMAb-binding sites. At IMP288's maximum specific activity of 90 MBq/nmol, no more than 26 MBq of ^{177}Lu could be administered. However, because pretargeting greatly minimizes radiation exposure, this amount was much lower than the MTD. Therefore, other strategies that could increase the total amount of radioactivity administered were evaluated.

Biodistribution studies revealed the amount of radioactivity delivered to a tumour from a single ^{177}Lu-IMP-288 injection could be increased nearly 2-fold by administering an additional 2 successive doses of the IMP288 after a single TF2 injection. However, further improvements could be achieved by administering successive cycles of the bsMAb followed by IMP288, and therefore this latter approach was selected. As expected, higher activity doses, administered in successive cycles, correlated with longer survival. Despite this clear trend, the survival achieved with 3 cycles was not significantly better than with 2 cycles. Evenmore, tumour volume curves in the groups of mice that received 2 or 3 cycles were quite similar. This could be due to the fact that by the third cycle tumour uptake had declined (11% ID/g) compared to the first two administrations (14% ID/g).

The limited toxicity observed indicates that the maximum tolerated dose had not been reached in these experiments. Three subsequent treatment cycles did not compromise body weight, blood counts or acute kidney function. The decrease in leukocyte counts (40% of baseline levels) was moderate, with rapid recovery in most animals. The kidneys had the highest ^{177}Lu-activity concentration of the normal organs, since the peptide is cleared by urinary elimination. A small fraction of the dose is reabsorbed by the proximal tubular cells and thus retained in the kidney. Serum creatinine was not increased after treatment, suggesting the absence of radiation nephritis; however,

since radiation effects on the kidneys can take many months to manifest, further studies would be required to assess the risk for chronic renal toxicity, which has been observed in preclinical and clinical testing of peptide radionuclide radioimmunotherapy *(29-31)*.

We initiated studies with ^{177}Lu primarily because the most promising results with radiolabelled antibodies in solid tumours have been observed in the treatment of small-volume disease (≤3 cm) or in an adjuvant setting *(32)*. ^{177}Lu is well suited for the treatment of small-volume disease with minimal radiation, given the medium-energy beta (maximum energy 0.497 MeV, mean energy 0.149 MeV, maximum penetration depth 2.5 mm). With an 11% abundance of 208 keV photons, the biodistribution of the ^{177}Lu-labelled IMP288 peptide by gamma camera imaging will be possible in a clinical setting, providing important insights into the kinetics of tumour binding and retention in patients.

In the current animal study, the wash-out of ^{177}Lu-IMP288 from the tumour was similar to that of the TF2 bsMAb. In this pretargeting approach, the kinetics of tumour binding might not take full advantage of ^{177}Lu's 6.7 day physical half-life. In contrast, the half-life of ^{90}Y (64.1 h) is more consistent with the pharmacokinetics of IMP288, but its longer tissue penetration range (maximum 12.0 mm) would be more appropriate for treating tumours >0.5 cm in diameter *(33-34)*. Because of its high energy (maximum energy 2.28 MeV, mean energy 0.935 MeV), a single dose of a ^{90}Y-labelled di-HSG peptide can be given to nude mice at or near MTD level with significant therapeutic effects *(23, 31)*. In contrast, in this model the lower energy of ^{177}Lu is less toxic, which allows for multiple dosing strategy improving therapeutic outcome well below the MTD. On the other, multiple treatment cycles might add to the complexity of PRIT, so one should aim administering MTD in one therapy cycle. The in vivo effects of these beta-emitters should be compared in the same animal model, or ultimately in clinical trials, to reveal the optimal combination for therapeutic effects and bone marrow and kidney toxicity.

Attempts to further enhance the activity dose in RIT for solid tumours are restricted by myelotoxicity. Therefore, PRIT was developed as an alternative primarily to circumvent problems associated with the long residence time of the antibody in the blood *(11)*. Several pretargeting approaches have been developed, with preclinical evidence universally indicating PRIT's benefits over direct targeting in terms of reduced toxicity with similar or improved efficacy *(11, 19)*. The clinical experience with pretargeting has been limited. Kraeber-Bodéré et al. optimized PRIT with a chemically conjugated bsMAb using a humanized anti-CEACAM5 Fab' x murine anti-DTPA Fab' and 1.9-5.5 GBq of an ^{131}I-di-DTPA -peptide, in patients with metastasized CEA-expressing tumours *(35-36)*. The tumour responses in the eight patients with colorectal cancer were modest, while patients with medullary thyroid cancer had much better therapeutic responses. However, this last group of patients experienced dose-limiting leuko- or thrombocytopenia, most likely due to diffuse metastatic involvement of the bone

marrow, while the patients with colorectal cancer only had mild hematologic toxicity (grade II). These results illustrate the relevance of determining the most effective and tolerable treatment strategy and dosing schedule for each different patient population.

Conclusions

In conclusion, in this study we show that pretargeted radioimmunotherapy with an anti-CEA bsMAb and a ^{177}Lu-labelled peptide could be an effective treatment modality for the treatment of CEA-positive colonic tumours.

References

1. Simmonds PC. Palliative chemotherapy for advanced colorectal cancer: systematic review and meta-analysis. Colorectal Cancer Collaborative Group. BMJ. 2000;321(7260):531-535.
2. Tappenden P, Jones R, Paisley S, Carroll C. Systematic review and economic evaluation of bevacizumab and cetuximab for the treatment of metastatic colorectal cancer. Health Technol Assess. 2007;11(12):1-iv.
3. Tol J, Koopman M, Cats A et al. Chemotherapy, bevacizumab, and cetuximab in metastatic colorectal cancer. N Engl J Med. 2009;360(6):563-572.
4. Gordon LI, Witzig T, Molina A et al. Yttrium 90-labeled ibritumomab tiuxetan radioimmunotherapy produces high response rates and durable remissions in patients with previously treated B-cell lymphoma. Clin Lymphoma. 2004;5(2):98-101.
5. Wiseman GA, Gordon LI, Multani PS et al. Ibritumomab tiuxetan radioimmunotherapy for patients with relapsed or refractory non-Hodgkin lymphoma and mild thrombocytopenia: a phase II multicenter trial. Blood. 2002;99(12):4336-4342.
6. Witzig TE, Flinn IW, Gordon LI et al. Treatment with ibritumomab tiuxetan radioimmunotherapy in patients with rituximab-refractory follicular non-Hodgkin's lymphoma. J Clin Oncol. 2002;20(15):3262-3269.
7. Witzig TE, Gordon LI, Cabanillas F et al. Randomized controlled trial of yttrium-90-labeled ibritumomab tiuxetan radioimmunotherapy versus rituximab immunotherapy for patients with relapsed or refractory low-grade, follicular, or transformed B-cell non-Hodgkin's lymphoma. J Clin Oncol. 2002;20(10):2453-2463.
8. Liersch T, Meller J, Kulle B et al. Phase II trial of carcinoembryonic antigen radioimmunotherapy with 131I-labetuzumab after salvage resection of colorectal metastases in the liver: five-year safety and efficacy results. J Clin Oncol. 2005;23(27):6763-6770.
9. Liersch T, Meller J, Bittrich M, Kulle B, Becker H, Goldenberg DM. Update of carcinoembryonic antigen radioimmunotherapy with (131)I-labetuzumab after salvage resection of colorectal liver metastases: comparison of outcome to a contemporaneous control group. Ann Surg Oncol. 2007;14(9):2577-2590.
10. Reardan DT, Meares CF, Goodwin DA et al. Antibodies against metal chelates. Nature. 1985;316(6025):265-268.
11. Boerman OC, van Schaijk FG, Oyen WJ, Corstens FH. Pretargeted radioimmunotherapy of cancer: progress step by step. J Nucl Med. 2003;44(3):400-411.
12. Chang CH, Sharkey RM, Rossi EA et al. Molecular advances in pretargeting radioimunotherapy with bispecific antibodies. Mol Cancer Ther. 2002;1(7):553-563.
13. Sharkey RM, Cardillo TM, Rossi EA et al. Signal amplification in molecular imaging by pretargeting a multivalent, bispecific antibody. Nat Med. 2005;11(11):1250-1255.
14. Le Doussal JM, Martin M, Gautherot E, Delaage M, Barbet J. In vitro and in vivo targeting of radiolabeled monovalent and divalent haptens with dual specificity monoclonal antibody conjugates: enhanced divalent hapten affinity for cell-bound antibody conjugate. J Nucl Med. 1989;30(8):1358-1366.
15. Griffiths GL, Chang CH, McBride WJ et al. Reagents and methods for PET using bispecific antibody pretargeting and 68Ga-radiolabeled bivalent hapten-peptide-chelate conjugates. J Nucl Med. 2004;45(1):30-39.

16. McBride WJ, Zanzonico P, Sharkey RM et al. Bispecific antibody pretargeting PET (immunoPET) with an 124I-labeled hapten-peptide. J Nucl Med. 2006;47(10):1678-1688.
17. Koppe MJ, Bleichrodt RP, Soede AC et al. Biodistribution and therapeutic efficacy of (125/131)I-, (186) Re-, (88/90)Y-, or (177)Lu-labeled monoclonal antibody MN-14 to carcinoembryonic antigen in mice with small peritoneal metastases of colorectal origin. J Nucl Med. 2004;45(7):1224-1232.
18. Schoffelen R, Sharkey RM, Goldenberg DM et al. Pretargeted Immuno-Positron Emission Tomography Imaging of Carcinoembryonic Antigen-Expressing Tumors with a Bispecific Antibody and a 68Ga- and 18F-Labeled Hapten Peptide in Mice with Human Tumor Xenografts. Mol Cancer Ther. 2010.
19. Sharkey RM, McBride WJ, Karacay H et al. A universal pretargeting system for cancer detection and therapy using bispecific antibody. Cancer Res. 2003;63(2):354-363.
20. Goldenberg DM, Rossi EA, Sharkey RM, McBride WJ, Chang CH. Multifunctional antibodies by the Dock-and-Lock method for improved cancer imaging and therapy by pretargeting. J Nucl Med. 2008;49(1):158-163.
21. Rossi EA, Goldenberg DM, Cardillo TM, McBride WJ, Sharkey RM, Chang CH. Stably tethered multifunctional structures of defined composition made by the dock and lock method for use in cancer targeting. Proc Natl Acad Sci U S A. 2006;103(18):6841-6846.
22. Sharkey RM, Karacay H, Litwin S et al. Improved therapeutic results by pretargeted radioimmunotherapy of non-Hodgkin's lymphoma with a new recombinant, trivalent, anti-CD20, bispecific antibody. Cancer Res. 2008;68(13):5282-5290.
23. Karacay H, Sharkey RM, Gold DV et al. Pretargeted radioimmunotherapy of pancreatic cancer xenografts: TF10-90Y-IMP-288 alone and combined with gemcitabine. J Nucl Med. 2009;50(12):2008-2016.
24. Morel A, Darmon M, Delaage M. Recognition of imidazole and histamine derivatives by monoclonal antibodies. Mol Immunol. 1990;27(10):995-1000.
25. Sharkey RM, Goldenberg DM, Goldenberg H et al. Murine monoclonal antibodies against carcinoembryonic antigen: immunological, pharmacokinetic, and targeting properties in humans. Cancer Res. 1990;50(9):2823-2831.
26. Lindmo T, Boven E, Cuttitta F, Fedorko J, Bunn PA, Jr. Determination of the immunoreactive fraction of radiolabeled monoclonal antibodies by linear extrapolation to binding at infinite antigen excess. J Immunol Methods. 1984;72(1):77-89.
27. Fraker PJ, Speck JC, Jr. Protein and cell membrane iodinations with a sparingly soluble chloroamide, 1,3,4,6-tetrachloro-3a,6a-diphrenylglycoluril. Biochem Biophys Res Commun. 1978;80(4):849-857.
28. Liu G, Hnatowich DJ. A semiempirical model of tumor pretargeting. Bioconjug Chem. 2008;19(11):2095-2104.
29. Rubin P, Constine LS, Nelson DF. Late effects of cancer treatment: radiation and drug toxicity. In: Perez CA BL, ed. Principles and Practice of Radiation Oncology. Philadelphia, PA: J.B. Lippincott; 1998:134-136.
30. Rolleman EJ, Krenning EP, Bernard BF et al. Long-term toxicity of [(177)Lu-DOTA (0),Tyr (3)]octreotate in rats. Eur J Nucl Med Mol Imaging. 2007;34(2):219-227.
31. Karacay H, Brard PY, Sharkey RM et al. Therapeutic advantage of pretargeted radioimmunotherapy using a recombinant bispecific antibody in a human colon cancer xenograft. Clin Cancer Res. 2005;11(21):7879-7885.
32. Behr TM, Liersch T, Greiner-Bechert L et al. Radioimmunotherapy of small-volume disease of metastatic colorectal cancer. Cancer. 2002;94(4 Suppl):1373-1381.
33. Cardillo TM, Ying Z, Gold DV. Therapeutic advantage of (90)yttrium- versus (131)iodine-labeled PAM4 antibody in experimental pancreatic cancer. Clin Cancer Res. 2001;7(10):3186-3192.
34. Stein R, Juweid M, Mattes MJ, Goldenberg DM. Carcinoembryonic antigen as a target for radioimmunotherapy of human medullary thyroid carcinoma: antibody processing, targeting, and experimental therapy with 131I and 90Y labeled MAbs. Cancer Biother Radiopharm. 1999;14(1):37-47.
35. Kraeber-Bodere F, Faivre-Chauvet A, Ferrer L et al. Pharmacokinetics and dosimetry studies for optimization of anti-carcinoembryonic antigen x anti-hapten bispecific antibody-mediated pretargeting of Iodine-131-labeled hapten in a phase I radioimmunotherapy trial. Clin Cancer Res. 2003;9(10 Pt 2):3973S-3981S.
36. Kraeber-Bodere F, Rousseau C, Bodet-Milin C et al. Targeting, toxicity, and efficacy of 2-step, pretargeted radioimmunotherapy using a chimeric bispecific antibody and 131I-labeled bivalent hapten in a phase I optimization clinical trial. J Nucl Med. 2006;47(2):247-255.

5

Quantitative immuno-SPECT monitoring of pretargeted radioimmunotherapy with a bispecific antibody in an intraperitoneal nude mouse model of human colon cancer

Rafke Schoffelen[1], Winette T.A. van der Graaf[2], Robert M. Sharkey[3], Gerben M. Franssen[1], W.J. McBride[4], Chien-Hsing Chang[5], Desirée L. Bos[1], David M. Goldenberg[3,4,5], Wim J.G. Oyen[1] and Otto C. Boerman[1]

Journal of nuclear medicine. Accepted for publication

[1] Radboud University Nijmegen Medical Centre, dept. of Nuclear Medicine, Nijmegen, Netherlands
[2] Radboud University Nijmegen Medical Centre, dept. of Medical Oncology, Nijmegen, Netherlands
[3] Garden State Cancer Center, Morris Plains, New Jersey, USA
[4] Immunomedics, Inc., Morris Plains, New Jersey, USA
[5] IBC Pharmaceuticals, Morris Plains, New Jersey, USA

Abstract

Background

The prospects for using pretargeted immuno-SPECT with a bispecific anti-carcinoembryonic antigen (CEA; CEACAM5; CD66e) x anti-hapten monoclonal antibody (bsMAb), TF2, and a small (1.5 kD) peptide, IMP288, labelled with ^{111}In to monitor the response to pretargeted radioimmunotherapy (PRIT) using ^{177}Lu-IMP288 in a nude mouse-human colon cancer model implanted in the peritoneal cavity was examined.

Methods

First, tumour uptake of ^{111}In-IMP288 and ^{177}Lu-IMP288, as determined by immuno-SPECT, was validated by ex vivo counting. Two groups of female BALB/c nude mice with i.p. LS174T tumours received i.v. injections of TF2, followed by 10 MBq of ^{111}In-IMP288 or 90 MBq of ^{177}Lu-IMP288. A control group of non-tumour-bearing mice received TF2 and ^{111}In-IMP288. One hour after the radiolabelled IMP288 was given, micro-SPECT/CT images were acquired, and subsequently animals were dissected. Furthermore, a survival study was performed in three groups of ten mice with i.p. tumours: mice received TF2 and ^{177}Lu-IMP288 (60 MBq), non-pretargeted ^{177}Lu-IMP288 (60 MBq), or PBS. Immuno-SPECT scans were acquired directly after therapy, and at 14 and 45 days after therapy. Tumour growth was analyzed in the successive scans in each animal.

Results

^{111}In- and ^{177}Lu-labelled IMP288 had identical in vivo distribution. The activity measured in the pretargeted immuno-SPECT images correlated well with the uptake measured in the dissected tumours (Pearson's $r = 0.99$, $p<0.05$). In the therapy study, the SPECT images showed rapid and selective tumour targeting with very high tumour-to-background contrast (30 ± 12) as early as one hour after injection. The successive images of the treated mice showed delayed tumour growth in the PRIT group, which corresponded with their prolonged survival.

Conclusion

Pretargeted immuno-SPECT with TF2 and ^{111}In- or ^{177}Lu-IMP288 can be used to predict and confirm tumor targeting and monitor the therapeutic effect of pretargeted radioimmunotherapy.

Introduction

Radiolabelled antibodies can be used for the diagnosis, detection and therapy of cancer. The diagnostic images acquired after injection of the radiolabelled antibody preparation can potentially predict the efficacy of radioimmunotherapy, an approach designated as theranostics. Theranostics is a useful concept for developing personalized targeted radionuclide therapies and has been applied for a long time in Nuclear Medicine. For example, diagnostic information obtained from pre-therapeutic PET or SPECT can ensure that the treatment is targeted specifically to tumours, which could aid in patient selection, and dosimetric analysis potentially could predict the benefit/risk ratio of a planned radionuclide therapy. This analysis also might aid in identifying the most appropriate prescribed therapeutic dose optimized for their radionuclide therapy (^{90}Y, ^{177}Lu, ^{213}Bi, etc.). Finally, imaging data could potentially assess therapeutic response, including the detection of unsuspected sites of disease. The feasibility of this approach has been shown in neuroendocrine tumours using ^{111}In- or ^{68}Ga-labelled somastatin analogues for diagnosis and the same peptides labelled with ^{177}Lu- or ^{90}Y for radionuclide therapy (*1, 2*).
In this study, the potential of theranostics for combined pretargeted radioimmunodetection and –therapy was evaluated. Pretargeting is a strategy that was developed to improve the imaging and therapeutic characteristics of directly radiolabelled monoclonal antibodies. Radiolabelled antibodies require several days to localize tumours effectively, due to the slow pharmacokinetics and accretion of intact antibodies in tumours. This slow uptake and clearance rate delays tumour detection by imaging and increases bone marrow toxicity for therapy. Pretargeting techniques achieve rapid accretion of the radionuclide in the tumour in combination with rapid blood clearance by first administering a non-radiolabelled bispecific monoclonal antibody (bsMAb). After the bsMAb localizes in the tumour and clears from the circulation, a small radiolabelled hapten-peptide is given, which leaves the bloodstream quickly, being trapped in the tumour by the anti-hapten arm of the bsMAb, while the remainder clears rapidly from the blood and is excreted via the kidneys. Coupling two haptens to the peptide improves peptide uptake, a phenomenon known as affinity enhancement (*3*). Chelate-metal complexes, such as DTPA-In, have been used as haptens (*4*). More recently, peptides substituted with the hapten, histamine-succinyl-glycine (HSG), in combination with anti-HSG antibody binding have provided a more flexible system, because these HSG-substituted peptides can be conjugated with various chelators (DOTA, NODA/NOTA, N_3S-chelates, etc.), allowing stable complexes with many radionuclides, such as ^{111}In and ^{99m}Tc for SPECT (*5-8*), ^{68}Ga and ^{18}F for PET(*9-13*), or ^{90}Y and ^{177}Lu for pretargeted radioimmunotherapy (PRIT) (*5, 8*). Including tyrosine in the peptide core also enables radioiodination (e.g., ^{124}I or ^{131}I) (*7, 14*).
For the studies described herein, a fully humanized anti-CEA x anti-HSG bsMAb

(TF2) (*15*), and a HSG-substituted hapten-peptide (IMP288) were applied in a nude mouse model for peritoneal dissemination of human cancer (*13*). Previous preclinical studies illustrated the enhanced sensitivity and specificity of this pretargeting system compared to FDG-PET (*7, 12, 13*).
The aim of the present study was to investigate whether pretargeted immuno-SPECT could predict the effectiveness of PRIT.

Materials and Methods

Pretargeting reagents TF2 and IMP288

The bsMAb, TF2, and the peptide IMP288, were provided by Immunomedics and IBC Pharmaceuticals (Morris Plains, NJ, USA). The preparation of TF2 and its binding properties have been described previously (*15, 16*). Gel filtration chromatography showed that TF2 bound >90% of radiolabelled peptide.
IMP288 was synthesized and purified as described by McBride et al. (*14*). It is a DOTA-conjugated D-Tyr-D-Lys-D-Glu-D-Lys tetrapeptide in which both lysine residues are substituted with a HSG-moiety via their ε-aminogroup: 7,10-tetra-azacyclododecane-N,N',N'',N'''-tetraacetic acid (DOTA)-D-Tyr-D-Lys(HSG)-D-Glu-D-Lys(HSG)-NH_2. IMP288 was labelled with ^{111}In (Covidien, Petten, The Netherlands) at a specific activity of 36 MBq/nmol and with ^{177}Lu (IDB Holland BV, Baarle Nassau, The Netherlands) at a specific activity of 321 MBq/nmol, under strict metal-free conditions. After adding 100 MBq ^{111}In to 4 μg (2.8 nmol) IMP288 or 900 MBq ^{177}Lu to 4 μg (2.8 nmol) IMP288 dissolved in 0.1 M 2-(*N*-morpholino) ethanesulfonic acid (MES) buffer, pH 5.5, the mixture was incubated for 20 min at 95 °C in a heating block. Subsequently, 10 μL 50 mM ethylenediaminetetraacetic acid (EDTA) was added to complex any unbound ^{111}In or ^{177}Lu. Radiochemical purity of the radiolabelled IMP288 preparations was determined by RP-HPLC as described previously (*5*). In all experiments, the radiochemical purity of radiolabelled IMP288 exceeded 95%.
Mice received TF2 and IMP288 intravenously in 0.2-0.3 mL phosphate-buffered saline (PBS), 0.5% bovine serum albumin (BSA).

Animal experiments

All studies were approved by the institutional Animal Welfare Committee of the Radboud University Medical Centre Nijmegen, and conducted in accordance with their guidelines (revised Dutch Act on Animal Experimentation, 1997). The experiments were performed in female nude BALB/c mice (6-8 weeks old) weighing 20 to 25 g. Mice were acclimated to laboratory conditions for at least one week before experimental use and were housed under non-sterile standard conditions

in filter-topped cages with free access to animal chow and water. Tumour growth was induced by an intraperitoneal (i.p.) injection of 0.5 mL of a suspension of 10^6 LS174T cells, a CEA-expressing human colon carcinoma cell line (CCL-188; passage 7; American Type Culture Collection), resulting in tumour nodules (1-3 mm) in the peritoneal cavity after 2-4 weeks (*17*).

Biodistribution and imaging studies

To investigate whether ^{111}In-IMP288 could be used as a surrogate for ^{177}Lu -IMP288 with pretargeted immuno-SPECT, the biodistribution of ^{111}In-IMP288 and ^{177}Lu -IMP288 was determined by micro-SPECT and by counting of dissected tumours. Two groups of five nude mice with i.p. tumours and one group of three mice without tumours (negative control) were injected intravenously with 5.0 nmol TF2 (0.2 mL). Sixteen hours later, 0.28 nmol IMP288 (0.2 mL) was administered intravenously. One group received ^{111}In-labelled IMP288 (10 MBq), and the other group received ^{177}Lu-labelled IMP288 (90 MBq). One hour after injection of the radiolabelled peptide, mice were euthanized by CO_2/O_2 asphyxiation. The control group of mice without any tumour received the same dose of TF2 and ^{111}In-IMP288. Before imaging, the total-body activity of each mouse was measured in a dose calibrator. A blood sample (50-100 μL) was drawn by cardiac puncture. Mice were imaged using an USPECT-II/CT scanner (MILabs, Utrecht, The Netherlands) with the 1.0-mm diameter pinhole rat collimator tube. The animals were placed in a supine position. SPECT scans were acquired for 60 min, followed by CT scans for anatomical reference (65 kV, 612μA, exposure time 240 msec).
After imaging, mice were dissected and the abdomen was systematically and meticulously examined for the presence of tumours. The location of each lesion was documented, and individually weighed, size measured, and the radioactivity detected in a gamma counter. The other organs of interest were weighed and counted in a gamma counter with standards prepared from the injected products, using appropriate energy windows for the radionuclide of interest. The percentage of the injected dose per gram tissue (%ID/g) was calculated.

Image analysis

Scans were reconstructed with MILabs reconstruction software, using an ordered-subset expectation maximization algorithm, with a voxel size of 0.375 mm. Images were analyzed with the Inveon Research Workplace software (version 2.2; Siemens Preclinical Solutions). Images were scored for the presence, number and localization of intraperitoneal tumours.
To estimate the absolute tumour uptake (% ID) from the images, calibration factors for ^{111}In and ^{177}Lu were determined; whole-body activity as measured in the scans was correlated to the activity measured in the animals measured in the dose calibrator.

VOIs were drawn around the tumour lesions. A VOI in the lower left abdomen (large intestines) was used as background activity. The activity concentrations in the tumours derived from the images were compared with the tumour uptake as measured in the gamma counter, assuming a tissue density of 1.0 g/mL.

PRIT study

The design of the PRIT study is summarized in Figure 1. Three groups of ten mice were inoculated i.p. with LS174T tumour cells. Two weeks after tumour cell inoculation, mice were given 5.0 nmol TF2 followed 16 h later with 60 MBq ^{177}Lu-IMP288 (previously determined to be the maximal tolerated dose). The two control groups received PBS or 60 MBq ^{177}Lu-IMP288 without pretargeting of TF2 on the same day that the treatment group received radiolabelled IMP288.
One hour after the PRIT group received the ^{177}Lu-IMP288, a baseline immuno-SPECT scan was acquired. The control groups were scanned after a diagnostic injection of ^{111}In-labelled IMP288 pretargeted with TF2, one day after therapy (*Figure 1*). Follow-up scans were acquired in all remaining animals of all groups at 14 and 45 days after therapy, after a diagnostic injection of ^{111}In-labelled IMP288 pretargeted with TF2. Animals were scanned under general anesthesia (isoflurane and O_2). The same imaging acquisition protocol, reconstruction, and calibration were used as in the biodistribution and imaging study. The scans were analyzed by drawing VOIs around tumour lesions, calculating the fraction administered dose, and by comparing the measurements of the same lesions in the follow-up scan and in the baseline scan, tumour growth of each tumour lesion was monitored.
Animals were observed daily by independent, experienced biotechnicians. When the humane endpoint was reached (failure to eat/drink and losing ≥15% of body weight in 1 or 2 days, or losing ≥20% of their starting weight, or in the case of tumour progression/abdominal distention or visual hemorrhagic ascites), mice were euthanized by CO_2/O_2 asphyxiation. All remaining animals were euthanized 120 days after therapy.

Statistical analysis

Biodistribution, SPECT and survival data were statistically analyzed using the software GraphPad Prism version 5.00 for Windows (GraphPad Software, San Diego USA). Means and standard deviations were used to describe continuous data, unless stated otherwise. Comparisons were analyzed using a non-parametric, two-tailed Mann Whitney test. Correlations were determined with the Pearson's correlation test. Survival was described with median survival times and survival curves were compared using the Log-rank test. The level of significance was set at $p<0.05$.

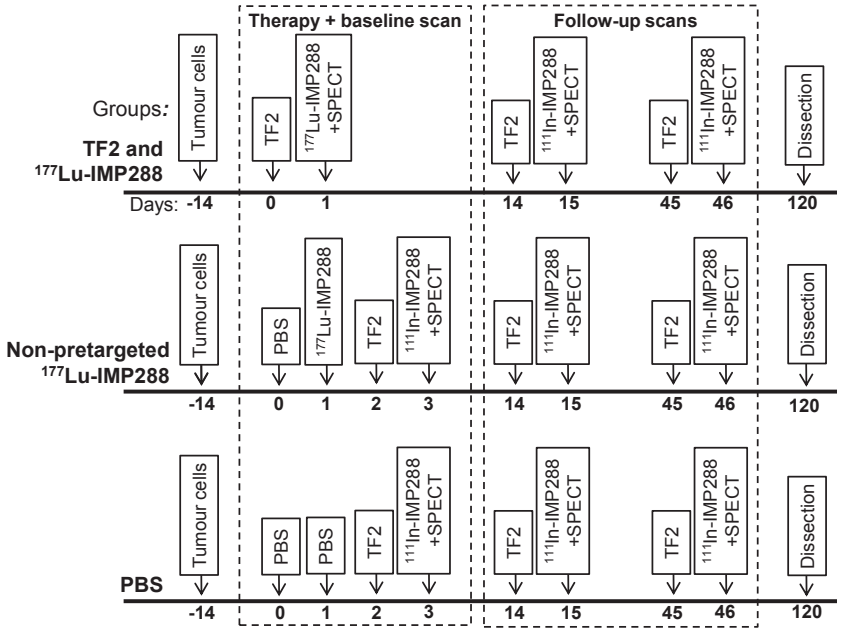

Figure 1: Treatment schedule for the three different therapy groups and the timing of the baseline and follow-up SPECT studies.

Results

Biodistribution and imaging study

Mice did not show clinical signs of discomfort or change in body weight for up to three weeks after inoculation of the LS174T tumour cells. Nevertheless, upon macroscopic inspection of their abdomen, multiple solid tumours were found, predominantly located at the rectovesical pouch, mesentery, subhepatic, -splenic and -phrenic spaces. Median number of tumour lesions per animal was 5 (range 0-9). Three-dimensional caliper measurements revealed that the median diameter of the tumour lesions was 5 mm (range 1-16 mm), corresponding with a median weight of 22 mg (range 0.6 to 840 mg). Two out of 10 mice did not develop any macroscopically visible tumours.

The biodistribution of ^{111}In-IMP288 and ^{177}Lu-IMP288 1 h p.i. in the mice that were pretargeted with TF2 was identical (*Figure 2*). Uptake of ^{111}In-IMP288 and ^{177}Lu-IMP288 in the tumour lesions was similar (6.9 ± 2.7 % ID/g vs 7.1 ± 2.7 %ID/g, respectively, Mann-Whitney, $p>0.05$). Likewise, blood concentrations at 1 h p.i. were the same (0.17± 0.13 %ID/g vs 0.16 ± 0.08 %ID/g, respectively, Mann-Whitney, $p>0.05$). At 1 h p.i., the ratios of uptake in the tumour to that in the other organs were 31.0 ± 30.8 (blood), 66.2 ± 23.4 (intestine), 3.7 ± 2.4 (kidney), and 27.4 ± 20.5 (liver)

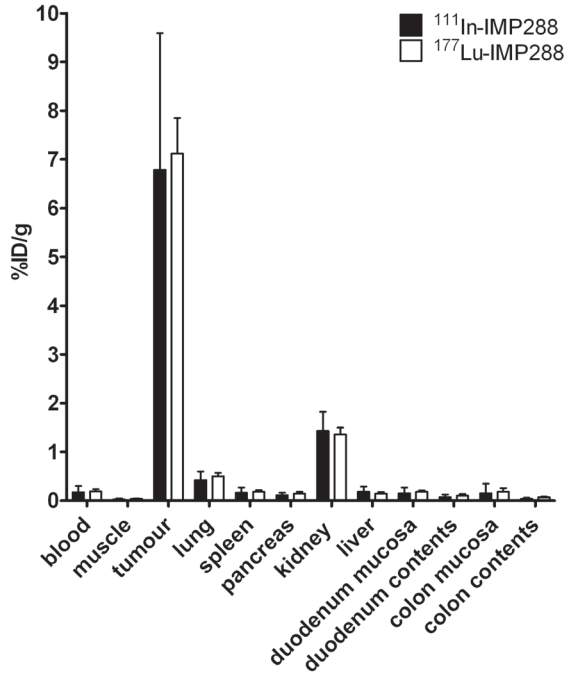

Figure 2: Biodistribution of 0.25 nmol ^{111}In- or ^{177}Lu-IMP288, following pretargeting with 6.0 nmol ^{125}I-TF2 (interval 16 h), 1 h after i.v. injection, in BALB/c nude mice with Intraperitoneal, CEA-expressing LS174T tumours.
Values are given as means ± standard deviations (n=5).

for ^{111}In-IMP288 and 34.6 ± 11.4 (blood), 58.0 ± 18.0 (intestine), 4.2 ± 0.3 (kidney), and 40.4 ± 49.1 (liver) for ^{177}Lu-IMP288, respectively. Normal tissue biodistribution of ^{111}In-IMP288 in the non-tumour-bearing mice was not significantly different from that of the tumour-bearing animals (data not shown), indicating that the presence of the intraperitoneally growing tumours did not affect clearance of the peptide from the normal tissues.

Image analysis

Clear and specific targeting of the tumour lesions was seen in SPECT images that were acquired one hour after injection of ^{111}In- and ^{177}Lu-IMP288. A typical example of an immuno-SPECT image of a tumour-bearing mouse is shown in *Figure 3A*. The corresponding photographs show all the tumours that were dissected from the abdomen of this animal. Each lesion was clearly visualized in the SPECT images. An example of a SPECT image of a non-tumour-bearing mouse is shown in *Figure 3B*, showing renal uptake and only very low accretion in the other normal organs. Normal tissue uptake was low in the majority of the tumour- and non-tumour-bearing mice. In some mice, low uptake in spleen (3/15), uterus and ovaries (2/15), and intestines (2/15) was seen, which could easily be discriminated from tumour lesions by their activity concentration, shape and location.

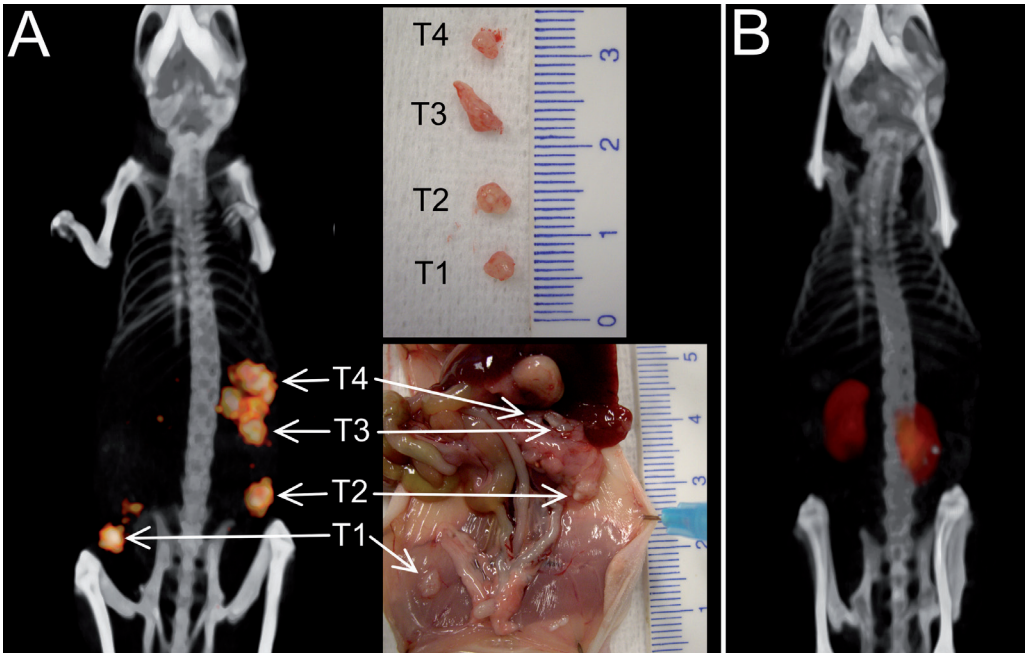

Figure 3: 3D-volume rendering of pretargeted immuno-SPECT/CT images of a tumour-bearing mouse (A) and a non-tumour-bearing mouse (B). The animals were imaged one hour after ^{111}In-IMP288 injection. Corresponding digital pictures are shown, that were made during dissection to localize and measure individual tumours. All dissected tumours (T1-4) are very clearly distinguishable on the pretargeted immuno-SPECT/CT images, with low normal tissue uptake.

Using the lower left abdomen as background region, tumour-to-background ratios were very high: 30 ± 12, and did not differ between the groups that received the ^{111}In- or ^{177}Lu-labelled peptide (33 ± 15 vs 27 ± 9, Mann-Whitney, $p>0.05$). All lesions ≥ 2 mm in diameter (≥ 4 mg) were detected as separate lesions with immuno-SPECT. Tumour uptake, as determined by immuno-SPECT and ex-vivo counting, showed a good correlation (Pearson's $r = 0.99$, $p<0.05$; *Figure 4*). Furthermore, the absolute values (%ID) of both methods showed good agreement, with a mean difference of only 13 ± 38% (Bland-Altman analysis). In all tumours ≥ 22 mg (=median tumour weight), the difference between the two measurements was <25%. In smaller tumours, the uptake measured with immuno-SPECT was less reliable, where uptake measured by SPECT in 40% of the lesions was > 25% different.

Pretargeted radioimmunotherapy studies

In two animals in the PBS group and in three animals in the PRIT group the baseline or follow-up scans did not disclose any tumours. These animals did not show any tumours at dissection 120 days after tumour inoculation. In the majority of the

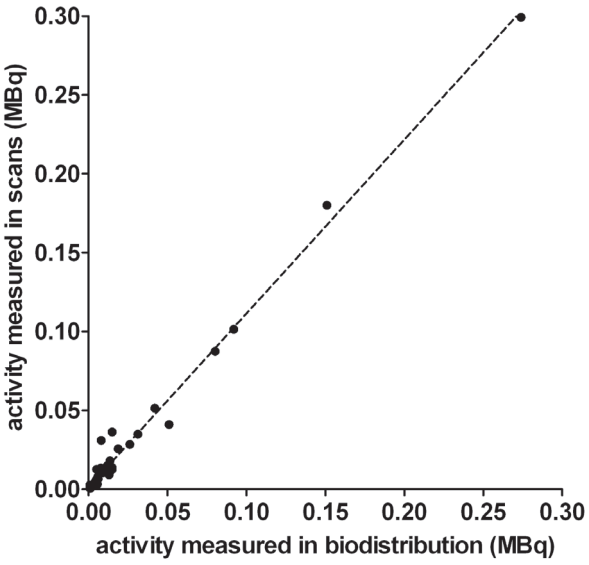

Figure 4: Correlation between tumour uptake measured in the pretargeted immuno-SPECT images (y-axis) and by ex vivo biodistribution (x-axis) (Spearman's rho = 0.99, $p<0.05$). Values are given for individual tumour lesions. Dotted line is linear fitted trend-line.

animals, micro-SPECT scans directly after therapy revealed multiple tumour lesions per animal: the median number of visualized tumours per animal was 4 (range 1- 10). One mouse in the PBS group had to be euthanized before the first follow-up scan (14 days p.i.), because of excessive tumour growth.

Tumour growth was monitored with immuno-SPECT after therapy by measuring the fraction of the injected dose ^{111}In- and ^{177}Lu-IMP288 for each lesion, drawing VOIs around the tumours in the baseline and in the follow-up scan. *Figure 5* shows a typical example of an animal of the control group that received non-pretargeted ^{177}Lu-IMP288. Tumour activity concentrations were similar in both scans, but the fraction of the injected dose per lesion was 10-fold higher in the follow-up scan on day 14 (*Figure 5A and 5B*). The excessive tumour growth that was prospectively monitored by imaging was confirmed when the animal had to be euthanized due to abdominal distension and ascites, nine days after the follow-up scan. Dissection of this animal revealed 2.0 gram of tumour tissue (*Figure 5C*).

PRIT resulted in a significant delay in tumour growth, demonstrated in the follow-up scans 14 days after therapy. Tumour uptake calculated as fraction of the administered dose increased 13- to 16-fold in the non-pretargeted group and the PBS group, respectively (mean 1289% (SEM 154%) and 1584% (SEM 167%), respectively), while in the PRIT group a 5-fold increase (535% (SEM 118%)) in tumour growth was observed 14 days after therapy (Mann Whitney, $p<0.05$) (*Figure 6*). At time of the second follow-up scan (45 days after therapy), only 1-3 mice per group were still alive.

Delayed tumour growth due to PRIT resulted in a median survival of 50 days (95%

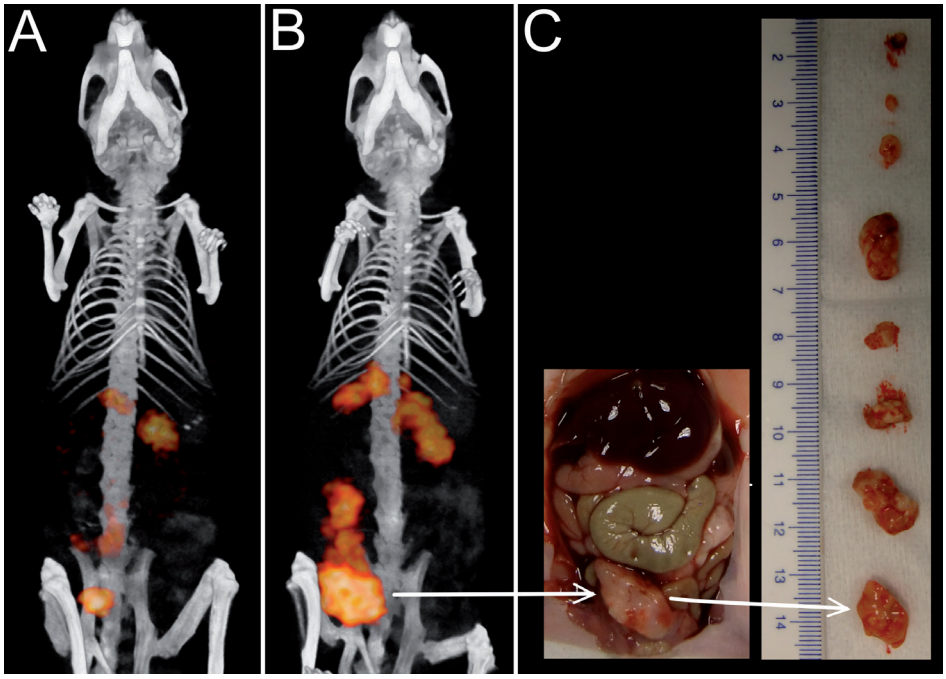

Figure 5: 3D-volume rendering of pretargeted immuno-SPECT/CT images of a mouse that was treated with not-pretargeted ^{177}Lu-IMP288 at the time of therapy (A) and the follow-up scan at 14 days after therapy (B), which shows a 10-fold increase in tumour size in this animal. Corresponding digital pictures (C) were made when the animal had to be euthanized nine days after the follow-up scan, showing the multiple tumours (total weight: 2-g) that were dissected from the abdomen, with the arrows indicating one of the tumours in the images and pictures.

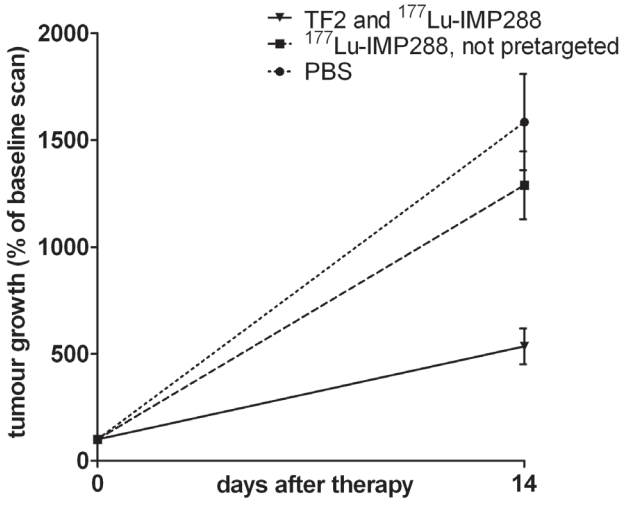

Figure 6. Difference in tumour growth between the therapy groups (TF2 and ^{177}Lu-IMP288, not-pretargeted ^{177}Lu-IMP288, or PBS), measured in the pretargeted immuno-SPECT images at time of therapy and follow-up scan made 14 days after therapy, and calculated as % increase of fraction administered dose. Values are given as means ± SEM of all individual tumours per therapy group.

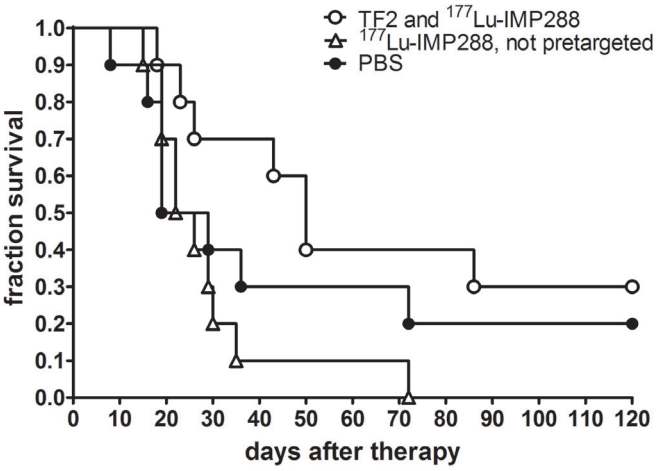

Figure 7: Kaplan-Meier survival curves for tumour-bearing mice that received pretargeted ^{177}Lu-IMP288, ^{177}Lu-IMP288 alone, or untreated (PBS). PRIT resulted in a median survival of 50 days (95% CI: 41-59 days), while the mice in the non-pretargeted group and the PBS group had a median survival of 22 and 19 days, respectively (95% CI: 15-29 and 9-29 days, respectively).

CI: 41-59 days), while the mice in the non-pretargeted group and the PBS group had a median survival of 22 and 19 days, respectively (95% CI: 15-29 and 9-29 days, respectively) (*Figure 7*). Kaplan-Meier survival analysis showed that overall survival curve of the groups treated with PRIT was significantly better than the overall survival of the group with non-pretargeted peptide ($p<0.05$). All animals in the PBS and non-pretargeted group had to be euthanized due to tumour progression; animals presented either with abdominal distension or with ascites. In the treated animals that had to be euthanized in the same period (<4 weeks after therapy), the main reason for euthanization was loss of body weight, while at dissection they had a low total tumour weight (9-fold lower than in the control animals).
Two animals in the PBS group and three in the PRIT group survived for more than 120 days after therapy. None of these animals had tumours visible in the scans or at dissection (134 days after tumour inoculation). As a result, Kaplan-Meier survival analysis of those two curves did not show significant differences.

Discussion

The present study shows that pretargeted immuno-SPECT is an excellent imaging method for monitoring the therapeutic effect of PRIT or, for that matter, monitoring any form of therapy. The biodistribution showed that the ^{111}In-labelled peptide is a reliable surrogate for the ^{177}Lu-labelled peptide. Pretargeted immuno-SPECT with TF2 and ^{111}In- or ^{177}Lu-IMP288 showed rapid and selective tumour targeting with very high tumour-to-background contrast as early as one hour after injection, which led to the detection of tumours as small as 2 mm. The activity in the tumour lesions as measured with SPECT correlated well with uptake measured

with ex vivo biodistribution. In a previous study, we showed that successive administrations of PRIT within a three-day interval resulted in similar uptake in the tumours (*5*). Therefore, images acquired after diagnostic or therapeutic administrations of PRIT can be compared quantitatively. Furthermore, tumour size could be derived accurately from the activity uptake (%ID) measured with SPECT, as in small tumour lesions the uptake (%ID/g) is relatively independent of tumor size. This allowed monitoring of tumour growth. The delayed tumour growth due to PRIT corresponded to the prolonged survival in the treated group. Hence, this report shows the feasibility and additional value of imaging to monitor the efficacy of with the same pretargeting agents, TF2 and radiolabelled IMP288.

The orthotopic LS174T human colon carcinoma model for peritoneal disease had been characterized previously (*17*). This animal model is more relevant than the widely used models of subcutaneously growing tumours to investigate the sensitivity of an imaging method, because background activity levels can be better appreciated. Furthermore, it is also more clinically relevant to monitor therapy effects.

We radiolabelled IMP288 with ^{111}In for pretargeted immuno-SPECT, because ^{111}In is used as a validated surrogate for ^{177}Lu, as it has the same in vivo behavior. Both radionuclides are residualizing radiometals. Therefore, predictive dosimetry can be performed with ^{111}In-data to estimate the radiation dose to the tumour. For calculation of absorbed doses, imaging during several days is required to determine the residence time of the radiolabell in the tissues. It would have been very interesting to estimate tumour and normal organ doses. However, for dosimetry multiple scans (≥ 3) are required within 7 days after injection, to calculate the area-under-the-curve for tumour/organ uptake. Multiple sessions of general anaesthesia within several days would have negatively affected the condition of the mice, which would have affected the toxicity and survival data. Therefore, we decided to acquire one SPECT scan 1 h after injection, and not to perform dosimetry in this animal study. In patients multiple scans can easily be acquired to estimate the radiaiton dose to the tumour lesions and to the dose limiting tissues.

The half-life of ^{111}In perfectly matches the biological half-life of the radiolabelled peptide. Former studies showed pretargeted immuno-PET and -SPECT with radionuclides, such as ^{68}Ga, ^{18}F, ^{124}I, and Tc^{99m} (*7, 12-14*), but these methods cannot be used for dosimetric calculations for therapy. The half-life of ^{68}Ga (68 min) is not matched with the therapeutic radionuclide. Using ^{99m}Tc for dosimetry on immuno-SPECT images is not feasible either, because ^{99m}Tc clears more rapidly from the (tumour) cells after binding and internalization, in contrast to (residualizing) radiometals like ^{111}In and ^{177}Lu.

The established valuable combination of imaging and therapy, designated as theranostics, could be a useful strategy in the clinical practice of PRIT. The therapeutic efficacy of PRIT with TF2 and ^{177}Lu-IMP288 was demonstrated previously in mice with subcutaneous LS174T xenografts (*5*). Furthermore, several

clinical studies with bsMAb and ^{111}In-labelled haptens for pretargeted immuno-SPECT showed high sensitivity (*18-21*). In patients, immuno-SPECT can be used to guide individual treatment, since this imaging modality can be repeated at multiple time points. In a pre-therapy diagnostic cycle, tumour targeting can be demonstrated in an imaging cycle with ^{111}In-labelled peptide, and dosimetric analysis of multiple pre-therapy diagnostic scans can be used to adjust activity doses for subsequent therapy cycles. Furthermore, images can be acquired directly after therapy to observe the distribution of therapeutic injections and calculate their absorbed doses. In the follow-up period after therapy, the effect on disease progression can be evaluated by implementing a diagnostic cycle.
In our institution, a phase I clinical study of pretargeted radioimmunotherapy with TF2 and ^{177}Lu-IMP288 in colorectal cancer patients is ongoing, using pre-therapy diagnostic cycles with TF2 and ^{111}In-IMP288 for dosimetric calculations. Preliminary results of this clinical study for theranostics in PRIT are encouraging. This and other future studies will provide more information on dose-response rates, the predictive value of dosimetry, and how it can contribute to more personalized medicine, or theranostics, in targeted radionuclide therapy.
In conclusion, the present study showed that pretargeted immuno-SPECT with TF2 and ^{111}In- or ^{177}Lu-IMP288 can be used to predict and confirm tumour uptake and monitor the therapeutic effect of pretargeted radioimmunotherapy.

Acknowledgements

We thank Bianca Lemmers-van de Weem, Iris Lamers-Elemans, Henk Arnts, and Jonathan Disselhorst for technical assistance. The work was supported by the Dutch Cancer Society (KWF Kankerbestrijding) grant no. KUN 2008-4038, and National Institutes of Health grant (National Institute of Biomedical Imaging and Bioengineering, R43 EB003751).

References

1. Baum RP, Rosch F. 1 World Congress on Ga-68 and Peptide Receptor Radionuclide Therapy (PRRNT), June 23-26, 2011, Zentralklinik Bad Berka, Germany. World J Nucl Med. Jan 2011;10(1):1-2.
2. Goldenberg DM, Chang C-H, Rossi EA, Mcbride WJ, Sharkey RM. Pretargeted molecular imaging and radioimmunotherapy. Theranostics. 2012.
3. Le Doussal JM, Martin M, Gautherot E, Delaage M, Barbet J. In vitro and in vivo targeting of radiolabeled monovalent and divalent haptens with dual specificity monoclonal antibody conjugates: enhanced divalent hapten affinity for cell-bound antibody conjugate. J Nucl Med. Aug 1989;30(8):1358-1366.
4. Karacay H, McBride WJ, Griffiths GL, et al. Experimental pretargeting studies of cancer with a humanized anti-CEA x murine anti-[In-DTPA] bispecific antibody construct and a (99m)Tc-/(188)Re-labeled peptide. Bioconjug Chem. Nov-Dec 2000;11(6):842-854.

5. Schoffelen R, van der Graaf WT, Franssen G, et al. Pretargeted 177Lu radioimmunotherapy of carcinoembryonic antigen-expressing human colonic tumors in mice. J Nucl Med. Nov 2010;51(11):1780-1787.
6. Sharkey RM, Cardillo TM, Rossi EA, et al. Signal amplification in molecular imaging by pretargeting a multivalent, bispecific antibody. Nat Med. Nov 2005;11(11):1250-1255.
7. Sharkey RM, Karacay H, Vallabhajosula S, et al. Metastatic human colonic carcinoma: molecular imaging with pretargeted SPECT and PET in a mouse model. Radiology. Feb 2008;246(2):497-507.
8. Sharkey RM, McBride WJ, Karacay H, et al. A universal pretargeting system for cancer detection and therapy using bispecific antibody. Cancer Res. Jan 15 2003;63(2):354-363.
9. Griffiths GL, Chang CH, McBride WJ, et al. Reagents and methods for PET using bispecific antibody pretargeting and 68Ga-radiolabeled bivalent hapten-peptide-chelate conjugates. J Nucl Med. Jan 2004;45(1):30-39.
10. Karacay H, Sharkey RM, McBride WJ, Rossi EA, Chang CH, Goldenberg DM. Optimization of hapten-peptide labeling for pretargeted immunoPET of bispecific antibody using generator-produced 68Ga. J Nucl Med. Apr 2011;52(4):555-559.
11. McBride WJ, D'Souza CA, Sharkey RM, et al. Improved 18F labeling of peptides with a fluoride-aluminum-chelate complex. Bioconjug Chem. Jul 21 2010;21(7):1331-1340.
12. Schoffelen R, Sharkey RM, Goldenberg DM, et al. Pretargeted immuno-positron emission tomography imaging of carcinoembryonic antigen-expressing tumors with a bispecific antibody and a 68Ga- and 18F-labeled hapten peptide in mice with human tumor xenografts. Mol Cancer Ther. Apr 2010;9(4):1019-1027.
13. Schoffelen R, van der Graaf WT, Sharkey RM, et al. Pretargeted immuno-PET of CEA-expressing intraperitoneal human colonic tumour xenografts: a new sensitive detection method. EJNMMI Res. Jan 27 2012;2(1):5.
14. McBride WJ, Zanzonico P, Sharkey RM, et al. Bispecific antibody pretargeting PET (immunoPET) with an 124I-labeled hapten-peptide. J Nucl Med. Oct 2006;47(10):1678-1688.
15. Rossi EA, Goldenberg DM, Cardillo TM, McBride WJ, Sharkey RM, Chang CH. Stably tethered multifunctional structures of defined composition made by the dock and lock method for use in cancer targeting. Proc Natl Acad Sci U S A. May 2 2006;103(18):6841-6846.
16. Goldenberg DM, Rossi EA, Sharkey RM, McBride WJ, Chang CH. Multifunctional antibodies by the Dock-and-Lock method for improved cancer imaging and therapy by pretargeting. J Nucl Med. Jan 2008;49(1):158-163.
17. Koppe MJ, Soede AC, Pels W, et al. Experimental radioimmunotherapy of small peritoneal metastases of colorectal origin. Int J Cancer. Oct 10 2003;106(6):965-972.
18. Aarts F, Boerman OC, Sharkey RM, et al. Pretargeted radioimmunoscintigraphy in patients with primary colorectal cancer using a bispecific anticarcinoembryonic antigen CEA X anti-di-diethylenetriaminepentaacetic acid F(ab')2 antibody. Cancer. Feb 15 2010;116(4 Suppl):1111-1117.
19. Barbet J, Peltier P, Bardet S, et al. Radioimmunodetection of medullary thyroid carcinoma using indium-111 bivalent hapten and anti-CEA x anti-DTPA-indium bispecific antibody. J Nucl Med. Jul 1998;39(7):1172-1178.
20. Le Doussal JM, Chetanneau A, Gruaz-Guyon A, et al. Bispecific monoclonal antibody mediated targeting of an indium-111-labeled DTPA dimer to primary colorectal tumors: pharmacokinetics, biodistribution, scintigraphy and immune response. J Nucl Med. Oct 1993;34(10):1662-1671.
21. Chetanneau A, Barbet J, Peltier P, et al. Pretargetted imaging of colorectal cancer recurrences using an 111In-labelled bivalent hapten and a bispecific antibody conjugate. Nucl Med Commun. Dec 1994;15(12):972-980.

6

Development of an imaging-guided CEA-pretargeted radionuclide treatment of advanced colorectal cancer: First clinical results

Rafke Schoffelen[1], Otto C. Boerman[1], David M. Goldenberg[2], Robert M. Sharkey[2], Carla M.L. van Herpen[3], Gerben M. Franssen[1], William J. McBride[4], Chien-Hsing Chang[5], Edmund A. Rossi[5], Winette T.A. van der Graaf[3] and Wim J.G. Oyen[1]

Submitted

[1] Radboud University Nijmegen Medical Centre, dept. of Nuclear Medicine, Nijmegen, Netherlands
[2] Garden State Cancer Center, Morris Plains, New Jersey, USA
[3] Radboud University Nijmegen Medical Centre, dept. of Medical Oncology, Nijmegen, Netherlands
[4] Immunomedics, Inc., Morris Plains, New Jersey, USA
[5] IBC Pharmaceuticals, Morris Plains, New Jersey, USA

Abstract

Background

Radiolabelled antibody targeting of cancer is limited by slow blood clearance. Pretargeting a non-radiolabelled bispecific antibody (bsMAb) followed by a rapidly clearing radiolabelled hapten-peptide improves tumour localization. The primary goals of this first pretargeting study in patients with the anti-CEACAM5 x anti-hapten (HSG) bsMAb, TF2, and the radiolabelled hapten-peptide IMP288, were to assess various pretargeting conditions and safety in patients with metastatic colorectal cancer (CRC).

Methods

Different dose schedules were studied in 4 cohorts of 5 patients (n=21): [1] shortening the interval between the bsMAb and peptide administration (5 days vs 1 day), [2] escalating the TF2 dose (from 75 to 150 mg), and [3] reducing the peptide dose (from 100 to 25 μg). After confirmation of tumour targeting by ^{111}In-IMP288, patients were treated with a bsMAb/^{177}Lu-IMP288 cycle. Toxicity was evaluated according to the NCI-CTC v3.0.

Results

Rapid and selective tumour targeting of the radiolabelled peptide was visualized within 1 h with high tumour-to-tissue ratios (>20 at 24 h). Improved tumour targeting was achieved with a 1-day interval between the administration of the bsMAb and the peptide, with the 25 μg peptide dose. High ^{177}Lu-IMP288 doses were well tolerated with some manageable TF2 infusion reactions, and transient grades 3-4 thrombocytopenia in 10% of the patients who received ^{177}Lu-IMP288.

Conclusions

This phase I radioimmunotherapy study demonstrates for the first time that pretargeting with TF2 anti-CEACAM5 bsMAb and radiolabelled IMP288 in patients with CEA-expressing CRC is feasible and safe. Tumours are specifically and rapidly targeted with limited toxicity.

Introduction

Tumour targeting with monoclonal antibodies is an attractive modality for targeted cancer therapy. For metastatic colorectal cancer (CRC), the anti-VEGF antibody, bevacizumab, and the anti-EGFR antibodies, cetuximab or panitumumab, can improve patient outcome when combined with chemotherapy (*1-7*). Antibodies conjugated with cytotoxic agents, such as drugs or radionuclides, have shown promising results in several indications (*8, 9*). Radiolabelled antibodies have proven effective in patients with non-Hodgkin lymphoma (*10-13*), but, successful adaptation of radioimmunotherapy (RIT) in solid tumours has been challenging (*9*). An ^{131}I-labelled anti-CEACAM5 IgG given as an adjuvant therapy to CRC patients after liver metastasectomy improved survival compared to a comparable contemporaneous group of patients without adjuvant therapy (5-year survival, 42.1% *vs.* 15.8% for RIT *vs.* controls, respectively) (*14, 15*). In addition, a recent clinical trial reporting objective responses and disease control in patients with advanced pancreatic cancer using a fractionated ^{90}Y-labelled antibody to a pancreatic mucin, PAM4, combined with low-dose gemcitabine is another example of promising results in solid tumours (*16*).

However, the slow blood clearance and delayed tumour uptake of directly radiolabelled antibodies causes continuous radiation exposure to the bone marrow and a high background signal, limiting therapeutic dosage. Pretargeting techniques were developed to overcome these deficiencies. With pretargeting, a non-radiolabelled humanized bispecific monoclonal antibody (bsMAb) is administered first intravenously. After the bsMAb localizes in the tumour and clears from the circulation, a smaller, radiolabelled molecule is given that is rapidly trapped in the tumour by the bsMAb, while the remainder clears from the blood very quickly, being eliminated via the kidneys. Pretargeting reduces the radiation exposure to radiosensitive normal tissues, such as bone marrow, as well as other tissues (*17-21*).

In this first-in-man phase I study, we investigated pretargeting with the bsMAb, TF2, for targeting CRC. TF2 is a humanized bsMAb construct, which was produced using the Dock-and-Lock-technology, resulting in a stable humanized tri-Fab molecule (*22*). It contains two Fab fragments with high affinity for CEACAM5 and another Fab-fragment with affinity for the hapten, histamine-succinyl-glycine (HSG). IMP288 is a peptide that contains two HSG moieties to preserve affinity enhancement properties for improved hapten-peptide uptake and retention (*23, 24*), and another moiety capable of stable binding of a radionuclide, in this case 1,4,7,10-tetraazacyclododecane-1,4,7,10-tetraacetic acid (DOTA) for binding ^{90}Y, ^{177}Lu, and ^{111}In (*21, 22, 25, 26*). The rapid and specific targeting of human tumour xenografts and the therapeutic potential of pretargeted, radiolabelled peptides were reported previously (*27-29*). The primary goals of this trial were to evaluate several pretargeting conditions and to assess the safety of pretargeting of CRC with TF2 and radiolabelled IMP288 in patients with metastatic CRC for whom no standard treatment was available.

Methods

Patient eligibility

Patients ≥18 years of age with progressive metastatic CRC for whom no standard treatment was available were enrolled. Eligibility criteria included Eastern Cooperative Oncology Group (ECOG) performance status ≤1, no previous therapies within four weeks (bevacizumab within eight weeks), and adequate hematopoiesis (absolute neutrophil count ≥1.5 x 10^9/L; platelets ≥150 x 10^9/L without transfusion during the previous month; hemoglobin ≥5.6 mmol/L), hepatic (total bilirubin ≤ 2 x ULN (upper limit of normal), aspartate transaminase (AST)/alanine transaminase (ALT) ≤ 3 x ULN) and renal function (serum creatinine ≤ 2 x ULN, Cockcroft clearance > 50 ml/min). Evidence of CEA expression by tissue staining or elevated plasma levels was required. Patients with a life expectancy of less than six months, known brain metastases, or cardiac disease with New York Heart Association classification of III or IV, were excluded.

The regional ethics review committee (CMO Regio Arnhem-Nijmegen) approved the study protocol and amendments. Written informed consent was obtained from all patients. The study was registered at ClinicalTrials.gov (NCT00860860) (*30*).

Study design

Preclinical studies showed successful pretargeting of tumours depends on three factors: the bsMAb dose, the interval between the administration of the antibody and the radiolabelled peptide, and the peptide dose (*28, 31*). Tumour targeting of the radiolabelled hapten-peptide will be affected by [i] the amount bsMAb in the tumour, which should be high enough to capture as much of the radiolabelled peptide as possible and [ii] the bsMAb concentration in the circulation, which should be as low as possible at the time of the radiolabelled hapten-peptide administration to prevent complex formation with the bsMAb in the circulation. This would increase the circulatory half-life of the radiolabelled hapten-peptide, in turn increasing the radiation exposure to normal tissues. Additionally, animal studies showed that increasing the specific activity of the radiolabelled hapten-peptide increases the fraction that targets the tumour (*28*). On the other hand, a low peptide dose may result in a higher fraction of the radiolabelled hapten-peptide dose being captured by circulating bsMAb, which again would result in more immune complex formation of the bsMAb and the radiolabelled peptide in the circulation.

To evaluate these interacting and interdependent factors relevant for tumour targeting, we studied four dose schedules in cohorts of five patients (*Table 1*). First, the effect of the interval between bsMAb and hapten-peptide was studied: cohort 1 received TF2 (75 mg) and IMP288 (100 μg) with a 5-day interval, while cohort 2 received the same doses with a 1-day interval. Bispecific antibody dose also was examined, with cohort 3

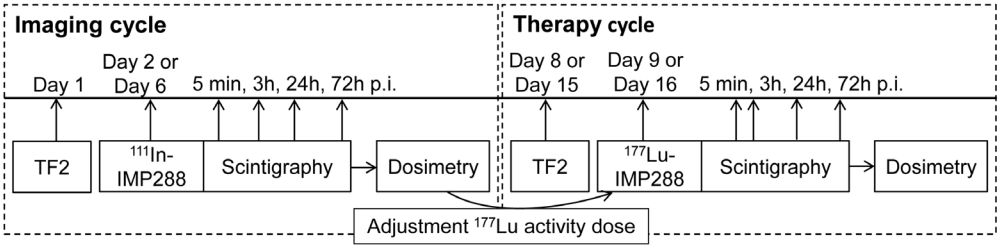

Figure 1: Treatment schedule.
Patients received an imaging cycle with TF2 and ^{111}In-IMP288 to determine the pharmacokinetics and radiation doses to the red bone marrow and kidneys. A safe, cumulative ^{177}Lu-activity dose was estimated, and one-fourth of this amount was administered in the first therapy cycle.

receiving a higher bsMAb dose (150 mg TF2, 1-day interval, 100 μg IMP288). Finally, in cohort 4, a lower IMP288 dose was tested (75 mg TF2, 25 μg IMP288, 1-day interval), with 25 μg being the minimal amount IMP288 required to prepare the maximum amount of administered ^{177}Lu activity (7.4 GBq) per treatment. Patients first underwent a diagnostic imaging cycle with TF2 and ^{111}In-IMP288. If tumour targeting of the radiolabelled peptide was observed, patients received a therapeutic cycle of TF2 and ^{177}Lu-IMP288 the following week (*Figure 1*). By quantitatively analyzing the scintigraphic images and blood pharmacokinetics after the ^{111}In-IMP288 injection, the radiation doses to the kidneys and bone marrow were estimated. The safe starting therapeutic dose of ^{177}Lu-IMP288 was calculated for each patient, being set at a threshold not to exceed a cumulative dose of 1.25 Gy to the bone marrow and 15 Gy to the kidneys. This total dose was then split into four equally divided treatment cycles. Since the nadir of hematologic toxicity after RIT with directly radiolabelled IgG is reached at five to six weeks, each fraction was to be administered every 8 weeks. The maximum allowed dose per cycle was 7.4 GBq, but for safety reasons in the first cohort it was limited to 3.7 GBq.

Table 1: Study design. Four cohorts were evaluated, using two TF2 dose levels, adjusting the interval between bsMAb and peptide administrations from five to one day, and reducing the peptide dose (i.e., increasing specific activity).

Cohort (n=5)	TF2 dose (mg)	Interval (days)	IMP288 dose (μg)
1	75	5	100
2	75	1	100
3	150	1	100
4	75	1	25

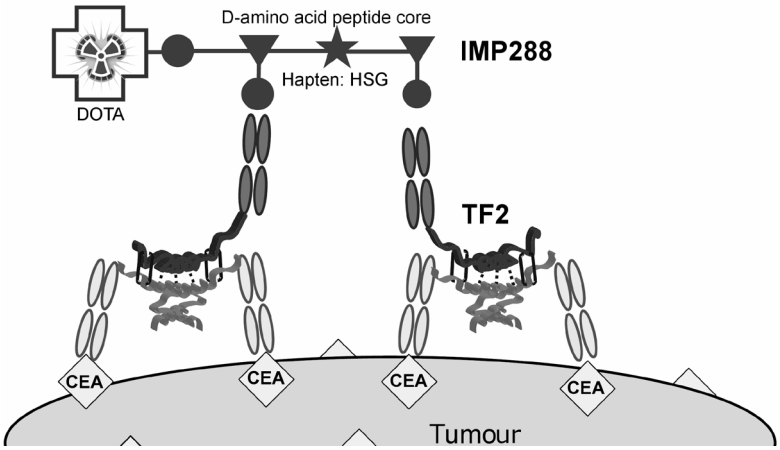

Figure 2: Schematic representation of the pretargeting agents. The trivalent bispecific antibody construct, TF2, binds divalently to CEACAM5, the tumour-associated antigen that is overexpressed on the cell surface of colorectal tumour cells. After the bsMAb has localized the tumour and cleared from the blood, a radiolabelled divalent peptide is given, substituted with the hapten, histamine-succinyl-glycine (HSG). This is rapidly targeted to the tumours and bound by high affinity to the anti-HSG Fab-fragment of the bsMAb. Due to its bivalency, it has the ability to crosslink the bsMAbs at the tumour surface, forming a stable complex. The peptide is conjugated with the chelator, DOTA, which can be labelled with a wide variety of radionuclides.

Investigational drugs

The clinical-grade trivalent anti-CEACAM5 x anti-HSG bsMAb construct, TF2, and the IMP288 hapten-peptide were provided by Immunomedics (Morris Plains, NJ, USA). TF2 (157 kD) is a recombinantly-engineered trivalent bsMAb composed of a humanized anti-histamine-succinyl-glycine (HSG) Fab-fragment derived from the 679 anti-HSG monoclonal antibody, and two humanized anti-CEACAM5 Fab-fragments derived from the humanized anti-CEACAM5 MAb, hMN-14 or labetuzumab (*Figure 2*). The binding characteristics of the bispecific antibody, TF2, were described previously (*22*). IMP288 (molecular weight 1456 Da) was synthesized as described by McBride et al. (*25*).

Preparation and administration of investigational drugs

The TF2 dose (75 or 150 mg) was diluted in 60 mL 0.9% w/v NaCl, and administered by i.v. infusion over a period of two hours. Starting from the second patient of cohort 2, all patients received a prophylactic dose of clemastine (2 mg) i.v. 15 min prior to start of the second TF2 infusion. Dexamethasone, 10 mg i.v., was added subsequently as an additional prophylactic medication prior to the second TF2 infusion, starting from the last patient of cohort 3.

IMP288 was labelled with either ^{111}In, a gamma-emitter, or with ^{177}Lu, a beta-emitter, for imaging or radionuclide therapy, respectively, as described previously (*28*). IMP288 was labelled with ^{111}In (Covidien, Petten, The Netherlands) at a specific activity of 1.9 or 7.4 MBq/μg (2.6 or 10.6 MBq/nmol), or with ^{177}Lu (IDB Holland BV, Baarle Nassau, The Netherlands, and Isotope Technologies Garching GmbH, Garching, Germany) at a specific activity of 37-296 MBq/μg (53-423 MBq/nmol). Radiochemical purity (RCP) of the radiolabelled IMP288 was determined using instant thin-layer chromatography and reverse-phase high-performance liquid chromatography, as described elsewhere (*28*). RCP always exceeded 95%. ^{111} In-IMP288 was dissolved in 10 mL 0.9% NaCl and ^{177}Lu- IMP288 in 20 mL 0.9% NaCl, and administered by an i.v. 2-min bolus.

Pharmacokinetic assessment

TF2 pharmacokinetics were assessed by collecting serum samples after the end of the infusion, and then at 0.5, 1, 2, 4, 6, and 24 h, with the last sample shortly before the IMP288 injection. Serum concentrations were determined with a sandwich enzyme-linked immunosorbent assay (ELISA) assay, using plates coated with an HSG-conjugated peptide coupled to bovine serum albumin. After incubating with dilutions of the patient's serum samples, binding was revealed with an anti-idiotype antibody directed against the humanized anti-CEACAM5 portion of TF2 (*32*).
^{111}In- and ^{177}Lu-IMP288 pharmacokinetics were determined by collecting blood samples 2 minutes, 0.5, 1, 2, 4, 24, and 72 h after injection, and counting in a gamma counter (Wizard, Pharmacia-LKB, Sweden) with standards prepared from the injected products, using appropriate energy windows for the radionuclide used. The percentage of the injected dose per gram tissue (% ID/g) in the blood samples was calculated.

Scintigraphic assessment and analysis

Anterior and posterior whole-body planar scintigraphic images (Siemens Ecam, Hoffmann Estates, IL, USA) were acquired at four time points: within 5 min after the injection of IMP288 and before voiding, 3 h after injection, after voiding, and at 24 h and 72 h. SPECT scans were also taken of regions with ≥1 tumours in the field of view. Radioactivity concentrations were determined by drawing regions of interest at tumours and muscle in the psoas region in the SPECTs that were acquired 24 h after injection of ^{111}In-IMP288. Tumour-to-normal tissue ratios were calculated.

Patient evaluation and follow-up

Toxicity assessment, hematology, clinical biochemistry, physical examination and ECOG performance status were performed at baseline and weekly during follow-up, up to eight weeks after therapy. As a measure for radiation-related renal toxicity,

weekly urinary analysis was performed to monitor proteinuria. Patients were monitored closely during and up to five hours after the TF2 infusions and IMP288 injections. Toxicity was evaluated according to the NCI-Common Terminology Criteria for Adverse Events v3.0 (NCI-CTCAE).

In the present study, no conventional one-drug dose escalation was performed, but four different dose schedules were studied cohort-wise, in which every cohort would ideally lead to a higher tumour-to-normal tissue ratio. Significant toxicities were defined as possibly or probably related to TF2 or ^{111}In-IMP288/^{177}Lu-IMP288 administration: any ≥ grade 3 non-hematologic toxicity, with the exception of nausea, vomiting, and diarrhea; thrombocytes <10 x 10^9/L, grade 4 thrombocytopenia lasting for ≥4 weeks, ≥ grade 3 thrombocytopenia with bleeding; grade 4 neutropenia lasting for ≥7 days, or ≥ grade 3 neutropenia with fever of at least 38.5 °C)

.To evaluate tumour response, a baseline FDG-PET/CT (contrast-enhanced) scan was performed within two weeks before therapy, and eight weeks after the ^{177}Lu-IMP288 injection. Responses were evaluated according to the Response Evaluation Criteria in Solid Tumours (RECIST).

Human-anti-human-antibody (HAHA) measurements

HAHA serum concentrations were determined before each TF2 infusion and up to eight weeks after the last TF2 infusion. HAHA directed against TF2 was measured with a sandwich ELISA assay (Immunomedics, Inc.), adding serial dilution of patient serum TF2-coated plates and then probing with a TF2-horseradish peroxidase conjugate, with binding revealed using o-phenylenediamine dihydrochloride (Sigma). Concentration (ng/mL) of anti-TF2 responses were based on a standard curve using a rat anti-idiotype antibody specific to hMN-14, WI2 (Immunomedics, Inc.) (*33*). The detection limit of the assay is 50 ng/mL, and therefore a positive HAHA was arbitrarily set as any value above this level.

Statistical analysis

Statistical analysis was performed using GraphPad Prism version 5.00 for Windows (GraphPad Software, San Diego, CA). Means and standard deviations were used to describe continuous data, unless stated otherwise. Statistical analysis was performed to compare tumour targeting between the different cohorts, using a non-parametric, two-tailed Mann Whitney test. The level of significance was set at $p<0.05$.

Results

Twenty-one patients were enrolled in the study between July 2009 and July 2011. One patient (patient 1) was withdrawn from the study prior to the ^{177}Lu-IMP288 treatment. He experienced a hypoxia grade 2 during the second TF2 infusion, and therefore the TF2 infusion was discontinued and not restarted.
Baseline characteristics of the patients who received TF2 ^{111}In/^{177}Lu-IMP288 cycles are reported in *Table 2*. Most patients had large tumour loads, with many large lesions in multiple organs. The low estimated red marrow doses allowed administration of high activity doses of ^{177}Lu-IMP288: four, two and three patients in cohort 2, 3 and 4, respectively, received 7.4 GBq. The other patients in cohort 2-4 received ^{177}Lu activity doses ranging from 2.5 to 6.2 GBq to avoid exceeding one-fourth of the maximum cumulative red marrow absorbed dose (1.25 Gy).

Table 2: Patient characteristics. Baseline patient characteristics are described: age, sex, site of primary tumour, sites of diseases at study entry, prior treatments, baseline CEA serum levels, and administered ^{177}Lu activity dose.

Age:	Median (range)	63 (39-76) years
Male/Female:		12/9
Performance score:	0 1	8 (38%) 13 (62%)
Site of primary tumour:	Colon Rectum	15 (71%) 6 (29%)
Site of disease:	Primary Liver Lungs Lymph nodes Bones Soft tissue Peritoneum	8 (38%) 18 (86%) 14 (67%) 8 (38%) 4 (19%) 3 (14%) 1 (5%)
Tumour load:	Baseline sum diameters of all lesions per patient, median (range)	27.6 (9.2-111.0) cm
Prior treatment:	Surgery Chemotherapy Bevacizumab Anti-EGFR therapy External radiotherapy	17 (81%) 21 (100%) 17 (81%) 7 (33%) 6 (29%)
CEA plasma level:	Baseline, median (range)	120 (12-2200) µg/L
Administered ^{177}Lu dose:	Median (range)	5.6 (2.5-7.4) GBq

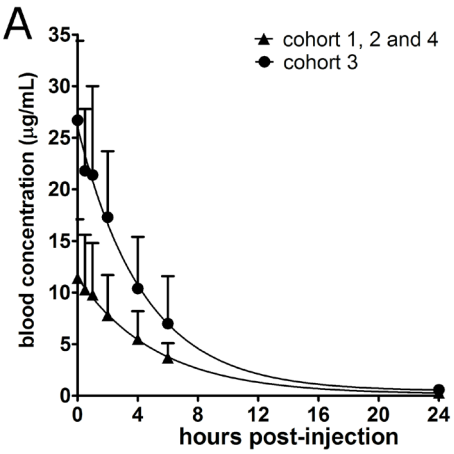

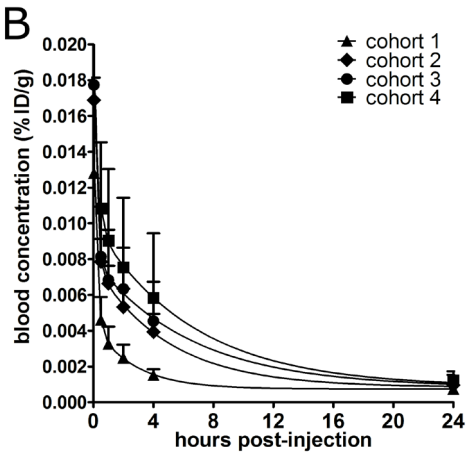

Figure 3: Pharmacokinetics.
A: Serum clearance of TF2 in cohorts 1, 2 and 4, that received 75 mg of TF2, and in cohort 3, 150 mg (mean ± standard deviation; n=5 per cohort), determined by ELISA. TF2 cleared rapidly from the serum, with cohort 3 having twice as high serum concentrations.

B: ^{111}In-IMP288 blood clearance per cohort (mean ± standard deviation; n=5 per cohort). In all cohorts >98% ID was cleared at 24 h p.i, although peptide blood clearance was somewhat delayed by shortening the interval between bsMAb and peptide administration, and to a lesser extent due to a higher antibody and a lower peptide doses.

Pharmacokinetic assessment

TF2 cleared rapidly from the blood, with 86% of the injected dose (ID) eliminated at 6 h after completion of the infusion, and 99% ID after 24 h in all cohorts. TF2 clearance was not related to the CEA plasma level at the time of infusion (data not shown). TF2 concentrations in the blood increased proportionally to the dose administered (*Figure 3A*). Radiolabelled IMP288 cleared the fastest in cohort 1, where the initial interval was 5 days (*Figure 3B*). Because TF2 cleared quickly, the interval was then adjusted to 1 day for cohort 2. In this cohort, the clearance rate of IMP288 slowed, but it was still very rapid. As conditions changed so the amount of TF2 in the serum at the time IMP288 was injected increased or the peptide dose was reduced, IMP288 clearance gradually slowed. For example, IMP288 concentrations were twice as high in cohort 3 that received 150 mg *vs* 75 mg in cohort 2 (*Figure 3B*). Overall, most of the administered activity cleared from the blood at 24 h post-injection in all cohorts (100%, 99%, 98% and 98% ID, cohorts 1-4, respectively).

Scintigraphic imaging analysis

In all patients, the ^{111}In-IMP288 images showed clear and selective targeting of known tumour lesions, and thus all patients were eligible to receive a therapeutic TF2/^{177}Lu-IMP288 cycle. Primary tumours, as well as metastases in the lungs, liver, lymph nodes,

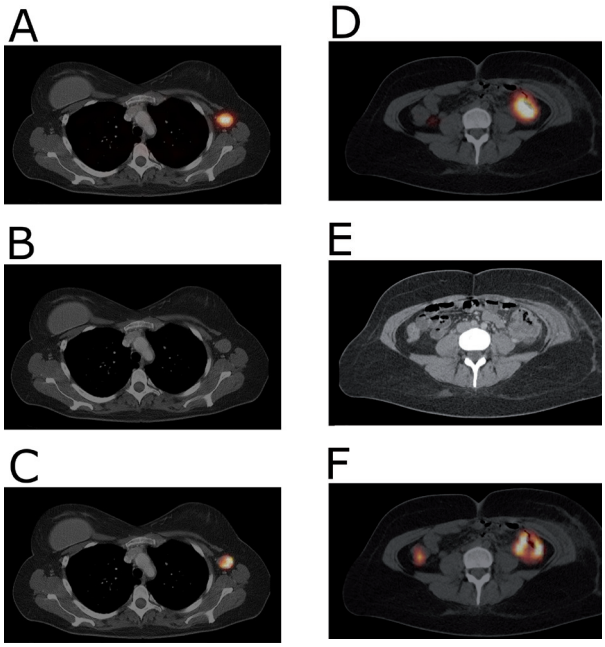

Figure 4: Scintigraphic images. The SPECT/CT image (A), acquired 24 h after injection of ^{111}In-IMP288 (185 MBq, 25 μg), pretargeted with 75 mg TF2 (1-day interval), in a 38-year-old patient (cohort 4), shows very clear tumour targeting of an axillary lymph node metastasis, with very low concentrations of radioactivity in normal tissues. Corresponding contrast-enhanced CT scan and a fused FDG-PET/CT scan are shown (B and C, respectively). The primary colon tumour (50 cm ab ano) also shows highly specific tumour targeting in the SPECT-image (D), confirmed by the CT-scan and FDG-PET/CT (E and F, respectively), with non-specific FDG-uptake in the ascending colon.

and soft tissue, were visualized as early as one hour after injection. Representative images of patient 21 in cohort 4 are shown in *Figure 4*.

The pre-therapy ^{111}In-scans and the post-therapy ^{177}Lu-scans were congruent, with somewhat stronger signal in the ^{177}Lu-scans due to higher levels of activity given. After one day, most activity had cleared from the normal tissues, with very limited retention in the kidneys, resulting in high tumour-to-normal tissue ratios (>20:1 at 24 h) in all cohorts (*Table 3*). Although highly variable between patients, liver metastases had higher uptake of the radiolabelled peptide than lung metastases. Shortening the interval between the bsMAb and peptide administration in cohort 2 resulted in significantly higher absolute activity concentrations in all tumours compared to cohort 1 (p=0.0079) and in higher tumour-to-normal tissue ratios (p=0.046). Furthermore, all patients in cohort 4 with liver metastases (n=3) appeared to have higher tumour activity concentrations (6.3, 9.7, 23.6 %ID/kg) and tumour-to-normal tissue ratios (33, 38, 84) than the patients in cohort 2 with liver metastases (n=4) (tumour activity concentrations: 3.2, 4.7, 5.4, 5.7 %ID/kg, and tumour-to-normal tissue ratios: 20, 24, 27, 29 at 24 h p.i.), indicating improved tumour targeting at the lower peptide dose (25 μg *vs.* 100 μg) due to a higher specific activity, although this was not statistically different (p=0.057).

Overall, the combined effect of shortening the interval and reducing the peptide dose resulted in significantly higher tumour activity concentrations and tumour-to-normal tissue ratios (cohort 1 *vs* cohort 4, p=0.0079 and p=0.035, respectively).

Table 3: Tumour targeting. Pretargeting conditions were varied in four cohorts: adjusting the interval between the bsMAb and peptide administration, escalating the bsMAb dose, and reducing the peptide dose. This resulted in improved tumour activity concentrations and tumour-to-normal tissue ratios. The uptake of ^{111}In-IMP288 in tumour and muscle tissue was determined with SPECT 24 h post injection of the radiolabelled peptide.

		bsMAb dose / interval / peptide dose			
		75 mg /5 days/ 100 µg Cohort 1	75 mg/1 day/ 100 µg Cohort 2	150 mg/1 day/ 100 µg Cohort 3	75 mg/1 day/ 25 µg Cohort 4
Activity concentration (%ID/kg, mean (range))	Tumour	1.4 (0.8-2.0)	4.4 (2.7-5.7)	5.9 (3.1-10.4)	9.4 (2.2-23.6)
	Normal tissue	0.068 (0.042-0.093)	0.18 (0.12-0.24)	0.19 (0.08-0.31)	0.21 (0.10-0.28)
Tumour-to-normal tissue ratio (mean (range))		20 (17-22)	24 (20-29)	32 (22-43)	40 (21-84)

Efficacy, safety, and tolerability

According to RECIST based on the FDG-PET/contrast-enhanced CT scans prior to therapy and eight weeks after therapy, all patients showed progressive disease eight weeks after the first therapy cycle with TF2 and ^{177}Lu-IMP288, and therefore none of the patients was eligible for a second treatment cycle. Thus, only the safety and tolerability of just one of the four planned treatment cycles can be reported.

Toxicity was limited in most patients, with no apparent differences between cohorts (*Table 4*). The majority of the patients with liver metastases had liver enzyme elevations prior to drug administrations (e.g., 43% had grade 3-4 GGT elevation at baseline). In many patients, GGT increased during the trial, which was deemed to be disease-related, since all patients had progression of liver metastases, as seen on the FDG-PET/CT-scans.

Seven patients (33%) experienced a mild grade 2 infusion reaction during onset of their second TF2 infusion. They experienced flushes, dyspnea, chest pain, back pain or coughing. They did not have cutaneous, cardiovascular or gastrointestinal signs or symptoms. All reactions were easily controlled by interrupting the infusion, and with intravenous administration of clemastine (2 mg) and dexamethasone (10 mg). Except for patient 1, with grade 2 hypoxia, the infusion was restarted in all patients at a slower infusion rate for fifteen minutes, and could be completed at the planned infusion rate without any recurrence of symptoms. After three infusion reactions (from patient 8), prophylactic intravenous clemastin (2 mg) was added prior to the patients' second TF2 infusion. After patient 15, prophylactic intravenous dexamethasone (10 mg) was added. With this regimen, infusion reactions occurred in 2 out of 5 patients, but the TF2 infusions could be completed as described above.

Following the single therapy cycle, bone marrow toxicity was mild in most patients (grade 1-2 in 30% of patients). More severe hematological toxicity (grade 3-4 throm-

Table 4: Toxicity. All grade 2, 3 and 4 toxicities, as well related and unrelated, scored according to the Common Terminology Criteria for Adverse Events (CTCAE v3.0) (n=21).

		Grade			Total of grade 2-4
		2	3	4	
Category	Adverse event	(No. of patients)			(%)
Blood/ bone marrow	Platelets	1	1	1	14
	Lymphocytopenia	1	2		14
	Haemoglobin	2	1		19
Syndromes	Acute infusion-related reaction	7			33
Constitutional symptoms	Fatigue	4			19
	Fever	1			5
	Sweating	1			5
Pulmonary	Dyspnoea	1	1		10
Gastrointestinal	Nausea	1			5
	Anorexia	4			19
	Diarrhea		2		10
Pain	Abdomen	3	1		19
	Tumour	1			5
Neurology	Somnolence	2			10
	Pyramidal tract dysfunction°	1			5
Infection	Biliary tree‡		1		5
Musculoskeletal	Arthritis (non-septic)	1			5
Renal	Urinary frequency	1			5
Metabolic/ laboratory	AST	4	1		24
	ALT	2	1		14
	Bilirubin	1	2		14
	Albumin, serum-low	6			29
	Alkaline phosphatase	5	5		48
	GGT	4	7	3	67

‡liver metastases with biliary tract obstruction confirmed by PET/CT
° brain metastases confirmed by MRI-cerebrum

bocytopenia, and grade 3 lymphopenia) occurred in two patients (10%; 1 in cohort 2 and 1 in cohort 3), with the nadir 5-6 weeks after ^{177}Lu-administration. Recovery was rapid, returning to grade ≤ 1 level at 7-8 weeks after therapy. None of these patients had complications or needed intervention. None of the patients showed signs or symptoms of renal toxicity.

One patient (in cohort 3) was admitted to the hospital due to severe dyspnea four days after the administration of ^{177}Lu-IMP288. High-resolution CT of the chest was unremarkable, lung function tests were normal and blood or sputum cultures, as well as viral serology, remained negative. The event was reported as probably related to the drug administrations, either TF2 or ^{177}Lu-IMP288, and thus recorded as a Suspected Unexpected Serious Adverse Reaction (SUSAR). The patient's dyspnea decreased, but remained at a lower level, which might have been related to rapid progression of disease, since this patient had progressive lung metastases.

HAHA measurements

Human antibodies against TF2 >50 ng/mL were detected in 11 of 21 patients, starting one week after the second TF2 infusion, gradually increasing in the follow-up period of eight weeks, indicating that the humanized trivalent bsMAb TF2 was immunogenic in ~50% of the patients upon repeated injection, but without clinical sequelae. Titers varied widely amongst patients (mean 386 ng/mL, range 53-800 ng/mL).

Discussion

Pretargeting was developed to improve the efficacy of tumour targeting with monoclonal antibodies. Recently, Kraeber-Bodéré et al. reported the efficacy of pretargeted RIT with an ^{131}I-di-DTPA-peptide (1.9-5.5 GBq) in patients with medullary thyroid carcinoma (*34, 35*). In this study, a survival benefit was observed compared with a historical untreated control group (*36*).

The pretargeting system described in this study, with the new bsMAb construct TF2, and HSG-substituted hapten-peptide IMP288 (*21, 22*), can utilized various chelating moieties (DTPA, NOTA, DOTA, N_3S-chelates, etc.) and radionuclides for PET or SPECT imaging (*25, 26, 37, 38*), or for pretargeted radioimmunotherapy (*27, 28, 31, 39*). Accurate dosing of the bsMAb and the radiolabelled peptide was demonstrated to be crucial for improved tumour targeting (*28*).

In this first-in-man pretargeting study with the new bsMAb construct, TF2, and ^{111}In/^{177}Lu-labelled IMP288, we showed that pretargeting provided rapid and efficient targeting of CEACAM5-expressing tumours with low normal tissue activity levels. The main objective of this study was to evaluate several dosing conditions to assess their effect on biodistribution and tumour targeting. The starting interval of 5 days was selected based on blood clearance studies of TF2 in rabbits (*32*), but when it became clear that TF2 cleared rapidly in humans, the interval was reduced to one day. The blood clearance of TF2 was much faster than that of similarly-sized IgG molecules (157 kD and 150 kD, respectively), which could be explained by the fact that TF2 lacks a C_H2 domain (*40, 41*). In nude mouse-human tumour xenograft models, an interval of 16-24 h was favorable, also because the bsMAb cleared very quickly from the blood (>99% cleared) (*28, 31*). In addition, TF2's peak tumour uptake occurred ~6 h postinjection in these models, decreasing gradually over time, and thus minimizing the interval allowed the hapten-peptide to be captured when more bsMAb is present in the tumour.

Overall, we found that reducing the interval and the IMP288 dose improved tumour targeting. Higher bsMAb doses also can enhance tumour uptake of the radiolabelled peptide (*26, 28*). While we did not observe improved tumour uptake by increasing the TF2 dose 2-fold at a 1-day interval (75 to 150 mg), these patients all had considerable tumour burden, suggesting that higher bsMAb doses could further improve tumour

targeting. However, we did observe a trend toward increased tumour uptake using 75 mg of TF2 when the IMP288 dose was lowered from 100 to 25 μg. Thus, further studies need to be performed before we are able to select the most appropriate set of conditions for pretargeting.

This study demonstrated the safety of pretargeted RIT with TF2 at doses of ^{177}Lu-IMP288 ranging from 3.7 to 7.4 GBq. The immune responses, i.e., symptomatic infusion reactions and the formation of anti-TF2 antibodies that were observed following the administration of the 2nd TF2 infusion, were unexpected, since TF2 is a humanized antibody construct. Murine precursors of anti-CEA bsMAb frequently showed immune responses (*42, 43*), which was reduced by using chimeric and humanized antibodies (*34*). However, the mild, grade 2, acute infusion related reactions that were observed in one-third of the patients at the second infusion of the humanized bsMAb did not preclude continuation of treatment, except for one patient who had extensive pulmonary metastases. We expect that reducing the infusion rate and the pre-administration of prophylactic antihistamines and corticosteroids will reduce this adverse event, and this is advised for future studies. The human antibodies against TF2 detected in half the patients were not yet present at the time of the second TF2 infusion (i.e., therapy cycle), so the TF2 pharmacokinetics was not affected. No correlation was found between the infusion reactions and the anti-TF2 antibody titers that started to increase only one week after the second TF2 infusion. In future studies, treatment should be more condensed to prevent accelerated TF2 blood clearance due to the presence of HAHA in part of the patients at subsequent cycles.

Overall, hematological toxicity of pretargeted RIT was minimal, particularly when considering that these patients all had received several lines of chemotherapy and up to 7.4 GBq of ^{177}Lu-IMP288. The two patients with transient grade $\geq$ 3 bone marrow toxicity had a somewhat higher bone marrow absorbed dose after administration of ^{177}Lu-IMP288. However, the radiation dose to the red marrow was very low, and therefore we suspect that underlying patient specific factors (age, performance status, effects of prior treatments on hematopoietic stem cell reserve) likely contributed to these toxicities. The dosimetric analysis has been reported previously (*44*), and will be described in more detail elsewhere.

The only unexpected major toxicity was severe dyspnea in one patient four days post TF2 infusion. However, several other reasons might have contributed to the adverse event, such as very high CEA serum levels, pre-existing pulmonary atelectases, and prior cardiac history. Since we could not identify the exact pathophysiological or immunological mechanism, it is unclear if this single case represents a truly drug-related adverse event. Of note, this patient appeared to have rapidly progressive disease and died within 14 weeks after study entry.

This trial was designed with the intent to administer high levels of ^{177}Lu-IMP288 using dosimetry to predict a safe dose. The radiolabelled hapten-peptide used in pretargeting can be viewed in a similar manner as radiolabelled peptides that are being used to treat neuroendocrine tumours (*45*) where dosimetry has gained a role in predicting the

potential for renal toxicity. In our protocol design, we determined the total therapeutic dose based on a pre-therapy imaging study and using conservative estimates of the red marrow and renal doses that should not be exceeded. However, for further safety, this total dose was to be split into four fractions, allowing sufficient time between each treatment to monitor toxicity, primarily hematological toxicity. Unfortunately our study population had extensive metastatic disease, and thus all patients showed disease progression at first evaluation eight weeks after the first therapy cycle with TF2 and ^{177}Lu-IMP288, before subsequently planned additional treatment cycles could be given.

Previously, RIT has been shown to be more effective in small-volume disease (*14, 15, 46*), but the phase I character of the current study prevented us from studying pretargeted RIT in a less heavily pretreated patient population. Recent clinical data in patients with advanced pancreatic cancer suggest a fractionated dosing regimen using a ^{90}Y-labelled antibody given in combination with low-dose (radiosensitizing) gemcitabine can provide disease control and even objective responses (*16*), giving credibility to pursuing ^{90}Y instead of ^{177}Lu for patients with advanced metastatic disease. Indeed ^{90}Y's physical half-life (64 h) matches the residence time in the tumour better than ^{177}Lu-IMP288 (6.7 days).

In conclusion, the results of this phase I clinical study with pretargeted RIT showed rapid and specific tumour targeting of the anti-CEA x anti-HSG bsMAb TF2 and the ^{111}In- or ^{177}Lu-hapten-peptide IMP288. Tumour targeting was improved by shortening the interval between the bsMAb and peptide administration, and by lowering the peptide dose. The procedure is safe, and infusion reactions are transient and manageable with appropriate medication and lowering the infusion rate. Further studies will be needed to determine if improvements in targeting can be obtained by additional adjustments to the pretargeting conditions, as well as revising the protocol design to allow full treatment to be given over a shorter duration, most likely retaining a fractionated regimen. Continuation with ^{177}Lu-IMP288 would be warranted for patients with less bulky disease.

References

1. Amado RG, Wolf M, Peeters M, et al. Wild-type KRAS is required for panitumumab efficacy in patients with metastatic colorectal cancer. *J Clin Oncol.* Apr 1 2008;26(10):1626-1634.
2. Bokemeyer C, Bondarenko I, Makhson A, et al. Fluorouracil, leucovorin, and oxaliplatin with and without cetuximab in the first-line treatment of metastatic colorectal cancer. *J Clin Oncol.* Feb 10 2009;27(5):663-671.
3. Giantonio BJ, Catalano PJ, Meropol NJ, et al. Bevacizumab in combination with oxaliplatin, fluorouracil, and leucovorin (FOLFOX4) for previously treated metastatic colorectal cancer: results from the Eastern Cooperative Oncology Group Study E3200. *J Clin Oncol.* Apr 20 2007;25(12):1539-1544.
4. Hurwitz H, Fehrenbacher L, Novotny W, et al. Bevacizumab plus irinotecan, fluorouracil, and leucovorin for metastatic colorectal cancer. *N Engl J Med.* Jun 3 2004;350(23):2335-2342.
5. Saltz LB, Clarke S, Diaz-Rubio E, et al. Bevacizumab in combination with oxaliplatin-based chemotherapy

as first-line therapy in metastatic colorectal cancer: a randomized phase III study. *J Clin Oncol.* Apr 20 2008;26(12):2013-2019.
6. Tol J, Koopman M, Cats A, et al. Chemotherapy, bevacizumab, and cetuximab in metastatic colorectal cancer. *N Engl J Med.* Feb 5 2009;360(6):563-572.
7. Van Cutsem E, Kohne CH, Hitre E, et al. Cetuximab and chemotherapy as initial treatment for metastatic colorectal cancer. *N Engl J Med.* Apr 2 2009;360(14):1408-1417.
8. Govindan SV, Goldenberg DM. New antibody conjugates in cancer therapy. *ScientificWorldJournal.* 2010;10:2070-2089.
9. Sharkey RM, Goldenberg DM. Cancer radioimmunotherapy. *Immunotherapy.* Mar 2011;3(3):349-370.
10. Gordon LI, Witzig T, Molina A, et al. Yttrium 90-labeled ibritumomab tiuxetan radioimmunotherapy produces high response rates and durable remissions in patients with previously treated B-cell lymphoma. *Clin Lymphoma.* Sep 2004;5(2):98-101.
11. Wiseman GA, Gordon LI, Multani PS, et al. Ibritumomab tiuxetan radioimmunotherapy for patients with relapsed or refractory non-Hodgkin lymphoma and mild thrombocytopenia: a phase II multicenter trial. *Blood.* Jun 15 2002;99(12):4336-4342.
12. Witzig TE, Flinn IW, Gordon LI, et al. Treatment with ibritumomab tiuxetan radioimmunotherapy in patients with rituximab-refractory follicular non-Hodgkin's lymphoma. *J Clin Oncol.* Aug 1 2002;20(15):3262-3269.
13. Witzig TE, Gordon LI, Cabanillas F, et al. Randomized controlled trial of yttrium-90-labeled ibritumomab tiuxetan radioimmunotherapy versus rituximab immunotherapy for patients with relapsed or refractory low-grade, follicular, or transformed B-cell non-Hodgkin's lymphoma. *J Clin Oncol.* May 15 2002;20(10):2453-2463.
14. Liersch T, Meller J, Bittrich M, Kulle B, Becker H, Goldenberg DM. Update of carcinoembryonic antigen radioimmunotherapy with (131)I-labetuzumab after salvage resection of colorectal liver metastases: comparison of outcome to a contemporaneous control group. *Ann Surg Oncol.* Sep 2007;14(9):2577-2590.
15. Liersch T, Meller J, Kulle B, et al. Phase II trial of carcinoembryonic antigen radioimmunotherapy with 131I-labetuzumab after salvage resection of colorectal metastases in the liver: five-year safety and efficacy results. *J Clin Oncol.* Sep 20 2005;23(27):6763-6770.
16. Ocean AJ, Pennington KL, Guarino MJ, et al. Fractionated radioimmunotherapy (RAIT) with 90Y-clivatuzumab tetraxetan (90Y-hPAM4) and low-dose gemcitabine is active in advanced pancreatic cancer: A phase I trial *Cancer* In press.
17. Reardan DT, Meares CF, Goodwin DA, et al. Antibodies against metal chelates. *Nature.* Jul 18-24 1985;316(6025):265-268.
18. Boerman OC, van Schaijk FG, Oyen WJ, Corstens FH. Pretargeted radioimmunotherapy of cancer: progress step by step. *J Nucl Med.* Mar 2003;44(3):400-411.
19. Chang CH, Sharkey RM, Rossi EA, et al. Molecular advances in pretargeting radioimunotherapy with bispecific antibodies. *Mol Cancer Ther.* May 2002;1(7):553-563.
20. Sharkey RM, Cardillo TM, Rossi EA, et al. Signal amplification in molecular imaging by pretargeting a multivalent, bispecific antibody. *Nat Med.* Nov 2005;11(11):1250-1255.
21. Goldenberg DM, Rossi EA, Sharkey RM, McBride WJ, Chang CH. Multifunctional antibodies by the Dock-and-Lock method for improved cancer imaging and therapy by pretargeting. *J Nucl Med.* Jan 2008;49(1):158-163.
22. Rossi EA, Goldenberg DM, Cardillo TM, McBride WJ, Sharkey RM, Chang CH. Stably tethered multifunctional structures of defined composition made by the dock and lock method for use in cancer targeting. *Proc Natl Acad Sci U S A.* May 2 2006;103(18):6841-6846.
23. Karacay H, McBride WJ, Griffiths GL, et al. Experimental pretargeting studies of cancer with a humanized anti-CEA x murine anti-[In-DTPA] bispecific antibody construct and a (99m)Tc-/(188)Re-labeled peptide. *Bioconjug Chem.* Nov-Dec 2000;11(6):842-854.
24. Le Doussal JM, Martin M, Gautherot E, Delaage M, Barbet J. In vitro and in vivo targeting of radiolabeled monovalent and divalent haptens with dual specificity monoclonal antibody conjugates: enhanced divalent hapten affinity for cell-bound antibody conjugate. *J Nucl Med.* Aug 1989;30(8):1358-1366.
25. McBride WJ, Zanzonico P, Sharkey RM, et al. Bispecific antibody pretargeting PET (immunoPET) with an 124I-labeled hapten-peptide. *J Nucl Med.* Oct 2006;47(10):1678-1688.
26. Schoffelen R, Sharkey RM, Goldenberg DM, et al. Pretargeted immuno-positron emission tomography im-

aging of carcinoembryonic antigen-expressing tumors with a bispecific antibody and a ^{68}Ga- and ^{18}F-labeled hapten peptide in mice with human tumor xenografts. *Mol Cancer Ther.* Apr 2010;9(4):1019-1027.
27. Karacay H, Sharkey RM, Gold DV, et al. Pretargeted radioimmunotherapy of pancreatic cancer xenografts: TF10-90Y-IMP-288 alone and combined with gemcitabine. *J Nucl Med.* Dec 2009;50(12):2008-2016.
28. Schoffelen R, van der Graaf WT, Franssen G, et al. Pretargeted 177Lu radioimmunotherapy of carcinoembryonic antigen-expressing human colonic tumors in mice. *J Nucl Med.* Nov 2010;51(11):1780-1787.
29. Sharkey RM, Karacay H, Litwin S, et al. Improved therapeutic results by pretargeted radioimmunotherapy of non-Hodgkin's lymphoma with a new recombinant, trivalent, anti-CD20, bispecific antibody. *Cancer Res.* Jul 1 2008;68(13):5282-5290.
30. www.clinicaltrials.gov/ct2/results?term=NCT00860860
31. Sharkey RM, Karacay H, Richel H, et al. Optimizing bispecific antibody pretargeting for use in radioimmunotherapy. *Clin Cancer Res.* Sep 1 2003;9(10 Pt 2):3897S-3913S.
32. Sharkey RM, Rossi EA, McBride WJ, Chang CH, Goldenberg DM. Recombinant bispecific monoclonal antibodies prepared by the dock-and-lock strategy for pretargeted radioimmunotherapy. *Semin Nucl Med.* May 2010;40(3):190-203.
33. Losman MJ, Novick KE, Goldenberg DM, Monestier M. Mimicry of a carcinoembryonic antigen epitope by a rat monoclonal anti-idiotype antibody. *Int J Cancer.* Feb 15 1994;56(4):580-584.
34. Kraeber-Bodere F, Faivre-Chauvet A, Ferrer L, et al. Pharmacokinetics and dosimetry studies for optimization of anti-carcinoembryonic antigen x anti-hapten bispecific antibody-mediated pretargeting of Iodine-131-labeled hapten in a phase I radioimmunotherapy trial. *Clin Cancer Res.* Sep 1 2003;9(10 Pt 2):3973S-3981S.
35. Kraeber-Bodere F, Rousseau C, Bodet-Milin C, et al. Targeting, toxicity, and efficacy of 2-step, pretargeted radioimmunotherapy using a chimeric bispecific antibody and 131I-labeled bivalent hapten in a phase I optimization clinical trial. *J Nucl Med.* Feb 2006;47(2):247-255.
36. Chatal JF, Campion L, Kraeber-Bodere F, et al. Survival improvement in patients with medullary thyroid carcinoma who undergo pretargeted anti-carcinoembryonic-antigen radioimmunotherapy: a collaborative study with the French Endocrine Tumor Group. *J Clin Oncol.* Apr 10 2006;24(11):1705-1711.
37. Griffiths GL, Chang CH, McBride WJ, et al. Reagents and methods for PET using bispecific antibody pretargeting and 68Ga-radiolabeled bivalent hapten-peptide-chelate conjugates. *J Nucl Med.* Jan 2004;45(1):30-39.
38. Koppe MJ, Bleichrodt RP, Soede AC, et al. Biodistribution and therapeutic efficacy of (125/131)I-, (186)Re-, (88/90)Y-, or (177)Lu-labeled monoclonal antibody MN-14 to carcinoembryonic antigen in mice with small peritoneal metastases of colorectal origin. *J Nucl Med.* Jul 2004;45(7):1224-1232.
39. Sharkey RM, McBride WJ, Karacay H, et al. A universal pretargeting system for cancer detection and therapy using bispecific antibody. *Cancer Res.* Jan 15 2003;63(2):354-363.
40. Chinn PC, Morena RA, Santoro DA, et al. Pharmacokinetics and tumor localization of (111)in-labeled HuCC49DeltaC(H)2 in BALB/c mice and athymic murine colon carcinoma xenograft. *Cancer Biother Radiopharm.* Apr 2006;21(2):106-116.
41. Ghetie V, Ward ES. FcRn: the MHC class I-related receptor that is more than an IgG transporter. *Immunol Today.* Dec 1997;18(12):592-598.
42. Kraeber-Bodere F, Bardet S, Hoefnagel CA, et al. Radioimmunotherapy in medullary thyroid cancer using bispecific antibody and iodine 131-labeled bivalent hapten: preliminary results of a phase I/II clinical trial. *Clin Cancer Res.* Oct 1999;5(10 Suppl):3190s-3198s.
43. Vuillez JP, Kraeber-Bodere F, Moro D, et al. Radioimmunotherapy of small cell lung carcinoma with the two-step method using a bispecific anti-carcinoembryonic antigen/anti-diethylenetriaminepentaacetic acid (DTPA) antibody and iodine-131 Di-DTPA hapten: results of a phase I/II trial. *Clin Cancer Res.* Oct 1999;5(10 Suppl):3259s-3267s.
44. Schoffelen R, Boerman, O.B., van der Graaf, W.T.A., van Herpen, C.M.L., McBride W.J., Chang, C-H., Rossi, E.A., Goldenberg, D.M., Oyen, W.J.G. Phase I clinical study of the feasibility of pretargeted radioimmunotherapy (PT-RAIT) in patients with colorectal cancer (CRC): First results. . *J Nucl Med.* Vol 52; 2011.
45. Baum RP, Rosch F. 1 World Congress on Ga-68 and Peptide Receptor Radionuclide Therapy (PRRNT), June 23-26, 2011, Zentralklinik Bad Berka, Germany. *World J Nucl Med.* Jan 2011;10(1):1-2.
46. Jain RK. Physiological barriers to delivery of monoclonal antibodies and other macromolecules in tumors. *Cancer Res.* Feb 1 1990;50(3 Suppl):814s-819s.

7

Predictive patient-specific dosimetry and individualized dosing of pretargeted radioimmunotherapy in patients with advanced colorectal cancer

Rafke Schoffelen[1], Wietske van der Weg[1], Eric P. Visser[1], David M. Goldenberg[2], Robert M. Sharkey[2], William J. McBride[3], Chien-Hsing Chang[4], Edmund A. Rossi[4], Winette T.A. van der Graaf[5], Wim J.G. Oyen[1] and Otto C. Boerman[1]

Submitted

[1] Radboud University Nijmegen Medical Centre, dept. of Nuclear Medicine, Nijmegen, Netherlands
[2] Garden State Cancer Center, Morris Plains, New Jersey, USA
[3] Immunomedics, Inc., Morris Plains, New Jersey, USA
[4] IBC Pharmaceuticals, Morris Plains, New Jersey, USA
[5] Radboud University Nijmegen Medical Centre, dept. of Medical Oncology, Nijmegen, Netherlands

Abstract

Background

Pretargeted radioimmunotherapy (PRIT) with bispecific monoclonal antibodies (bsMAb) and a radiolabelled peptide reduces the radiation dose to normal tissues. Here, we report the accuracy of an ^{111}In-labelled pre-therapy scout dose for personalized dosing and prediction of radiation dose of PRIT with the anti-CEA x anti-hapten bsMAb TF2 and the ^{177}Lu-labelled hapten-peptide IMP288 in a phase I study in metastatic colorectal cancer (CRC) patients.

Methods

Twenty patients received an imaging cycle with TF2 and ^{111}In-IMP288 followed by PRIT with TF2 and ^{177}Lu-IMP288. Absorbed doses to bone marrow and kidneys were predicted based on blood samples and scintigrams acquired after ^{111}In-IMP288 injection, and individual ^{177}Lu activity doses were determined. Different dose schedules were studied varying the interval between the bsMAb and peptide administration (5 days vs 1 day), increasing the bsMAb dose (75 mg vs 150 mg), and lowering the peptide dose (100 μg vs 25 μg). Toxicity was scored using NCI-CTC v3.0.

Results

TF2 and ^{111}In/^{177}Lu-IMP288 clearance was highly variable, although a strong correlation was observed between peptide residence times and individual TF2 blood concentrations at the time of peptide injection (Spearman's ρ=0.94, $p<0.0001$). Specific tumour uptake of ^{111}In/^{177}Lu-IMP288 was visualized as early as 1 h p.i. High tumour-to-background ratios were observed. Therapeutic ^{177}Lu activity doses resulted in low absorbed radiation doses to normal tissues (red bone marrow <0.5 Gy, kidneys <3 Gy). In the majority of patients who received 7.4 GBq or adjusted ^{177}Lu activity doses, red marrow doses did not exceed 0.31 Gy as predicted (11/13, 85%). Simulated ^{177}Lu-IMP288 absorbed red marrow doses were in good agreement with the actual measured doses (mean difference -0.0026 mGy/MBq, SD 0.028 mGy/MBq). Hematologic toxicity was mild in most patients, with only two cases (10%) of grade 3-4 thrombocytopenia. Most importantly, platelet toxicity correlated significantly with red marrow dose (Spearman's ρ=0.58, $p=0.008$).

Conclusion

These results show that individual high therapeutic activity doses in pretargeted radioimmunotherapy in patients with CEA-expressing CRC could be safely administered, by predicting the radiation dose to red marrow and kidneys based on dosimetric analysis of a scout dose of TF2 and ^{111}In-IMP288.

Introduction

Selective targeting of tumour-associated antigens with radiolabelled antibodies can be used for diagnosis and therapy of cancer. In combining imaging with treatment, a concept designated as theranostics, targeted radionuclide therapies can be personalized. For example, diagnostic information obtained from pre-therapeutic PET or SPECT, can be used to predict the efficacy of the treatment. In this way, patients can be selected for radioimmunotherapy by estimating the probability of tumour control versus the risk of toxicity of a planned treatment. This analysis might also aid in identifying the most appropriate radionuclide (^{90}Y, ^{177}Lu, ^{213}Bi, etc.) to deliver the therapeutic dose to ensure that the patient receives a unique dose optimized for their radionuclide therapy (^{90}Y, ^{177}Lu, ^{213}Bi, etc.). Finally, imaging data could potentially assess therapeutic response. The feasibility of this approach has been demonstrated in patients with neuroendocrine tumours using ^{111}In- or ^{68}Ga-labelled somastatin analogues for diagnosis and the same peptides labelled with ^{177}Lu- or ^{90}Y for radionuclide therapy (*1, 2*). In this clinical study, the potential of theranostics for combined pretargeted radioimmunoscintigraphy and –therapy was evaluated. Pretargeting is a strategy that was developed to improve the imaging and therapeutic characteristics of directly radiolabelled monoclonal antibodies. Radiolabelled antibodies require several days to effectively target tumours, due to the slow pharmacokinetics and slow accretion of intact antibodies in tumours. This slow uptake and clearance rate delays the optimal timing for imaging and increases bone marrow toxicity for therapy. Pretargeting techniques achieve rapid accretion of the radionuclide in the tumour in combination with rapid blood clearance by first administering a non-radiolabelled bispecific monoclonal antibody (bsMAb). After the bsMAb has localized in the tumour and has cleared from the circulation, a small radiolabelled hapten-peptide is administered, which extravasates quickly, is trapped in the tumour by the bsMAb, while the remainder is cleared rapidly from the blood and is excreted via the kidneys. The retention of the radiolabelled hapten-peptide in the tumour is increased when the peptide carries two haptens (*3*). In our pretargeting system, peptides are substituted with the hapten histamine-succinylglycine (HSG), creating a flexible pretargeting system. The peptide can be conjugated with various chelating moieties (DTPA, NOTA, DOTA, N_3S-chelates, etc.), so that it can be radiolabelled with a variety of radionuclides, such as ^{111}In and ^{99m}Tc for SPECT imaging (*4*), ^{18}F and ^{68}Ga for PET imaging (*5-8*), or ^{131}I, ^{90}Y, and ^{177}Lu for pretargeted radioimmunotherapy (PRIT) (*9, 10*).

Until recently, bsMAbs used in pretargeting were either produced by chemical conjugation of Fab-fragments or via the quadroma technology. A novel method, the Dock-and-Lock (DNL) technology, has been developed to produce humanized trivalent Fab bsMAb constructs with two binding Fab's for the tumour-associated antigen and one for the hapten on the radiolabelled peptide (*11, 12*). Using DNL constructs to target B-cell lymphoma and pancreatic cancer, significant therapeutic responses have been

reported in animals with subcutaneous xenografts, using di-HSG-peptide (*9, 13*).
In preclinical studies, we applied the fully humanized anti-CEA x anti-HSG DNL-constructed bsMAb (TF2), and a HSG-substituted hapten-peptide (IMP288) in a nude mouse model for peritoneal presentation of human cancer (*11, 14*). These studies showed the enhanced sensitivity and specificity of this pretargeting system compared to FDG-PET (*8, 15, 16*). Furthermore, we showed that PRIT with TF2 and ^{177}Lu-peptide can be an effective treatment modality of colon cancer with limited toxicity (*9*). Pretargeted immuno-SPECT images acquired after diagnostic ^{111}In-IMP288 or therapeutic ^{177}Lu-IMP288 administrations could be quantitatively compared and could be used to predict and monitor the therapeutic effect of PRIT. Therefore, to administer an appropriate activity dose, an individual pre-therapy diagnostic cycle with the same compounds can be used to estimate absorbed doses (*17, 18*).
Here, we report the accuracy of an ^{111}In-labelled pre-therapy scout dose for personalized dosing and prediction of radiation dose of PRIT with TF2 and the ^{177}Lu-IMP288 in a first-in-man study in metastatic colorectal cancer (CRC) patients.

Methods

Patients

Inclusion criteria included age ≥18 years, histologically or serologically confirmed CEA-expressing advanced colorectal malignancies refractory to conventional treatment or without any standard therapeutic option, Eastern Cooperative Oncology Group performance status ≤1, no chemotherapy, external beam radiation, immunotherapy or prior angiogenesis inhibitors within four weeks prior to study entry, adequate hematopoietic function (absolute neutrophil count ≥1.5 x 10^9/L; platelets ≥150 x 10^9/L without transfusion during the previous month; hemoglobin ≥5.6 mmol/L), hepatic (total bilirubin ≤2x upper limit of normal (ULN), aspartate transaminase (AST)/alanine transaminase (ALT) ≤3 x ULN) and renal function (serum creatinine ≤2 x ULN, Cockcroft clearance >50 ml/min). Exclusion criteria were a life expectancy ≤ 6 months, known brain metastases, cardiac disease with New York Heart Association classification of III-IV, or any other illness significantly affecting the patients' clinical condition. The protocol (ClinicalTrials.gov NCT00860860) was approved by the Institutional Review Board of the Radboud University Nijmegen Medical Centre. Written confirmed consent was obtained from all patients prior to any study-related procedures.

Preparation and administration of investigational drugs

The pretargeting agents were provided by Immunomedics (Morris Plains, NJ, USA). The clinical grade trivalent anti-CEACAM5 x anti-HSG bsMAb construct, TF2, is

an engineered trivalent bsMAb composed of a humanized anti-histamine-succinyl-glycine (HSG) Fab-fragment derived from the 679 anti-HSG monoclonal antibody, and two humanized anti-CEACAM5 Fab-fragments derived from the humanized anti-CEACAM5 MAb, hMN-14 antibody or labetuzumab. Their binding characteristics have been described previously (*12*).
The IMP288 peptide (molecular weight 157 kDa) was synthesized and purified as described by McBride *et al. (7).* IMP288 was labelled with ^{111}In (Covidien, Petten, The Netherlands) at a specific activity of 185 MBq/100 or 25 μg (2.6 or 10.6 MBq/nmol) and with ^{177}Lu (IDB Holland BV, Baarle Nassau, The Netherlands, and Isotope Technologies Garching GmbH, Garching, Germany) at a specific activity of 3.7-7.4 GBq/100 or 25 μg (53-423 MBq/nmol). Radiochemical purity of the radiolabelled IMP288 preparations was determined using instant thin-layer chromatography and reversed phase high-performance liquid chromatography as described previously *(9)*, and always exceeded 95%.
The TF2 dose (75 or 150 mg) was dissolved in 60 mL 0.9% w/v NaCl, and was administered by intravenous infusion over a period of two hours. Patients received a prophylactic gift of clemastine (2 mg) and dexamethason 10 mg intravenously 15 minutes prior to start of their second TF2 infusion to suppress infusion-related symptoms. ^{111}In-IMP288 was dissolved in 10 mL 0.9% NaCl and ^{177}Lu- IMP288 in 20 mL 0.9% NaCl, and administered by an intravenous bolus.

Study design

Each therapy cycle patients received a pre-therapy cycle with TF2 and ^{111}In-labelled IMP288. The ^{111}In-IMP288 data were used to simulate absorbed doses of ^{177}Lu-IMP288 and to calculate a safe individual ^{177}Lu activity dose (see paragraph: *Dosimetric calculations and individual ^{177}Lu doses*). Subsequently, the therapy cycle was administered, with the same interval, bsMAb and IMP288 dose (*Figure 1A*). Four different dosing schedules were studied in cohorts of five patients per cohort (*Figure 1B*), varying the interval between the bsMAb and peptide administration (cohort 1: 5 days interval vs next cohorts: 1 day). TF2 dose was varied (cohort 3: 150 mg TF2, vs other cohorts: 75 mg). Furthermore, two IMP288 doses were studied (cohort 4: 25 μg IMP288 vs other cohorts: 100 μg). 25 μg IMP288 was the minimal peptide dose required to label the peptide with the maximum ^{177}Lu dose, 7.4 GBq.

Pharmacokinetics

Serum samples were collected at the end of the TF2 infusion, 30 min, 1 h, 2 h, 4 h, 6 h, and 24 h after infusion, the last sample being taken shortly before peptide infusion. TF2 concentrations were determined with a sandwich enzyme-linked immuno sorbent assay (ELISA) assay, using HSG-conjugated peptide as a catcher and anti-MN-14 anti-idiotype antibody as a tracer antibody, developed at Immunomedics to determine

A

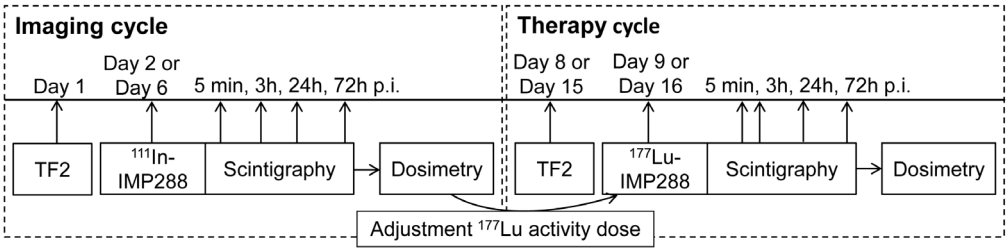

B

Cohort (n=5)	TF2 dose (mg)	Interval (days)	IMP288 dose (μg)
1	75	5	100
2	75	1	100
3	150	1	100
4	75	1	25

Figure 1: Study design. A: Patients received an imaging cycle with TF2 and ^{111}In-IMP288 to determine the pharmacokinetics and radiation doses to the red bone marrow and the kidneys. Based on the dosimetric calculations a safe ^{177}Lu-activity dose was estimated, which was administered in the therapy cycle one week later. B: Four cohorts in which different dose schedules of the pretargeting system were studied, varying the bsMAb dose, the interval between bsMAb dose, and the peptide dose.

TF2 concentrations, as described previously (*19*).
Blood samples were collected 2 min after ^{111}In- and ^{177}Lu-IMP288 injection, 30 min, 1 h, 2 h, 4 h, 24 h and 72 h p.i., and counted in a gamma counter (Wizard, Pharmacia-LKB, Sweden) with standards prepared from the injected products, using appropriate energy windows. The percentage of the injected dose per gram tissue (% ID/g) and blood residence time were calculated.

Scintigraphy

Whole body planar scintigraphic images were acquired, directly followed by SPECT imaging of kidneys and ≥ 1 tumour lesion in the same field of view, using a Siemens dual-head gamma camera (Ecam, Hoffmann Estates, IL), equipped with medium energy collimators. Symmetric 15% windows were used over both the 172 KeV and 246 KeV energy peaks of ^{111}In-scintigraphy, and over both 113 and 208 KeV for ^{177}Lu-scintigraphy.
Scans were acquired within 15 min after the injection of IMP288 before voiding, 3 h after injection after voiding, 24 h and 72 h after injection. If scintigraphic images showed adequate ^{111}In-IMP288 accumulation in metastatic lesions, patients were eligible for ^{177}Lu-IMP288 therapy.

Dosimetric analysis and individual ^{177}Lu doses

^{111}In-IMP288 data were used as surrogate to calculate predicted radiation dose of ^{177}Lu-IMP288, assuming identical pharmacokinetics and biodistribution of ^{111}In-IMP288 and ^{177}Lu-IMP288. Simulation of the ^{111}In scans and blood data for ^{177}Lu and calculation of residence times were performed as described previously (*18*). In OLINDA, the dynamic bladder model was used, (bi-exponential model, bladder voiding at 3 h interval).

The dose to the red bone marrow was calculated using two methods: (I) quantification of the radioactivity in an ROI over the cranium in the scintigraphic images (=imaging-based method), (II) based on the radioactivity concentrations in the blood as described by Shen et al (=blood-based method) (*20*). For the imaging method the residence time was divided by the fraction of the red marrow mass in the cranium to the mass in the total body, for which the default value 0.119 was taken from ICRP23's Reference Man. For the blood method, a red marrow-to-blood activity concentration of 1 was applied, as was determined for ^{177}Lu-peptide (*21*).

As the red marrow and the kidneys were considered as the organs primarily at risk for radiation-induced toxicity, the simulated absorbed doses to these organs were used to calculate a safe total activity dose of ^{177}Lu that would guide no more than 1.25 Gy to the red marrow or no more than 15 Gy to the kidneys, as these thresholds are generally accepted to be below thresholds for radiation-induced toxicity (*22, 23*). For the red bone marrow, the radiation dose calculated with either the imaging or blood-based method was used, whichever was the highest. The calculated total ^{177}Lu activity dose that could be administered safely was divided into four successive cycles, i.e. per cycle a quarter of the calculated total ^{177}Lu activity dose would be administered. In the first cohort, the maximum total ^{177}Lu activity dose per cycle was 3.7 GBq, even when dosimetric calculations would allow a higher ^{177}Lu dose. In the next cohorts the maximum dose per cycle was 7.4 GBq.

Patient follow-up

Patients were closely monitored during and weekly up to eight weeks after therapy, with physical examination, clinical biochemistry, hematology, and toxicity assessment according to the Common Toxicity Criteria for Adverse Events (CTCAE v3.0).

Significant toxicities were defined as: thrombocytes $<10 \times 10^9$/L, grade 4 thrombocytopenia lasting for ≥4 weeks, grade 4 neutropenia for ≥7 days, ≥grade 3 thrombocytopenia with bleeding, ≥ grade 3 neutropenia with fever at least 38.5 °C, or any ≥ grade 3 non-hematologic toxicity, with the exception of nausea, vomiting, and diarrhea.

Therapeutic efficacy was evaluated by Response Evaluation Criteria in Solid Tumours (RECIST), comparing a baseline FDG-PET-CT scan performed within two weeks prior to start on study, and a FDG-PET-CT acquired eight weeks after ^{177}Lu-IMP288 injection.

Statistics

Statistical analysis was performed with GraphPad Prism software version 5.00 for Windows (San Diego USA), using two-tailed Mann Whitney test. Bonferonni correction was applied when multiple groups were compared, Spearman's correlation tests were used for not normally distributed and categorical data, and Bland Altman plots were determined for agreement tests. The level of significance was set at $p<0.05$.

Results

The baseline patient characteristics are summarized in *Table 1* for the patients that were treated with ^{177}Lu-IMP288. Patient 1 had to be withdrawn and replaced for medical safety reasons. His second TF2 infusion had to be discontinued due to hypoxia grade 2 as symptom of a grade 2 infusion reaction. Although this adverse event resolved rapidly, we decided not to restart the infusion.

Pharmacokinetic assessment

Overall, TF2 showed fast blood clearance in all patients; >99% of the administered dose cleared in 24 h. A longer interval for antibody clearance (cohort 1: 5 days vs cohort 2: 1 day) resulted in even lower concentrations at the time of peptide injection (cohort 1: 5 days vs cohort 2: 1 day, p=0.01, Mann-Whitney) (*Figure 2A*). Patients that received a higher TF2 dose (cohort 3: 150 mg) showed a wide variation in antibody blood concentrations compared to those that received the lower dose (cohort 2 and 4: 75 mg) at 24 h p.i (range 0.077-1.2 μg/mL vs 0.16-0.59 μg/mL in cohort 3 vs cohort 2 and 4 respectively). Similar variations in peptide blood residence time were observed for the patients that had the higher bsMAb dose (cohort 3: 1.5-7.5 h vs cohort 2: 2.0-5.5 h), as well for the patients that received the lower peptide dose (cohort 4: 1.7-9.3 h) (*Figure 2B*). The individual peptide blood residence times correlated strongly with the individual TF2 blood concentration at the time of peptide injection, as compared within the cohorts that received the same peptide dose (100 μg in cohort 1-3) (Spearman's $\rho=0.94$, $p<0.0001$) (*Figure 2C*).

Scintigraphic images

Tumour lesions were visualised as early as one hour after injection of the radiolabelled peptide in all patients, with ^{111}In-scans and ^{177}Lu-scans being highly congruent. The whole body planar and SPECT images of one of the patients are shown in *Figure 3*, along with the FDG-PET images. ^{111}In- and ^{177}Lu-IMP288 cleared from the blood and renal system within 24 h, with very limited kidney or other normal tissue retention, resulting in very high tumour-to-background ratios.

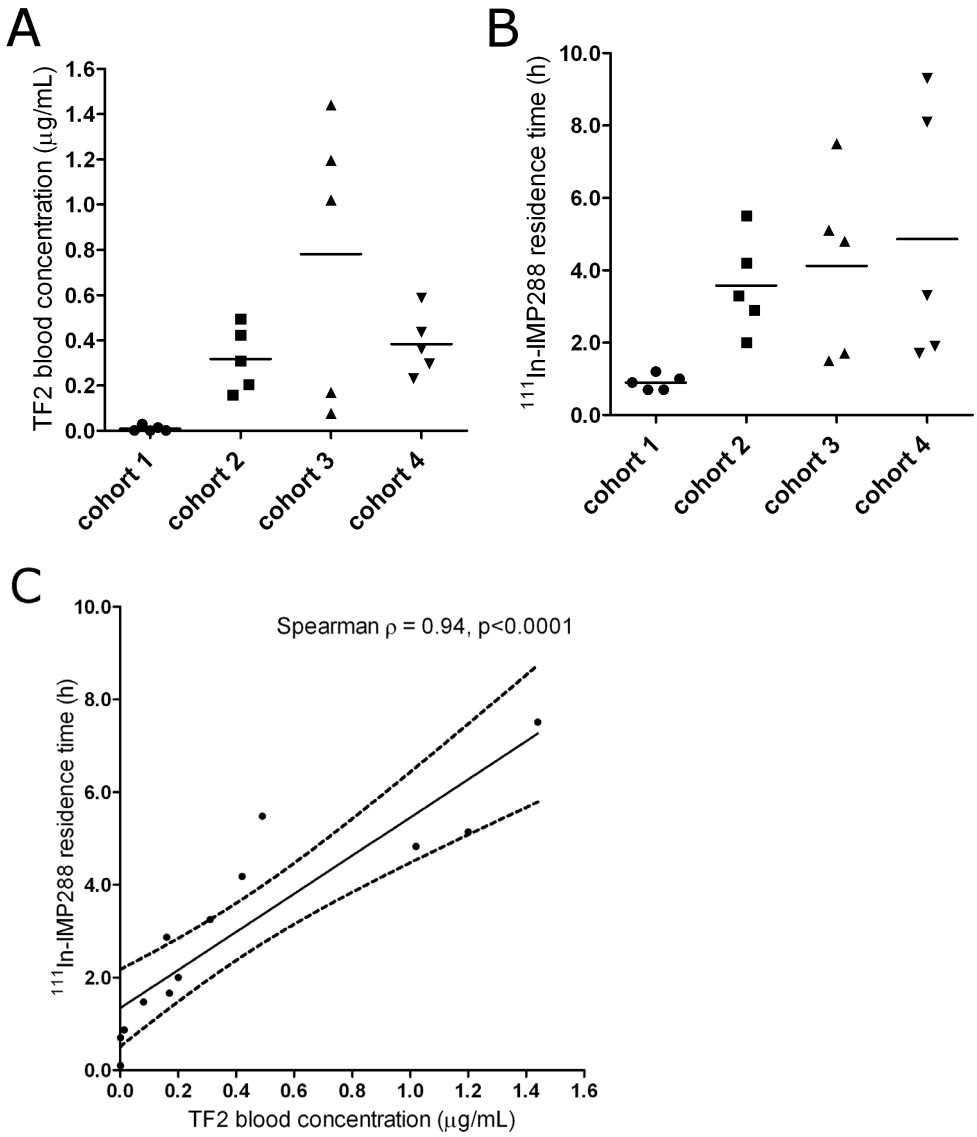

Figure 2: TF2 and IMP288 blood pharmacokinetics.
A: TF2 blood concentration at the moment of IMP288 injection (individual patients).
B: ^{111}In-IMP288 residence times of the four cohorts (individual patients).
C: Correlation between TF2 and IMP288 blood pharmacokinetics. Individual TF2 blood concentration at the moment of peptide injection plotted against the blood residence time of ^{111}In-IMP288 (Spearman r=0.94, P<0.0001), with linear regression line (solid line) and the 95% confidence interval.

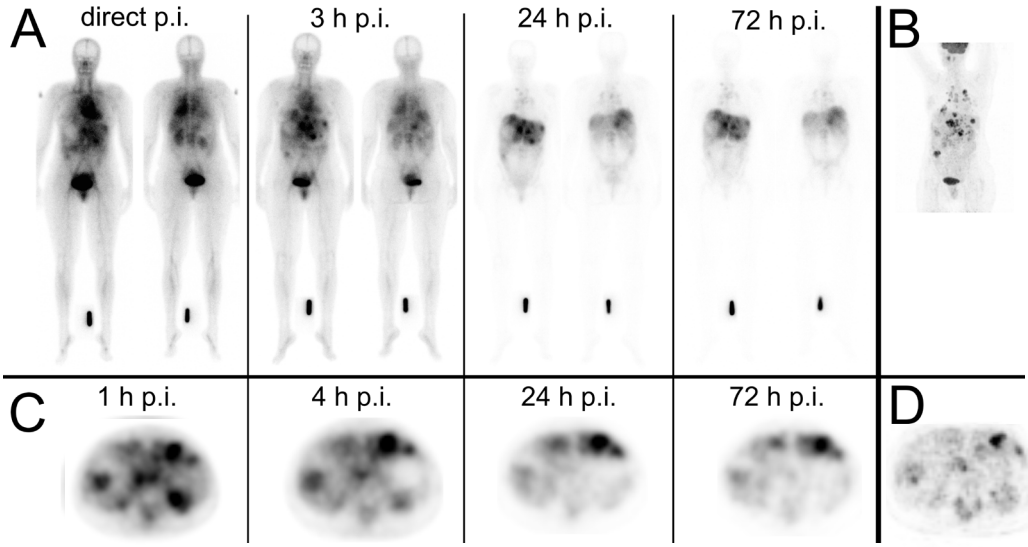

Figure 3: Scintigraphic images. Scintigraphic images acquired after injection of ^{111}In-IMP288 (185 MBq, 100 μg), pretargeted with 150 mg TF2 (1-day interval), in a 52-year-old patient (cohort 3), with a primary colon tumour, liver, lymph nodes (mediastinum) and bone (lumbar vertebrae) metastases.
A: Whole body planar anterior and poster images (10 min p.i., 3 h p.i., 24 h p.i., 72 h p.i.) with an aliquot of the injected dose was kept near the feet in all scans. B: corresponding FDG-PET.
B: SPECT images of same patients, acquired directly after planar images (3D volume rendered, 1 h p.i., 4 h p.i., 24 h p.i., 72 h p.i.). D: corresponding FDG-PET.
The scintigraphic images show very clear tumour targeting and low concentrations of radioactivity in normal tissues.

Absorbed doses and individual ^{177}Lu activity doses

Kidney uptake of the radiolabelled peptide was low and the predicted kidney absorbed doses (<0.50 mGy/MBq) were not limiting the maximum acitivity doses that could be administered, as in none of the patients four cycles of 7.4 GBq ^{177}Lu would exceed the limit of 15 Gy radiation dose to the kidneys. The predicted radiation doses to the red bone marrow were relatively low, and showed some increase in subsequent cohorts (mean ± SD of blood-based method: 0.008 ± 0.003, 0.034 ± 0.011, 0.045 ± 0.028, and 0.060 ± 0.040 for cohort 1, 2, 3 and 4 respectively, *Figure 4*), although the only significant difference was between cohort 1 vs cohort 2-4 (p= 0.02, Mann-Whitney, with Bonferonni correction). Individual patients in cohort 2, 3 and 4 showed a wider variation in red marrow doses, which corresponded with the larger range measured in the individual peptide blood residence times within these cohorts.
The low predicted red marrow doses allowed high therapeutic doses to be administered, up to 7.4 GBq (Table 1). In several patients of cohort 2-4, the ^{177}Lu activity

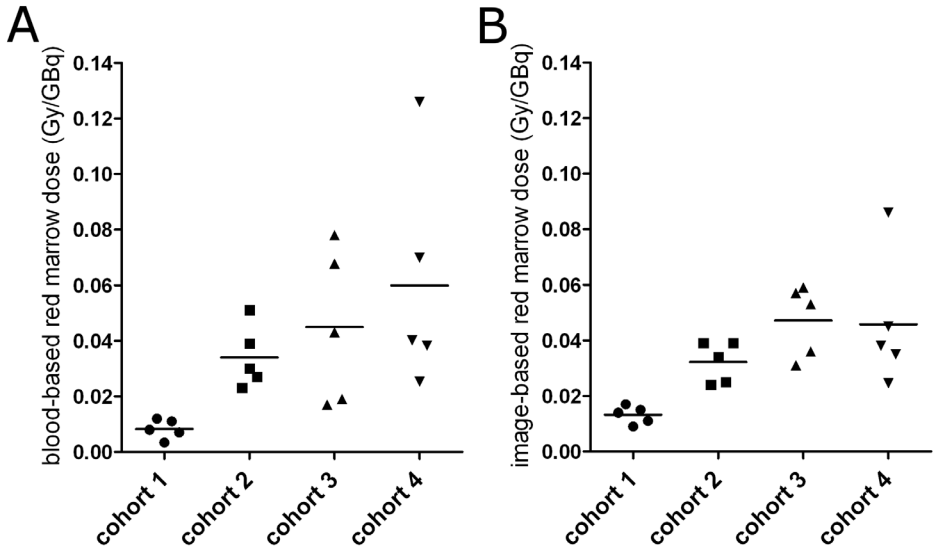

Figure 4: Simulated ^{177}Lu absorbed doses. The simulated ^{177}Lu-IMP288 absorbed doses for kidneys (A), and red marrow (blood-based (B), image-based (C)) (individual patients per cohort).

doses were adjusted to keep the red marrow dose below 1.25 Gy in four successive cycles (0.31 Gy per treatment cycle), as defined in the per protocol. The results of two different methods that were used to estimatered marrow doses (blood- versus image-based method) were in good agreement (mean difference: 0.0040 mGy/MBq, SD: 0.017 mGy/MBq, Bland-Altman).

Patient 20 and 21 were also allowed to receive 7.4 GBq, but due to lower labelling efficiency, they only received 5.6 GBq ^{177}Lu. The radiolabelling of 7.4 GBq ^{177}Lu to 25 μg IMP288 had been successful in pre-study tests procedures and for patient 19.

The red marrow doses that were measured after administration of ^{177}Lu-IMP288, were in good agreement with the predicted absorbed doses. The Bland-Altman plot in *Figure 5* shows a mean difference of -0.0026 mGy/MBq (SD: 0.014 mGy/MBq). As a consequence, the measured red marrow doses did not exceed the aimed 0.31 Gy in the majority of patients (11 out of 13 patients (85%); excluding cohort 1, patient 20 and 21 from the analysis, as described above).

Hematologic toxicity

Hematologic toxicity was limited in most patients (grade 1-2 in 30% of the patients). Only two patients (10%) had ≥ grade 3: patient 10 (cohort 2) and patient 16 (cohort 3) had grade 3-4 thrombocytopenia, and grade 3 lymphopenia. The nadir was 5-6 weeks after ^{177}Lu-IMP288 administration, and both patients showed fast and complete recovery at 7-8 weeks p.i., without any complications or need for intervention.

Table 1: Baseline patient characteristics and individual ^{177}Lu administered activity doses based on the individual dosimetric calculations of the ^{111}In-imaging cycle.

Patient code	Cohort	Age (years)	Sex	Site of primary	Site of disease at study entry	Prior treatments	CEA (µg/L)	^{177}Lu- dose (GBq)
2	1	60	M	Colon	Liver, lungs, lymph nodes	Surgery, external radiotherapy, chemotherapy, immunotherapy	820	3.7
3	1	63	F	Colon	Liver	Surgery, chemotherapy, immunotherapy	990	3.7
4	1	54	F	Colon	Liver, lungs	Surgery, chemotherapy, immunotherapy	1600	3.7
5	1	68	F	Rectum	Liver, lungs, lymph nodes, bone	Surgery, external radiotherapy, chemotherapy, immunotherapy	13	3.7
6	1	61	M	Colon	Liver, lungs, lymph nodes	Chemotherapy, immunotherapy	79	3.7
7	2	63	F	Rectum	Peritoneum, soft tissue	Surgery, chemotherapy	140	6.2
8	2	63	M	Rectum	Rectum, liver, lungs	External radiotherapy, chemotherapy, immunotherapy	12	7.4
9	2	72	M	Rectum	Rectum, liver	Surgery, external radiotherapy, chemotherapy, immunotherapy	150	7.4
10	2	70	M	Colon	Liver	Surgery, chemotherapy, immunotherapy	120	7.4
11	2	55	F	Colon	Liver	Surgery, chemotherapy, immunotherapy	220	7.4
12	3	70	M	Colon	Liver, lungs, bone	Surgery, chemotherapy, immunotherapy	2200	7.4
13	3	76	M	Colon	Colon, lungs, lymph nodes, bone	Chemotherapy, immunotherapy	280	7.4
14	3	52	F	Colon	Colon, liver, lungs, lymph nodes, bone, soft tissue	Chemotherapy, immunotherapy	85	4.0
15	3	58	M	Colon	Liver, lungs	Surgery, chemotherapy, immunotherapy	16	5.9
16	3	76	M	Colon	Colon, liver, lymph nodes	Surgery, chemotherapy, immunotherapy	140	4.6
17	4	73	M	Colon	Lungs, liver	Surgery, chemotherapy, immunotherapy	32	4.5
18	4	63	F	Colon	Colon, lungs, liver	Surgery, chemotherapy, immunotherapy	81	2.5
19	4	66	F	Rectum	Rectum, lungs, liver, lymph nodes	Surgery, chemotherapy, immunotherapy	28	7.4
20	4	72	M	Colon	Lungs	Surgery, chemotherapy, immunotherapy	60	5.6
21	4	39	F	Colon	Colon, liver, lymph nodes, soft tissue	Surgery, external radiotherapy, chemotherapy, immunotherapy	17	5.6

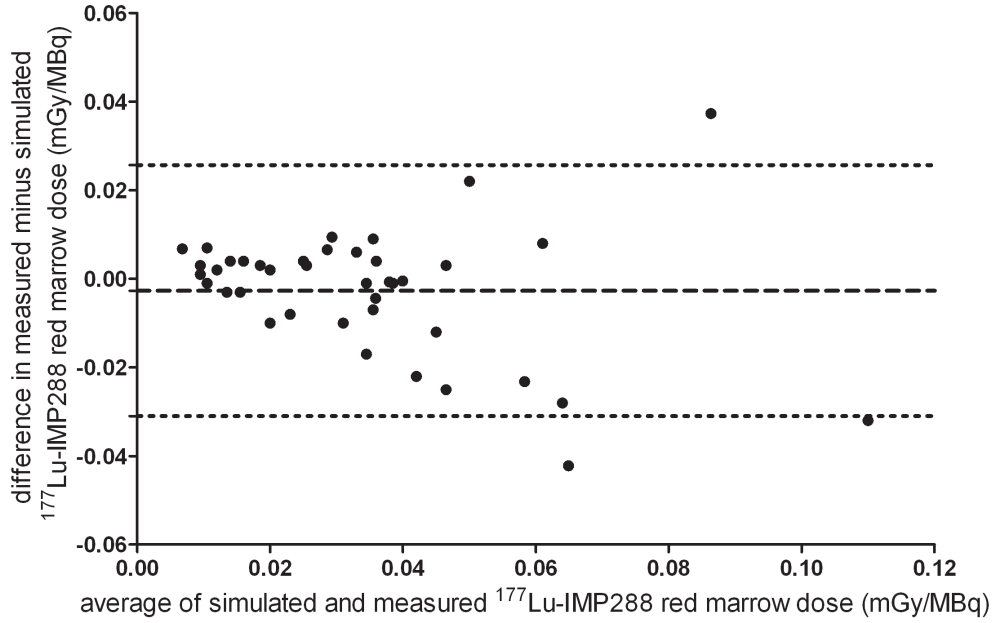

Figure 5: Agreement between predicted and measured ^{177}Lu doses. Bland-Altman plot showing the difference between the measured minus predicted data plotted against their average. Dashed line is mean difference (-0.0026 mGy/MBq), dotted lines are 95% agreement limits (-0.031 and 0.026 mGy/MBq).

Remarkably, those two patients has somewhat higher ^{177}Lu absorbed doses than predicted by the imaging cycle (0.45 and 0.48 Gy for patient 10 and 16, respectively), while the red marrow dose of all other patients, did not exceed 0.31 Gy and only had grade 0-2 thrombocytopenia. The measured ^{177}Lu-IMP288 absorbed doses correlated significantly with platelet toxicity (Spearman's ρ=0.58, p=0.008) (*Figure 6*).

Therapeutic efficacy

At evaluation by FDG-PET/CT-scan eight weeks after the first therapy cycle with TF2 and ^{177}Lu-IMP288, all patients still had progressive disease, therefore none of the patients could receive a next therapy cycle.

Discussion

Patient-specific treatment planning in radioimmunotherapy is an attractive strategy to reduce the risk of hematologic toxicity. In this study, we showed that individualized dosing of PRIT with TF2 and ^{177}Lu-IMP288 at fixed radiation dose thresholds, estimated using a pre-therapeutic scout dose of TF2 and ^{111}In-IMP288 is feasible

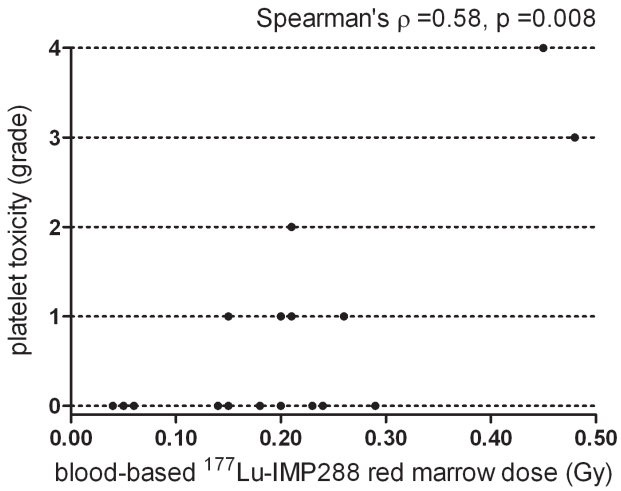

Figure 6: Correlation between ^{177}Lu absorbed doses and platelet toxicity. The measured ^{177}Lu-IMP288 absorbed doses (calculated with blood-based method) correlated significantly with platelet toxicity (Spearman r=0.58, P=0.008).

and safe in patients with progressive metastatic CRC. Individualized activity dosing seemed essential, as relatively large inter-patient variations were observed in TF2 and IMP288 pharmacokinetics. We were able to identify those patients that were at the lowest risk for hematologic toxicity and who were eligible to receive the maximum activity dose of 7.4 GBq. At the same time, in those patients in which the peptide blood and marrow residence time was somewhat slower in the pre-therapy cycle, the ^{177}Lu therapeutic activity doses could be reduced to prevent toxicity. As a consequence, red bone marrow radiation doses were low (<0.5 Gy).

Most importantly, our data showed a correlation between red marrow doses and bone marrow toxicity. This observation is in accordance with the results of some previous clinical radioimmunotherapy studies (*18, 24, 25*), while various other studies reported a lack of correlation between dosimetric estimations and severity of toxicity (*26-30*). The discrepancy between the lack of correlation of the other studies and the correlation in this study might be due to differences in dose rate (*31-33*).

Our study showed some interesting features of the bsMAb and peptide pharmacokinetics. First, in all patients, the blood clearance of TF2 was much faster than that of similarly sized IgG molecules (157 kD and 150 kD, respectively), which could be explained by the fact that TF2 lacks a C_H2 domain, while this part of an antibody enables recycling via FcRn-receptors (*34*). Our findings are in line with observation that C_H2 domain-deleted IgG variants (121 kDa) clear much faster from the blood than intact IgG (*35*). Due to the fast blood clearance of TF2, the interval between TF2 and IMP288 administrations could safely be shortened from five days to one day. However, the short

residence time of TF2 in the blood reduces the tumour uptake, as large molecules like antibodies have several barriers to cross that limit their localization in tumours (*36*). Rapid blood clearance reduces the driving force of tumour accumulation. In pretargeting, it would be preferable to have a bsMAb construct with a longer circulatory half-life, like IgGs, as this would result in higher antibody-concentrations in the tumour.
Secondly, our data suggest that the inter-patient variety in peptide blood residence time could be explained by individual variation in bsMAb clearance rates, and consequently the bsMAb blood concentration at the time of peptide administration. If the concentration of circulating bsMAb is relatively high at the time the radiolabelled peptide is injected, a larger portion of the injected peptide dose will form an immune complex with the antibody in the circulation, which will enhance the residence time of the radiolabelled peptide in the blood (and thus will enhance the red marrow dose). These data are in accordance with the clinical results of the phase I study, where patients with CEA-expressing tumours received an anti-CEA x anti-DTPA bsMAb in combination with an ^{131}I-di-DTPA-hapten (*37*).
In our study, no clear patient-specific distinctions were found that could explain differences in bsMAb clearance rates. Theoretically, the variation in TF2 blood clearance could be influenced by differences in individual baseline plasma CEA levels, as antigen-antibody complexes could be formed in serum, but no such correlation was observed (data not shown). Furthermore, TF2 clearance could be affected by liver function, as the antibody is captured and degraded in the liver. However, in this study, none of the patients showed impairment of hepatic function.
In the four patient cohorts we studied the effects of three important pretargeting paramaters: (1) the interval between injection of the bsMAb and the peptide, (2) the bsMAb dose, and (3) the peptide dose (*9*). First, we aimed to determine the minimal interval required for sufficient serum bsMab clearance, to maximize uptake of the bsMAb in the tumour. Secondly, tumour uptake of the radiolabelled peptide could be improved by administrating a higher antibody dose. We also demonstrated that tumour uptake of the radiolabelled peptide increased at lower peptide doses. It remains to be established whether these parameters could be optimized any further, because at some point the residence time of the radiolabelled peptide will be enhanced to such an extent that it will cause enhanced red marrow toxicity.
In our dosimetric calculations, we used two different methods to estimate the red marrow dose. Using blood concentrations as surrogate for bone marrow concentrations was permitted, because the pretargeting agents do not bind to any blood, marrow, or bone component, and metastatic bone involvement is limited in CRC. For imaging quantification the cranium was used, because this region does not have overlapping organs. For example, the use of lumbar vertebrae is hindered by overlapping intestines (*38*). We showed that both dosimetry methods are feasible and reveal similar results.
Hematological toxicity was limited in most patients, with only two patients who had transient grade 3-4 thrombocytopenia. Several mechanisms may explain these two

sporadic cases. First, they had slightly higher measured than predicted red marrow doses, which was not the case in the other patients, who had grade 0-2 hematologic toxicity. Furthermore, patient specific factors can contribute to the risk of hematologic toxicity due to (P)RIT, such as age, prior treatments such as radio- or chemotherapy, or extensive bone marrow involvement. Both patients with grade 3-4 thrombocytopenia were ≥70 years (median age of the other patients: 63 years). They did not have bone marrow metastases, and they had received similar lines and cycles chemotherapy compared to the other patients, and had a similar interval between this study and their last treatment compared to the other study patients.

In this study, ^{177}Lu was selected as a radionuclide for radioimmunotherapy as it has several advantages over the use of other β-emitting radionuclides like ^{90}Y and ^{131}I. The low energy of the beta particles with a short tissue penetration range is ideally suited for treatment of smaller sized tumours and low radiation doses to adjacent normal tissues and red bone marrow. Its 11% abundance of photons allows scintigraphy to monitor the pharmacodynamics of therapeutic administrations. We performed a pre-therapy imaging cycle with ^{111}In-labelled IMP288, as ^{111}In- and ^{177}Lu-labelled peptides are known to have similar biodistribution. ^{177}Lu is a residualizing radionuclide which means that the radionuclide is retained in tumour cells after internalization. The half-life of ^{90}Y (64.1 h) matches better with the residence time of the IMP288-peptide in the tumour, which will enhance the radiation dose to the tumour. Therefore, this could be an approach to further widen the therapeutic window to evaluate the safety and dose-escalation with TF2 and ^{90}Y-labelled IMP288. Another advantage of ^{90}Y is its longer tissue penetration range (maximum 12.0 mm), which could irradiate non-targeted regions in the tumour in case of inhomogeneous intratumoural distribution of the radiolabelled peptide.

In conclusion, these first clinical results show that pretargeted radioimmunotherapy in CEA-expressing CRC is feasible and safe. Individual high therapeutic activity doses could be safely administered, based on patient-specific dosimetry in a pre-therapy cycle with TF2 and ^{111}In-IMP288. Tumours are specifically and rapidly targeted with TF2 and ^{177}Lu-IMP288, with limited hematological toxicity. Further clinical investigation should focus on therapeutic efficacy in patients with smaller volume disease and evaluating potential advantages of ^{90}Y over ^{177}Lu for labelling the peptide, especially when treating larger tumours with inhomogeneous uptake.

References

1. Baum RP, Rosch F. 1 World Congress on Ga-68 and Peptide Receptor Radionuclide Therapy (PRRNT), June 23-26, 2011, Zentralklinik Bad Berka, Germany. *World J Nucl Med.* Jan 2011;10(1):1-2.
2. Goldenberg DM, Chang, C.-H., Rossi, E.A., McBride, W.J., Sharkey, R.M. Pretargeted molecular imaging and radioimmunotherapy. . *Theranostics.* 2012.
3. Le Doussal JM, Martin M, Gautherot E, Delaage M, Barbet J. In vitro and in vivo targeting of radiolabeled monovalent and divalent haptens with dual specificity monoclonal antibody conjugates: enhanced divalent

hapten affinity for cell-bound antibody conjugate. *J Nucl Med.* Aug 1989;30(8):1358-1366.
4. Sharkey RM, Cardillo TM, Rossi EA, et al. Signal amplification in molecular imaging by pretargeting a multivalent, bispecific antibody. *Nat Med.* Nov 2005;11(11):1250-1255.
5. Griffiths GL, Chang CH, McBride WJ, et al. Reagents and methods for PET using bispecific antibody pretargeting and 68Ga-radiolabeled bivalent hapten-peptide-chelate conjugates. *J Nucl Med.* Jan 2004;45(1):30-39.
6. Koppe MJ, Bleichrodt RP, Soede AC, et al. Biodistribution and therapeutic efficacy of (125/131)I-, (186) Re-, (88/90)Y-, or (177)Lu-labeled monoclonal antibody MN-14 to carcinoembryonic antigen in mice with small peritoneal metastases of colorectal origin. *J Nucl Med.* Jul 2004;45(7):1224-1232.
7. McBride WJ, Zanzonico P, Sharkey RM, et al. Bispecific antibody pretargeting PET (immunoPET) with an 124I-labeled hapten-peptide. *J Nucl Med.* Oct 2006;47(10):1678-1688.
8. Schoffelen R, Sharkey RM, Goldenberg DM, et al. Pretargeted immuno-positron emission tomography imaging of carcinoembryonic antigen-expressing tumors with a bispecific antibody and a 68Ga- and 18F-labeled hapten peptide in mice with human tumor xenografts. *Mol Cancer Ther.* Apr 2010;9(4):1019-1027.
9. Schoffelen R, van der Graaf WT, Franssen G, et al. Pretargeted 177Lu radioimmunotherapy of carcinoembryonic antigen-expressing human colonic tumors in mice. *J Nucl Med.* Nov 2010;51(11):1780-1787.
10. Sharkey RM, McBride WJ, Karacay H, et al. A universal pretargeting system for cancer detection and therapy using bispecific antibody. *Cancer Res.* Jan 15 2003;63(2):354-363.
11. Goldenberg DM, Rossi EA, Sharkey RM, McBride WJ, Chang CH. Multifunctional antibodies by the Dock-and-Lock method for improved cancer imaging and therapy by pretargeting. *J Nucl Med.* Jan 2008;49(1):158-163.
12. Rossi EA, Goldenberg DM, Cardillo TM, McBride WJ, Sharkey RM, Chang CH. Stably tethered multifunctional structures of defined composition made by the dock and lock method for use in cancer targeting. *Proc Natl Acad Sci U S A.* May 2 2006;103(18):6841-6846.
13. Sharkey RM, Karacay H, Litwin S, et al. Improved therapeutic results by pretargeted radioimmunotherapy of non-Hodgkin's lymphoma with a new recombinant, trivalent, anti-CD20, bispecific antibody. *Cancer Res.* Jul 1 2008;68(13):5282-5290.
14. Chang CH, Sharkey RM, Rossi EA, et al. Molecular advances in pretargeting radioimunotherapy with bispecific antibodies. *Mol Cancer Ther.* May 2002;1(7):553-563.
15. Schoffelen R, van der Graaf WT, Sharkey RM, et al. Pretargeted immuno-PET of CEA-expressing intraperitoneal human colonic tumour xenografts: a new sensitive detection method. *EJNMMI Res.* Jan 27 2012;2(1):5.
16. Sharkey RM, Karacay H, Vallabhajosula S, et al. Metastatic human colonic carcinoma: molecular imaging with pretargeted SPECT and PET in a mouse model. *Radiology.* Feb 2008;246(2):497-507.
17. Brouwers AH, Buijs WC, Mulders PF, et al. Radioimmunotherapy with [131I]cG250 in patients with metastasized renal cell cancer: dosimetric analysis and immunologic response. *Clin Cancer Res.* Oct 1 2005;11(19 Pt 2):7178s-7186s.
18. Stillebroer AB, Zegers CM, Boerman OC, et al. Dosimetric Analysis of 177Lu-cG250 Radioimmunotherapy in Renal Cell Carcinoma Patients: Correlation with Myelotoxicity and Pretherapeutic Absorbed Dose Predictions Based on 111In-cG250 Imaging. *J Nucl Med.* Dec 12 2011.
19. Sharkey RM, Rossi EA, McBride WJ, Chang CH, Goldenberg DM. Recombinant bispecific monoclonal antibodies prepared by the dock-and-lock strategy for pretargeted radioimmunotherapy. *Semin Nucl Med.* May 2010;40(3):190-203.
20. Shen S, DeNardo GL, Sgouros G, O'Donnell RT, DeNardo SJ. Practical determination of patient-specific marrow dose using radioactivity concentration in blood and body. *J Nucl Med.* Dec 1999;40(12):2102-2106.
21. Forrer F, Krenning EP, Kooij PP, et al. Bone marrow dosimetry in peptide receptor radionuclide therapy with [177Lu-DOTA(0),Tyr(3)]octreotate. *Eur J Nucl Med Mol Imaging.* Jul 2009;36(7):1138-1146.
22. Valkema R, Pauwels SA, Kvols LK, et al. Long-term follow-up of renal function after peptide receptor radiation therapy with (90)Y-DOTA(0),Tyr(3)-octreotide and (177)Lu-DOTA(0), Tyr(3)-octreotate. *J Nucl Med.* Jan 2005;46 Suppl 1:83S-91S.
23. Scala RJ. Biologic effects of ionizing radiation. In: P.J. Early BDS, ed. *Principles and Practice of Nuclear Medicine*. St Louis: Mosby; 1995:123-127.
24. Juweid ME, Zhang CH, Blumenthal RD, Hajjar G, Sharkey RM, Goldenberg DM. Prediction of hematologic toxicity after radioimmunotherapy with (131)I-labeled anticarcinoembryonic antigen monoclonal

antibodies. *J Nucl Med.* Oct 1999;40(10):1609-1616.
25. Vallabhajosula S, Goldsmith SJ, Hamacher KA, et al. Prediction of myelotoxicity based on bone marrow radiation-absorbed dose: radioimmunotherapy studies using 90Y- and 177Lu-labeled J591 antibodies specific for prostate-specific membrane antigen. *J Nucl Med.* May 2005;46(5):850-858.
26. Behr TM, Sharkey RM, Juweid ME, et al. Phase I/II clinical radioimmunotherapy with an iodine-131-labeled anti-carcinoembryonic antigen murine monoclonal antibody IgG. *J Nucl Med.* Jun 1997;38(6):858-870.
27. Divgi CR, Bander NH, Scott AM, et al. Phase I/II radioimmunotherapy trial with iodine-131-labeled monoclonal antibody G250 in metastatic renal cell carcinoma. *Clin Cancer Res.* Nov 1998;4(11):2729-2739.
28. O'Donoghue JA, Baidoo N, Deland D, Welt S, Divgi CR, Sgouros G. Hematologic toxicity in radioimmunotherapy: dose-response relationships for I-131 labeled antibody therapy. *Cancer Biother Radiopharm.* Aug 2002;17(4):435-443.
29. Vose JM, Wahl RL, Saleh M, et al. Multicenter phase II study of iodine-131 tositumomab for chemotherapy-relapsed/refractory low-grade and transformed low-grade B-cell non-Hodgkin's lymphomas. *J Clin Oncol.* Mar 2000;18(6):1316-1323.
30. Wiseman GA, White CA, Sparks RB, et al. Biodistribution and dosimetry results from a phase III prospectively randomized controlled trial of Zevalin radioimmunotherapy for low-grade, follicular, or transformed B-cell non-Hodgkin's lymphoma. *Crit Rev Oncol Hematol.* Jul-Aug 2001;39(1-2):181-194.
31. Behr TM, Memtsoudis S, Sharkey RM, et al. Experimental studies on the role of antibody fragments in cancer radio-immunotherapy: Influence of radiation dose and dose rate on toxicity and anti-tumor efficacy. *Int J Cancer.* Aug 31 1998;77(5):787-795.
32. Behr TM, Sharkey RM, Sgouros G, et al. Overcoming the nephrotoxicity of radiometal-labeled immunoconjugates: improved cancer therapy administered to a nude mouse model in relation to the internal radiation dosimetry. *Cancer.* Dec 15 1997;80(12 Suppl):2591-2610.
33. Howell RW, Goddu SM, Rao DV. Design and performance characteristics of an experimental cesium-137 irradiator to simulate internal radionuclide dose rate patterns. *J Nucl Med.* May 1997;38(5):727-731.
34. Ghetie V, Ward ES. FcRn: the MHC class I-related receptor that is more than an IgG transporter. *Immunol Today.* Dec 1997;18(12):592-598.
35. Chinn PC, Morena RA, Santoro DA, et al. Pharmacokinetics and tumor localization of (111)in-labeled HuCC49DeltaC(H)2 in BALB/c mice and athymic murine colon carcinoma xenograft. *Cancer Biother Radiopharm.* Apr 2006;21(2):106-116.
36. Jain RK. Physiological barriers to delivery of monoclonal antibodies and other macromolecules in tumors. *Cancer Res.* Feb 1 1990;50(3 Suppl):814s-819s.
37. Kraeber-Bodere F, Faivre-Chauvet A, Ferrer L, et al. Pharmacokinetics and dosimetry studies for optimization of anti-carcinoembryonic antigen x anti-hapten bispecific antibody-mediated pretargeting of Iodine-131-labeled hapten in a phase I radioimmunotherapy trial. *Clin Cancer Res.* Sep 1 2003;9(10 Pt 2):3973S-3981S.
38. Visser E, Postema E, Boerman O, Visschers J, Oyen W, Corstens F. Software package for integrated data processing for internal dose assessment in nuclear medicine (SPRIND). *Eur J Nucl Med Mol Imaging.* Mar 2007;34(3):413-421.

8

SPECT-based patient-specific tumour and red bone marrow dosimetry for pretargeted radioimmunotherapy

Wietske van der Weg[1], Rafke Schoffelen, Robert F. Hobbs[2], Martin Gotthardt[1], David M. Goldenberg[3], Robert M. Sharkey[3], Wim J.G. Oyen[1], Otto C. Boerman[1], George Sgouros[2], Eric P. Visser[1]

In preparation

[1] Radboud University Nijmegen Medical Centre, dept. of Nuclear Medicine, Nijmegen, Netherlands
[2] Johns Hopkins University, dept. of Radiology, Baltimore, Maryland, USA
[3] Garden State Cancer Center, Morris Plains, New Jersey, USA

Abstract

Background

Red bone marrow (RBM) toxicity is a dose limiting factor in (pretargeted) radioimmunotherapy. Dosimetric analysis could be improved by using three-dimensional (3D)-based methods instead of planar gamma camera imaging, avoiding organ overlap and to enable tumour dosimetry. Therefore, the aim of this study was to develop an RBM dosimetry approach using the Monte Carlo-based 3D-Radiobiological Dosimetry (3D-RD) software, and to determine its additional value for predicting RBM toxicity.

Methods

RBM and tumour doses were determined by the 3D-RD for thirteen colorectal cancer patients after pretargeted radioimmunotherapy (PRIT) with the two-step administration of an anti-CEA x anti-HSG bispecific monoclonal antibody and a ^{177}Lu -labelled di-HSG-peptide. The 3D-RD dosimetry was based on SPECT scans acquired directly, 3 h, 24 h and 72 h after the ^{177}Lu administration. 3D-RD RBM doses were correlated to the grade of thrombocytopenia after treatment, graded according to NCI Common Terminology Criteria v3. The results were compared with RBM doses calculated based on whole body planar scintigraphic images and blood samples that were also acquired after ^{177}Lu-labelled peptide injection. Furthermore, tumour doses for the ^{177}Lu-therapy were estimated and tumour-to-RBM dose ratios were simulated for PRIT with ^{90}Y.

Results

3D-RD RBM doses were higher (median 0.43 Gy) than the blood-based and 2D image-based doses (median 0.21 and 0.20 Gy, respectively). 3D-RD RBM doses for the patients with thrombocytopenia (n=7) were higher (range 0.43-0.97 Gy) compared to patients without gradable thrombocytopenia (n=6, range 0.12-0.39 Gy), except in one patient with a RBM dose of 0.48 Gy who had no thrombocytopenia, but a grade 2 leukopenia. Blood- and 2D image-based RBM doses for patients with grade 1-2 RBM toxicity were in the same range as for the patients without toxicity (0.14–0.29 Gy and 0.11-0.26 Gy, respectively), whereas blood-based RBM doses for two grade 3-4 patients were higher (0.66 Gy and 0.51 Gy, respectively). The median 3D-RD tumour dose was 1.45 Gy (range 0.46-3.76 Gy) for the ^{177}Lu-therapy. When simulated for ^{90}Y instead of ^{177}Lu the median increase in the tumour-to-RBM dose ratio was 21%.

Conclusion

3D-RD dosimetry based on the SPECT images may more accurately predict RBM toxicity than blood- or 2D image-based methods. The 3D image-based dosimetry has additional value to estimate tumour doses and to predict the benefit-versus-risk ratios for different radionuclides.

Introduction

The aim of radioimmunotherapy (RIT) is to selectively target radioactivity to tumour lesions, with limited radiation doses to healthy tissues. The absorbed dose (AD) depends on the patient-specific pharmacokinetics of the tracer, the administered activity and the radionuclide. After pre-therapeutic diagnostic administration of a trace amount of the radiolabelled compound, dosimetric calculations lead to a patient-specific insight in where which amount of energy is deposited. This information can be used to adjust the individual therapy dose, or even be useful to select the most suitable radionuclide for therapy. Ideally, this leads to an improved benefit-versus-risk ratio for individual patients.

In external beam radiation, this patient-specific treatment planning is common practice, as quite some data on the AD and its effect on tumour and normal tissues are available. However, for RIT the information on dose-response correlation is hardly known, and dose estimations are les adequate. Therefore further investigation of dose-response relations and development of accurate dosimetry methods for the clinical practice of radioimmunotherapy are required.

Since the red bone marrow (RBM) is often dose limiting in RIT (*1-5*), the focus of this work will be on the RBM dose calculation and dose-response relation. Commonly used methods to calculate the RBM AD are the blood-based method (*1, 3, 6, 7*), a two-dimensional (2D) image-based method, or a combination of these two methods. Although blood-based (or partially blood-based) dosimetry is an accepted method for estimation of the RBM dose (*1, 3, 6, 7*), the correlation with the observed hematologic toxicity is not sufficiently high for clinical use (*5, 8*). Especially when the radiopharmaceutical shows RBM retention, 2D image-based dosimetry seems to be a better predictor for hematological toxicity (*5*).

In our institution, both above-mentioned methods were prospectively applied in a clinical phase I pretargeted radioimmunotherapy (PRIT) study in twenty patients with advanced colorectal cancer (*9*). Dosimetric data based on a diagnostic administration of an ^{111}In-labelled tracer were used to predict the RBM AD in a subsequent treatment with the same tracer labelled with ^{177}Lu. Despite low predicted RBM absorbed doses (<0.5 Gy), five patients developed a grade 1-2 and two patients a grade 3-4 thrombocytopenia after treatment. The dosimetric results guided activity dosing to some extent, but no clear-cut discrimination could be made between the patients with or without toxicity. This indicates that an improved dosimetry method for prediction, and ideally prevention, of RBM toxicity is warranted.

A major improvement could be the use of three-dimensional (3D) images for dosimetry (*10-13*) instead of planar scintigraphic images. It has been shown that single photon emission computed tomography (SPECT)-based dosimetry leads to smaller errors than planar image-based dosimetry (*14*). The major advantage of 3D dosimetry is that, due to the lack of overlapping organs and more adequate attenuation correc-

tion, the output is a rather reliable measurement of the dose in a particular volume. The measured activity as well as the size of the volume of interest is more accurately estimated in 3D dosimetry. In contrast, using 2D dosimetry one has to rely on the extrapolation of the standard mean percentage RBM in the delineated area compared to the whole body RBM mass.
Therefore, we hypothesized that 3D SPECT-based RBM dosimetry results may better correlate with bone marrow toxicity. Although 2D image-based dosimetry is more and more replaced by 3D dosimetry in research settings, to date no 3D RBM dosimetry results have been validated and correlated to RBM toxicity.
Only recently, Schwartz et al. (*4*) introduced a combined positron emission tomography (PET) and blood-based RBM dosimetry method, mainly focusing on the red marrow-to-plasma activity concentration ratio. The activity in the lumbar vertebrae (LV) was used to calculate this ratio. Subsequently OLINDA (*15*) was used for S-factor-based dose calculation, using a phantom-based RBM mass, although a more patient-specific approach might be preferred (*4*). Therefore, a voxel based method using Monte Carlo simulations or dose-point kernel convolution would be advantageous, because this directly leads to the RBM dose. However, more than two or three images are required for these methods, in contrast to the PET study.

Here we applied a method for 3D RBM dosimetry, using the Monte Carlo-based 3D Radiobiological Dosimetry (3D-RD) software (*16*), to accurately estimate the RBM dose and the tumour dose in patients who underwent pretargeted RIT with a bispecific antibody and a ^{177}Lu-labelled peptide.

Materials and Methods

Patients

In this report, data acquired in a phase I study in metastasized colorectal cancer patients was used. Patients with advanced colorectal cancer gave informed consent to undergo pretargeted RIT. Patients received the anti-CEACAM5 x anti-hapten humanized trivalent bispecific antibody TF2. One day later the ^{177}Lu-labelled di-hapten peptide (2500-7400 MBq) was administered. Thirteen out of twenty patients had a complete image-data set, i.e. four SPECT scans and four whole-body planar scintigraphies acquired after treatment, and these patients were selected for 3D-dosimetry.

Image acquisition and use in dosimetry

Anterior and posterior whole body planar images were acquired immediately (at 8 cm/minu), 3 h (6 cm/min), 24 h and 72 h (both 4 cm/min) after administration of ^{177}Lu-labelled peptide, and followed by a SPECT scan made by continuous, circular scan-

ning with a 180° scan arc, 64 views per camera head and 19s/view. For each patient a region for the SPECT scanning was selected that contained lumbar vertebrae (LV) and at least one tumour lesion.
A Siemens dual-head gamma camera (ECAM, Hoffmann Estates, IL), equipped with medium energy collimators was used with a symmetric 15% window over the 208 keV energy peak for the SPECT scanning, and an additional 15% window over the 113 keV peak for the planar images.
Subsequently, these SPECT scans were used for tumour and bone marrow dosimetry of the ^{177}Lu dose and simulation of ^{90}Y doses (matched pair dosimetry). ^{90}Y has a shorter half-life than ^{177}Lu (2.66 days versus 6.71 days for ^{177}Lu), which corresponds better to the peptide residence time in the tumour. Therefore, it was suggested to replace ^{177}Lu with ^{90}Y in pretargeted RIT. The longer range of β-radiation from ^{90}Y versus ^{177}Lu (maximum penetration range in tissue of 12 and 2.5 mm, respectively) lead to concerns about the influence on the RBM dose. This is why we simulated ^{90}Y treatment with 3D-RD in order to estimate the effect on the tumour versus RBM dose. The planar ^{177}Lu images were only used to calculate the ^{177}Lu RBM dose. Due to organ overlap tumour dosimetry could not be performed on planar images.
A baseline FDG-PET – low-dose (130 kV, 50 mAs) computed tomography (CT), and a contrast enhanced diagnostic CT scan were performed within two weeks prior to study entry, and for follow up, eight weeks after ^{177}Lu injection. For the PET-CT an integrated camera (Biograph BGO duo, Siemens Medical Solutions, Malvern, PA,USA) was used, after FDG administration according to the EANM guidelines (*17*).

2D image and blood-based bone marrow dosimetry

During the PRIT study the dose to red bone marrow was calculated with a blood-based (*3*) and a 2D image-based dosimetry method (*18*). The blood-based RBM dose was based on blood samples collected 2 minutes, 30 minutes, 1 h, 2 h, 4 h, 24 h and 72 h after peptide injection and the total body activity (retrieved from the whole body planar images). These samples were counted in a gamma counter (Wizard, Pharmacia-LKB, Sweden) with reference samples prepared from the injected products, using appropriate energy windows. Whole body activities were calculated and combined with the blood counts for the final dose calculation as described by Shen et al.(*3*) This was performed with the SPRIND software (*18*) using a red marrow-to-blood activity concentration of one, as was determined for ^{177}Lu-peptide (*19*).
For the 2D image-based method, SPRIND was used to delineate the cranium, representing the activity in the RBM and to calculate the residence times. The residence time of the cranium activity was divided by the fraction of the RBM mass in the cranium to the mass in the total skeleton, for which the default value 0.119 was taken from ICRP23's Reference Man. Subsequently, OLINDA software (*15*) was used to calculate the RBM dose.

SPECT image reconstruction

SPECT scans were reconstructed with the iterative reconstruction software ReSPECT (Scivis, Germany), in six iterations, without noise reduction, with background subtraction and attenuation correction of 0.13 cm^{-1}, based on the results of Brown et al. (*20*). Because attenuation correction with the Chang-like method (*21*) as used by ReSPECT is based on the body contours, a correct body contour is needed for quantitative use of the images.
In ReSPECT the 'threshold object background' is used for definition of the body contour; voxels with a value higher than this threshold are assigned to the body. The contour can be defined correctly with the default threshold as long as the target (body)-to-background activity ratio is high enough. The scans acquired directly and 3 h post-injection were reconstructed with ReSPECT's default settings for 'threshold object background', because body-to-background activity ratios were sufficiently high. For the scans 24 h and 72 h post-injection the contour was fitted to the contour of the first scan, by lowering the threshold value, as the lower whole body activity would lead to a smaller body contour with the default settings.

Calibration

For the callibration of the SPECT scans, a cylindrical phantom was filled with 440 MBq ^{177}Lu, dissolved in 9.1 L water, and imaged using the same scanning and reconstruction protocol as used for the patient-SPECTs. The known activity at the time of acquisition, combined with the number of counts in a volume drawn around the phantom, resulted in a calibration factor of 6.23 x 10^{-6} MBq per count.

Delineation and co-registration

Tumour orientated co-registration of the SPECT scans and the low-dose CT was performed with the HERMES Gold 2.10 software (HERMES Medical Solutions, Stockholm, Sweden). The co-registered CT was scaled to the same matrix size as the SPECT (128x128x78).
For each patient VOIs were manually delineated for RBM in the LV (VOI_{LV}) on the SPECT scans, and for one tumour lesion (VOI_{tumour}) on the CT.
For the VOI_{LV}, at each time point, the RBM rich parts of at least two LV were delineated and further processed as one VOI. If delineation on the SPECT scans was not possible because the LV could not be distinguished from the background, the co-registered CT was used for delineation.
To confirm the location and presence of tumour, the contrast-enhanced CT, SPECT and PET scans were used. To limit the impact of the partial volume effect, tumours with a diameter of at least 2 cm were selected.

3D-RD

For the 3D dosimetry the Monte Carlo-based 3D-RD dosimetry package, developed by George Sgouros' group at the Johns Hopkins Medical Institute (Baltimore, USA), was used (*13, 16*). The voxel values of the SPECT scans were multiplied by the calibration factor, resulting in activity maps. The low-dose CT scan was used to assign a density and composition (soft tissue, lung or bone) to each voxel of the SPECT scans. The activity, density, and composition maps were the input for the Monte Carlo (MC) simulations. For each SPECT scan 10^6 MC simulations were accomplished, using the spectra probability distributions obtained from MIRD (*22*), resulting in a dose rate per voxel for each scan.
The dose per voxel was calculated by integrating the dose rates for each voxel after exponential extrapolation of energy deposition after the last scan, based on the third and fourth scan. This finally resulted in a dose map. Integration of the dose rates per VOI lead to the VOI specific mean absorbed doses.

3D tumour dosimetry

For the VOI_{tumour} the mean absorbed dose (AD_{tumour}) and a dose volume histogram (DVH) were determined. The DVH provides insight in the heterogeneity of the AD in the tumour. For comparison, the AD in VOI_{tumour} were also calculated with the sphere model in OLINDA (*15*). Therefore, the mass of the VOI was calculated with the density map, created from the low-dose CT, and the total activity in the VOI_{tumour} at the four different time points (and extrapolated for the period after the last scan) was used to calculate the residence time.

3D LV-based RBM dosimetry

The LV were delineated on each scan because the co-registration was tumour oriented, which meant that using one VOI_{LV} for all scans would introduce an additional error. Therefore, the integrated mean dose rate per VOI_{LV} was used. This gives a mean absorbed dose for the RBM (AD_{RBM}), but no DVH.
To investigate the biological effect of the dose rate, also the biological effective dose (BED) was calculated for the RBM:

$$R_{t-RBM} = \frac{AD_{tumour}}{AD_{RBM}} \qquad Eq.\ 1$$

with the radiobiological parameters from the linear quadratic equation model (α and β, and α/β = 10 Gy (*23*)), the absorbed dose (AD) and the Lea-Catchside G-factor ($G(T_\mu)$), depending on the DNA repair rate (μ): 0.46 h (*23*).

The 3D LV-based AD_{RBM} was compared to the blood-based and the 2D cranium-based RBM dosimetry results, and correlated with the grade of thrombocytopenia (graded according to NCI Common Terminology Criteria v3.

Tumour-to-RBM dose ratios

In adequate treatment settings, the AD_{tumour} is sufficiently higher than the AD_{RBM}. To evaluate this, the tumour-to-RBM dose ratio ($R_{t\text{-}RBM}$) was calculated:

$$BED = AD_{RBM}\left(1 + \frac{G(T_\mu)}{\alpha/\beta} AD_{RBM}\right) \qquad \textit{Eq. 2}$$

This calculation was done for the ^{177}Lu dose and the simulated ^{90}Y dose, because a higher ratio would indicate a more suitable radionuclide for this treatment.

Results

Patients, VOIs and RBM toxicity

To estimate the tumour dose we used liver metastases (8 patients), lung metastases (2 patients) or the primary tumour or local recurrence (3 patients). The patient and VOI characteristics are summarized in *Table 1*.
The hematologic toxicity is represented by the grade of thrombocytopenia. Of the included patients, three patients scored grade 4, grade 3 and grade 2 thrombocytopenia respectively, and three other patients grade 1 thrombocytopenia. One patient (patient 18) just without a thrombocytopenia (120 x 10^9 platelets/L, while <120 x 10^9 platelets/L is defined as grade 1), did show a grade 2 leucopenia. Whereas in two other patients (patient 10 and 16) a leucopenia (grade 1 and 2 respectively) was seen complementary to the thrombocytopenia (grade 3 and 4).

3D tumour and RBM doses

The ^{177}Lu AD_{tumour} ranged from 0.46 to 3.76 Gy (median 1.45 Gy). In the subgroup of patients with delineated liver metastases the mediantumour dose was 2.50 Gy. A typical DVH of a tumour is shown in *Figure 1*.
The AD_{tumour} calculated with 3D-RD was similar in most patients, and only slightly higher than with OLINDA (<5.0%), except for one patient (patient 10) who showed a 9% higher 3D-RD tumour dose and one patient (patient 18) who showed a higher dose (36 %) for OLINDA.
RBM doses ranged from 0.12 to 0.97 Gy (median 0.43). In all patients the BED was very similar to the AD (≤0.1% difference) (data not shown).

Table 1: Patient, and VOI_{tumour} details and dose results

Patient	Age (years)	Sex	Location VOI_{tumour}	AA (GBq)	Volume VOI_{tumour} (mL)	Platelet toxicity (grade)	AD_{RBM} (Gy)	3D-RD AD_{tumour} (Gy)	OLINDA AD_{tumour} (Gy)
7	63	F	Rectum	6.2	14	0	0.39	0.73	0.71
10	70	M	Liver	7.4	70	4	0.51	2.94	2.67
11	55	F	Liver	7.4	44	0	0.29	2.53	2.47
12	70	M	Liver	7.4	386	0	0.30	1.54	1.47
13	76	M	Colon	7.4	23	0	0.12	0.52	0.51
14	52	F	Liver	4.0	23	1	0.70	3.70	3.72
15	58	M	Liver	5.9	285	1	0.58	0.86	0.83
16	76	M	Colon	4.6	121	3	0.97	0.66	0.64
17	73	M	Lung	4.5	65	2	0.43	0.63	0.62
18	63	F	Liver	2.5	104	0	0.48	3.76	5.12
19	66	F	Liver	7.4	141	0	0.28	1.45	1.38
20	72	M	Lung	5.6	723	1	0.72	0.46	0.45
21	39	F	Liver	5.6	154	0	0.23	2.47	2.45
Median (range)	66 (39-76)				104 (14-723)		0.43 (0.12-0.97)	1.45 (0.46-3.76)	1.38 (0.45-5.12)

RBM = red bone marrow. AA = administered activity, tox = toxicity: grade thrombocytopenia

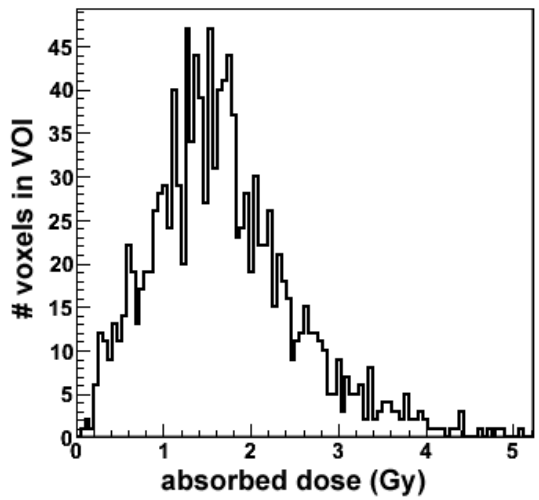

Figure 1: Dose volume histogram of the tumour volume of interest, located in the liver of patient 19.

Correlation between RBM dose and RBM toxicity

All blood-based, cranium-based and 3D-RD-based RBM doses are plotted against the grade of platelet toxicity in *Figure 2*. 3D-RD-based RBM doses (*Figure 2A*) were in general higher (median 0.43 Gy) than the doses calculated with the blood-based and 2D-image-based methods (*Figure 2B* and *2C*, median 0.21 and 0.20 Gy, respectively). The highest 3D-RD-based RBM dose without RBM toxicity was 0.39 Gy. All other patients, with RBM doses in the range of 0.43-0.97 Gy, showed RBM toxicity; the only patient in this range (0.48 Gy) without thrombocytopenia had a grade 2 leucopenia. Blood- and 2D image-based RBM doses for patients with grade 1-2 RBM toxicity were in the same range as for the patients without toxicity (0.14–0.29 Gy and 0.11-0.26 Gy, respectively), whereas blood-based RBM doses for two grade 3-4 patients were higher (0.51 and 0.66 Gy).

Tumour to RBM dose ratios for ^{177}Lu compared to ^{90}Y

The effect of ^{90}Y versus ^{177}Lu was shown by the simulated ^{90}Y dosimetry based on the ^{177}Lu images, co-registration and VOIs (*Table 2*). The median tumour-to-RBM dose ratios was 5.08 for ^{177}Lu and 4.97 for ^{90}Y, with a median percentage increase of 21%, though with a wide inter-patient variation (range -3-56%).
Interestingly, patients with a high RBM dose using ^{177}Lu treatment showed the largest percentage increase in tumour to RBM dose ratio when changing to ^{90}Y (*Figure 3*).

Table 2: The difference between the tumour-to-RBM dose ratios for treatment with ^{177}Lu and simulated for ^{90}Y. A positive difference represents a higher tumour to RBM dose ratio for ^{90}Y compared to ^{177}Lu.

Patient	Tumour-to-RBM dose ratios		Difference in tumour-to-RBM ratios for ^{90}Y minus ^{177}Lu (%)
	^{177}Lu	^{90}Y	
7	1.88	2.13	13%
10	5.72	6.54	14%
11	8.84	9.78	11%
12	5.08	7.27	43%
13	4.33	4.33	0%
14	5.26	6.37	21%
15	1.49	2.29	54%
16	0.68	1.06	56%
17	1.46	2.02	39%
18	7.77	8.87	14%
19	5.11	4.97	-3%
20	0.64	0.99	54%
21	10.91	13.72	26%
Median (range)	5.08 (0.64-10.91)	4.97 (0.99-13.72)	21% (-3-56%)

RBM = red bone marrow

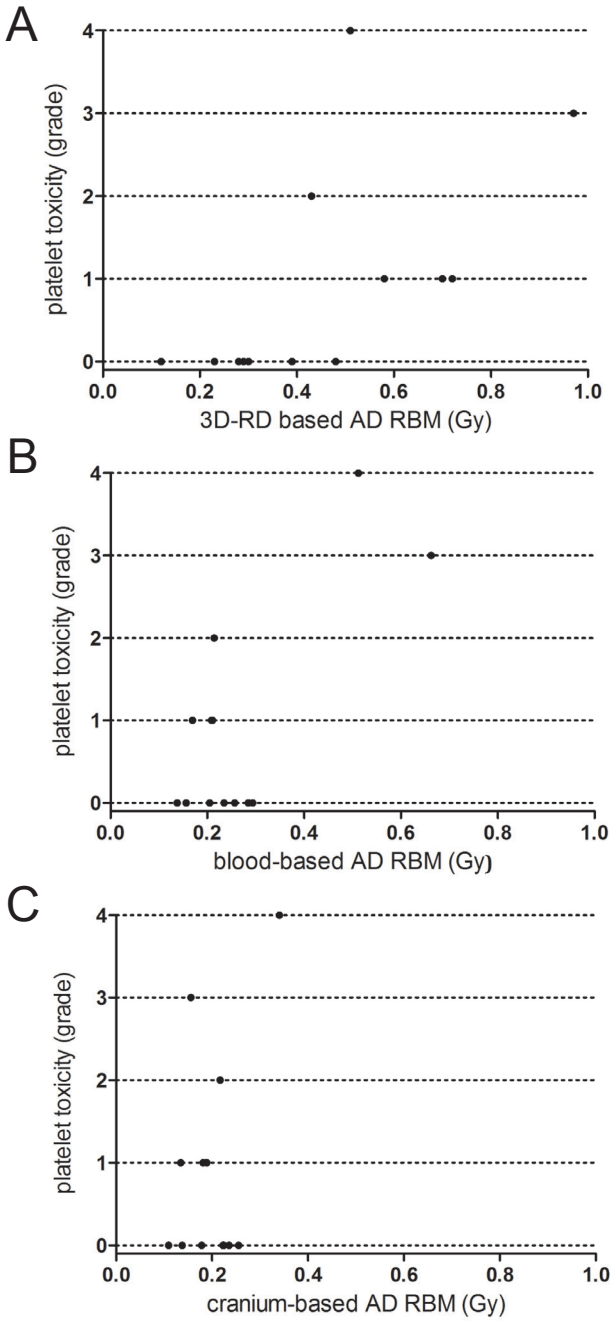

Figure 2: 3D-RD-based (A), blood-based (B) and cranium-based (C) absorbed dose in the red bone marrow, versus the grade of platelet toxicity. *AD RBM = absorbed dose red bone marrow.*

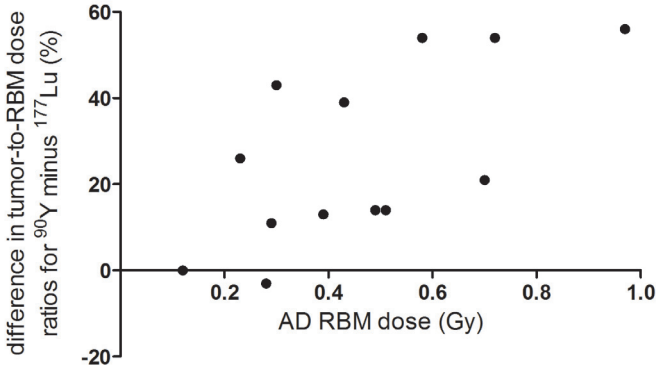

Figure 3: Per patient RBM doses plotted versus the percentage difference in tumour-to-RBM dose ratios for ^{90}Y (simulated) minus ^{177}Lu (measured). A positive difference represents a higher ratio for ^{90}Y compared to ^{177}Lu.

Discussion

Accurate dosimetric calculations of tumour and RBM doses are essential for patient-specific treatment planning in pretargeted RIT. In this study, we demonstrated how 3D-RD can be used for advanced quantification of the tumour and RBM dose and the prediction of RBM toxicity.

With 3D-RD all patients with RBM toxicity (including grade 1-2) had a higher RBM dose than the patients without any RBM toxicity. This distinction was not observed with the blood-based and 2D-cranium-based methods. RBM doses were in most patients higher when calculated with 3D-RD than with the blood-based method (11 patients) and the cranium-based method (12 patients). In blood-based RBM dosimetry it is assumed that the blood activity concentration is an accurate surrogate for the bone marrow concentration at all time points. However, in some patients we observed some bone marrow retention at the later imaging time point (24 h and 72 h post injection). Therefore, the blood-based method could result in an underestimation for the AD_{RBM}. The 2D cranium-based dosimetry might also have resulted in an underestimation of the AD_{RBM}. The fraction RBM in the cranium is used to represent the activity in the total RBM. In the SPRIND software package, this fraction was defined as 0.119, based on the ICRP23's Reference Man, representing a 40-year old male. For our patient-population (median age 63 year), this might have been an overestimation. Since the distribution of the RBM over the skeleton is age and patient-specific, ideally this fraction should be individually measured, and a patient-specific percentage of the RBM in a certain VOI should be used for this method.

In addition, the difference between the 3D LV-based and 2D cranium-based AD_{RBM} could be explained by inhomogeneous uptake in the RBM (*2, 5*), and the influence of activity surrounding the LV on the AD_{LV}. We would have preferred to use the same

VOI for both methods. Unfortunately, it is not feasible to use a VOI for the lumbar vertebrae in the SPRIND software, because an appropriate background ROI could not be defined. The cranium does not suffer from overlapping organs, which is an important criterium in planar image dosimetry. For the 3D dosimetry, it is more favorable to use the lumbar vertebrae, as the larger bone marrow volume is less affected by the partial volume effect.

An absorbed dose of 2 Gy in the RBM is a generally accepted limit above which RBM toxicity could occur. Nonetheless, based on the 3D-RD dosimetry we observed thrombocytopenia or leukocytopenia (≥ grade 1) in all patients receiving >0.4 Gy on the RBM, while none of the patients had bone marrow involvement or marrow reserve reducing treatments within 4 weeks before entering the study.

Bone marrow toxicity has been described before in patients receiving doses lower than 2 Gy (*6, 24*). This might suggest that to avoid any grade of toxicity, a limit lower than 2 Gy should be used for some dosimetry methods, radiolabelled compounds, or patient populations. This might be due to methodological differences in the dosimetry, i.e. correction for the partial volume effect. Furthermore, dose rate might be an important factor influencing the dose-reponse correlation (*25-27*). Some patient specific factors are also likely to contribute to the risk of hematologic toxicity, such as age, previous treatments influencing the bone marrow reserve, elapsed time since the last chemotherapy, etc (*28, 29*). Therefore, the dose-toxicity correlation found for a certain compound in a specific patient population cannot easily be generalized for other studies. However, the intra-study results in a large group of patients calculated with the same dosimetry method can lead to adequate treatment planning for that specific (experimental) treatment.

3D-image based dosimetry, either PET, or SPECT-based, is methodologically the most direct approach for RBM dose calculation in pretargeted RIT. Morover, 3D dosimetry above 2D dosimetry in bypassing the influence of overlapping organs, the advantage of 3D-RD LV dosimetry is the more accurate VOI drawing. and provides a result that contributes to the general knowledge about RBM response. Therefore, we advocate that further investigation of the dose-response relation in the RBM should be 3D-based. Nevertheless, it seems reasonable not to disqualify the simpler methods for future use in the clinic. These less demanding methods might, combined with 3D-imaging based methods (i.e. as in the method described by Schwartz et al.(*4*), be sufficient and better suited for use in daily practice.

The OLINDA-based results of the tumour absorbed doses were comparable to the 3D-RD results. In general OLINDA leads to a somewhat lower dose, which can be explained by the influence of activity surrounding the VOI. For use of the OLINDA sphere model, the VOI is assumed to be isolated. In 3D-RD, surrounding activity does contribute to the tumour dose, which is more realistic.

On the other hand, using the OLINDA sphere model instead of MC simulations is much faster, it only provides a mean dose, and therefore might be less useful for dose-

response monitoring. Besides this, OLINDA RBM dosimetry, or in general S-factor-based RBM dosimetry, is not feasible without a known (or model based) RBM mass. Therefore, the MC-based dosimetry is advantageous for RBM dosimetry.
The results of the ^{90}Y simulation that replacing ^{177}Lu by ^{90}Y would lead to a percentage increase in the tumour-to-RBM dose ratio, especially in patients with a higher RBM dose. The increase in tumour-to-RBM dose ratio for ^{90}Y suggests that the impact of the shorter half-life of ^{90}Y for the tumour dose is somewhat larger than for the RBM dose in most patients. However, with the low tumour doses and tumour-to-RBM dose ratio that were obtained with ^{177}Lu and ^{90}Y, a clinically relevant increase seems out of reach.
It seems that matched pair dosimetry, as shown for ^{177}Lu and ^{90}Y, could be a convenient and relatively inexpensive alternative for an animal or patient study, in order to investigate the effect of a different radionuclide on the tumour-to-RBM dose ratio. However, simulation does not account for therapeutic differences due to inhomogeneous distribution of the radioactivity within the tumour.

Conclusions

This work outlines how patient-specific dosimetry with 3D-RD can quantify RBM absorbed doses based on the lumbar vertebrae and tumour doses. The 3D-RD RBM doses seem to be a more sensitive predictor for patients showing any grade of RBM toxicity than blood-based and planar image-based RBM doses.
In addition, with comparing the ^{177}Lu doses with the simulated ^{90}Y doses, it was shown that matched pair dosimetry with both RBM and tumour dose calculation might be useful for the selection of a radionuclide for therapy.

References

1. Hindorf C, Glatting G, Chiesa C, Linden O, Flux G. EANM Dosimetry Committee guidelines for bone marrow and whole-body dosimetry. *Eur J Nucl Med Mol Imaging.* Jun 2010;37(6):1238-1250.
2. Sgouros G, Jureidini IM, Scott AM, Graham MC, Larson SM, Scheinberg DA. Bone marrow dosimetry: regional variability of marrow-localizing antibody. *J Nucl Med.* Apr 1996;37(4):695-698.
3. Shen S, DeNardo GL, Sgouros G, O'Donnell RT, DeNardo SJ. Practical determination of patient-specific marrow dose using radioactivity concentration in blood and body. *J Nucl Med.* Dec 1999;40(12):2102-2106.
4. Schwartz J, Humm JL, Divgi CR, Larson SM, O'Donoghue JA. Bone Marrow Dosimetry Using 124I-PET. *J Nucl Med.* Apr 2012;53(4):615-621.
5. Ferrer L, Kraeber-Bodere F, Bodet-Milin C, et al. Three methods assessing red marrow dosimetry in lymphoma patients treated with radioimmunotherapy. *Cancer.* Feb 15 2010;116(4 Suppl):1093-1100.
6. Siegel JA, Yeldell D, Goldenberg DM, et al. Red marrow radiation dose adjustment using plasma FLT3-L cytokine levels: improved correlations between hematologic toxicity and bone marrow dose for radioimmunotherapy patients. *J Nucl Med.* Jan 2003;44(1):67-76.
7. Wessels BW, Bolch WE, Bouchet LG, et al. Bone marrow dosimetry using blood-based models for radiolabeled antibody therapy: a multiinstitutional comparison. *J Nucl Med.* Oct 2004;45(10):1725-1733.
8. Brouwers AH, Buijs WC, Mulders PF, et al. Radioimmunotherapy with [131I]cG250 in patients with metastasized renal cell cancer: dosimetric analysis and immunologic response. *Clin Cancer Res.* Oct 1

2005;11(19 Pt 2):7178s-7186s.
9. Schoffelen R, Boerman OC, Goldenberg DM, et al. Development of an imaging-guided CEA-pretargeted radionuclide treatment of advanced colorectal cancer: First clinical results. *Submitted for publication.*
10. Assie K, Dieudonne A, Gardin I, Buvat I, Tilly H, Vera P. Comparison between 2D and 3D dosimetry protocols in 90Y-ibritumomab tiuxetan radioimmunotherapy of patients with non-Hodgkin's lymphoma. *Cancer Biother Radiopharm.* Feb 2008;23(1):53-64.
11. Lyra M, Lagopati N, Charalambatou P, Vamvakas I. Patient-specific dosimetry in radionuclide therapy. *Radiat Prot Dosimetry.* Sep 2011;147(1-2):258-263.
12. Fukuoka M, Taki J, Mochizuki T, Kinuya S. Comparison of diagnostic value of I-123 MIBG and high-dose I-131 MIBG scintigraphy including incremental value of SPECT/CT over planar image in patients with malignant pheochromocytoma/paraganglioma and neuroblastoma. *Clin Nucl Med.* Jan 2011;36(1):1-7.
13. Sgouros G, Frey E, Wahl R, He B, Prideaux A, Hobbs R. Three-dimensional imaging-based radiobiological dosimetry. *Semin Nucl Med.* Sep 2008;38(5):321-334.
14. He B, Wahl RL, Du Y, et al. Comparison of residence time estimation methods for radioimmunotherapy dosimetry and treatment planning--Monte Carlo simulation studies. *IEEE Trans Med Imaging.* Apr 2008;27(4):521-530.
15. Stabin MG, Sparks RB, Crowe E. OLINDA/EXM: the second-generation personal computer software for internal dose assessment in nuclear medicine. *J Nucl Med.* Jun 2005;46(6):1023-1027.
16. Prideaux AR, Song H, Hobbs RF, et al. Three-dimensional radiobiologic dosimetry: application of radiobiologic modeling to patient-specific 3-dimensional imaging-based internal dosimetry. *J Nucl Med.* Jun 2007;48(6):1008-1016.
17. Boellaard R, O'Doherty MJ, Weber WA, et al. FDG PET and PET/CT: EANM procedure guidelines for tumour PET imaging: version 1.0. *Eur J Nucl Med Mol Imaging.* Jan 2010;37(1):181-200.
18. Visser E, Postema E, Boerman O, Visschers J, Oyen W, Corstens F. Software package for integrated data processing for internal dose assessment in nuclear medicine (SPRIND). *Eur J Nucl Med Mol Imaging.* Mar 2007;34(3):413-421.
19. Forrer F, Krenning EP, Kooij PP, et al. Bone marrow dosimetry in peptide receptor radionuclide therapy with [177Lu-DOTA(0),Tyr(3)]octreotate. *Eur J Nucl Med Mol Imaging.* Jul 2009;36(7):1138-1146.
20. Brown S, Bailey DL, Willowson K, Baldock C. Investigation of the relationship between linear attenuation coefficients and CT Hounsfield units using radionuclides for SPECT. *Appl Radiat Isot.* Sep 2008;66(9):1206-1212.
21. Chang L-T. A Method for Attenuation Correction in Radionuclide Computed Tomography. *Nuclear Science, IEEE Transactions on.* 1978;25(1):638-643.
22. Eckerman KF, Endo A. *MIRD: Radionuclide Data and Decay Schemes*. 1st ed. Reston, VA: Society of Nuclear Medicine; 2008.
23. Baechler S, Hobbs RF, Prideaux AR, Wahl RL, Sgouros G. Extension of the biological effective dose to the MIRD schema and possible implications in radionuclide therapy dosimetry. *Med Phys.* Mar 2008;35(3):1123-1134.
24. Juweid ME, Sharkey RM, Behr T, et al. Radioimmunotherapy of patients with small-volume tumors using iodine-131-labeled anti-CEA monoclonal antibody NP-4 F(ab')2. *J Nucl Med.* Sep 1996;37(9):1504-1510.
25. Behr TM, Memtsoudis S, Sharkey RM, et al. Experimental studies on the role of antibody fragments in cancer radio-immunotherapy: Influence of radiation dose and dose rate on toxicity and anti-tumor efficacy. *Int J Cancer.* Aug 31 1998;77(5):787-795.
26. Behr TM, Sharkey RM, Sgouros G, et al. Overcoming the nephrotoxicity of radiometal-labeled immunoconjugates: improved cancer therapy administered to a nude mouse model in relation to the internal radiation dosimetry. *Cancer.* Dec 15 1997;80(12 Suppl):2591-2610.
27. Howell RW, Goddu SM, Rao DV. Design and performance characteristics of an experimental cesium-137 irradiator to simulate internal radionuclide dose rate patterns. *J Nucl Med.* May 1997;38(5):727-731.
28. Baechler S, Hobbs RF, Jacene HA, Bochud FO, Wahl RL, Sgouros G. Predicting hematologic toxicity in patients undergoing radioimmunotherapy with 90Y-ibritumomab tiuxetan or 131I-tositumomab. *Journal of nuclear medicine : official publication, Society of Nuclear Medicine.* Dec 2010;51(12):1878-1884.
29. O'Donoghue JA, Baidoo N, Deland D, Welt S, Divgi CR, Sgouros G. Hematologic toxicity in radioimmunotherapy: dose-response relationships for I-131 labeled antibody therapy. *Cancer Biother Radiopharm.* Aug 2002;17(4):435-443.

9

Summary

The working hypothesis for this thesis was that pretargeting could improve radioimmunotherapy (RIT) of tumours. RIT is the selective targeting of tumour-associated antigens expressed on the tumor cells with radiolabeled antibodies. However, the slow uptake and clearance rate of intact antibodies delays tumour detection by imaging and increases bone marrow toxicity during therapy. Pretargeting techniques were developed to overcome these problems, and to allow rapid and selective delivery of radionuclides to tumours. In this approach, a bispecific monoclonal antibody (bsMAb) is administered intravenously and given time to accumulate in the tumour and clear from the circulation. Subsequently, a radiolabeled hapten-peptide is given that clears rapidly from the blood and body, but is trapped in the tumor by the anti-hapten binding arm of the bsMAb.

We investigated pretargeting for carcinoembryonic (CEACAM5)-expressing tumours with the bsMAb TF2, and the peptide IMP288. TF2 is a humanized anti-CEACAM5 x anti-HSG bsMAb construct produced using the Dock-and-Lock-technology, resulting in a stable humanized tri-Fab molecule. TF2 contains two Fab fragments with high affinity for CEACAM5 and another Fab-fragment with affinity for the hapten, histamine-succinyl-glycine (HSG). IMP288 is a peptide that contains two HSG moieties for improved hapten-peptide uptake and retention, and the chelating moiety 1,4,7,10-tetraazacyclododecane-1,4,7,10-tetraacetic acid (DOTA), capable of stable binding of a variety of radionuclides, such as ^{111}In for SPECT imaging, with ^{18}F and ^{68}Ga for PET imaging, or ^{90}Y and ^{177}Lu for pretargeted radioimmunotherapy (PRIT).

First we studied this pretargeting system in murine tumour models, to guide the translation into the clinical situation. In our animal studies we used BALB/c nude mice with small CEA-expressing LS174T human colonic tumours either subcutaneously (s.c.) or intraperitoneally (i.p.).

In the studies described in **Chapter 2 and 3** the effects of the antibody and peptide dose on their uptake in the tumour and normal tissues was investigated. The TF2 and IMP288 dose were escalated to find which administered dose resulted in the maximum amount that could be targeted specifically to the tumours. We found that the optimal dose of TF2 was 5.0-6.0 nmol/mouse and the optimal dose of IMP288 was 0.28 nmol/mouse.

In **Chapter 2** we studied the specificity of pretargeted immuno-PET with TF2 and ^{68}Ga-labelled IMP288 in BALB/c nude mice with a s.c. LS174T tumour, a s.c. CEA-negative tumour, or an inflammation in thigh muscle. Within one hour, the PET-images and dissected tissues showed high and specific targeting of the ^{68}Ga-IMP288 in the tumour and very low uptake in normal tissues, in a CEA-negative tumour, and inflamed muscle. The same mice were also imaged after injection of ^{18}F-FDG.

^{18}F-FDG localized efficiently in the tumour, but also in the inflamed muscle and in various normal tissues (brain, myocardium, kidney, focally in intestines). A similar hapten-peptide was labelled with ^{18}F and tested in mice with a s.c. LS174T tumour. ^{18}F-labelled peptide distributed similarly in the tumour and normal tissues as the ^{68}Ga-labelled peptide, indicating that either radiolabelled hapten-peptide could be used. It was concluded that pretargeted immuno-PET with TF2 and a ^{68}Ga- or ^{18}F-hapten-peptide is a rapid and highly specific imaging modality for the detection CEA-positive tumours, and is more specific than ^{18}F-FDG-PET.

The advantages of an orthotopic animal model compared to a s.c. tumour model for demonstrating the sensitivity of a new imaging method are that such a model also includes the effect of tumour-to-background ratios, and tumours of variable sizes within one animal can be studied. Therefore, in **Chapter 3**, we assessed the sensitivity of the pretargeted immuno-PET with TF2 and ^{68}Ga-IMP288 in mice with small intraperitoneal xenografts. Again, we compared pretargeted immuno-PET with ^{18}F-FDG-PET. After injection of the ^{68}Ga-labelled peptide high tumour-to-background ratios were observed, resulting in clear visualization of the tumours, and detection of all intra-abdominal tumour lesions ≥ 10 μL. ^{18}F-FDG also visualized some of these tumours, but also showed physiological uptake in various normal tissues, with lower tumour-to-intestines ratios. These results suggest that pretargeted immuno-PET with bsMAb and a ^{68}Ga-labelled peptide could be a very sensitive imaging method for colonic cancer.

After having optimized the TF2 and IMP288 doses and having demonstrated the potential of pretargeted immuno-PET imaging, in **Chapter 4** the therapeutic efficacy and toxicity of pretargeted radioimmunotherapy (PRIT) with TF2 and ^{177}Lu-labelled IMP288 was determined in mice with s.c. LS174T tumours. Because pretargeting reduced the radiation dose to the bone marrow, the total amount of radioactivity that could be administered in one treatment cycle was much lower than the maximum tolerable dose. Therefore, the tumour targeting of two regimens of repeated administrations of radiolabelled IMP288 were investigated in a biodistribution experiment. The first regimen consisted of one TF2 injection followed by multiple IMP288 administrations in a 3 hour interval. The second regimen consisted of multiple cycles where each IMP288 administration was preceded by a new TF2 injection (72 hour interval). The last dosing schedule resulted in the highest radioactivity dose delivered to the s.c. tumours. In the therapy experiment, mice received one, two or three successive treatment cycles. PRIT effectively delayed tumour growth and significantly prolonged survival significantly, with longer survival of the groups that received successive cycles without relevant toxicity. No relevant changes in mean body weight, leukocyte or platelet counts, or serum creatinine were measured. This study indicated that in mice PRIT could be an effective treatment modality against colon cancer with limited toxicity.

To predict the efficacy of pretargeted radioimmunotherapy, diagnostic images can be acquired after injection of the radiolabeled agent. This strategy of combining imaging with therapy is designated as theranostics, and was the subject of the study described in **Chapter 5**. The prospects for using pretargeted immuno-SPECT with TF2 and IMP288 labelled with ^{111}In to monitor the response to PRIT using ^{177}Lu-IMP288 in mice with i.p. growing LS174T tumours was examined. In this model pretargeted immuno-SPECT showed rapid and selective tumour targeting with very high tumor-to-background contrast, which led to the detection of very small tumours. The activity in the tumour lesions as measured with SPECT correlated well with uptake measured in dissected tissues. A survival study was performed in mice that received TF2 and ^{177}Lu-IMP288, non-pretargeted ^{177}Lu-IMP288, or PBS. In the treated group, immuno-SPECT-imaging allowed non-invasive monitoring of the delayed tumour growth non-invasively which corresponded to prolonged survival. These results showed the feasibility and additional value of imaging to monitor the efficacy of with the same pretargeting agents, TF2 and radiolabelled IMP288.

The preclinical studies were used to translate the pretargeting system into a first-in-men phase I study (**Chapter 6**). The main objectives of this study were to assess various pretargeting conditions and safety in patients with metastatic colorectal cancer (mCRC). For the participating patients no standard treatment options were available. Different dose schedules were studied in four cohorts of five patients [1] shortening the interval between the bsMAb and peptide administration (5 days *vs* 1 day), [2] escalating the TF2 dose (from 75 to 150 mg), and [3] reducing the peptide dose (from 100 to 25 μg). Rapid and selective tumour targeting of the radiolabelled peptide was visualized within one hour with high tumour-to-tissue ratios (>20 at 24 h). Improved tumour targeting was achieved with a 1-day interval between the administration of the bsMAb and the peptide, with the 25 μg peptide dose. High ^{177}Lu-IMP288 activity doses were well tolerated with some manageable TF2 infusion reactions, and transient grades 3-4 thrombocytopenia in two patients. It was concluded that pretargeting with TF2 and ^{177}Lu-IMP288 in patients with CEA-expressing mCRC is feasible and safe.

In **Chapter 7** the dosimetric analysis that was performed based on the whole body planar scintigraphic images and blood sampling was described. Before each therapy cycle patients received an imaging cycle with TF2 and ^{111}In-labeled IMP288. The ^{111}In-IMP288 data were used to simulate absorbed doses of ^{177}Lu-IMP288 and to calculate the maximum ^{177}Lu activity dose that could be administered safely. Individualized activity dosing seemed essential, as relatively large inter-patient variations were observed in TF2 and IMP288 pharmacokinetics in the phase I study. A strong and significant correlation was observed between IMP288 residence times and individual TF2 blood concentrations at the time of IMP288 injection. Therapeutic ^{177}Lu activity doses re-

sulted in low absorbed radiation doses to normal tissues. In the majority of patients who received the maximum or adjusted ^{177}Lu activity doses, the measured red bone marrow (RBM) doses did not exceed the threshold set in the protocol. Simulated ^{177}Lu-IMP288 absorbed red marrow doses were in good agreement with the actual measured doses. Hematologic toxicity correlated significantly with RBM dose.

The SPECT images acquired in the phase I study were also analysed with a new, sophisticated method, the Monte Carlo-based Three-Dimensional -Radiobiological Dosimetry (3D-RD) method (**Chapter 8**). The voxel values of the SPECT scans were converted to activity maps and a low-dose CT scan was converted to a densitiy map, and both maps were the input for the Monte Carlo simulations. This resulted in the energy deposition per voxel per scan time, and combining the results of the four SPECT scans per injection led to a dose map per VOI. In contrast to the previous described dosimetry methods, for 3D-RD the SPECT scans were used instead of the whole body planar images, and the lumbar vertebrae instead of cranium for RBM dosimetry, and 3D-RD allowed tumour dosimetry. Furthermore, this new dosimetry method did take in account tissue density and showed tumour heterogeneity. The feasibility of the 3D-RD software and its value for predicting RBM toxicity and therapeutic efficacy in the phase I clinical study of PRIT were studied and compared with the blood-based and planar image-based results. 3D dosimetry showed 2-fold higher RBM doses compared to the blood-based and planar image-based methods, and a better RBM dose-toxicity correlation. Furthermore, tumour and RBM ^{177}Lu doses acquired by the 3D-RD method were simulated for ^{90}Y. The mean increase of tumour-to-RBM ratio when simulating for ^{90}Y compared to ^{177}Lu was 21%. These results suggest that the 3DRD software may more accurately predict bone marrow toxicity and tumour doses than blood or 2D-image-based methods.

In **chapter 10** the results are discussed and future perspectives are outlined.

10

General discussion and future prospects

High morbidity and mortality rates of patients with metastatic colorectal cancer (mCRC) (*1*) demonstrate the need for better, effective imaging and therapeutic strategies. Despite the increase of treatment options since 2000 (*2-6*), eventually the disease progresses in most patients. In addition, current therapeutic regimens cause significant early and sometimes late toxicity, negatively affecting the patient's quality of life (*7*). Several therapies that have been approved as standard treatment for mCRC, such as cetuximab or panitumumab, show only limited increase of median overall survival (*5, 6*). Curative liver metastatectomy is an established approach (*8, 9*). Unfortunately, large population data revealed high recurrence rates (>50%) (*10*). Other attempts to combine different treatments, such as pre-operative concomitant chemo-radiation in advanced stage rectal cancer, have improved surgical results, but do not result in cure of all patients.

The prognosis of mCRC patients can be improved by early detection of disease, i.e. small tumour lesions that allow minimal invasive but adequate surgery (*11*). Furthermore, targeted systemic therapies with limited side effects are preferred to widen the arsenal of therapies and to circumvent drug resistance. Radionuclide targeting using monoclonal antibodies or receptor binding peptides could be a very effective technique, as has been demonstrated for non-Hodgkin's lymphoma and neuroendocrine tumours. However, for mCRC the results of radioimmunotherapy (RIT) with radiolabelled monoclonal antibodies are modest (*12*). In general, solid tumour lesions are less radiosensitive than hematologic tumours. So, in RIT further activity dose escalation is required to guide therapeutic radiation doses to these tumours. However, the long-circulating radiolabelled antibody causes continuous irradiation of the bone marrow. This results in dose-limiting bone marrow suppression before sufficient radiation doses can be delivered to solid tumours. Therefore, to maintain acceptable normal tissue absorbed doses, the tumour-to-normal tissue ratio should be improved.
A very promising strategy to improve this ratios is pretargeting, in which the targeting of the tumour and the radionuclide delivery are separated in two steps.

In this thesis, we have studied such a pretargeting system in preclinical studies, to guide the translation into the clinical situation. To develop a sensitive and specific imaging modality, tumour-to-normal tissue ratios should be maximal, and to achieve therapeutic efficacy, the amount of activity targeted to the tumours should be maximized, without increasing normal tissue radiation doses. Important pretargeting parameters to be optimized are: the bsMAb dose, the interval between injection of the bsMAb and the radiolabelled peptide and the peptide dose. As these parameters are interdependent, the process of optimization is rather challenging.

As pretargeted imaging/therapy is a two-step strategy including the subsequent administration of two agents, the first parameter to be examined is the optimal interval

between the bsMAb and radiolabelled peptide. Ideally, the peptide should be administered at the time that the highest amount of bsMAb is in the tumour, whereas it should be low in the circulation. At later time points, when blood concentration is low, bsMAb concentration in the tumour can also start to decrease. However, if the interval would be too short, and the bsMAb is not sufficiently cleared from the circulation yet, the antibody and the peptide will complex in the blood. This will not only reduce tumour targeting, but will also increase the circulatory half-life of the radiolabelled hapten-peptide complex. Thus, the optimal interval is the best compromise between the time at which the highest amount of bsMAb is in the tumour and the time needed required to have a low bsMAb concentration in the blood.
The amount of the bsMAb in the tumour can be enhanced by increasing the dose of bsMAb. It should be noted that when administering a higher bsMAb dose, a longer interval could be required to allow the bsMAb to clear from the blood. Furthermore, when the antigen sites on the tumour are saturated at a certain bsMAb dose, the maximal amount of bsMAb targeted to the tumour is achieved and a further increase of the bsMAb dose does not result in further improvement.
Another important factor in pretargeting is the peptide dose. The minimum peptide dose is determined by radiochemistry: the radiolabelling procedures determine the minimum amount of peptide that is required to label the amount of radioactivity that needs to be administered. For imaging, the radioactivity dose should be sufficiently high for reasonable image statistics, while for therapy it should be sufficient to guide a therapeutic radiation doses to the tumour. Conversely, a lower peptide dose radioabelled with a fixed amount of radioactivity, will increase the fraction of the radioactivity that will be delivered to tumour. On the other hand, a low peptide dose may result in a lower ratio between the circulating bsMAb and the administered peptide dose. Consequently, a higher fraction of the radiolabelled peptide in the blood could be captured by the circulating bsMAb, increasing the circulatory half-life of the radiolabelled peptide.

In our studies in mice, we investigated the optimal conditions for the pretargeted imaging and therapy application. The interval between TF2 and IMP288 administration we used in mice was 16 hours, as this was already studied by Sharkey *et al*. First, we escalated the TF2 dose to find which administered dose resulted in the maximum amount of TF2 that could be targeted specifically to the tumour and its effect on IMP288 tumour capture (chapter 2 and 4). We found that the optimal TF2 dose was 5.0-6.0 nmol per mouse, as higher TF2 doses did not result in a higher tumour uptake of TF2 or IMP288. Apparently, at higher doses saturation of CEA antigens in the subcutaneous xenografts occurred.
Subsequently, we determined the optimal peptide dose in this mouse model. For the application of micro-PET-imaging, the minimal IMP288 dose (400 ng) to be administered was determined by the amount required for a minimum of ^{68}Ga activity dose (5

MBq) to make high quality PET-images (chapter 2). For therapeutic application, we aimed at to find the maximum absolute amount of radioactivity that could be delivered to the tumour lesions. Therefore, we increased the IMP288 dose to determine the dose at which the maximum absolute amount of peptide was specifically targeted to the tumor. We found that the optimal dose was 0.28 nmol IMP288, and 26 MBq ^{177}Lu could be radiolabelled to this amount of peptide. In our preclinical therapy study, we observed that this activity dose was well below the maximal tolerable dose. Therefore, our treatment strategy included the use of repeated treatment cycles.

After the successful dose optimization in our preclinical studies, we showed that pretargeted immuno-PET with an anti-CEA bsMAb and a ^{68}Ga- or ^{18}F-hapten-peptide is a rapid, highly specific and sensitive imaging modality for the detection CEA-positive tumours (chapter 2 and 3). Within 1 h, tumour lesions showed high and specific uptake of the radiolabeled IMP288, while its uptake in normal tissues and inflamed muscle was low. This resulted in clear visualization of small intra-abdominal tumour lesions by pretargeted immuno-PET. In the same animal models, ^{18}F-FDG showed uptake in tumours as well as in various normal tissues (brain, heart, intestines) and the inflamed muscle, which complicated tumour discrimination. Although a high sensitivity and specificity for FDG-PET in detecting recurrent colorectal cancer lesions has been reported in patients, FDG-PET images could lead to diagnostic dilemmas in discriminating malignant from benign, highly metabolic lesions, such as inflamed tissues. Therefore, we concluded that pretargeted immuno-PET with bsMAb and a ^{68}Ga-labelled peptide could be an imaging method of additional value for colonic cancer.
Short-lived radionuclides, such as ^{68}Ga and ^{18}F, are ideally suited for pretargeted PET imaging, and their half-lives match the pharmacokinetics of the peptide for imaging. In our preclinical studies we showed similar if not identical distribution in vivo of the ^{18}F-labelled peptide and the ^{68}Ga-labelled peptide (chapter 2). The selection of the most suitable radionuclide depends on multiple factors. ^{68}Ga can be eluted twice daily from a ^{68}Ge/^{68}Ga generator, avoiding the need for an on-site cyclotron. For these studies, the procedure to label IMP288 with ^{68}Ga was optimized, resulting in a one-step labelling technique that could be completed within 45 minutes. ^{18}F, the most widely used radionuclide in PET, has an even more favourable half-life for pretargeted PET imaging (t½ = 110 min). Its shorter positron range in tissue (median 0.62 mm), results in better image quality in preclinical imaging. It is abundantly available and inexpensive. However, the chemistry involved in preparing ^{18}F-labelled products can be challenging. McBride *et al.* recently reported a simplified approach for preparing ^{18}F-labelled peptides that involves the formation of ^{18}F-aluminum complexes that can then be simply chelated by a chelate like NOTA (*13*). Translation to the clinical situation will show the feasibility of upscaling the radiolabelling procedure, and the effect of the intrinsic resolution of the clinical PET-scanner in combination with the spatial resolution of the radionuclides on imaging tumours.

To study the therapeutic effect of PRIT with TF2 and ^{177}Lu-IMP288, we compared the tumour growth and survival in mice with subcutaneous colorectal xenografts after PBS versus one, two or three cycles of PRIT. We demonstrated that using the optimal dose schedule and multiple treatment cycles of PRIT, it could be an effective treatment modality with limited toxicity for CEA-expressing human colonic tumours (chapter 4). Higher activity doses, administered in successive cycles, resulted in significantly longer survival compared to PBS, while the repeated treatment cycles did not cause significant changes in body weight, blood counts or acute kidney function.
In addition, we showed that pretargeted immuno-SPECT is an excellent imaging method to monitor the therapeutic effect of PRIT, using the same pretargeting agents (chapter 5). The pretargeted immuno-SPECT images showed rapid and selective tumor targeting with very high tumor-to-background contrast as early as one hour after injection. The successive images of the treated mice showed delayed tumor growth in the PRIT group, which corresponded with their prolonged survival. The combination of pretargeted immuno-SPECT during PRIT, as tested in our preclinical model, could also be a valuable strategy in clinical practice. The efficient combination of imaging and therapy using the same agents is designated as theranostics. Diagnostic information obtained from pre-therapeutic PET or SPECT, can be used to ensure that the radionuclide is specifically targeted to tumours, which guides patients selection. Dosimetric analysis of the images can be used to predict the benefit/risk ratio of a planned radionuclide therapy. Moreover, it can be crucial to estimate the optimal dose or radionuclide in radioimmunotherapy studies. Furthermore, imaging data can be used to assess therapy response.

The knowledge acquired in the preclinical studies was used to design the phase I study with TF2 and IMP288 in patients with progressive mCRC. The main objective of this first-in-men study was to optimize the dose schedule for tumour targeting in patients, while maintaining tolerable and reversible toxicity. Therefore we studied different dose schedules in four cohorts of five patients, assessing the effect of shortening the interval between the bsMAb and peptide administration (5 days *vs* 1 day), escalating the TF2 dose (from 75 to 150 mg), and reducing the peptide dose (from 100 to 25 μg). We demonstrated that PRIT with these agents in patients with CEA-expressing CRC is feasible and safe. Tumours were targeted specifically and rapidly. Tumour targeting was improved targeting when the interval between the bsMAb and peptide administration was reduced and at a lower peptide dose (chapter 6). In an attempt to reach higher concentrations in the tumour, we tested a 2-fold higher TF2 dose, but we did not observe improved tumour targeting. For future studies, it might be interesting to study the effect of a further TF2 dose escalation, e.g. 300 mg. However, with a higher infused TF2 dose a 2-day interval might be required to ensure rapid blood clearance of the radiolabeled peptide.

Overall, our preclinical and clinical studies indicated the limited uptake of radioactivity in normal tissue and limited radiation related toxicity in PRIT. Low normal tissue absorbed radiation doses were measured at high therapeutic ^{177}Lu activity doses (chapter 6), which resulted in minimal hematologic toxicity. The sporadic cases of grade 3-4 bone marrow toxicity correlated significantly with absorbed red marrow dose (chapter 7). 3D voxel based patient-specific dosimetry was shown to be a more accurate method for predicting bone marrow toxicity than the blood based and 2D methods (chapter 8). Therefore, PRIT will allow further activity dose escalation, which is required to achieve therapeutic radiation doses in solid tumours like CRC.

Apart from the hematologic toxicity, that was clearly radiation-induced, we monitored patients for potentially immunologic responses to the antibody infusions. Despite the fact that TF2 is a fully humanized antibody construct, infusion reactions were observed in one third of the patients at the second infusion of the bsMAb, which could not be completely prevented by prophylactic medications. The infusion reactions were transient and manageable by lowering the infusion rate and adding appropriate medication, and did not preclude continuation of treatment in most patients. In fact, further analysis of the serum samples acquired up to 24 h after the infusions, suggested that the allergic reactions are most likely due to complement-activation, rather than histamine release (data not shown). Therefore, critical situations with anaphylaxis upon repeated exposure are considered unlikely. So, the clinical relevance of this adverse event should be evaluated in larger patient groups and infusion schedules can be further optimized.
Another immunologic adverse effect was the formation of human antibodies against TF2 in ~50% of the patients after two infusions with the bsMAb. Increasing HAHA titers during at least eight weeks after the second administration were observed (chapter 5). No correlation was found between the formation of anti-TF2 HAHAs and the observed infusion reactions. High HAHA levels could further accelerate TF2 blood clearance at subsequent injection, which would further reduce tumour accumulation of TF2 at subsequent cycles.

Despite improved tumour targeting in the four successive patient cohorts, absolute tumour concentrations remained relatively low, and tumour retention was relatively short. The 3D voxel based dosimetry method confirmed the tumour absorbed doses to be sub-therapeutic, and no clinical therapy responses were measured by successive FDG-PET/CT.
This lack of efficacy could be due to various factors. First, all patients had gross metastatic disease, with mostly large tumours. MAb uptake in those larger lesions is known to be limited and inhomogeneous, due to high interstitial pressure. In the current first-in-man study, we were allowed only to include patients who had already been treated

with all standard therapies. For CRC, many lines of therapy were recently added to the list of approved treatments. Medical oncologist and patients consider experimental therapies only after standard treatment options. The long period of less effective treatment, in general results in large volume of disease at the time the patient is fit for experimental therapies. By then, only a small fraction of the patients is in a physical condition to be safely included in phase I clinical trials.

Due to the fast progression of disease in our patient population, patients could not be given the subsequently planned additional treatment cycles, while the therapy trial was designed to offer four repeated dosing cycles every eight weeks. So, all patients only received a quarter of the planned activity dose. However, in this first-in-men study a safe interval of eight weeks between treatment cycles was required to allow evaluation of the myelotoxicity of each treatment cycle. As we have confirmed the initial safety of PRIT with these agents and high acitivity doses, in future studies patients can be treated with a shorter interval between the treatments.

Another way to improve therapeutic efficacy could have been to switch from ^{177}Lu to ^{90}Y as a therapeutic radionuclide. ^{90}Y's physical half-life (64 h) better matches the residence time in the tumour (6.7 days), which would enhance the radiation dose to the tumour. However, the tissue penetration range of both radionuclides is markedly different (maximum: 12.0 vs 2.5 mm, respectively). And the retention in the bone marrow of the pretargeted radiolabeled peptide might be low but not negligible. Therefore, the radiation dose to the bone marrow might also be enhanced using ^{90}Y instead of ^{177}Lu. So, the safety profile of ^{90}Y could be different as well. The 3D-RD dosimetry results predicted that the tumor-to-red marrow dose ratios would not improve when switching to ^{90}Y. Unfortunately, we could not test these effects in our preclinical studies. Due to the major effect of the difference in tissue penetration range, and the inevitably differences in size between mice and humans, the experimental data from mouse models are challenging to extrapolate. For example, in mice the retention of a radiolabelled compound in the kidneys could be the radiation source of adjacent liver tissue and cause liver toxicity, as was shown in preclinical studies with radiolabelled Fab-fragments (*14*), while this would not be the case in humans due to the larger distance between those organs.

Furthermore, the current pretargeting system based on TF2 and radiolabelled IMP288 could be substantially improved by enhancing the circulatory half-life of bsMAb. High amounts of bsMAb in the tumour are required to capture as much of the radiolabelled peptide as possible, and to fully exploit the pretargeting technique of a two-step targeting of radioactivity. This can only be achieved by sustained high antibody blood levels during multiple days, as this is the driving force for accumulation of the bsMAb in the tumor. However, in patients the blood clearance of TF2 was much faster than that of similarly sized IgG molecules. This unexpected result could be explained by the fact that TF2 lacks a C_H2 domain (*15, 16*).

In conclusion, based on the knowledge acquired in this thesis, pretargeted immuno-PET with TF2 and IMP288 could be a very powerful imaging modality in patients with mCRC. Further studies should determine its added value in specificity compared to FDG-PET, and potentially similar or superior sensitivity in (CRC) patients.
As a therapeutic option, we did not find any evidence that PRIT with TF2 and ^{177}Lu-IMP288 can be effective in patients with advanced large-volume metastatic disease. However, in future studies several factors can be varied to increase the therapy effect, like testing PRIT in patients with smaller volume disease, and using a bsMAb with enhanced circulatory half-life.

References

1. Global Cancer Facts & Figures 2nd Edition, American Cancer Society. 2011.
2. de Gramont A, Figer A, Seymour M, et al. Leucovorin and fluorouracil with or without oxaliplatin as first-line treatment in advanced colorectal cancer. *J Clin Oncol.* 2000;18:2938
3. Saltz LB, Cox JV, Blanke C, et al. Irinotecan plus fluorouracil and leucovorin for metastatic colorectal cancer. Irinotecan Study Group. *N Engl J Med.* 2000;343:905.
4. Hurwitz H, Fehrenbacher L, Novotny W, et al. Bevacizumab plus irinotecan, fluorouracil, and leucovorin for metastatic colorectal cancer. *N Engl J Med.* 2004;350:2335
5. Jonker DJ, O'Callaghan CJ, Karapetis CS, et al. Cetuximab for the treatment of colorectal cancer. *N Engl J Med.* 2007;357:2040.
6. Douillard JY, Siena S, Cassidy J, et al. Randomized, phase III trial of panitumumab with infusional fluorouracil, leucovorin, and oxaliplatin (FOLFOX4) versus FOLFOX4 alone as first-line treatment in patients with previously untreated metastatic colorectal cancer: the PRIME study. *J Clin Oncol.* 2010;28:4697.
7. Eng C. Toxic effects and their management: daily clinical challenges in the treatment of colorectal cancer. *Nat Rev Clin Oncol.* 2009;6:207-18.
8. Jones RP, Jackson R, Dunne DF, et al. Systematic review and meta-analysis of follow-up after hepatectomy for colorectal liver metastases. *Br J Surg.* 2012;99:477-86.
9. Neeff H, Hörth W, Makowiec F, et al. Outcome after resection of hepatic and pulmonary metastases of colorectal cancer. *J Gastrointest Surg.* 2009;13:1813-20.
10. de Jong MC, Pulitano C, Ribero D, et al. Rates and patterns of recurrence following curative intent surgery for colorectal liver metastasis: an international multi-institutional analysis of 1669 patients. *Ann Surg.* 2009 Sep;250:440-8.
11. Fong Y, Fortner J, Sun RL, Brennan MF, Blumgart LH. Clinical score for predicting recurrence after hepatic resection for metastatic colorectal cancer: analysis of 1001 consecutive cases. *Ann Surg.* Sep 1999;230:309-318; discussion 318-321.
12. Behr TM, Sharkey RM, Juweid ME, et al. Phase I/II clinical radioimmunotherapy with an iodine-131-labeled anti-carcinoembryonic antigen murine monoclonal antibody IgG. *J Nucl Med.* 1997;38:858-870.
13. McBride WJ, Sharkey RM, Karacay H, et al. A novel method of 18F radiolabeling for PET. *J Nucl Med.* Jun 2009;50:991-998.
14. Behr TM, Sharkey RM, Sgouros G, et al. Overcoming the nephrotoxicity of radiometal-labeled immunoconjugates: improved cancer therapy administered to a nude mouse model in relation to the internal radiation dosimetry. *Cancer.* Dec 15 1997;80:2591-2610.
15. Chinn PC, Morena RA, Santoro DA, et al. Pharmacokinetics and tumor localization of (111)in-labeled HuCC49DeltaC(H)2 in BALB/c mice and athymic murine colon carcinoma xenograft. *Cancer Biother Radiopharm.* Apr 2006;21:106-116.
16. Ghetie V, Ward ES. FcRn: the MHC class I-related receptor that is more than an IgG transporter. *Immunol Today.* Dec 1997;18(12):592-598.

Samenvatting

De studies in dit proefschrift beschrijven radioimmunotargeting (RIT) van tumoren door middel van een pretargeting methode/benadering. Bij RIT worden radioactief gelabelde antilichamen toegediend, die gericht zijn tegen antigenen op tumorcellen en die daardoor specifiek in tumoren accumuleren. Omdat intacte antilichamen slechts langzaam in tumoren accumuleren en traag uit het bloed worden geklaard, kunnen de tumoren pas enkele dagen na injectie gedetecteerd worden en worden tijdens therapie het beenmerg aan een relatief hoge stralendosis blootgesteld. Om deze problemen te omzeilen zijn nieuwe pretargeting technieken ontwikkeld die zorgen voor een snelle en selectieve opname van de radioactiviteit in tumoren. Bij deze toepassing wordt eerst een niet-radioactief bispecifiek monoclonaal antilichaam (bsMAb) toegediend. Er wordt gewacht tot het antilichaam is geaccumuleerd in de tumor en geklaard uit de circulatie. Daarna wordt een radioactief gelabeld hapteen-peptide toegediend dat snel wordt geklaard uit het bloed en lichaam, maar wordt gebonden in de tumor door de anti-hapteen arm van het bsMAb.
Wij hebben een pretargeting systeem onderzocht gebaseerd op het bsMAb TF2 en het peptide IMP288 voor carcinoembryonic antigen (CEACAM5)-expresserende tumoren. TF2 is een gehumaniseerd anti-CEACAM5 x anti-HSG bsMAb dat is geproduceerd door middel van de zogenaamde Dock-and-Lock technologie, met een stabiel tri-Fab-molekuul als resultaat. TF2 bestaat uit twee Fab-fragmenten met hoge affiniteit voor CEACAM5 en een Fab-fragment met hoge affiniteit voor het hapteen histamine-succinyl-glycine (HSG). IMP288 is een peptide met twee HSG-groepen, met als doel een verbeterde hapteen-peptide opname en retentie in de tumor. Ook heeft IMP288 een chelator 1,4,7,10-tetraazacyclododecaan-1,4,7,10-tetraacetic acid (DOTA) die een groot scala aan radionucliden stabiel kan binden, zoals ^{111}In voor SPECT scans, ^{18}F en ^{68}Ga voor PET scans of ^{90}Y en ^{177}Lu voor pretargeted radioimmunotherapie (PRIT).

Allereerst hebben we het pretargeting systeem onderzocht in diermodellen ter oriëntatie voor de translatie naar de klinische situatie. In deze dierexperimenten maakten wij gebruik van naakte BALB/c muizen die werden geïnoculeerd met een LS174T-tumorcellen, van een CEA-expresserende, humane, colorectale cellijn. De subcutane (s.c.) injectie van 1 x 10^6 LS174T cellen resulteerde in s.c. tumoren van ongeveer 0.1-0.3 gram in 10-14 dagen. Hetzelfde aantal LS174T cellen werd intraperitoneaal geïnoculeerd, wat 2-3 weken na injectie resulteerde in peritoneale carcinomatosis met meerdere solide tumoren in het abdomen die veel variatie vertoonden in gewicht (0.3-650 mg), zonder tekenen van ongerief of verandering in lichaamsgewicht.

In de studies beschreven in **hoofdstuk 2 en 3** werd onderzocht wat het effect van de dosis van het bsMAb en het peptide was op de opname van het radioactief gelabelde IMP288 in de tumor en in de normale organen. De TF2 en IMP288 dosis werden opgehoogd om de dosis vast te stellen waarbij een maximale hoeveelheid radioac-

tiviteit specifiek naar de tumoren geleid kon worden. Uit deze studies bleek dat de optimale TF2 dosis in dit model 5.0-6.0 nmol/muis is en de optimale IMP288 dosis 0.28 nmol/muis.

In **hoofdstuk 2** hebben we de specificiteit van pretargeted immuno-PET met TF2 en ^{68}Ga-gelabelled IMP288 onderzocht in BALB/c naakte muizen met een s.c. LS174T-tumor, een s.c. CEA-negatieve tumor, of een steriele ontsteking in de dijbeenspier. In minder dan een uur toonden de PET-scan en de gedissecteerde weefsels een specifieke opname van het ^{68}Ga-IMP288 in de LS174T-tumor en zeer lage opname in de normale organen, in de CEA-negatieve tumor en in de ontstoken spier. Dezelfde muis werd ook gescand na injectie van ^{18}F-FDG. ^{18}F-FDG accumuleerde efficiënt in de tumor, maar ook in de ontstoken spier en in meerdere normale weefsels (hersenen, myocard, nieren en focaal in de darmen). Een soortgelijk hapteen-peptide werd radioactief gelabeld met ^{18}F en getest in muizen met een s.c. LS174T-tumor. ^{18}F-gelabeld peptide accumuleerde op dezelfde manier in de tumor en de normale weefsels als het ^{68}Ga-gelabelled peptide. Deze studies toonden aan dat pretargeted immuno-PET met TF2 en ^{68}Ga- of ^{18}F-hapteen-peptide een snelle, specifieke beeldvormende techniek is voor de detectie van CEA-positieve tumoren en dat het specifieker is dan ^{18}F-FDG-PET.

Voor het aantonen van de sensitiviteit van een nieuwe beeldvormende techniek heeft een orthotoop diermodel enkele voordelen in vergelijk met een s.c. tumormodel, nl. dat een dergelijk model ook de effecten van de tumor-vs-achtergrond-ratio's en tumoren van verschillende groottes binnen één dier onderzocht kunnen worden. In de studie beschreven in **hoofdstuk 3** werd de sensitiviteit van de pretargeted immuno-PET met TF2 en ^{68}Ga-IMP288 onderzocht in muizen met kleine intraperitoneale tumoren. Ook in deze studie werd pretargeted immuno-PET vergeleken met ^{18}F-FDG-PET. Na injectie van het ^{68}Ga-gelabelde peptide werd een hoog contrast tussen de tumor en de normale weefsels gevonden, wat resulteerde in een duidelijke afbeelding van alle tumoren in de buikholte met een volume ≥ 10 μL. Met ^{18}F-FDG konden enige tumoren ook worden afgebeeld, maar werd ook fysiologische opname gezien in normale organen, waardoor bijvoorbeeld de tumoren moeilijker van de normale darm onderscheiden konden worden. Deze resultaten suggereren dat pretargeted immuno-PET met bsMAb en ^{68}Ga-gelabeld peptide een zeer gevoelige beeldvormende techniek kan zijn voor het opsporen van colorectaal kanker.

Nadat de TF2- en IMP288-dosis waren geoptimaliseerd en de potentie van pretargeted immuno-PET was aangetoond, werd de therapeutische effectiviteit en toxiciteit van pretargeted radioimmunotherapie (PRIT) met TF2 en ^{177}Lu-gelabelled IMP288 bepaald in muizen met s.c. LS174T-tumoren (**hoofdstuk 4**). Aangezien pretargeting een verlaging van de stralingsdosis naar het beenmerg gaf, konden veel hogere doses radioactiviteit aan de muizen worden toegediend dan met directe radioimmuno-

therapie. Ook werden verschillende schema's met herhaalde toediening van radioactief gelabelled IMP288 onderzocht in een biodistributie-experiment. Het eerste schema bestond uit één TF2-injectie gevolgd door meerdere IMP288-injecties (interval van 3 uur). Het tweede schema bestond uit meerdere cycli waarbij elke IMP288 toediening werd voorafgegaan door een nieuwe TF2-injectie (interval van 72 uur). Het laatstgenoemde dosisschema resulteerde in de hoogste opname van radioactiviteit in de s.c. tumoren. In het therapie-experiment kregen de muizen één, twee of drie opeenvolgende cycli. PRIT vertraagde de tumorgroei effectief en verlengde de overleving van de muizen met s.c. tumoren significant, waarbij de overlevingswinst groter was in de muizen die meerdere werden behandeld met meerdere cycli TF2 en Lu177-IMP288 zonder dat relevante bijwerkingen gezien werden. Deze studie in muizen wijst erop dat PRIT bij colorectale kanker een mogelijk effectieve nieuwe behandeloptie met beperkte toxiciteit kan zijn.

Om de effectiviteit van pretargeted radioimmunotherapie te kunnen voorspellen, kunnen diagnostische scans worden vervaardigd na injectie van het radioactief gelabelde hapteen-peptide. De strategie waarbij beeldvorming en behandeling worden gecombineerd, wordt ook wel 'theranostics' genoemd. Dit was het onderwerp van de studie die wordt beschreven is in **hoofdstuk 5**. De mogelijkheid om pretargeted immuno-SPECT met TF2 en IMP288 gelabeld met ^{111}In te gebruiken voor monitoring van het therapeutisch effect van PRIT met ^{177}Lu-IMP288 werd onderzocht in muizen met intraperitoneaal groeiende LS174T-tumoren. In dit model toonde pretargeted immuno-SPECT een snelle en selectieve opname van het gelabelde hapteen-peptide in de tumor. Hierdoor konden zeer kleine tumoren gedetecteerd worden. De radioactiviteit in de tumorlesies gemeten in de SPECT scans correleerde goed met de opname die werd gemeten in de gedissecteerde weefsels. Er werd een overlevingsstudie uitgevoerd in muizen die TF2 en ^{177}Lu-IMP288, niet-gepretargeted ^{177}Lu-IMP288, of PBS kregen toegediend gevolgd door immuno-SPECT scans direct, 14 en 45 dagen na therapie. Tijdens PRIT met TF2 en ^{177}Lu-IMP288 kon de tumorgroei in de proefdieren in de opeenvolgende scans worden gevolgd. De resultaten van deze studie toonden de toegevoegde waarde van beeldvorming voor het monitoren van de effectiviteit PRIT.

De kennis die werd verzameld in de pretargeting studies in muizen-modellen werd gebruikt om een een fase I studie in patiënten met dikkedarmkanker in een vergevorderd stadium te ontwerpen (**hoofdstuk 6**). Het belangrijkste doel van deze studie was het bepalen van [1] de verschillende variabelen die bij pretargeting een rol spelen en [2] de veiligheid in patiënten met gemetastaseerd colorectaal carcinoom (CRC). Voor patiënten die in aanmerking kwamen voor deze studie waren geen standaard therapeutische opties meer beschikbaar. Er werden verschillende dosisschema's bestudeerd in vier cohorten van vijf patiënten door [1] het inkorten van het interval tussen de

toediening van het bsMAb en het peptide (5 dagen vs 1 dag), [2] het verhogen van de TF2 dosis (van 75 naar 150 mg) en [3] het verlagen van de peptide dosis (van 100 naar 25 μg). Er werd ook in de patiënten een snelle en selectieve tumoropname van het radioactief gelabelde hapteen-peptide waargenomen in minder dan een uur tijd met hoge tumor/normale weefsels ratio's (>20 na 24 uur). De tumoropname van het radioactief gelabelde hapteen-peptide was hoger bij een interval tussen de toediening van het bsMAb en het peptide van 1 dag en bij een peptide dosis van 25 μg. Hoge ^{177}Lu-IMP288 activiteitsdoses konden veilig aan patiënten worden toegediend. Wel werden bij enkele patiente infusiereacties waargenomen na herhaalde toediening van het TF2. Deze infusiereacties konden goed worden behandeld. Ook werd in twee patienten een tijdelijk graad 3-4 trombocytopenie waargenomen. Er werd geconcludeerd dat pretargeting met TF2 en ^{177}Lu-IMP288 in patiënten met CEA-expresserende CRC uitvoerbaar en veilig is.

In **hoofdstuk 7** is de dosimetrische analyse van de planaire scintigrammen en bloedsamples beschreven. Voorafgaand aan elke behandelcyclus kregen patiënten een diagnostische cyclus met TF2 en ^{111}In-gelabeld IMP288. De ^{111}In-IMP288 data werden gebruikt om de stralingsdosis van het ^{177}Lu-IMP288 te voorspellen, om zo te berekenen welke ^{177}Lu activiteitsdosis veilig kon worden toegediend. Er werd een sterke correlatie gevonden tussen de TF2 bloedspiegel op het moment van IMP288 toediening en de verblijftijd van het IMP288 in het bloed. Therapeutische ^{177}Lu activiteitsdoses resulteerden in lage stralingsdoses in de normale weefsels. In de meerderheid van de patiënten die de maximale of aangepaste ^{177}Lu activiteitsdoses ontvingen, overschreed de gemeten beenmergdosis niet de in het protocol vastgestelde limiet. Er was goede overeenstemming tussen de gesimuleerde ^{177}Lu-IMP288 beenmergdoses en de werkelijk gemeten doses. De hematologische toxiciteit correleerde met de stralendosis naar het beenmerg.

De SPECT-scans die werden verkregen in de fase I studie werden ook geanalyseerd met een nieuwe, geavanceerde methode, de Three-Dimensional Radiobiological Dosimetry (3D-RD) methode die gebaseerd is op Monte-Carlo simulaties (**hoofdstuk 8**). De voxel-waarden van de SPECT scans werden gebruikt om de activiteitsverdeling in de scan te bepalen en een CT-scan om de dichtheid van de weefsels te bepalen. De data van deze scans vormden de input van de Monte Carlo simulaties, die resulteerden in een schatting van de energie-depositie per voxel per scan. Met de combinatie van de resultaten van de vier SPECT-scans na een injectie werd de dosis binnen een VOI berekend. In tegenstelling tot de eerder beschreven dosimetrie-methodes, werden voor 3D-RD de SPECT-scans i.p.v. de planaire scintigrammen gebruikt en de lumbale wervels i.p.v. het cranium voor de beenmergdosis. Bovendien kon met de 3D-RD dosimetrie-methode naast de beenmergdosis ook de tumordosis worden bepaald. Daarnaast werd met 3D-RD ook rekening gehouden met het effect van de

weefseldichtheid en heterogeniteit van de stralingsdosis binnen een tumorlesie. De uitvoerbaarheid en de voorspellende waarde van deze 3D-RD software methode werd bestudeerd voor het voorspellen van beenmergtoxiciteit en therapeutische effectiviteit in de fase I klinische PRIT-studie en vergeleken met de resultaten van de methodes gebaseerd op de planaire scans en de bloedsamples. De 3D-dosimetrie toonde twee keer zo hoge beenmergdoses in vergelijking met de bloed- en planaire methode en een betere dosis-toxiciteitscorrelatie. Ook werden de tumor en beenmergdoses van het ^{177}Lu verkregen d.m.v. de 3D-RD methode gesimuleerd voor ^{90}Y. De tumor-vs-beenmerg-ratio van de data gesimuleerd voor ^{90}Y in vergelijking met ^{177}Lu lagen in dezelfde range. Er werd geconcludeerd dat met de 3D-RD methode de beenmergtoxiciteit en de stralingsdoses naar de tumoren beter voorspeld kunnen worden dan met de conventionele methoden.

In **hoofdstuk 9** worden de studies in het Engels samengevat en in **hoofdstuk 10** worden de resultaten bediscussieerd en het toekomstperspectief uiteengezet.

List of publications

Schoffelen R, Sharkey RM, Goldenberg DM, Franssen GM, McBride WM, Rossi EA, Chang CH, Laverman P, Disselhorst JA, Eek A, van der Graaf WTA, Oyen WJG and Boerman OC. Pretargeted immuno-positron emission tomography imaging of carcinoembryonic antigen-expressing tumors with a bispecific antibody and a 68Ga- and 18F-labeled hapten peptide in mice with human tumor xenografts. *Molecular cancer therapeutics. 2*010;9:1019-1027.

Schoffelen R, van der Graaf WT, Franssen GM, Sharkey RM, Goldenberg DM, McBride WJ, Rossi EA, Eek A, Oyen WJG and Boerman OC. Pretargeted 177Lu radioimmunotherapy of carcinoembryonic antigen-expressing human colonic tumors in mice. *Journal of nuclear medicine.* 2010;51:1780-1787.

Jaspers HC, Verbist BM, Schoffelen R, Mattijssen V, Slootweg PJ, van der Graaf WT, van Herpen CM. Androgen receptor-positive salivary duct carcinoma: a disease entity with promising new treatment options. *Journal of clinical oncology.* 2011;29:e473-476.

Schoffelen R, van der Graaf WT, Sharkey RM, Franssen GM, McBride WJ, Chang CH, Laverman P, Goldenberg DM, Oyen WJG and Boerman OC. Pretargeted immuno-PET of CEA-expressing intraperitoneal human colonic tumor xenografts: a new sensitive detection method. *EJNMMI research.* 2012;2:5.

Schoffelen R, van der Graaf WT, Sharkey RM,Franssen GM, McBride WJ, Chang CH, Bos DL, Goldenberg DM, Oyen WJG and Boerman OC. Quantitative immuno-SPECT monitoring of pretargeted radioimmunotherapy with a bispecific antibody in an intraperitoneal nude mouse model of human colon cancer: Pretargeting theranostics. *Journal of nuclear medicine. Accepted for publication.*

Schoffelen R, Boerman OC, Goldenberg DM, Sharkey RM, van Herpen CML ,Franssen GM, McBride WJ, Chang CH, Rossi EA, van der Graaf WT and Oyen WJG. Development of an imaging-guided CEA-pretargeted radionuclide treatment of advanced colorectal cancer: First clinical results. *Submitted.*

Schoffelen R, van der Weg W, Visser EP, Goldenberg DM, Sharkey RM, McBride WJ, Chang CH, Rossi EA, van der Graaf WT, Oyen WJG and Boerman OC. Predictive patient-specific dosimetry and individualized dosing of pretargeted radioimmunotherapy in patients with advanced colorectal cancer. *Submitted.*

Van der Weg W, Schoffelen R, Hobbs R, Gotthardt M, Oyen WJG, Boerman OCB, Sgouros G, Visser EP. SPECT-based patient-specific tumor and red bone marrow dosimetry for pretargeted radioimmunotherapy. *In preparation.*

Curriculum vitae

Born:	May 30, 1983 in Tilburg, the Netherlands
1995-2001:	Gymnasium (cum laude) Theresialyceum, Tilburg, The Netherlands
2001-2008:	Medical Doctor degree (bene meritum) Radboud University Nijmegen Medical Centre (RUNMC), Nijmegen, The Netherlands
2005:	Research project: "Use of complementary and alternative medicines among cancer patients enrolled onto phase I clinical trials at The Royal Marsden Hospital" Royal Marsden Cancer Centre, Drug Development Unit, Sutton, UK supervised by prof. dr. P.H.M. de Mulder and prof. dr. S.B. Kaye
2007:	Clinical internship: health care in developing countries Sengerema District Designated Hospital, Sengerema, Tanzania supervised by dr. M. Keuter and drs. M.J. Voeten
2008:	Start of PhD project RUNMC, Nijmegen, The Netherlands
2009-2011:	Chair Clinical PhD council RUNMC, Nijmegen, The Netherlands
2009:	Honorable Mention Siemens Inveon Image of the Year, Preclinical Solutions World Molecular Imaging Congress, Montreal, Canada
2010:	Best Oral Presentation 20th IRIST International Congress, Groningen, The Netherlands
2011:	Nomination for Marie Curie Award Annual Congress of European Association of Nuclear Medicine, Birmingham, UK
2011:	Frye Stipendium, RU, Nijmegen, The Netherlands Invested in research project: "Three-dimensional voxel-based dosimetry" Johns Hopkins Hospital, Dept. Nuclear Medicine, Baltimore, USA supervised by prof. G. Sgouros and dr. R. Hobbs
2012:	Start of internal medicine training Rijnstate Hospital, Arnhem, The Netherlands

Dankwoord

Op de kaft staat slechts één naam, maar eigenlijk horen alle onderstaande namen erbij. Daarnaast had dit onderzoek natuurlijk nooit kunnen plaatsvinden zonder de muizen: het proefdieronderzoek opende de deuren voor de klinische studie. Ook de deelname van de patiënten was onmisbaar. Ik heb erg veel respect voor hun enorme lef en toewijding bij dit geneesmiddelenonderzoek, in een poging om voor hun toekomstige lotgenoten nieuwe behandelopties te ontwikkelen.

Allereerst wil ik mijn eerste promotor bedanken: Otto, ik had het niet beter kunnen treffen dan met jou! Onze besprekingen waren inhoudelijk altijd zeer opbouwend. Maar naast je wetenschappelijke kwaliteiten, heb ik ook veel waardering voor je openheid, gelijkwaardigheid en oprechte interesse voor alle leden van je onderzoeksgroep. Dit heeft mijn promotie-tijd tot een leerzame en aangename periode gemaakt.
Wim, bedankt voor je lef, je snelle inzicht en doortastende besluiten bij onverwachtse resultaten bij deze toch wel spannende studie met twee nieuwe preparaten.
Winette, jij wist mij en de bovengenoemde Heren altijd weer even bij de oncologische les te houden als wij soms wat afdwaalde op het Nucleaire Pad.
Gerben, Gerrie, eigenlijk is dit ook jouw proefschrift! Het lab-werk in de vroege ochtenden, het CDL-werk in de late uurtjes: zonder ooit te mopperen. En ook nog een opbeurende schouderstomp op de juiste momenten. Thanks. Duck is my middle-name.
Annemarie, Eek, ook jij bedankt voor al je lab-werk voor mijn project. Maar vooral ook voor de enorm leuke, sociale events die je altijd weer organiseert
Jonathan, Sjonnie, ik heb je geduld regelmatig op de proef gesteld en daarbij aangetoond dat die onuitputtelijk is bij jouw hulp aan anderen. Het heeft mijn proefschrift van de Digibetische Afgrond gered. Maar vooral dank ook voor je mentale steun en vriendschap.
Peter, Laborman, dank je voor de prettige samenwerking en praktische hulp bij de Inveonperikelen en ^{18}F-praktijken en de gezelligheid buiten het werk om.
Gabie, dankzij jou heb ik 'leren promoveren'. En ik vond je enorme inzet bij het opstarten van de Clinical PhD Council geweldig en ik heb het heel leuk gevonden dat ik daarna je stokje mocht overnemen, bedankt voor je vertrouwen.
Sandra, Messie, het was heel fijn om af en toe mijn hart bij je te luchten over gedeelde frustraties en daarna weer met frissere moed door te gaan.
En natuurlijk alle andere Aquarium-genoten, Maarten, Stijn, Inge, Willem, Cathelijne, Janneke, Desirée, Lieke, Danny, Peter (Z), Karolina, Mark, Edwin, Samantha, dank voor jullie hulp en gezelligheid!
Bianca, Kitty, Henk en Iris, alleen dankzij jullie onvermoeibare en ervaren zorg voor de dieren is het mogelijk op een verantwoorde en zorgvuldige manier het onderzoek te doen!
Carla, heel veel dank dat je mij onder je hoede hebt genomen en dat ik bij jouw fase I team mocht aansluiten! Je stond altijd klaar met raad en daad, om het allerbeste voor de patiënten te regelen. Ik heb veel geleerd van je doeltreffende aanpak.
Anja, bedankt voor al je geduld en verstandige woorden op de belangrijke momenten. Ik voel me al een beetje vóór-opgeleid en hoop dat we dat over een paar jaartjes voortzetten.
Marye, ik vond het fijn dat ik altijd bij je terecht kon bij fase I-dillemma's, dank je wel!
Claudia, Iris, Michiel, Mirjam, Maartje, Researchvpk, jullie wisten altijd weer orde op zaken te stellen, als het in de praktijk nét weer even anders liep dan ik had gepland.
Wilmy, Yvonne, Lidwien, Tonnie, Brechje, Mark, Riet, Ria, Eveline, Ine, verpleegkundigen

en secretaressen van de oncologische dagbehandeling en verpleegafdeling, zonder jullie grote inzet bij de planning en uitvoering van de infusies was het niet gelukt, dank!
Maichel en Miranda, jullie zijn dé Hotlab-Helden, altijd bereid om de PRIT-medicatie op tijd te leveren, zelfs als wij haast onmogelijke eisen stelden aan de specifieke activiteit.
Katja, dank je wel dat je hebt volgehouden ondanks de vaak moeizame samenwerking met de verscheidene andere partijen.
Marjo en Eddy, bedankt voor al jullie hulp bij de opname- en scan-planning, ik heb jullie betrokkenheid erg gewaardeerd.
Martin, English, jouw toewijding maakte de vele scanuren (187 uren in totaal) voor zowel de patiënten als voor de arts-onderzoeker een stuk dragelijker . Nog meer uren maakte je als mijn favoriete, kletsende wandelcoach, voor de Once-in-a-Lifetime-Experience!
Michel, Bernadette, Marie Claire, Tineke, Peter K, Diane, Jurrian, jullie ook hartelijk bedankt voor jullie vaardige hulp bij de extra logistiek bij de scans.
Eric, de analyse van de klinische scans bleek toch een beetje ingewikkelder dan ik als Dosimetrie-Dummie had gedacht. Dankzij onze complementaire kennis en doorzettingsvermogen is het toch gelukt, met name dankzij de Technische Geneeskunde studenten:
Karen en Wietske, jullie ook superbedankt voor jullie zeer zinvolle bijdrage bij mijn project en de brug die jullie sloegen tussen techniek en kliniek.
Dennis, Marcel en Martin G, dank jullie wel voor jullie klinisch wetenschappelijke input, die was onmisbaar voor dit proefschrift!
Sandra, Jacqueline, Judith, Sylvia, Carola, Jolanda, Steven en Monique, jullie secretariële hulp heeft me zeer geholpen.
CPC'ers, Dagmar, Nathalie en Mieke, ik vond het heel leuk om samen met jullie voor de UMCN-promovendi een netwerk, cursussen etc. op te zetten.
Prof. Sgouros en Rob, thank you very much for your hospitality and for helping us to apply your 3D-RD-software on our data. It was a very worthy analysis for our research project, as it will be for many others in the future. Good luck with the validation and implementation.
Dr Sharkey, thank you very much for your throughout reviews of our data and manuscripts, You have taught me a lot about pretargeting specifically and (pre)clinical research in general.

Lieve Ankie, Arjanne, Esther, Heleen, Irma, Jorien, Josje, Kristel, Lucie, Marieke, Tessa, en Willemien, wat ben ik blij dat jullie mijn vriendinnen zijn! Al zoveel mooie en soms moeilijke dingen samen meegemaakt. Al lopen onze levens soms geografisch wat verder uit elkaar, we komen toch altijd weer samen en dan voelt het weer als vanouds: fijn!
Lieve Mayk, Henry, Thijs, Mayk, Lot, San, Morten, Tes en Marnix, jullie zijn de fijnste zussen, broer, schoonzus en zwagers die je je maar kan wensen, bedankt gewoon voor alles!
Lieve pap & mam, jullie zijn de allerbeste ouders! Dank jullie wel voor jullie onvoorwaardelijke zorg en steun!

AllerLiefste, Paul. Gelukkig weet je wat het is, een proefschrift schrijven en heb je me daarom mijn mopper-momenten vergeven. Twee boekjes op de plank, wat een opluchting. En nu door met de uitdagingen die we hebben gevonden in onze nieuwe banen, maar vooral genieten van alles daarbuiten. Heerlijk om samen met jou door het leven te gaan!